



National Library
of Canada

Bibliothèque nationale
du Canada

Canadian Theses Service

Service des thèses canadiennes

Ottawa, Canada
K1A 0N4

NOTICE

The quality of this microform is heavily dependent upon the quality of the original thesis submitted for microfilming. Every effort has been made to ensure the highest quality of reproduction possible.

If pages are missing, contact the university which granted the degree.

Some pages may have indistinct print especially if the original pages were typed with a poor typewriter ribbon or if the university sent us an inferior photocopy.

Reproduction in full or in part of this microform is governed by the Canadian Copyright Act, R.S.C. 1970, c. C-30, and subsequent amendments.

AVIS

La qualité de cette microforme dépend grandement de la qualité de la thèse soumise au microfilmage. Nous avons tout fait pour assurer une qualité supérieure de reproduction.

S'il manque des pages, veuillez communiquer avec l'université qui a conféré le grade.

La qualité d'impression de certaines pages peut laisser à désirer, surtout si les pages originales ont été dactylographiées à l'aide d'un ruban usé ou si l'université nous a fait parvenir une photocopie de qualité inférieure.

La reproduction, même partielle, de cette microforme est soumise à la Loi canadienne sur le droit d'auteur, SRC 1970, c. C-30, et ses amendements subséquents.

UNIVERSITY OF ALBERTA

**A Fluid Inclusion and Stable Isotope Study of Mesothermal
Au-Quartz Veins in the Klondike Schists, Yukon Territory.**

by

Ralph William Rushton

A THESIS

SUBMITTED TO THE FACULTY OF GRADUATE STUDIES AND RESEARCH
IN PARTIAL FULFILMENT OF THE REQUIREMENTS FOR THE DEGREE
OF MASTER OF SCIENCE

Department of Geology

Edmonton, Alberta

Fall, 1991



National Library
of Canada

Bibliothèque nationale
du Canada

Canadian Theses Service Service des thèses canadiennes

Ottawa, Canada
K1A 0N4

The author has granted an irrevocable non-exclusive licence allowing the National Library of Canada to reproduce, loan, distribute or sell copies of his/her thesis by any means and in any form or format, making this thesis available to interested persons.

The author retains ownership of the copyright in his/her thesis. Neither the thesis nor substantial extracts from it may be printed or otherwise reproduced without his/her permission.

L'auteur a accordé une licence irrévocable et non exclusive permettant à la Bibliothèque nationale du Canada de reproduire, prêter, distribuer ou vendre des copies de sa thèse de quelque manière et sous quelque forme que ce soit pour mettre des exemplaires de cette thèse à la disposition des personnes intéressées.

L'auteur conserve la propriété du droit d'auteur qui protège sa thèse. Ni la thèse ni des extraits substantiels de celle-ci ne doivent être imprimés ou autrement reproduits sans son autorisation.

ISBN 0-315-70092-0

Canada


UNIVERSITY OF ALBERTA

RELEASE FORM

NAME OF AUTHOR: Ralph William Rushton
TITLE OF THESIS: A Fluid Inclusion and Stable Isotope Study
of Mesothermal Au-Quartz Veins in the
Klondike Schists, Yukon Territory.
DEGREE FOR WHICH THESIS WAS PRESENTED: Master of Science
YEAR THIS DEGREE GRANTED: Fall, 1991

Permission is hereby granted to the UNIVERSITY OF ALBERTA LIBRARY to reproduce single copies of this thesis and to lend or sell such copies for private, scholarly or scientific research purposes only.

The author reserves other publication rights, and neither the thesis nor extensive extracts from it may be printed or otherwise reproduced without the author's written permission.


.....

PERMANENT ADDRESS:

Honey Bee Cottage,
Barfrestone,
Nr. Dover,
Kent,
ENGLAND.

DATE: July 16 1991

There's gold, and it's haunting and haunting;
It's luring me on as of old;
Yet it isn't the gold that I'm wanting,
So much as just finding the gold.
It's the great, big, broad land 'way up yonder,
It's the forests where silence has lease;
It's the beauty that thrills me with wonder,
It's the stillness that fills me with peace.

*The Spell of the Yukon,
Robert W. Service.*

UNIVERSITY OF ALBERTA
FACULTY OF GRADUATE STUDIES AND RESEARCH

The undersigned certify that they have read, and recommend to the Faculty of Graduate Studies and Research for acceptance, a thesis entitled A FLUID INCLUSION AND STABLE ISOTOPE STUDY OF MESOTHERMAL Au-QUARTZ VEINS IN THE KLONDIKE SCHISTS, YUKON TERRITORY submitted by RALPH WILLIAM RUSHTON in partial fulfilment of the requirements for the degree of MASTER OF SCIENCE.

.....
Supervisor: B. E. Nesbitt

.....
K. Muehlenbachs

.....
R. D. Morton

.....
D. Schmitt

Date: Oct 1, 1991.....

Dedication

To my parents.

ABSTRACT

Although over 300 metric tonnes of gold was extracted from the Klondike placer gold deposits, production from hardrock sources has been negligible, despite the occurrence of numerous gold-bearing quartz veins throughout the Klondike region.

Two dominant styles of quartz veining are recognized in the Klondike region of Yukon Territory, namely: (1) minor lens-shaped veins developed parallel to metamorphic foliation (foliaform) which are devoid of mineralization; foliaform vein mineralogy often reflects that of the immediate host rock, and no wallrock alteration has been noted around the veins; (2) massive quartz veins which are discordant to the foliation and often contain gold and/or sulfide mineralization. Carbonate-flooding and/or pyritisation of the wallrocks is commonly seen around Au-bearing veins. Both types of vein occur within middle to upper greenschist facies, Paleozoic (Devonian-Mississippian to Permian), metasedimentary and meta-igneous lithologies with Island arc affinities, which form part of the Yukon-Tanana terrane.

The Au-quartz veins are Earliest Cretaceous in age, and are hosted by brittle, extensional structures which may have developed during uplift of the Klondike region in the Late Jurassic to Early-Middle Cretaceous, following thrust-imbrication in the Early Jurassic. Foliaform veins probably formed as a result of elevated pore-fluid pressures within the rocks during thermal re-equilibration of the over-thickened imbricate stack, immediately post-thrusting in the Middle to Late Jurassic.

Fluid inclusion studies have delineated significant, regional P-X trends in primary inclusion fluids from the Au-quartz veins. The fluids have low salinities (<6 eq.wt.% NaCl) but variable CO₂ concentrations, decreasing from approximately 0.13-0.18 mole fraction CO₂ in the southeastern Klondike, through variable concentrations in the central Klondike (<0.01 to ≈1.00 mole fraction CO₂), to dominantly aqueous fluids (<0.01 mole fraction CO₂) in veins from the northwest of the region. Estimated trapping pressures decrease in a similar fashion, from 2070 ±420 bars to between 300-700 bars, from

southeast to northwest. Fluid temperatures ranged from 300-350°C in central and southern lodes, to 200-250°C in Au-quartz veins from the northwest Klondike. The P-X trends are interpreted as evidence for effervescence of a CO₂-rich phase from the mineralizing fluid, most likely in response to significant, regional uplift during the life of the hydrothermal system. Convection of the hydrothermal fluid may have been driven by an elevated geothermal gradient resulting from the rapid uplift.

The foliaform veins appear to have formed from variable salinity (0-14 eq.wt.% NaCl), H₂O+NaCl fluids with a low CO₂ content (<0.01 mole fraction CO₂), at temperatures of up to ≈400°C, and pressures of up to 3 kbars. The calculated isotopic composition of the foliaform vein fluids shows greater variation than Au-quartz vein fluids, probably as a result of host-rock control on the fluid isotopic signature. δ¹⁸O_{fluid} values range from 2.1 to 14 ‰ (average 7.9 ±3.3 ‰), with greater variation in veins hosted by metasedimentary lithologies. δD values of extracted inclusion fluids range from -102 to -183 ‰ (average -150 ±22 ‰). Although the fluid isotopic composition implies an evolved meteoric source for the foliaform vein fluids, the age and tectonic/rheological setting of vein formation (during, or immediately post-, retrograde metamorphism accompanying thrusting) argue against significant meteoric water involvement.

The isotopic composition of the Au-quartz vein fluids (averages: δ¹⁸O_{fluid} ≈7.8 ±1.5 ‰, δD_{fluid} ≈-150 ±18 ‰; compositional range: δ¹⁸O_{fluid} 3.2 to 9.8 ‰, δD_{fluid} -104 to -179 ‰) indicates that the mineralizing fluid was meteoric in origin, but underwent considerable isotopic evolution prior to mineralization. δD_{fluid} values of extracted inclusion fluids (-166 ±11‰) and from hydrothermal muscovites (-138 to -174 ‰) from the Sheba vein system are in good agreement, and indicate that the deuterium signature reflects that of the primary mesothermal fluid.

Acknowledgements

To adequately thank all those who have helped me over the past couple of years would take an extra chapter to do properly. However...

First and foremost, I would like to thank my supervisor, Bruce Nesbitt, for his patience, good-natured encouragement, and much appreciated financial support during the lengthy preparation of this thesis. Extra thanks also go to Bruce for initiating a study in such an historically interesting region. I will always be grateful to Jim Mortensen for introducing me to the geology and history of the Klondike, and for unselfishly sharing his knowledge of the geology of Yukon Territory with me. Without his help, much of this work would not have been possible. So who pays the 'phone bill, Jim?

Financial support for this project, in the form of a Boreal Alberta Research grant from the Circumpolar Institute at the University of Alberta, is gratefully acknowledged. Likewise, the help and travel assistance provided by the Geology Section of the Department of Indian and Northern Development in Whitehorse was invaluable. In addition, Jim McFaull and United Keno Hill Mines Ltd. provided welcome accommodation and assistance in the field, and are thanked for making things much easier. An honorable mention must also go to the Hughes-Lang group of companies for providing me with copies of unpublished company reports. Thanks to Scott Tomlinson, Bill Lebarge, Linda Matteson and Tashia for their help and company during the summer of 1989.

I am grateful to Karlis Muehlenbachs and all of his staff in the stable isotope laboratory at the University of Alberta, for analyzing innumerable samples, and for providing late-night liquid nitrogen during the frequent graveyard shifts. Thanks also to Tom Chacko for allowing me to use his unpublished calibration equation.

A special thank-you to the past Bubble Kings, Pierre Maheux and Bob Shaw, for initiating me into the myopic delights of the fluid inclusion stage, and to Bob Luth for cheerfully allowing me access to his printer in my times of direst need.

And last, but not least, to Susie, Ed and Rose, Heideh, Heather, and Bjami, all of the inmates of Room 3-01 past and present, the two other Shamools, all of the friends who gave me support and put up with my bad jokes, complaints and hangovers, and anyone I may have inadvertently forgotten. Thanks- I owe you one.

TABLE OF CONTENTS

Chapter	Page
I. INTRODUCTION	1
Historical and Geographical Setting	1
Bedrock Quartz veins	1
Results of Previous Studies	2
Objectives of the Present Study	5
II. REGIONAL AND LOCAL GEOLOGY	7
Regional Tectonic Setting	7
Omenica Crystalline Belt	7
Yukon-Tanana Terrane	7
The Paleozoic to Mesozoic Evolution of YTT	9
Paleozoic Evolution of YTT	9
<i>Regional Metamorphism</i>	11
Mesozoic Evolution of YTT	11
<i>Thrust Imbrication of YTT</i>	11
<i>Magmatic Lull and Regional Uplift</i>	12
Slide Mountain Terrane	12
The Geology of the Klondike Region	12
General Geology	12
<i>Assemblage I</i>	13
<i>Assemblage II</i>	14
<i>Assemblage III</i>	14
Deformation and Metamorphism	14
Thrust Imbrication	15
F1 Cooling Ages	15
Cretaceous Thermal Event	15
Faulting	16
III. HOST ROCK PETROGRAPHY	17
Principal Host Lithologies	17
Assemblage I Lithologies	17
Quartz-Augen Schist (QAS)	18
Chloritic Schist	18
Felsic Schist	19
Sulphur Creek Orthogneiss (SCO)	22
Assemblage II Lithologies	22
Micaceous Quartzites	22

TABLE OF CONTENTS (Continued)

Chapter	Page
Calc-Silicate Rocks	23
Garnet-Mica Schists	23
Mount Burnham Orthogneiss (MBO)	24
Assemblage III Lithologies	24
Serpentinite Lenses	24
IV. GEOLOGY OF THE QUARTZ VEINS	25
Eocene Epithermal Mineralization	26
Mesothermal Quartz Veins	26
Foliaform Veins	26
Discordant Quartz Veins	29
Age and Structure of Mesothermal Au-Quartz Veins	29
Au-Quartz Vein Structure	31
Au-Quartz Vein Geology	32
Gangue Mineralogy	32
Gold and Sulfide Mineralization	39
<i>Gold Morphology and Fineness</i>	<i>41</i>
Wallrock Alteration	43
<i>Carbonate Flooding</i>	<i>43</i>
<i>Pyritization</i>	<i>43</i>
Foliaform Vein Geology	44
V. FLUID INCLUSION STUDY	46
Introduction	46
Selection of Material	46
Results of Fluid Inclusion Study	47
Fluid Inclusion Types	47
Type 1: Aqueous Inclusions	48
Type 2: Intermediate XCO ₂ Inclusions	48
Type 3: High XCO ₂ Inclusions	49
Au-Quartz Veins	54
CO ₂ -Absent Au-Quartz Veins	54
<i>Final Melting Temperature of Ice: T_{ice}</i>	<i>54</i>
<i>Temperature of Total Homogenization: T_{htot}</i>	<i>55</i>
CO ₂ -Bearing Au-Quartz Veins	55
<i>Final Melting Temperature of CO₂: T_{mCO2}</i>	<i>58</i>

TABLE OF CONTENTS (Continued)

Chapter	Page
<i>Final Melting Temperature of Ice: $T_{m_{ice}}$</i>	58
<i>Final Melting Temperature of Clathrate: $T_{m_{clath}}$</i>	58
<i>Temperature of CO₂ Homogenization: T_{hCO_2}</i>	59
<i>Temperature of Total Homogenization: $T_{h_{tot}}$</i>	62
Foliaform Veins	62
Fluid Composition and Density	65
CO ₂ -Absent Au-Quartz Vein Fluids	65
CO ₂ -Bearing Au-Quartz Vein Fluids	68
<i>Vapor Phase Composition</i>	70
<i>Aqueous Phase Composition</i>	70
<i>Bulk Fluid Density and Composition</i>	71
Foliaform Vein Fluids	72
Pressure Calculations	72
Pressure at Total Homogenization: $P_{Th_{tot}}$	72
<i>Au-Quartz Veins</i>	72
<i>Foliaform Veins</i>	73
Pressure at Trapping: P_t	73
<i>Au-Quartz Veins in the Central Klondike</i>	75
<i>Au-Quartz Veins in the Southern Klondike</i>	76
<i>Au-Quartz Veins in the Northern Klondike</i>	77
<i>Foliaform veins</i>	78
Interpretation of Discordant Vein Data	79
Effervescence of CO ₂	79
<i>Criteria for Demonstrating Immiscibility</i>	82
VI. LIGHT STABLE ISOTOPE STUDY	86
Introduction	86
Results	86
Oxygen and Carbon Isotopes	87
Hydrogen Isotopes	95
Mineral Pair Geothermometry	95
Fluid Isotopic Signature	100
Choice of Equilibrium Fractionation Expressions	100
Fluid temperature	101
<i>Au-Quartz Veins</i>	101
<i>Foliaform Veins</i>	102

TABLE OF CONTENTS (Continued)

Chapter	Page
Mesothermal Vein Fluid Composition	102
<i>Au-Quartz Veins</i>	102
<i>Foliaform Veins</i>	105
<i>Hunker Dome Amethyst</i>	106
Eocene(?) Epithermal Veins	106
Ultramafic-Hosted Carbonate Veins	106
Discussion of Mesothermal Vein Data	107
Reliability of Deuterium Analyses	107
Compositional Range of Klondike Mesothermal Fluids	108
VII. DISCUSSION AND CONCLUSIONS	111
Au-Quartz Veins	111
Regional Structural Relationships	111
<i>Structures Related to Thrusting</i>	114
<i>Structures Related to Regional Uplift</i>	114
Au-Quartz Vein Fluid Source	116
Models of Mesothermal Fluid Genesis	116
Klondike Au-Quartz Vein Fluid Source	118
<i>Metamorphic/Magmatic Fluids</i>	118
<i>Meteoritic Fluids</i>	120
<i>Yukon Meteoric Waters</i>	121
<i>D-depleted Fluids: Other Examples</i>	122
Depth of Au-Mineralization: Hydrostatic vs. Lithostatic Fluid Pressures	123
Effervescence of CO ₂	124
Heat Source	130
Gold Transport and Deposition Mechanisms	130
Origin of Gangue Barite in the Violet Lode	133
Foliaform Veins	133
Foliaform Vein Fluid Source	135
Hunker Dome Amethyst Fluid Source	137
Eocene Epithermal Vein Fluid Source	138
A Model for Foliaform and Au-Quartz Vein Formation	138
Implications	141
REFERENCES	144

TABLE OF CONTENTS (Continued)

Chapter	Page
APPENDICES	154
Appendix 1. <i>Correction of FCO_2 and XCO_2 using the procedure of Diamond (1986)</i>	155
Appendix 2. <i>Microthermometric data for Au-bearing and foliaform vein quartz.</i>	158
Appendix 3. <i>Fluid composition calculations</i>	173
Appendix 4. <i>Equilibrium fractionation expressions used in isotope geothermometry and fluid isotopic composition calculations (see Chapter VI)</i>	174
Appendix 5. <i>Location and description of vein quartz and host rock samples from the Klondike</i>	175
Appendix 6. <i>The geology of selected Au-quartz vein locations</i>	187
Appendix 7. <i>Graphical construction methods for inclusion fluid pressure estimation</i>	191

LIST OF TABLES

Table		Page
1	Summary of microthermometric and inclusion fluid composition data for the principal Au-quartz vein occurrences	67
2	Inclusion fluid pressures for principal Au-quartz veins, calculated at the temperature of homogenization and the estimated temperature of trapping (see Table 1 for fluid compositions)	74
3	Light stable isotope analyses of vein minerals from Au-quartz and foliaform veins, Klondike District (see Appendix 5 for detailed sample locations)	90
4	Summary of fluid isotopic compositions from the principal Au-quartz veins, Klondike region	103
5	Comparison of some geochemical characteristics of inclusion fluids and mineral separates from Phanerozoic, Mesothermal Au-deposits	112

LIST OF FIGURES

Figure		Page
1	A. Location of the Klondike District and regional distribution of Yukon-Tanana and Slide Mountain terranes. B. Geology of the Klondike District, modified from Mortensen (1990). C. Distribution of the three principal lithotectonic assemblages, after Mortensen (1990) (see text).	3
2	Map of the Klondike District showing the locations of the principal, mesothermal Au-quartz veins in relation to the major thrust faults mapped by Mortensen (1990). Also shown are two ultramafic-hosted, carbonate vein occurrences and the Germaine Creek epithermal prospect.	4
3	A. Composite lithotectonic section for the Yukon-Tanana terrane in western Yukon, including the Klondike District. B. Schematic northwest-southeast lithotectonic section of the Klondike District illustrating the probable structural levels of the three main lithotectonic assemblages (modified after Mortensen, 1990).	10
4	Field sketch of a foliaform quartz+K-feldspar vein occupying and F2 fold hinge in quartz-augen schists, near California Gulch, Lower Bonanza Creek.	28
5	Geology of A.the Hunker Dome and B. Lone Star areas, with Au-quartz vein locations. Modified after Mortensen (1990).	33
6	Geological sketch map of exploration trenches in the Hunker Dome area, showing relationship between discordant quartz veining and a possible splay from the major thrust fault (see Figure 5).	34
7	Generalized paragenetic sequence for Au-bearing, discordant quartz veins at the Mitchell, Sheba and Hunker Dome lode occurrences. Modified from Friedrich and Hoymann (1989).	40
8	Map of the Klondike District showing the principal Au-quartz vein occurrences examined in this study, the most abundant type of primary inclusion found in quartz from each location, and the average Th_{10t} and Th_{CO_2} for each location.	52
9	Map of the Klondike District showing the locations of foliaform quartz vein occurrences examined in this study, the most abundant type of primary inclusion found in quartz from each location, and the average Th_{10t} , Th_{CO_2} (where applicable) and fluid salinity for each vein.	53
10	Ice melting temperatures ($T_{m_{ice}}$) for type 1 inclusions in A. CO_2 -absent, northern Klondike Au-quartz veins, B. CO_2 -bearing Au-quartz veins from the central Klondike, excluding Hunker Dome amethyst.	56
11	Temperature of total homogenization (Th_{10t}) for CO_2 -absent Au-quartz veins, broken down by location (see Figure 8, and Table 1).	57
12	A. Melting temperature of CO_2 ($T_{m_{CO_2}}$), and B. melting temperature of clathrate ($T_{m_{clath}}$), for CO_2 -bearing Au-quartz veins in central and southern Klondike.	60
13	Temperature and mode of homogenization of CO_2 phase (Th_{CO_2}) in CO_2 -bearing, Au-quartz veins, broken down by location.	61

LIST OF FIGURES (Continued)

Figure	Page
14	Temperature of total homogenization (Th_{tot}) for CO_2 -bearing Au-quartz veins, broken down by location (see Figure 8, and Table 1). 63
15	Plot of Th_{tot} of primary inclusions in Au-quartz veins, against distance along section line X-X' (see Figure 8). 64
16	A. Total Tm_{ice} data, and B. total Th_{tot} data, for foliaform vein quartz samples. 66
17	A. Isochores and estimated trapping pressures for fluids in type 1 primary inclusions in CO_2 -absent Au-quartz veins. Explanation: A. Virgin, B. Violet, C. range of isochores for 27 Pup, Lone Star, Hilchey, Sheba and Mitchell veins, D. Hunker amethyst. Boiling curve calculated for ≈ 4 eq. wt.% NaCl. B. Isochores for type 1 inclusion fluids in foliaform vein quartz, calculated for ≈ 5 eq. wt.% NaCl and $Th_{tot} \pm 1$ st.dev. (data from Haas, 1976; Potter and brown, 1977; Knight and Bodnar, 1989). 69
18	The shape of the solvus in the H_2O-CO_2-NaCl system, at 6 wt.% NaCl and varying pressures. Modified from Bowers and Helgeson (1983). Stippled rectangle represents the T-X area occupied by type 2a inclusion fluids in CO_2 -bearing Au-quartz veins (see text). 81
19	Isochores for type 2a and type 3 fluids from the Sheba vein. The estimated pressure at the intersection of the type 2a inclusion homogenization temperature range with the type 3 fluid isochore, and the pressure at the origin of the type 2a fluid isochore, are in close agreement. Isochores constructed from the data of Angus et al. (1976) and Bowers and Helgeson (1983). 2-phase curve constructed from the data of Takenouchi and Kennedy (1965). 83
20	Oxygen isotope analyses of quartz from: A. Au-bearing mesothermal veins, B. unmineralized, foliaform veins ($\delta^{18}O_{\text{‰}} \text{ SMOW}$). See also Table 3. 88
21	Hydrogen isotope analyses of inclusion fluids in quartz from A. Au-bearing mesothermal veins, B. unmineralized foliaform veins ($\delta D_{\text{‰}} \text{ SMOW}$) See also Table 3. 89
22	A. Comparison of $\delta^{18}O_{\text{quartz}}$ analyses, and B. comparison of δD of inclusion fluids, from Au-bearing and foliaform vein quartz samples. 96
23	$\delta^{18}O_{\text{quartz}}$ of Au-bearing and foliaform vein quartz, against vein host lithology. 97
24	Exchange equilibrium diagram for quartz-calcite, and quartz-muscovite mineral pairs from Au-bearing and foliaform vein quartz. Only two quartz-calcite pairs are approaching isotopic equilibrium over the estimated temperature range. Loci of tie lines calculated from equilibrium fractionation expressions of 1. Matsuhisa et al. (1979) and O'Neil et al. (1969), 2. Clayton et al. (1989), 3. unpublished quartz-muscovite fractionation expression (T. Chacko, pers. comm.). Diagram adapted from Rumble (1978). 99

LIST OF FIGURES (Continued)

Figure		Page
25	Plot of δD vs. calculated $\delta^{18}O$ of Klondike Au-quartz vein, and foliaform vein forming fluids, and other Cordilleran, mesothermal Au-quartz vein systems. Curve A illustrates the approximate isotopic evolution path of meteoric water at variable water rock ratios (<i>italics</i>), and temperatures of approximately 300-400°C. (* δD_{fluid} values calculated from hydrothermal mica). Data from Madu et al. (1990), Nesbitt et al. (1989), Goldfarb et al. (1988), Shaw et al. (1991), Sheppard (1986).	109
26	Schematic section through the Klondike Au-quartz vein system at the time of formation of the veins. In this model, the veins are coeval. The loss of CO_2 from the mineralizing fluid occurs at the transition from lithostatic or suprahydrostatic, to hydrostatic fluid pressures, at a depth of approximately 5-6 km within the fluid system (See text).	125
27	Schematic section through the Klondike Au-quartz vein system at the time of formation of the veins. The veins are coeval, and loss of CO_2 occurs as regional uplift forces the fluid system through the solvus in the H_2O-CO_2-NaCl system (See text).	127
28	Schematic section through the Klondike Au-quartz vein system at the time of formation of the veins. The veins are of different ages, with the youngest veins now exposed in the northwestern Klondike. Significant uplift occurred between episodes of vein formation. Regional uplift forces the fluid system through the solvus in the H_2O-CO_2-NaCl system, and the youngest veins formed from a CO_2 -depleted hydrothermal fluid.	129
29	The solubility of CO_2 in a 6 wt.% NaCl solution, at varying pressure and temperature. The shaded boxes represent the approximate P-T-X areas occupied by primary inclusion fluids in the Klondike Au-bearing veins, and illustrate the loss of CO_2 with decreasing fluid pressure. Diagram constructed from the data of Takenouchi and Kennedy (1965).	132

LIST OF PLATES

Plate	Page	
1	<p>A. Quartz-augen schist (QAS) cut by discordant quartz-carbonate vein. Note blue-grey quartz-feldspar augen, and yellow-green carbonate alteration around vein. B. Photomicrograph of unaltered QAS (crossed polars). Large quartz augen (qa) in groundmass of quartz, untwinned feldspar and muscovite, with ≈10% carbonate. C. Photomicrograph (crossed polars) illustrating carbonate flooding of QAS adjacent to discordant vein (qv) shown in Plate 1A (scale bar 0.5 mm for both plates).</p>	20
2	<p>Photomicrographs of, A. Chloritic schist with calcite (cc), in plane polarized light (ppl); B. Felsic schist, under crossed polars (xpl), showing crenulation cleavage defined by muscovite (m), in quartz groundmass; C. Micaceous quartzite (xpl); D. Garnet-muscovite schist (ppl) showing retrograde chlorite (c) growth on muscovite (m) and garnet (g). See text for full descriptions. Scale bar 0.5 mm for all plates.</p>	21
3	<p>A. Foliaform quartz lenses (ql) in altered quartz-muscovite schist from the Esperanza prospect (see Fig. 2). Head for scale; B. Au-bearing mesothermal quartz veins, discordant to foliation, at the French Gulch showing (see Fig. 2). Note intense Fe-staining on, and adjacent to, vein margins.</p>	27
4	<p>A. The Sheba vein (see Fig. 2): Massive, discordant, Au-bearing quartz vein cutting chloritic schists. Note host-rock foliation dipping towards the left of the photograph, and green Cu-staining from sulfide mineralization (see text). Hammer (arrowed) for scale; B. Minor discordant vein (dq) cutting foliaform quartz vein (fq). Note brown weathered Fe-carbonate along discordant vein margins.</p>	30
5	<p>White barite (ba) and quartz (q) in sample of vein material from the Violet mine dump (see Fig. 2); B. Photomicrograph (xpl) of zone of quartz brecciation in a discordant quartz vein from Hunker Dome. Note the introduction of late muscovite (m) and pyrite (py) along the zone. Scale bar is 0.5 mm.</p>	36
6	<p>A. Late quartz/amethyst cementing brecciated mesothermal quartz vein from Hunker Dome. B. Relatively fluid inclusion-free, unstrained amethyst (am) on strained, inclusion-rich, mesothermal quartz (mq) showing undulose extinction. C. Barite (ba) and euhedral quartz (qtz) from vein margin of discordant vein from the Virgin prospect (see Fig. 2). Scale bar for both photomicrographs is 0.5 mm.</p>	37
7	<p>A. Visible Au (Au) on limonite (after pyrite) in oxidized vein margin material from the 27 Pup vein (see Fig. 2). Scale bar is 1 cm; B. Foliaform quartz+ K-feldspar (K) vein, hosted by the Sulphur Creek orthogneiss, on Sulphur Creek.</p>	42
8	<p>Photomicrographs of type 1 and 2 fluid inclusions in discordant vein quartz, taken at room temperature (ca. 23°C); A. Field of large type 2a inclusions in sample YR64a (NB: CO₂-phases have homogenized); B. 3-phase type 2a inclusions, sample YR64a; C. 3-phase type 2a inclusions, sample YR64a (in plates B and C, sample was cooled briefly in liquid nitrogen to nucleate CO₂-vapor phase); D. 3-phase type 2b inclusion in</p>	

LIST OF PLATES

Plate		Page
8	<i>Continued.</i> mesothermal quartz, sample RR137; E. Type 1 inclusions (arrowed), sample RR322; F. Type 1 inclusion in amethyst, sample RR137. All scale bars are 100 microns, except plate E (50 microns).	50

I. INTRODUCTION

Historical and Geographical Setting

Despite historical production of over 300 metric tonnes of gold from placer deposits, the Klondike region of west-central Yukon Territory, Canada (Figures 1a and 2), has yet to produce significant quantities of gold from hardrock or lode sources (Whelan and Meixner, 1989; Morison and Hein, 1987; Gleeson, 1970). Placer gold production began in the area with the gold rush of 1896, reached a peak of approximately 30 metric tonnes of gold in 1900, and has continued to the present day despite a significant decline in output. The region is located approximately 400 km northwest of Whitehorse, southwest of the Tintina Trench (Figure 1a), and is bounded to the north and northeast by the Klondike River, and in the south and west by the Indian and Yukon rivers (Figures 1b and 2).

Bedrock Quartz Veins

Gold-bearing quartz veins, hosted by the schists and gneisses which underlie the area, were discovered at an early stage in the development of the Klondike placer deposits (e.g., McConnell and Tyrrell, 1898; Maclean, 1914). The common occurrence of gold-bearing quartz pebbles in placer gravels, the crystalline habit of some of the placer gold, and the apparent localization of placer pay streaks to gravels immediately downstream of known gold-bearing lodes, convinced McConnell (1905) and others (Tyrrell, 1912; Brock, 1909) that the placer gold must have been derived from the quartz veins. Nevertheless, the "mother lode", which many believed must eventually be found within the area, remained elusive.

McConnell (1905) first noted the occurrence of more than one type of quartz vein within the schists. Foliaform quartz veins (ffm), which resemble typical metamorphic "segregation" veins (e.g., Yardley, 1975), are lensoid, parallel to the metamorphic foliation, and are generally devoid of any sulfide or gold mineralization. In contrast, the gold-bearing veins are generally discordant to the foliation, are poor in sulfides and are

known to contain local, high-grade, gold mineralization (Mortensen et al., in press). Intensive exploration has identified nearly two dozen gold-bearing discordant quartz veins, distributed in a broad, northwest-southeast trending belt across the Klondike region; in addition numerous smaller unnamed veins occur throughout the area.

The most economically and historically important of the known vein occurrences are shown on Figure 2. Gold grades are often spectacular but very erratic, with values of up to 9 kg/tonne recorded for high-grade sulfide mineralization, although the sporadic nature of the mineralization has rendered most of the veins uneconomical at current Au prices. The Lone Star mine was the only mine to achieve significant production: gold worth an estimated \$25,000 at 1912 prices (ca. 40 kg of gold) was recovered from nearly 8,500 tons of ore between 1912 and 1914 (Northern Cordilleran Mineral Inventory, 1972). Overall, contributions from lode sources accounted for less than 0.5 % of the total Klondike production in 1912 (Maclean, 1914), and soon afterwards ceased altogether.

Results of Previous Studies

Preliminary geological, fluid inclusion and light stable isotope investigations of the gold-bearing veins (e.g., Friedrich and Hoymann, 1989; Rushton et al., 1990; Mortensen et al., in press) suggested that they are part of an extensive mesothermal vein system with geological and genetic similarities to other documented mesothermal deposits, for example, the gold-bearing quartz veins in the Otago Schists, New Zealand (McKeag and Craw, 1989), the Mother Lode, California (Weir and Kerrick, 1987), and the Jungwon gold area in the Republic of Korea (Shelton et al., 1988). However, the Klondike veins differ from the more generally accepted empirical and geologic models of mesothermal vein systems in two important aspects.

Firstly, prevailing geological thought on the genesis of mesothermal lode gold deposits in the Cordillera falls essentially into two different camps: (1) the generation of mineralizing fluids during prograde, metamorphic devolatilization of subducted sediments

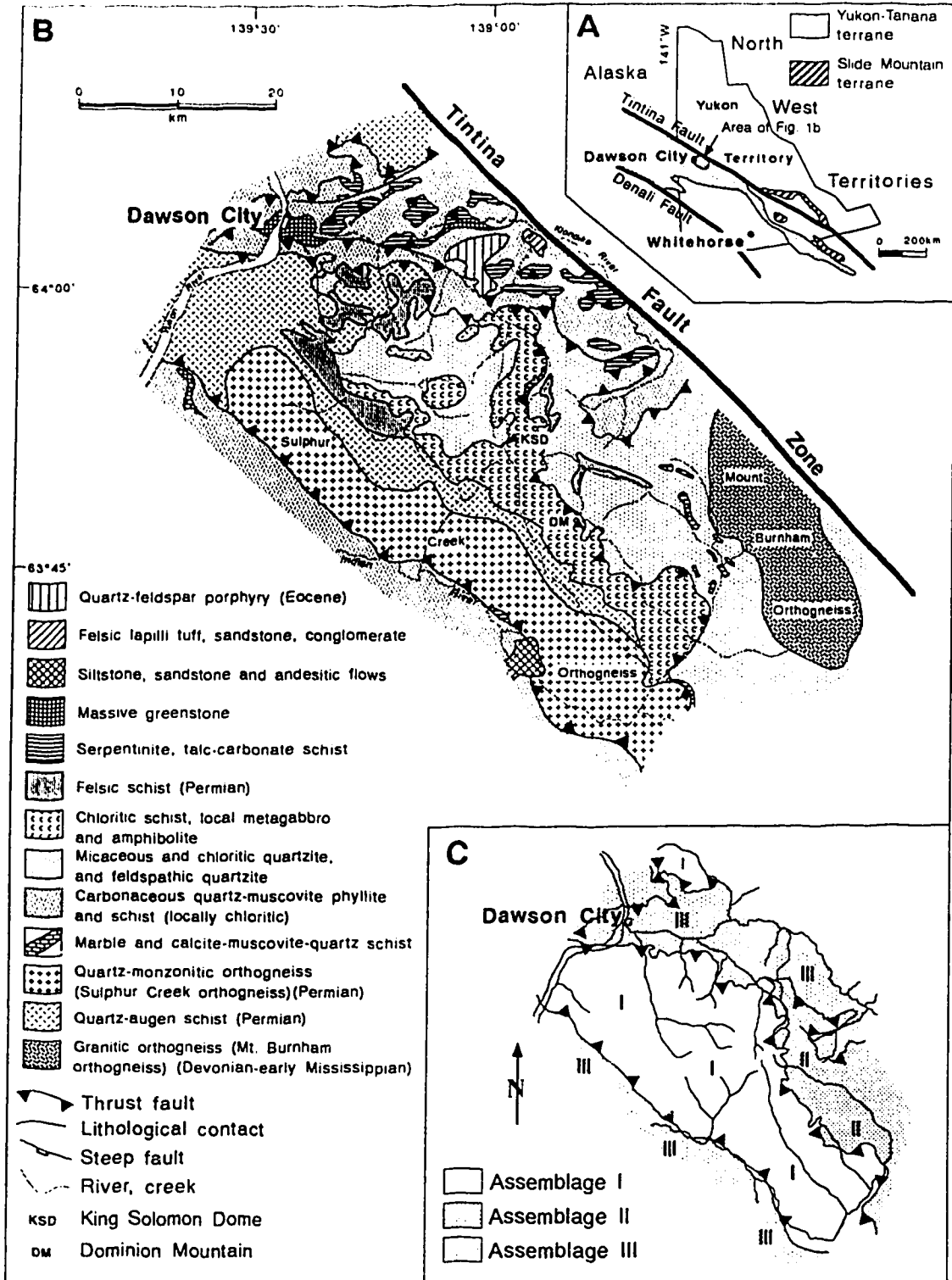


Figure 1. A. Location of the Klondike District and regional distribution of Yukon-Tanana and Slide Mountain terranes. B. Geology of the Klondike District, modified from Mortensen (1990). C. Distribution of the three principal lithotectonic assemblages, after Mortensen (1990) (see text).

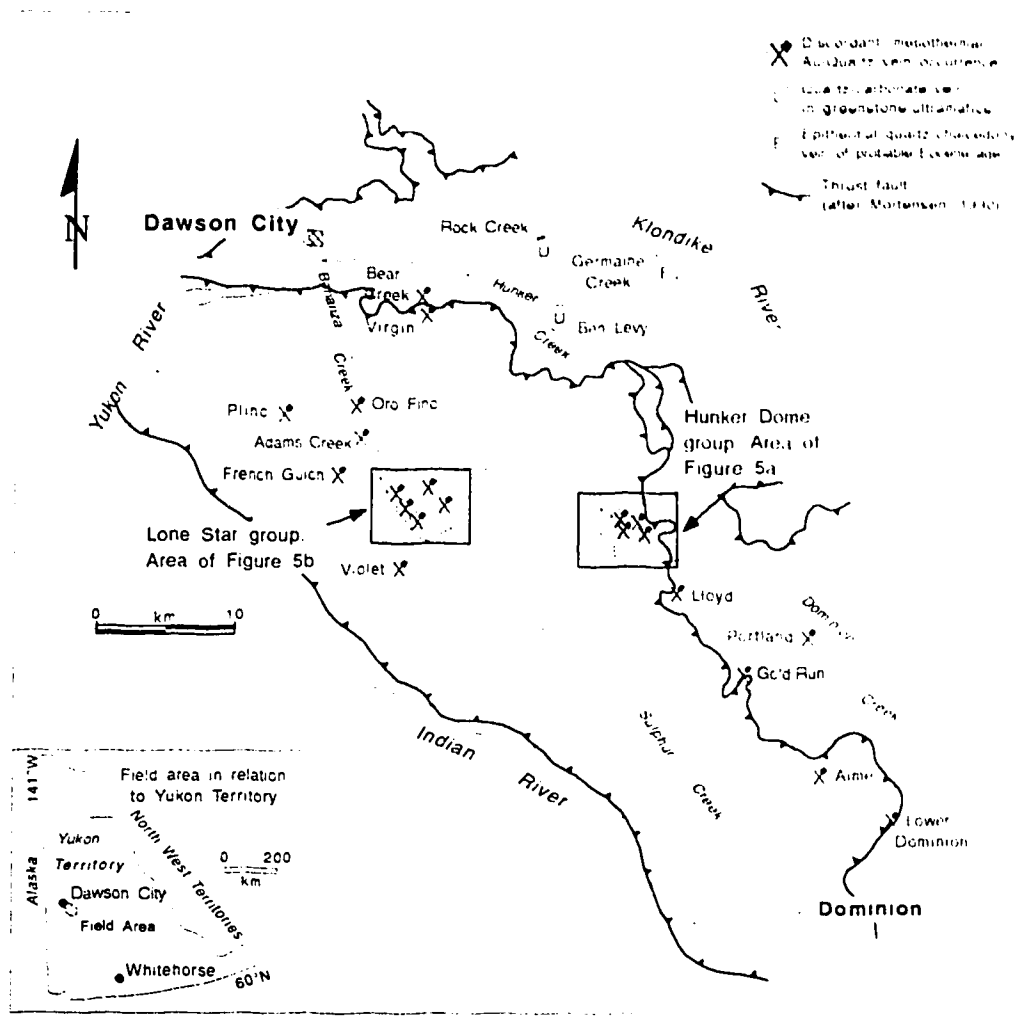


Figure 2. Map of the Klondike District showing the locations of the principal, mesothermal Au-quartz veins in relation to the major thrust faults mapped by Mortensen (1990). Also shown are two ultramafic-hosted, carbonate vein occurrences and the Germaine Creek epithermal prospect.

and igneous rocks (e.g., Goldfarb et al., 1989; Goldfarb et al., 1988), and (2) deep convection and chemical evolution of meteoric waters (e.g., Nesbitt, 1988; Nesbitt and Muehlenbachs, 1989). Most authors currently favor the first model which has been applied in studies of Archean and Phanerozoic Au-quartz vein systems (e.g., Goldfarb et al., 1988; Kyser and Kerrich, 1990; Groves and Phillips, 1987).

However, the initial hydrogen isotope analyses of extracted inclusion fluids reported in Rushton et al. (1990) and Mortensen et al. (in press) suggest that inclusion fluids from discordant vein quartz are depleted in deuterium relative to the metamorphic or magmatic water fields; an observation which is incompatible with the involvement of metamorphogenic fluids in the mesothermal mineralizing process. Also, K-Ar ages, obtained by Mortensen (in press) for hydrothermal muscovite from a gold-quartz vein in the Klondike, suggest that the mesothermal veins post-date prograde metamorphism by as much as 60 Ma, and cast doubt upon the applicability of the metamorphic devolatilization model to the Klondike veins (see below). These results are more easily explained by the involvement of chemically evolved meteoric waters, the model favored by Nesbitt (1988) and Shelton et al. (1988), which is currently a source of some controversy (e.g., Kyser and Kerrich, 1990; Nesbitt, 1990; Pickthorn et al., 1987; Nesbitt et al., 1987; Peters et al., 1990; Nesbitt and Muehlenbachs, 1991).

Secondly, the common association of Au-quartz veins and major crustal structures such as terrane-bounding faults (Kerrich and Wyman, 1990) has not been recognized in the Klondike. Rather, the veins appear to be hosted by relatively minor, extensional structures which bear no obvious relationship to any of the regional structures currently recognized in the Klondike (Mortensen et al., in press; J. Mortensen, pers. comm.).

Objectives of the Present Study

The current study focuses on the geochemistry of the gold-bearing mesothermal veins, and had a number of initial objectives. In a regional context, the study is part of an

on-going investigation of crustal fluid regimes, and related mineralized and non-mineralized vein systems, across the Canadian Cordillera (e.g., Nesbitt, 1990; Nesbitt and Muehlenbachs, 1989; Nesbitt, 1988).

In addition, to resolve some of the problems raised by the preliminary studies, a more detailed fluid inclusion and stable isotope study of discordant and foliaform vein minerals was undertaken, in order to determine the nature, P-T conditions and potential source of the vein-forming fluids, and to define any regional variations in the fluid geochemistry.

On a local scale, the current work is one of three related geochemical studies which are focusing on the mesothermal veins as a possible source for much of the Klondike placer gold (see Knight et al., in prep.; Mortensen, in prep.). Recent work by Dufresne (1987), suggested that much of the gold contained within the rich, elevated bench gravels on Hunker and Bonanza creeks (the White Channel gravels) was introduced during a Pliocene-Pleistocene age epithermal mineralizing event, and may subsequently have been incorporated into younger placer deposits along the same creeks by erosion. However, the White Channel gravels are absent from many of the central and southern Klondike creeks, suggesting that the placer gold in these areas must have been derived from other sources. Thus, the results of the study presented below, have a number of implications for genetic models of mesothermal Au-quartz vein systems in regionally metamorphosed areas, and for the probable source of much of the Klondike placer gold.

II. REGIONAL AND LOCAL GEOLOGY

Regional Tectonic Setting

Omenica Crystalline Belt

The rocks of the Klondike district belong to two distinct, although perhaps related terranes; the Yukon-Tanana Terrane (YTT), and the Slide Mountain Terrane (SMT) (Mortensen, 1990; Hansen, 1990). These terranes form part of the northern extension of the Omineca Crystalline Belt, one of five tectonic belts which make up the Canadian Cordillera (Templeman-Kluit, 1976; Monger, 1984; Gabrielse and Yorath, 1989).

The Omenica Crystalline Belt is an assemblage of Middle Proterozoic to Middle Paleozoic miogeoclinal rocks, with Paleozoic and lower Mesozoic volcanogenic and sedimentary rocks, which were deformed and variably metamorphosed in Middle Mesozoic to Early Tertiary times (Monger, 1984). Much of the deformation and metamorphism which has affected the rocks of the Omenica belt occurred as a result of the collision between a large composite, allochthonous terrane (Terrane 1) and the North American Continental margin (NACM), sometime in the Middle Jurassic (Monger et al., 1982). The smaller terranes which together make up Terrane 1, are believed to have come together by the Late Triassic to Early Jurassic times (Monger et al., 1982).

Yukon-Tanana Terrane

The YTT is an assemblage of metamorphic and plutonic rocks with island arc affinities, of Middle Paleozoic to Early Mesozoic age, exposed over a large part of Yukon Territory and east-central Alaska (Figure 1a) (Mortensen, 1990; Hansen, 1988; Mortensen and Jilson, 1985). It is one of the most easterly of the transported, "suspect" terranes which abut the autochthonous strata of the NACM. In west-central Yukon and eastern Alaska, the YTT is faulted to the north against miogeoclinal strata of the NACM along the Tintina Fault. In southwestern Yukon and southern Alaska, the southern margin of the YTT is defined by the Denali Fault (Figure 1a) (Mortensen and Jilson, 1985). In the Late

Cretaceous and/or Early Tertiary, up to 450 km of dextral, strike-slip movement along the Tintina fault offset a significant portion of the YTT, which now crops out in southern Yukon Territory, to the northeast of the fault (Figure 1a) (Mortensen and Jilson, 1985).

The origin and nature of the YTT are still open to question. Some authors suggest that the YTT is pericratonic with stratigraphic affinities to North America, and has not been significantly displaced from its site of origin (Gabrielse and Yorath, 1989), while others maintain that the YTT is allochthonous with respect to the NACM (Templeman-Kluit, 1979). Most recently, Mortensen (in press) argues against a direct link between rocks of the YTT and the autochthonous strata of the NACM.

The nomenclature used to describe the YTT is confusing, partly because of its complex geological history with multiple episodes of deformation, metamorphism and magmatism (Hansen et al., 1989; Mortensen, in press). In recent literature, the terrane has been referred to as the Kootenay terrane, with Barkerville and Nisutlin subterrane (e.g., Wheeler et al., 1984; Gabrielse and Yorath, 1989), the Cassiar terrane (Anderson and Hodgson, 1989), and also the Yukon-Tanana terrane (Mortensen, in press; Aleinikoff et al., 1986). A detailed discussion of the terrane nomenclature is beyond the scope of this paper, and the interested reader is referred to Mortensen (in press) for further discussion. The name YTT as used by Monger and Berg (1987), and Mortensen (in press) is used in this paper (Figure 1a).

Recent work on the YTT in Yukon Territory (Templeman-Kluit, 1976, 1979; Mortensen and Jilson, 1985; Mortensen, 1990, in press; Hansen, 1988; Hansen et al., 1989), and on the northwestern extension of the YTT into Alaska (Dusel-Bacon and Aleinikoff, 1985; Aleinikoff et al., 1986), has helped to resolve many of the problems in the interpretation of the regional geological and tectonic evolution of the YTT. Detailed mapping has revealed significant regional similarities in the geology and tectonic evolution of the YTT, wherever it has been encountered in Yukon Territory and Alaska (Mortensen,

1990; Mortensen and Jilson, 1985). The following discussion is taken mainly from Mortensen (in press) and Hansen (1988).

The Paleozoic to Mesozoic Evolution of YTT

Paleozoic Evolution of YTT

The oldest rocks recognised within YTT are quartz-rich metasedimentary units, with local marbles and pelitic units, of Late Devonian age or older, which appear to have been deposited in a passive continental margin environment (Figure 3). These rocks are overlain by an interlayered sequence of Middle Devonian to Mississippian metasedimentary rocks and submarine metavolcanic units, which have been intruded by two suites of metaplutonic rocks with similar Devono-Mississippian ages.

Metaluminous quartz diorite, granodiorite and quartz-monzonite bodies with local gabbroic units which occur in Yukon and Alaska, have yielded U-Pb ages of 375 to 348 Ma and are coeval, and probably cogenetic, with the Devono-Mississippian metavolcanics (Mortensen, 1990). Peraluminous granitic orthogneiss bodies, which give similar zircon U-Pb ages of 364 to 340 Ma, have also been mapped across much of YTT, although it is uncertain whether an extrusive equivalent of these rocks exists. This metavolcanic and metaplutonic assemblage is believed to have formed above a north- to northeast-dipping subduction zone (Mortensen, in press).

Middle Permian metavolcanic, metaplutonic and metasedimentary rocks have recently been described by Mortensen (in press) from the Klondike area of Yukon Territory. The meta-igneous rocks are calc-alkaline in character and yield Middle Permian U-Pb zircon ages (see below). These rocks have not been reported from any other exposures of YTT rocks, possibly because of their lithological similarity to the Devono-Mississippian intrusives (Mortensen, in press). This assemblage may have formed in an east facing magmatic arc above a Late Paleozoic, southwest- to west-dipping subduction zone, outboard of North America (Mortensen, in press; Hansen, 1988).

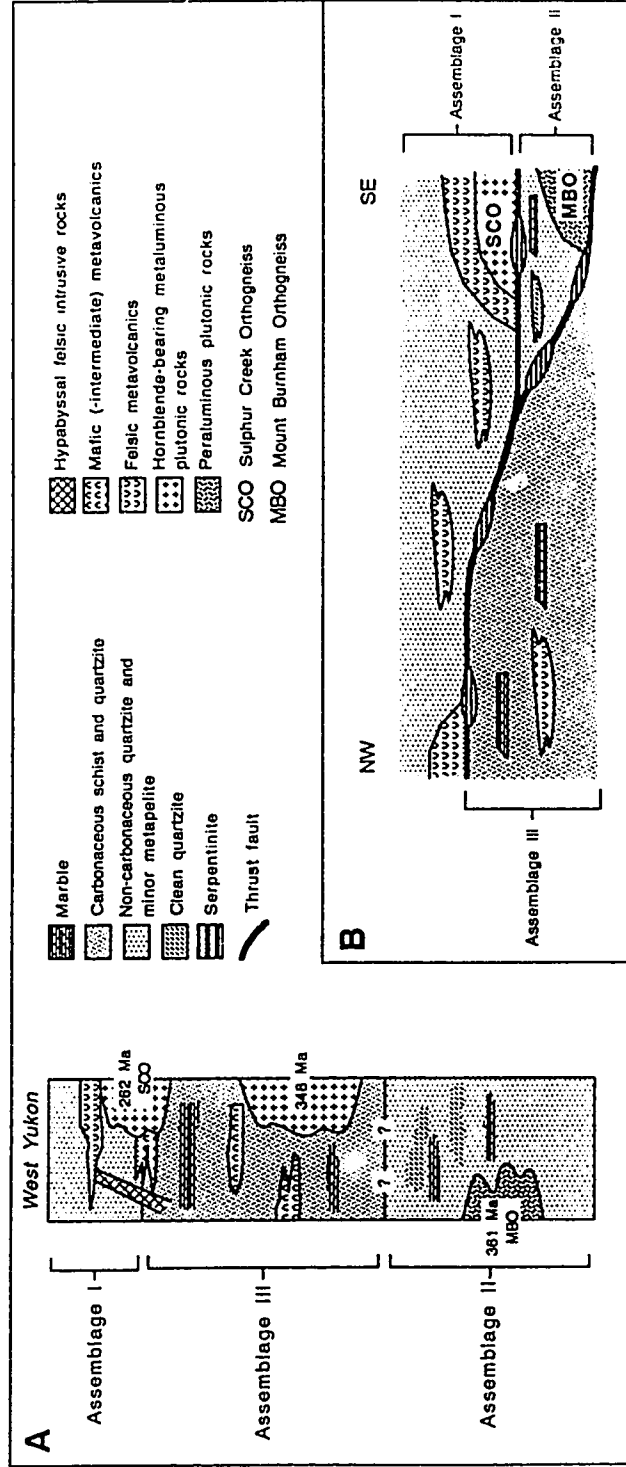


Figure 3. A. Composite lithotectonic section for the Yukon-Tanana terrane in western Yukon, including the Klondike District. B. Schematic northwest-southeast lithotectonic section of the Klondike District illustrating the probable structural levels of the three main lithotectonic assemblages (modified after Mortensen, 1990).

Regional Metamorphism

Following development of the Late Paleozoic arc complex, between Middle Permian to Late Triassic times, extensive, penetrative ductile deformation (D1) and regional metamorphism (F1-locally up to lower amphibolite facies) affected most of YTT (Mortensen, in press; Hansen, 1988). Mortensen suggests that D1 deformation and the accompanying metamorphism was caused by collision of YTT with another continental land mass, possibly North America, at this time. Metamorphic cooling ages range from Jurassic to Middle Cretaceous and imply that cooling was prolonged across much of the YTT.

Mesozoic Evolution of YTT

Late Triassic to Middle Jurassic age plutonic activity has been recognised across much of the YTT. Mortensen (in press) reports U-Pb, Ar-Ar and K-Ar ages of between 212 to 185 Ma for a suite of strongly differentiated intrusives ranging in composition from ultramafic, through dioritic to syenitic. These intrusives are probably related to a collision between YTT, and other terranes to the west; it is probable that an easterly directed subduction zone existed at this time to the west of YTT, dipping beneath the terrane (Hansen, 1988).

Thrust Imbrication of YTT

Structural imbrication of much of the YTT along major thrust faults occurred towards the end of the Triassic-Jurassic plutonism, and has been constrained to Early to Middle Jurassic in Yukon (J. Mortensen, pers. comm.). Thrusting was probably initiated as a result of the continued plate convergence and amalgamation of other terranes to the west (Hansen, 1988; Mortensen, in press).

Magmatic Lull and Regional Uplift

Although Middle Cretaceous plutons are known to intrude YTT, the period from approximately 155 to 125 Ma ago is notable for the almost complete absence of magmatism across the entire Canadian Cordillera (Armstrong, 1988; Gabrielse and Yorath, 1989). Armstrong also notes that this period of inactivity is coincident with regional gaps in the stratigraphic record, suggesting that uplift and erosion, which probably began immediately post thrusting, were still taking place at this time.

Slide Mountain terrane

The SMT occurs as a northwest-southeast trending belt of relatively small, isolated allochthons which extends along the length of the Canadian Cordillera (Figure 1a) (Hansen, 1990). The terrane is comprised of weakly- to non-metamorphosed oceanic and arc-related strata including massive greenstone and altered ultramafic rocks, which range in age from Devonian to Triassic (Hansen, 1988). SMT rocks generally lie to the east of the YTT, but often occur along thrust surfaces, tectonically interleaved with YTT rocks (e.g., Mortensen, 1990).

The relationship between YTT and SMT is uncertain. Hansen (1988) argues that SMT rocks represent the subduction/accretionary complex which developed on the eastern edge of the Late Paleozoic YTT magmatic arc, above the westerly directed subduction zone.

The Geology of the Klondike Region

General Geology

The Klondike (Figure 1b), has been mapped by a number of workers (e.g., McConnell, 1905; Bostock, 1942; Green, 1972; Debicki, 1984, 1985), and most recently by Mortensen (1990). The region falls within an area which experienced significant uplift during the Neogene period, and which escaped Pleistocene glaciation (Dufresne, 1987). As a result, the area is deeply weathered, and outcrop is sparse (Mortensen, 1990). The

geology of the unconsolidated sediments, including the White Channel and other gold-bearing gravels, has been described by a number of authors (e.g., Milner, 1976; Templeman-Kluit, 1982; Morison and Hein, 1987; Dufresne, 1987).

Figure 1b, after Mortensen (1990), illustrates the general geology of the Klondike region. Mortensen recognized a sequence of regional-scale thrust sheets underlying the area (Figure 1c), termed Assemblages I, II, and III, made up of a variety of metamorphic rock types (see below). Sheets and lenses of serpentinite and ultramafic rocks with ophiolitic affinities, interpreted as belonging to the Slide Mountain terrane, have been structurally emplaced along many of the thrust surfaces (Figure 1b) (Mortensen, 1990). Unmetamorphosed, Late Cretaceous to Early Tertiary intrusive and extrusive rocks and sedimentary rocks are also exposed within the area, but do not host mesothermal mineralization. Locally, these late intrusives appear to cut the thrust surfaces (Mortensen, 1990). The stratigraphic and structural relationships between the various units are illustrated in Figure 3, after Mortensen (in press), and the metamorphic rocks are described in greater detail below.

Assemblage I

Within the imbricated package of metamorphic rocks, Assemblage I occupies the highest structural level, and is comprised of metasedimentary and metavolcanic schists, and orthogneisses (Figure 3). The most common lithologies in Assemblage I are chloritic schists, impure quartzites, felsic schists, quartz-augen schists and a quartz-monzonitic orthogneiss body, termed the Sulphur Creek orthogneiss (SCO) (Mortensen, 1990). The quartz-augen schist is thought to be a metamorphosed and deformed quartz-feldspar porphyry intrusive.

Similar U-Pb zircon ages from the SCO (262.4 ± 2.2 Ma), the quartz-augen schist (261 ± 4 Ma), and from samples of the metavolcanics (263 ± 4 Ma), suggest that the three units may be coeval and assign a Middle Permian age to Assemblage I (Mortensen, 1990).

The sequence is interpreted as upright, with many of the originally discordant, intrusive contacts rotated into near concordancy by shear strain (Mortensen, 1990). Metamorphic foliation is subhorizontal and roughly parallel to compositional layering.

Assemblage II

At a lower structural level than Assemblage I, Assemblage II is up to 800 m thick, and consists predominantly of metasedimentary units and metavolcanics. Lithologies include impure quartzites, marbles, and felsic schists, and a large body of granitic orthogneiss, the Mt. Burnham orthogneiss (MBO). The metasedimentary rocks and metavolcanics of Assemblage II are somewhat older than the rocks of Assemblage I; the MBO yielded Late Devonian to Early Mississippian U-Pb zircon ages (363.8 ± 1.5 Ma).

Assemblage III

Assemblage III, at the lowest structural level, is comprised of metasedimentary rocks for which no ages are available. Rock types present in the assemblage include abundant carbonaceous phyllites and quartzites (Mortensen, 1990).

Deformation and Metamorphism

The rocks of Assemblages I, II, and III were pervasively deformed and metamorphosed under middle greenschist facies conditions (chlorite-biotite grade) across most of the area (F1). The age of the F1 event has been bracketed to between Middle Permian and Late Triassic (Mortensen, 1990), and may represent the approximate timing of the collision between YTT and the NACM (see above). In the southwestern Klondike, in the vicinity of the Mt. Burnham orthogneiss (Figure 1b), garnet and hornblende occur in metasediments of Assemblage II, indicating that slightly higher metamorphic grades were attained in this area during F1 (Mortensen, 1990; Metcalfe, 1981; this study).

Thrust Imbrication

Thrust imbrication of the Klondike (F2), which occurred at some time between Late Triassic and Middle Cretaceous times across YTT, dismembered the package of metamorphic rocks and was probably accompanied by the development of northeast verging folds, and a crenulation cleavage (Mortensen, 1990). Thrust deformation in the Klondike and eastern Alaska has been bracketed to between 190 to 180 Ma (J. Mortensen, pers. comm.), which is also the approximate maximum age for the onset of regional uplift. F2 deformation was also accompanied by retrogression of the F1 metamorphic mineral assemblage to lower greenschist facies (Mortensen et al., in press). Ultramafic rocks belonging to the SMT which are emplaced along the thrust faults appear not to have been affected by F1.

F1 Cooling Ages

Middle Jurassic to Early Cretaceous K-Ar and Rb-Sr ages for metamorphic muscovite and hornblende obtained from a number of locations, are interpreted as F1 cooling ages and indicate an extended cooling history with uplift during the Middle to Late Jurassic, and during the Early Cretaceous (Mortensen, 1990; Mortensen et al., in press). Cooling through the closure temperatures of biotite and muscovite ($\approx 300\text{-}350^\circ\text{C}$) occurred soon after thrust deformation (Middle Jurassic) in some parts of the Klondike; the oldest cooling ages occur in the southwestern portion of the Klondike region, indicating early, differential uplift of this part of the region (J. Mortensen, pers. comm.).

Cretaceous Thermal Event

Mortensen (1990) reports concordant U-Pb ages of 111 Ma, for monazite from the Mt. Burnham orthogneiss, indicating a relatively young, thermal overprint of the F1 assemblage in the southeast of the field area. Similar thermal overprints have been reported

from a number of locations in Yukon and Alaska (Mortensen, in press). The significance of this event is uncertain, but may have a bearing on the fluid inclusion study (see below).

Faulting

The available structural data for the Klondike region is, at best, patchy. Sparse outcrop, and a deep weathering profile (ca. 75 m deep locally (Mortensen, 1990)) have hindered attempts at detailed structural mapping. A number of steep faults have been mapped within the area, and appear to cut F2 thrust faults, although poor exposure across most of the Klondike precludes a meaningful interpretation of the overall structure (Mortensen, 1990; Debicki, 1984, 1985; this study). In addition, minor faulting has been seen to cut discordant veins in a number of locations.

III. HOST ROCK PETROGRAPHY

Principal Host Lithologies

Au-quartz veins are hosted by the most abundant lithologies within assemblages I and II: no veins were seen within lithologies belonging to Assemblage III during the course of the present study. Foliaform veins occur, to a greater or lesser degree, in rocks of all three Assemblages.

Discordant veins in the southeast Klondike occur within the micaceous and chloritic quartzite unit of Assemblage II, and also within the chloritic schist unit of Assemblage I (Figures 1b and 2). The same lithologies host veins in the central Klondike, in the vicinity of Hunker and King Solomon Domes. Along Sulphur Creek, and in the vicinity of the Violet and Virgin occurrences, the lodes are hosted by quartz-augen schists belonging to Assemblage I. In the Lone Star/27 Pup/Hilchey claim group, veining occurs within felsic and chloritic schists.

The intensity and type of wallrock alteration surrounding the veins (see below) is at least in part controlled by the host lithology: the more Fe-rich chloritic schists show a higher degree of carbonate alteration and pyritization (Mortensen et al., in press; this study). The petrography of the dominant discordant vein-host lithologies is described briefly below. For more detailed petrographic descriptions of the principal lithologies which outcrop within the area, the reader is referred to Metcalfe (1981) and Mortensen (1990).

Assemblage I Lithologies

Assemblage I is comprised predominantly of metavolcanic and meta-intrusive lithologies of Permian age. This Assemblage underlies the bulk of the field area. The quartz-augen schist, felsic schist and chloritic schist units of Assemblage I host the most important of the known vein occurrences.

Quartz-Augens Schist (QAS)

The QAS unit is an areally extensive unit which occurs in a southeast-northwest trending belt, running up the middle of the Assemblage I thrust sheet. Mortensen (1990) assigned a Permian age to this lithology. The rock may be weakly to strongly foliated, and locally has a distinctive cherty appearance. In hand specimen, the presence of chlorite imparts a greenish-grey coloration to the rock. F1 foliation is defined by muscovite and chlorite, with local development of an F2 crenulation.

A distinctive feature of this rock are abundant blue-grey, opalescent quartz augen, often up to 1 cm across (Plate 1a). They are generally rounded, but both Mortensen (1990) and Metcalfe (1986) report that they are often tectonically flattened. The presence of magmatic embayments on some of the least recrystallized quartz grains appears to reflect remnants of an original igneous texture (Mortensen, 1990; Metcalfe, 1986).

The groundmass is predominantly quartz with variable grain size, depending on the degree of cataclasis (Metcalfe, 1986). Subhedral feldspar grains with dusty sericitic inclusions are also present within the matrix, but their abundance is highly variable. Ferroan calcite is a common accessory mineral in most samples, and may comprise greater than 50 % of the rock in zones of wallrock alteration adjacent to discordant veins (Plates 2b and 2c).

Metcalfe (1986) presents 19 whole rock analyses of the QAS which indicate a calc-alkaline composition. On the basis of the whole-rock chemistry, the petrography and field relationships, Mortensen (1990) suggests that the unit is a deformed quartz-feldspar porphyry intrusive and the felsic schist (see below) its extrusive equivalent.

Chloritic Schist

Chloritic schists, and local amphibolites, occur over much of the southeast and central portion of the Assemblage I thrust sheet. They are the dominant host lithology to Au-quartz veins in the central Klondike (e.g., Hunker Dome, Lloyd, Mitchell). In outcrop

the chloritic schists are dark green in color and generally well foliated. In trenching on the Mitchell and Sheba claim groups, they have a distinctive brown weathering color caused by weathering of Fe-carbonate alteration within the schists.

Thin sections examined in this study were comprised primarily of quartz and chlorite (50-70 %) with subordinate plagioclase feldspar, muscovite, epidote and minor oxide minerals (Plate 2a). Epidote may make up 20-30 % of the rock at some locations. Adjacent to discordant veins, pyrite often comprises up to 40-50 % of the rock. Metcalfe (1981) and Mortensen (1990) also report that actinolite is a locally important constituent, but none was seen in the course of the present study.

The primary foliation is generally defined by chlorite and muscovite, with parallel bands of granoblastic quartz \pm feldspar (An₆₋₃₄, Metcalfe, 1981). Development of crenulation fabrics is common. Carbonate is commonly seen in the groundmass and also infilling late fractures which cut foliation.

The chloritic schists have a similar Permian age to the QAS described above, but are mafic to intermediate in composition (Mortensen, 1990). Mortensen (1990) describes a close association between the chloritic schist and bodies of metagabbro which often show well preserved igneous textures. On the basis of this association and the compositional data, he suggests an igneous derivation for the schists, from mafic or intermediate volcanics with associated subvolcanic, gabbroic intrusives.

Felsic Schist

Patches of felsic schist occur throughout Assemblages I, sometimes apparently intimately folded with the QAS, and also sporadically within Assemblage II. Mapping by Mortensen (1990) suggests that the felsic schists overlie the quartz-augen- and chloritic-schists. In outcrop they are silvery-grey to brown (Fe-stained) in color, and are strongly foliated. A strong crenulation cleavage is often developed. Chlorite locally imparts a

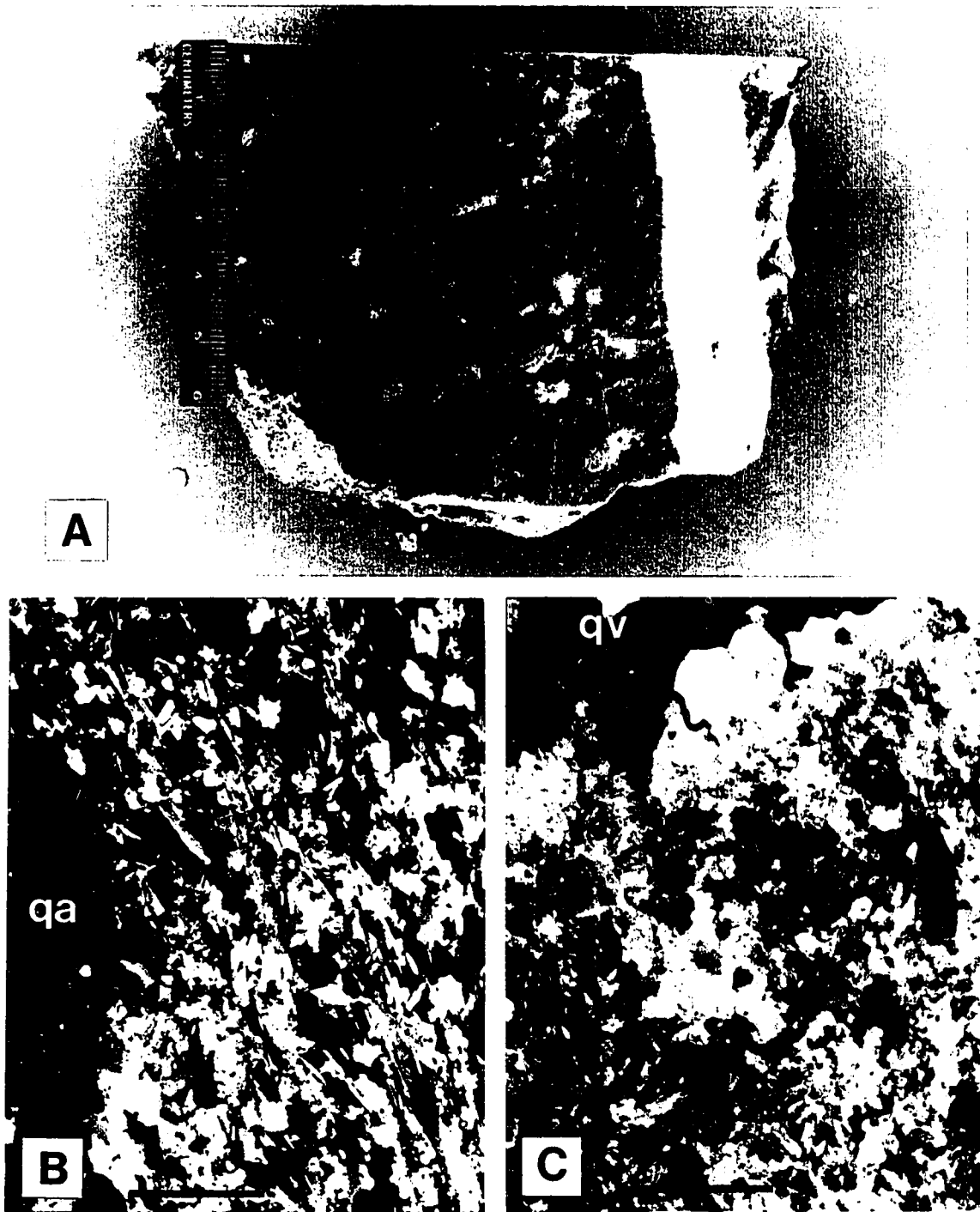


Plate 1. A. Quartz-augen schist (QAS) cut by discordant quartz-carbonate vein. Note blue-grey quartz-feldspar augen, and yellow-green carbonate alteration around vein. B. Photomicrograph of unaltered QAS (crossed polars). Large quartz augen (qa) in groundmass of quartz, untwinned feldspar and muscovite, with $\approx 10\%$ carbonate. C. Photomicrograph (crossed polars) illustrating carbonate flooding of QAS adjacent to discordant vein (qv) shown in Plate 1A (scale bar 0.5 mm for both plates).

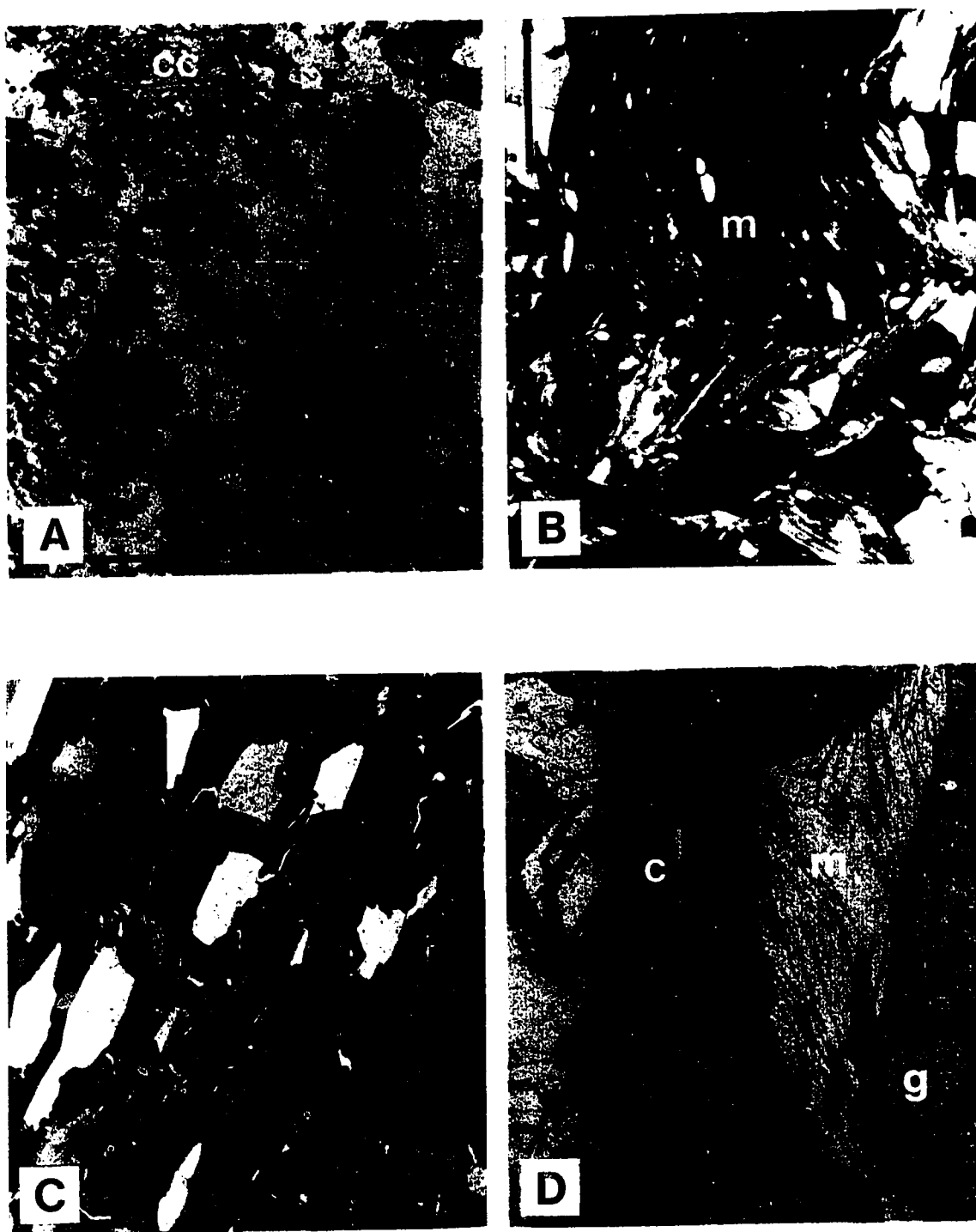


Plate 2. Photomicrographs of, A. Chloritic schist with calcite (cc), in plane polarized light (ppl); B. Felsic schist, under crossed polars (xpl), showing crenulation cleavage defined by muscovite (m), in quartz groundmass; C. Micaceous quartzite (xpl); D. Garnet-muscovite schist (ppl) showing retrograde chlorite (c) growth on muscovite (m) and garnet (g). See text for full descriptions. Scale bar 0.5 mm for all plates.

greenish tint to the coloration. The schists consist almost entirely of granoblastic quartz and lepidoblastic, variably chloritised muscovite, with local feldspar (Plate 2b).

Stratiform pyrite mineralization is common within the felsic schist (J. Mortensen, pers.comm.; this study). In the sulfide-rich zones, disseminated pyrite can comprise up to 20-30 % of the rock, and when weathered it gives the rock a distinctive yellow-brown coloration. No other sulfide minerals were seen within the pyrite-rich zones.

Mortensen (1990) considers the felsic schist to be a metamorphosed felsic tuff, probably the extrusive equivalent of the QAS. In addition, the presence of stratiform sulfide mineralization implies deposition in a submarine environment.

Sulphur Creek Orthogneiss (SCO)

The SCO is exposed along the southwestern margin of Assemblage I, and is truncated by the major thrust fault mapped by Mortensen (1990). It is a large intrusive body of quartz-monzonitic orthogneiss. No samples were available for thin section examination. Mortensen (1990) considers it to be comagmatic with the quartz-augen-schists described previously.

Assemblage II Lithologies

Rocks belonging to assemblage II are comprised of interlayered metasedimentary units and mafic and felsic volcanics of Devonian to Mississippian age or older (Mortensen, 1990). Lithologies include marbles and calc-silicates, micaceous and feldspathic quartzites, chloritic quartzites and garnet-mica schists. The extensive felsic schist and quartzitic units, although lithologically similar to felsic schists and quartzites exposed within Assemblage I, are probably of different ages (Mortensen, 1990). Discordant vein occurrences along Dominion Creek are hosted by rocks belonging to Assemblage II.

Micaceous Quartzites

Micaceous quartzites occur in Assemblages I and II. They generally have a granoblastic quartz groundmass, with locally variable grain size, and scattered anhedral crystals of plagioclase which are sericitized to varying degrees. Grain boundaries between quartz crystals are often sutured. F1 foliation is defined by lepidoblastic muscovite (Plate 2c), and increasingly towards the southeast of the field area, by biotite. Muscovite is usually less altered than biotite, which is often replaced by chlorite. One sample of quartzite contained subhedral, poikiloblastic garnets up to 4-5 mm in size.

Calc-Silicate Rocks

Quartz-calcite rocks from outcrops on Dominion Creek, are composed of layers of granoblastic calcite crystals interbanded with finer-grained quartz-rich layers, probably reflecting the original sedimentary layering. A poorly developed foliation is defined by biotite (phlogopite?) mica, locally retrograded to chlorite. Scattered throughout the sample are poikiloblastic clinozoisite crystals which show anomalous deep blue interference colors.

Garnet-Mica Schists

These rocks occur on Lower Dominion Creek. In hand specimen, the garnet-mica schists are moderately to well foliated, grey-green in color, with abundant sub-to euhedral garnets up to 7 mm across. Green bunches of chlorite up to 5 mm across are also visible in hand specimen. In thin section, primary F1 biotite, and retrograde chlorite (after biotite), define the foliation. Chlorite is also seen replacing garnet (Plate 2d). The matrix consists of equigranular quartz with abundant, untwinned, variably sericitized plagioclase. The garnet-biotite assemblage has also been described in metasediments from the southwestern part of the field area, along the Indian River (Mortensen, 1990).

Mount Burnham Orthogneiss (MBO)

A prominent feature of assemblage II, is the Mt. Burnham orthogneiss complex, which outcrops in the far southeast of the field area (Figure 1b). Due to problems with access, no samples were available from the complex for examination. However, Mortensen (1990) notes that it is granitic in composition with K-feldspar augen up to 8 cm across, in a groundmass of coarsely crystalline biotite, muscovite, quartz and feldspar. Garnet and tourmaline occur locally.

Assemblage III Lithologies

Rocks belonging to Assemblage III do not appear to host significant Au-quartz mineralization. Mortensen (1990) notes that Assemblage III lithologies are locally very similar to those of Assemblage II, with quartzites, chloritic schists and marble/calc-silicate lithologies common. However, the age of these lithologies is unknown. Dark- to medium-grey, carbonaceous quartzites are locally abundant in the northeastern portion of the field area (Figure 1b).

Serpentinite Lenses

Serpentinite occurs as lenses and slivers along thrust faults in the Hunker Dome area, and throughout the Klondike region. A single sample described by Metcalfe (1981) was comprised predominantly of variably sheared antigorite with subordinate chrysotile and Fe-oxides. Although no Au-quartz veining has been described from within serpentinite lenses, Mortensen et al. (in press) note that carbonate-rich veins occur within carbonate-altered serpentinite (listwanite) along lower Hunker Creek.

IV. GEOLOGY OF THE QUARTZ VEINS

Until recently, four distinct types of quartz vein were recognized in the Klondike region (Mortensen et al., in press; Friedrich and Hoymann, 1989; Dufresne, 1987):

- 1) Mesothermal quartz veins: these occur within the schists of Assemblages I, II, and III (e.g., Lone Star, Gold Run).
- 2) Quartz-carbonate veins in greenstones and ultramafic rocks (e.g., Ben Levy).
- 3) Epithermal quartz-chalcedony veining hosted by Eocene(?) igneous and sedimentary rocks (e.g., Germaine Creek).
- 4) Low temperature epithermal veins and associated alteration, presumed to be Pliocene to Pleistocene in age, within the White Channel Gravels (Dufresne, 1987).

However, in addition to the above, a fifth geochemically distinct (see below) type of quartz has recently been recognised:

- 5) Amethyst of unknown age, lining vugs and cementing brecciated mesothermal quartz veining in the Hunker Dome area, recognised by Mortensen (pers. comm.).

The current study examines the mesothermal veins in greater detail, although stable isotope analyses were also carried out on 4 samples of ultramafic hosted carbonate veins, and 2 of Eocene epithermal carbonate from Germaine Creek, by way of preliminary investigation of this mineralization.

Of the 5 styles of veining described above, types 1, 3 and 4 are known to be associated with anomalous precious metal enrichment. Gold mineralization associated with the mesothermal veins is described in detail below. Mineralization associated with the White Channel gravels was described by Dufresne (1987) and will not be considered further, here.

Eocene Epithermal Mineralization

The Germaine Creek epithermal prospect occurs in Eocene quartz-feldspar intrusives, felsic tuffs, and clastic sediments which crop out in the northeastern portion of the field area, adjacent to the Tintina trench (Figure 1b). Mortensen et al. (in press) describe quartz and chalcedony veining which is associated with pronounced alteration, and anomalous levels of As, Hg, Sb and Tl (Ballantyne, pers. comm. *in* Mortensen et al., in press). Au enrichment is present, but rare.

Preliminary work has suggested that the Germaine Creek mineralization is of a style similar to other epithermal systems in Yukon and the Cordillera, for example the Grew Creek deposit, near Faro, Yukon (see Christie et al., in press).

Mesothermal Quartz Veins

Quartz veining is a common feature of regional metamorphic terranes, particularly in greenschist facies rocks (Kyser and Kerrich, 1990). Two styles of mesothermal vein have been described from the Klondike region (e.g., McConnell, 1905; Mortensen et al., in press):

Foliaform Veins

Foliaform veins are ubiquitous in metamorphic rocks belonging to all three lithological assemblages. They are lensoid, discontinuous quartz veins which generally occur parallel to F1 foliation planes in the schists (Plate 3a). Foliaform veins resemble typical metamorphic "segregation" veins (e.g., Yardley, 1975; Fyfe et al., 1978), and comprise up to 10 % by volume of the rock mass locally (Mortensen et al., in press). They are often mineralogically similar to their host rocks, and are barren of gold mineralization.

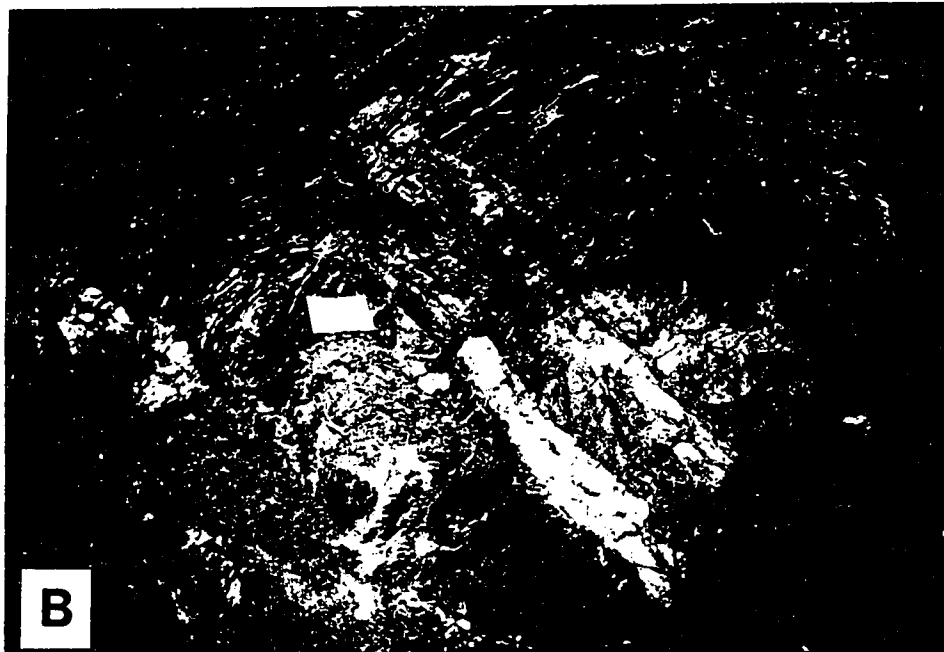
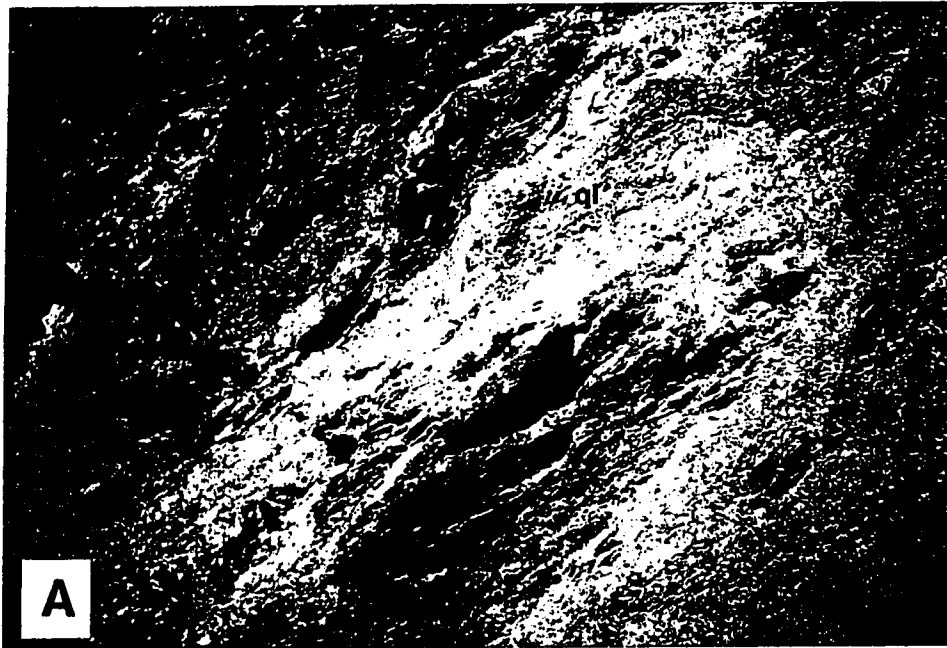


Plate 3. A. Foliaform quartz lenses (ql) in altered quartz-muscovite schist from the Esperanza prospect (see Fig. 2). Head for scale; B. Au-bearing mesothermal quartz veins, discordant to foliation, at the French Gulch showing (see Fig. 2). Note intense Fe-staining on, and adjacent to, vein margins.

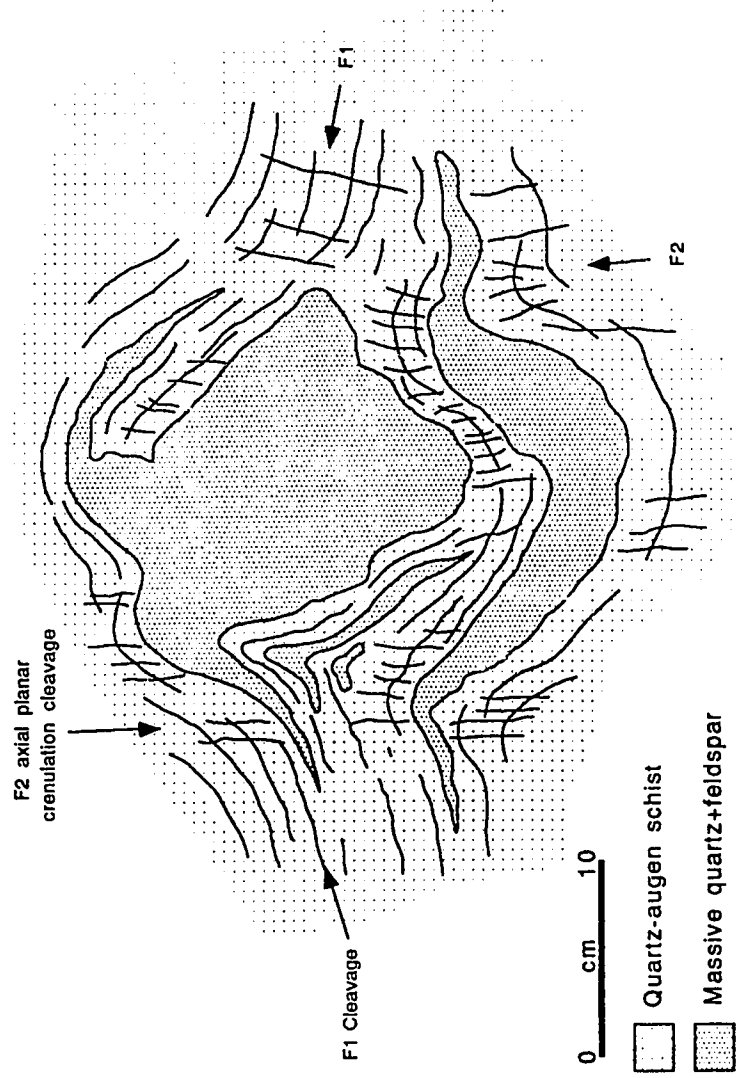


Figure 4. Field sketch of a foliaform quartz+K-feldspar vein occupying an F2 fold hinge in quartz-augen schists, near California Gulch, Lower Bonanza Creek.

Discordant Quartz Veins

In addition to the foliaform veins described above, numerous massive, milky quartz veins up to 2-3 m thick and often hundreds of meters in strike length, are exposed within the Klondike region (Plates 3b and 4a). These veins generally cross-cut the metamorphic foliation and occur sporadically throughout Assemblage I, and locally within Assemblages II and III (Figure 2). A number of the discordant veins have been found to contain significant Au mineralization, although Au is not a ubiquitous feature of the veins. In the past, a number of mining operations have attempted to exploit some of the richer discordant veins, for example the Lone Star and Violet mines, described by Maclean (1914).

Age and Structure of Mesothermal Au-Quartz Veins

The distribution of the most important known mesothermal Au-quartz vein occurrences are shown in Figure 2. Au-bearing discordant veins are essentially confined to the Assemblage I thrust sheet, with sporadic occurrences in Assemblage II, where it outcrops in the southeast of the field area. The abundance of veining decreases rapidly to the north of the Klondike River, and Au-bearing veins are unknown from this part of the region (Mortensen et al., in press).

On the basis of structural style and field relationships, the Au-bearing discordant quartz veins appear to be younger than the foliaform variety. Foliaform veins occur parallel to F1 foliation planes, and are sometimes found occupying F2 fold hinges (Figure 4). However, they appear to be essentially unaffected by the F2 deformation, suggesting a late- or post-F2 formation age. Mortensen (1990) notes that F2 deformation was probably syn-thrust faulting (ca. 190-180 Ma, J. Mortensen, pers. comm.), which is therefore taken as the maximum age of formation of the foliaform veins.

Discordant veins can be seen cutting foliaform veins at a number of localities. For example, at the Lone Star mine a discordant vein was seen cross-cutting, and slightly off-setting a foliaform vein. Also, Plate 4b shows a minor discordant quartz vein clearly cutting

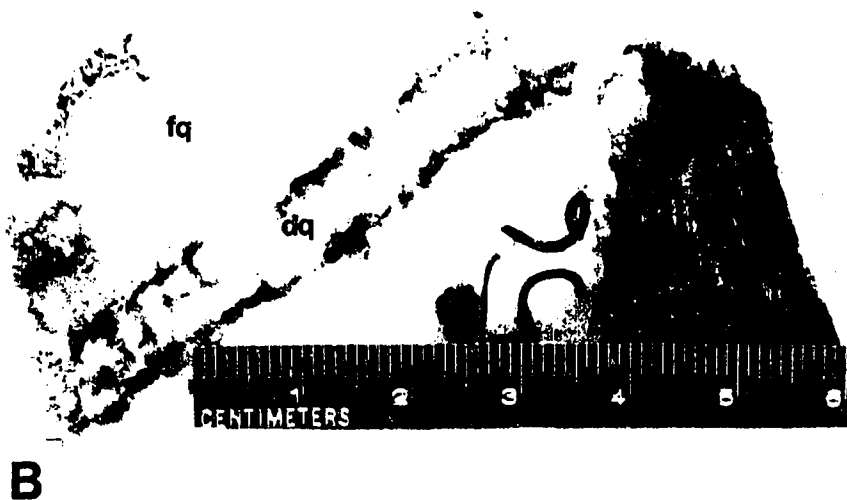


Plate 4. A. The Sheba vein (see Fig. 2): Massive, discordant, Au-bearing quartz vein cutting chloritic schists. Note host-rock foliation dipping towards the left of the photograph, and green Cu-staining from sulfide mineralization (see text). Hammer (arrowed) for scale; B. Minor discordant vein (dq) cutting foliaform quartz vein (fq). Note brown weathered Fe-carbonate along discordant vein margins.

across a foliaform vein. In apparent contradiction of these observations, Mortensen et al. (in press) report the occurrence of foliaform veins which appear to merge with discordant veins in outcrop, suggesting that there may be an overlap in the age of formation of the two types of vein.

Recently however, Early Cretaceous K-Ar ages of between 140.1 ± 2.0 and 134.5 ± 1.5 Ma, have been obtained for two samples of hydrothermal muscovite collected from Au-bearing discordant quartz veins at the Sheba prospect (Mortensen, in press). These ages are believed to represent the age of mineralization, implying that the discordant veins are significantly younger than the foliaform variety. The Early Cretaceous ages indicate that discordant vein formation occurred during late post-metamorphic cooling and uplift (Mortensen, in press).

It is noteworthy that similar Early Cretaceous formation ages have been reported for at least two other Cordilleran mesothermal Au-quartz vein systems. Sketchly et al. (1986) obtained an age of 131 ± 5 Ma for hydrothermal micas in wall-rock alteration associated with mesothermal lode-gold mineralization at the Erickson Mine, Cassiar, in British Columbia. Alldrick (1982) reports K/Ar ages of 139 ± 5 and 141 ± 5 Ma for sericite collected from mineralized quartz veins at the Mosquito Creek and Cariboo Gold Quartz mines, respectively.

Au-Quartz Vein Structure

The Au-quartz veins appear to be hosted by moderately to steeply dipping, brittle, extensional structures (Mortensen et al., in press). The vertical extent of individual veins is unknown, although the results of the fluid inclusion study suggest that the vertical extent of the regional vein system may have been on the order of several kilometres (see below). Laterally, the veins are generally only tens, to a few hundreds, of meters in length at most, and usually pinch out quite rapidly, implying that the host structures were fairly minor faults.

In the southeast and central parts of the Klondike, Au-quartz veins occur in both the hangingwall and footwall of the regional thrust faults (Figures 2, 5 and 6), and almost invariably occur within a few hundreds of meters of a thrust fault. This relationship is illustrated on a smaller scale by trench mapping in the Hunker Dome area, where discordant veins occur in the footwall and hanging wall of a splay from the main thrust fault, and strike roughly parallel to the trace of the thrust (Figures 5 and 6).

Discordant Au-quartz veins in the southeast and central parts of the Klondike are steeply dipping and generally trend roughly northwest-southeast or north-south. In the Hunker Dome area, the Mitchell, Sheba and Hunker Dome vein sets constitute a poorly defined, north-south trending, left-stepping en echelon array (Mortensen et al., in press; J. Mortensen, pers. comm.). In the northwest Klondike, Au-bearing veins trend between east-west, to roughly north-south, with variable dip.

Northwest of the central Klondike, with the exception of the Virgin lode, the association of Au-quartz veining with thrust faults is not apparent (Figures 1 and 5). Similarly, the relationship between the structures which host Au-quartz veins, and F3 folds -which are developed across the entire Klondike region (Mortensen, 1990)- is unknown.

A number of workers have commented on the possible existence of steep faults or lineaments along some of the Klondike creeks (e.g., Milner, 1977; Debicki, 1984). However, Mortensen (1990) notes that displacement along the faults/lineaments, if they in fact exist, must be minor because there is no apparent offset across them. The relationship between these postulated structures and the Au-quartz lodes is unknown.

Au-Quartz Vein Geology

Gangue Mineralogy

The mineralogy of the Au-bearing veins has been described in detail by Friedrich and Hoymann (1989), and Mortensen et al., (in press). The vein mineralogy is remarkably simple: most veins consist almost entirely (ca. >95 %) of milky-white, massive, anhedral,

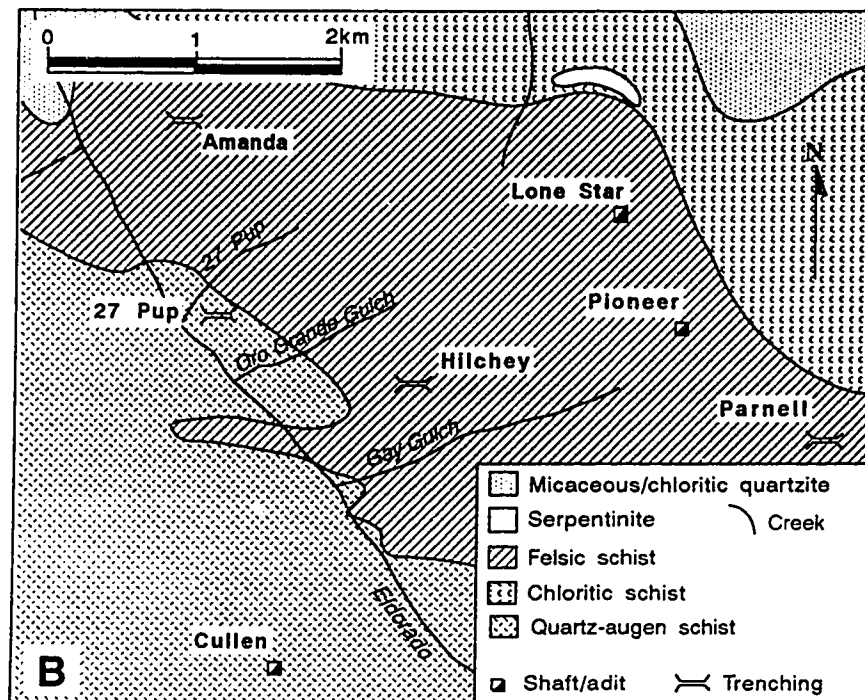
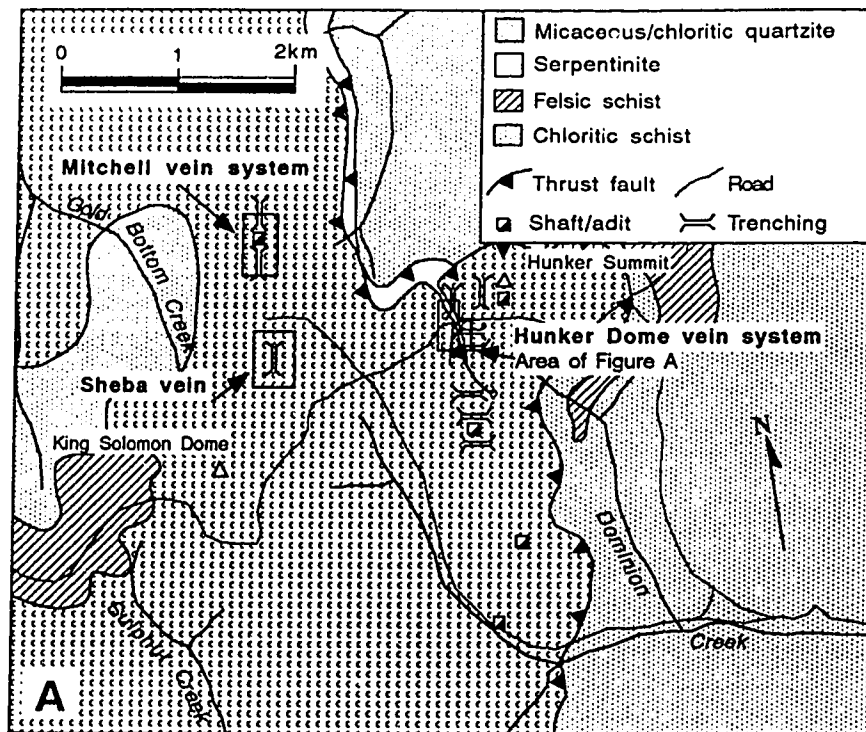


Figure 5. Geology of A. the Hunker Dome and, B. Lone Star areas, with Au-quartz vein locations. Modified after Mortensen (1990).

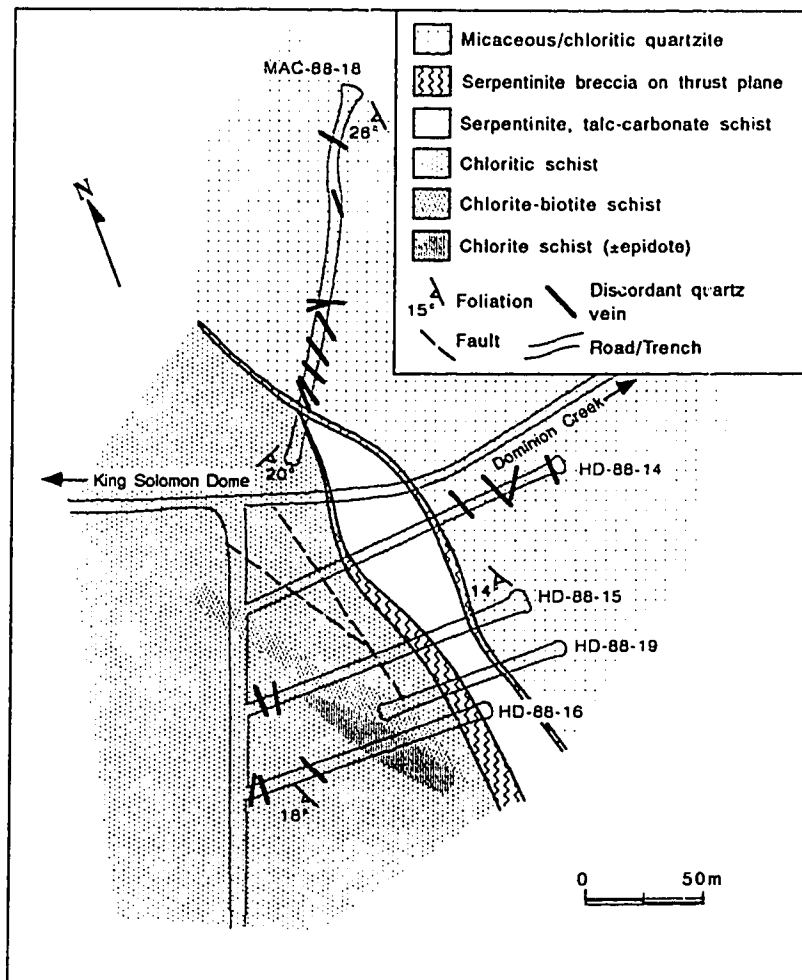


Figure 6. Geological sketch map of exploration trenches in the Hunker Dome area, showing relationship between discordant quartz veining and a possible splay from the major thrust fault (see Figure 5).

quartz with local vugs lined by euhedral quartz crystals. Ribbon textures and banding within discordant veins are rare, suggesting that most of the veins are the product of a single-stage mineralizing event (Mortensen et al., in press). Banding was seen in one float sample from the Mitchell vein, and ribbon textured quartz has been reported from the Aime and Hunker Dome occurrences (Mortensen et al., in press). In addition, infill breccia textures, in which the main component of the breccia matrix is a later phase (Dowling and Morison, 1989), have been seen in hand samples of discordant vein quartz from the Hunker Dome area (see below). Angular inclusions of wall-rock material are present in the Sheba, Lloyd and Gold Run veins. Minor development of stylolites has been reported from adjacent to some vein margins (Mortensen et al., in press).

In addition to quartz, the most common gangue phases are calcite/ferroan carbonate, barite, and mica with rare rutile and feldspar (Mortensen et al., in press; this study). Coarse grained, subhedral, white barite is abundant in samples of vein float material from the Violet shaft dump (Plate 5a) and has also been reported from the Virgin and Parnell veins (Mortensen et al., in press; this study). Scheelite has been recovered from numerous placer deposits in the Klondike and is believed to have been derived from mesothermal veins, but has not been seen in situ (J. Mortensen, pers. comm.).

White muscovite occurs in most discordant veins, usually as thin selvages along late fractures, and within thin brecciated bands cutting gangue quartz (Plate 5b). In thin-section muscovite is also commonly seen within crystals of vein quartz, suggesting that at least some mica is primary, and may be coeval with gold mineralization (see below). Mortensen (pers. comm.) also reports hydrothermal muscovite occurring with galena in a thin band from the centre of a minor, discordant vein from the Sheba prospect (see below). K-Ar ages for this muscovite are reported above.

Late stage amethyst occurs as large (ca. 2-3 cm), euhedral crystals lining vugs in a discordant vein from the Hunker Dome area, and also cementing fragments of milky quartz



Plate 5. A. White barite (ba) and quartz (q) in sample of mesothermal vein material from the Violet mine dump (see Fig. 2); B. Photomicrograph (xpl) of a zone of quartz brecciation in a discordant quartz vein from Hunker Dome, showing introduction of late muscovite (m) and pyrite (py) along the zone. Scale bar is 0.5 mm.

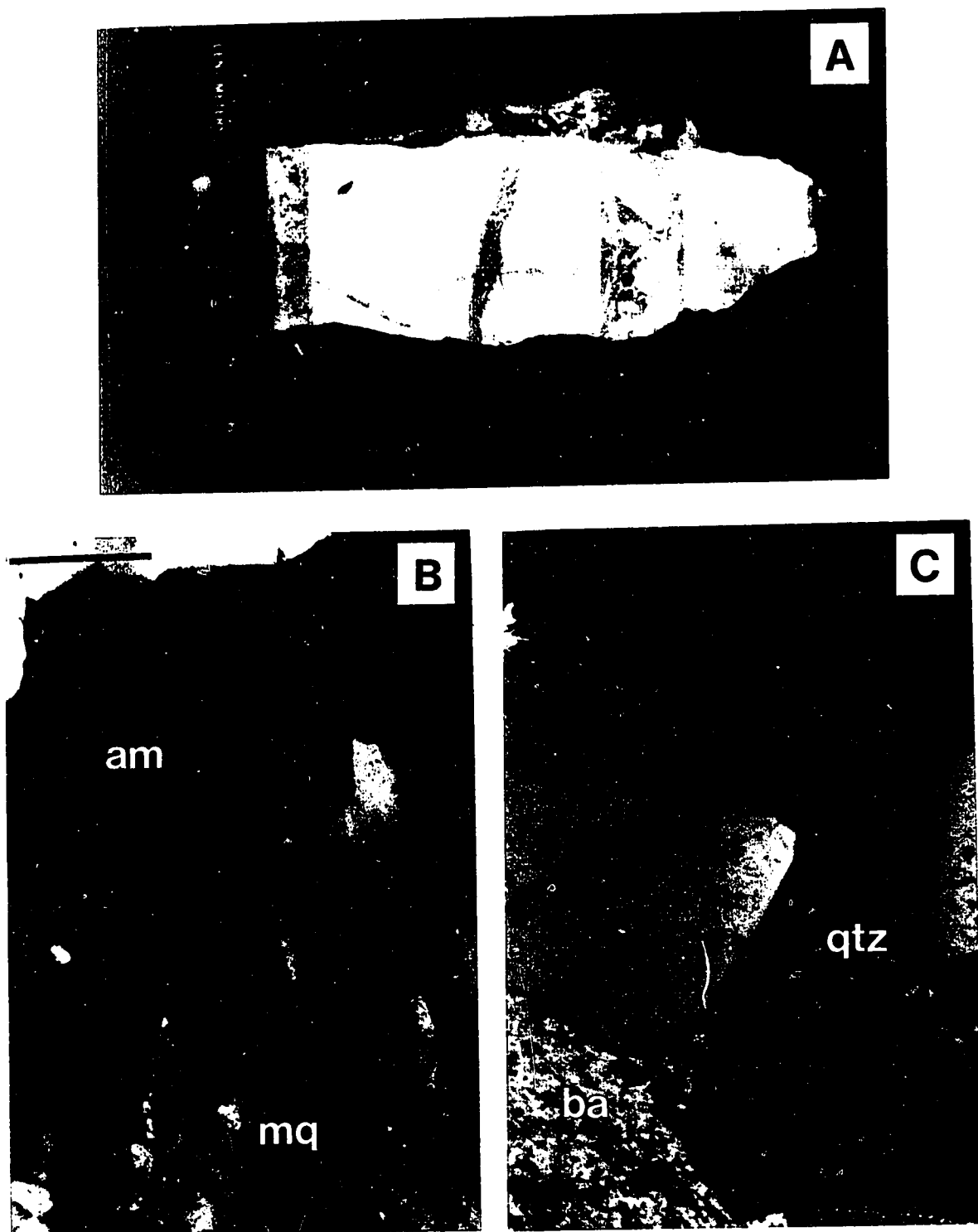


Plate 6. A. Late quartz/amethyst cementing brecciated mesothermal quartz vein from Hunker Dome. B. Relatively fluid inclusion-free, unstrained amethyst (am) on strained, inclusion-rich, mesothermal quartz (mq) showing undulose extinction. C. Barite (ba) and euhedral quartz (qtz) from vein margin of discordant vein from the Virgin prospect (see Fig. 2). Scale bar for both photomicrographs is 0.5 mm.

in a brecciated vein from the same area (Figure 7, Plate 6a). Although the amethyst is clearly younger than the milky vein quartz, the exact timing of its introduction is uncertain.

In thin section, Au-vein quartz is predominantly anhedral, with some elongation of crystals perpendicular to vein margins. Crystal size is highly variable, and ranges from a few millimetres to 3 to 4 cm or greater. Abundant trails of secondary and pseudosecondary fluid inclusions can be seen along healed fractures, and many samples are cut by anastomosing networks of brown, iron-stained cracks. Quartz typically displays low to moderate degrees of strain: undulose extinction is seen in most samples of vein quartz (Plate 6b) and grain boundaries between adjacent crystals are often highly sutured. Development of subgrains is common. Large anhedral quartz crystals are locally cut by thin anastomosing zones/veinlets of finer grained, relatively unstrained quartz, similar in appearance to the "spider veinlets" described by Dowling and Morrison (1989). Also, bands of minor brecciation and/or cataclasis, often marked by significant grain size reduction, can be seen within some samples (Plate 5b). Introduction of pyrite, white mica and carbonate has occurred along some of these fractured zones. With the exception of brecciated or vuggy veins, it was not possible to distinguish multiple generations of quartz within the discordant veins.

Carbonate occurs as large anhedral crystals apparently coeval with most quartz, or infilling late fractures and cracks within quartz. Barite was seen in thin sections of vein samples from the Virgin, Violet and Parnell lodes (Plate 6c). Two generations of barite may be present in some samples; an early phase developed against the vein margins, and a second phase in the centre of the vein.

One sample of amethyst-matrix breccia was examined in thin section. Veinlets of unstrained comb-textured/euhedral to anhedral amethyst infill fractures within strained, mesothermal quartz (Plate 6b). The amethyst is notably fluid inclusion-free in comparison to the cloudy, host quartz, although large primary inclusions were found in all samples. In

places, angular clasts of the host material are totally enclosed by, and in apparent optical continuity with, the amethyst.

Gold and Sulfide Mineralization

Most Au-quartz veins contain only trace amounts of sulfide mineralization, in the form of scattered crystals of pyrite and galena. Pyrite is found disseminated within vein quartz, as trails of crystals along late stage fractures (Plate 5b), and also as selvages and disseminations within, or adjacent to, the vein wallrocks (see below). It is commonly weathered to rusty brown limonite, which may contain very high (supergene?) gold grades (Plate 7a). In places, Au-bearing vein mineralization may be nothing more than pyritic/limonitic planes or fractures which cross-cut metamorphic foliation. Galena occurs as small (<1 cm), disseminated crystals within the veins (Mortensen et al., in press).

The Sheba vein is a notable exception to the majority of the sulfide-poor veins (Plate 4a). Massive sulfide aggregates, up to 20 to 30 cm across, occur throughout the Sheba vein. Also, Maclean (1914) reports that sulfide aggregates found underground in the Lone Star mine yielded particularly high Au grades. Detailed paragenetic studies of the Sheba, Mitchell and Hunker veins have identified a number of sulfide minerals including arsenopyrite, chalcopyrite, sphalerite, freibergite, pyrargite and galena (Friedrich and Hoymann, 1989). Their paragenetic scheme, slightly modified, is shown in Figure 7.

Gold has been reported from all of the principal discordant vein locations which were examined in this study (J. Mortensen, pers. comm.; J. Knight, pers. comm.; Friedrich and Hoymann, 1989; Maclean, 1914; Debicki, 1984, 1985; this study). It occurs in a number of forms within the lodes, but is most commonly associated with pyrite, or in limonitic pseudomorphs after pyrite. Visible gold, unassociated with sulfides, has been seen in hand samples occurring along late fractures within quartz.

Although gold is paragenetically coeval with quartz, pyrite, pyrrhotite and chalcopyrite, Friedrich and Hoymann (1989) note that in the Hunker Dome lode, a second

<i>Ore/Gangue Phase</i>	<i>Main Stage</i>	<i>Late Stage</i>	<i>Post</i>
Quartz	—————	—————	
Carbonate	—————	? —————	
Barite	—————	— — — ?	
Muscovite	—————	? —————	
Arsenopyrite	———		
Pyrite	—————	—————	
Pyrrhotite	———		
Chalcopyrite	———		
Gold	—————	? —————	
Sphalerite	———	———	
Freibergite	———	———	
Galena	? — — —	————— ?	
Limonite			—————
Amethyst		? —————	————— ?

Figure 7. Generalized paragenetic sequence for Au-bearing, discordant quartz veins at the Mitchell, Sheba and Hunker Dome lode occurrences. Modified from Friedrich and Hoymann (1989).

stage of gold mineralization occurred after most quartz had formed (Figure 7). This is in agreement with the observation that some visible gold occurs along late fractures, and has implications for the fluid inclusion study; fluids trapped within inclusions which are primary with respect to the main phase of Au-quartz mineralization may not necessarily be chemically representative of the fluids responsible for late-stage mineralization.

Gold grades within limonitic material are often extremely high, probably as a result of supergene enrichment, and visible gold is common. Mortensen et al., (in press) note a possible empirical correlation between the gold and pyrite/sulfide content of the Klondike veins.

Gold Morphology and Fineness

The fineness of gold from the Klondike placers and bedrock-lodes has been studied by Knight et al., (in prep.) and Friedrich and Hoymann (1989). Discordant lode gold fineness ranges from approximately 500 to 900. Friedrich and Hoymann (1989) report microprobe analyses of gold from the Hunker Dome lode which range from between 75 to 87 % Au, approximately 13 to 22 % Ag, with traces of Bi, Te, Hg, Cu and S. Additionally, geographical trends can be seen within the data, which appear to correlate with fluid P-T-X trends which are apparent in the results of the fluid inclusion study; gold-fineness decreases towards the northern part of the Klondike (J. Mortensen, pers. comm.).

Morphologically, all of the gold seen in the present study was either irregular in shape or sheet-like/flaky. However, occurrences of crystalline gold within the Lone Star lode and other veins have been reported (McConnell, 1905). Also, octahedral and dendritic crystalline gold is commonly found by placer miners in the area, although whether these are primary lode-derived textures, or form as a result of supergene processes, is unsure.

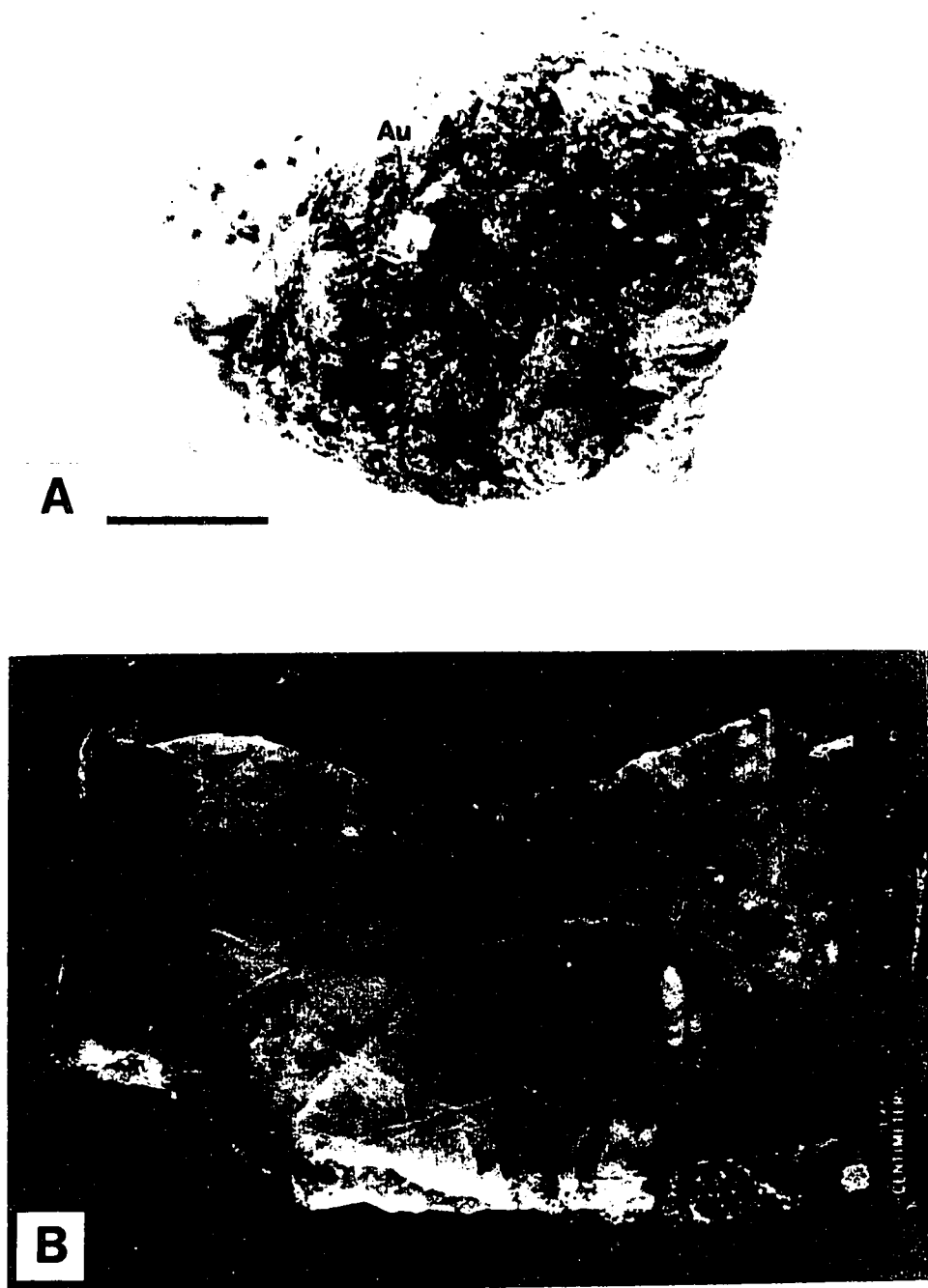


Plate 7. A. Visible Au (Au) on limonite (after pyrite) in oxidized vein margin material from the 27 Pup vein (see Fig. 2). Scale bar is 1 cm; B. Foliaform quartz+ K-feldspar (K) vein, hosted by the Sulphur Creek orthogneiss, on Sulphur Creek.

Wallrock Alteration

The styles of wallrock alteration seen in rocks adjacent to the Klondike veins are typical of alteration zones observed around other Cordilleran and Archean mesothermal lodes (e.g., Nesbitt et al., 1986; Phillips and Groves, 1983). Pyritization and carbonate-flooding of the wall rocks are the most common hydrothermal alteration types seen around the discordant lodes. The degree of alteration is partly dependent on the nature of the vein host rock; the more Fe-rich, chloritic schists tend to show more intense carbonate alteration than veins hosted by felsic units (Mortensen et al., in press; this study); quartz-augen schists and felsic schists commonly display little or no alteration other than slight pyritization.

Carbonate Flooding

Immediately adjacent to veins in the Hunker Dome and Mitchell claim groups, the chloritic schists often appear rusty brown in color. This coloration, which is due to ferroan-carbonate flooding, may extend up to 2-3 m into the wallrocks. Carbonate is also found along late fractures in discordant vein quartz. The effects of carbonatization are illustrated in Plates 1b and 1c. Plate 1b is unaltered quartz-augen schist from Sulphur Creek which contains only trace amounts of carbonate. In contrast, quartz-augen schist collected from the wall rock of a minor discordant vein on Sulphur Creek is stained yellow-green by ferroan calcite in hand sample (Plate 1a), and in thin section (Plate 1b), greater than 50 % of the rock is comprised of carbonate, which can also be seen replacing lepidoblastic muscovite.

Pyritization

Pyritization is seen adjacent to many of the veins. Pyrite may comprise up to 40% by volume of the rock locally (Mortensen et al., in press). In hand specimen, cubes and aggregates of pyrite, and limonitic pseudomorphs after pyrite, occur scattered throughout

the wallrocks within 2-3 cm of the veins. Locally, high-grade selvages of limonite (presumably after pyrite) up to 5 cm thick occur on the margins of some veins (Plates 3b and 7a) (e.g., 27 Pup, French Gulch).

Pyritization is most obviously developed in the more Fe-rich chloritic schists. Mortensen et al. (in press) report pyrite pseudomorphs after magnetite porphyroblasts in chloritic schists from the Mitchell vein. It is interesting to note that the most intense pyritic alteration, which is seen in the wallrocks of veins from the Mitchell and Sheba prospects, also corresponds to the most sulfide-rich of the known Klondike lodes.

Foliaform Vein Geology

Foliaform veins comprise up to 10 % by volume of the rock mass locally (Mortensen et al., in press). Although they are generally only between 5-20 cm thick, they may be as much as 3 m thick at some localities, for example the Cullen claim, near the Violet shaft.

The mineralogy of the foliaform veins is simple, and often reflects the dominant mineralogy of the host rock type. The veins consist primarily of quartz with common calcic and/or ferroan carbonate. K-feldspar is found in foliaform veins hosted by orthogneiss, for example along lower Sulphur Creek (Plate 7b) (Mortensen et al., in press). Sulfides are absent to rare: pyrite may occur in foliaform veins hosted by pyritic quartz augen schist, and galena was found in a single foliaform vein collected from the Plinc claim group (J. Mortensen, pers. comm.).

In hand sample, foliaform vein quartz varies in texture and appearance from clear and glassy, to massive milky quartz, and locally, sugary textured quartz. No wall-rock alteration was found associated with any foliaform veins. However, the immediate wall rocks to some veins do show a marked depletion in quartz, and an increase in the proportion of phyllosilicates relative to the bulk mineralogy of the rock mass, a

phenomenon also noted by Yardley (1975) in a study of lensoid veins in metamorphic rocks from the Connemara area in Ireland (see below).

In thin section, foliaform vein quartz is commonly highly strained and exhibits strong undulose extinction and sutured grain boundaries. Primary fluid inclusions are relatively rare in comparison to discordant vein quartz, and the microthermometric data reported for foliaform vein quartz in Chapter V contain a much higher proportion of secondary fluid inclusion analyses than the Au-quartz vein data.

Although gold has not been found in any of the foliaform veins, numerous adits and trenches were sited on the larger veins, which were presumably mistaken for Au-bearing discordant veins.

V. FLUID INCLUSION STUDY

Introduction

A fluid inclusion study of the Klondike veins (foliaform and Au-bearing) was undertaken in order to define the P-V-T-X state of the vein forming fluids, and to describe any regional variations in the fluid geochemistry and P-T conditions at the time of entrapment. Over 600 fluid inclusions were examined in approximately 160 doubly-polished quartz wafers; 100 chips from Au-quartz vein material and 60 from foliaform vein samples. Microthermometric analyses were carried out on a modified USGS gas-flow heating-freezing stage calibrated using liquid nitrogen, natural pure-CO₂ inclusions in Alpine vein quartz, a distilled water-ice bath, and Merck standards. Standard errors are $\pm 0.2^{\circ}\text{C}$ for freezing and $\pm 2^{\circ}\text{C}$ for heating to 300°C .

Selection of Material

Au-quartz vein material, collected from exploration trenches and adit dumps, consists of massive, milky, unbanded quartz with minor sulfide and gold mineralization (see above). Fields of relatively large (10-30 μm) primary inclusions were found in most samples of discordant vein quartz (Plate 8). Euhedral quartz crystals from vugs yielded particularly high quality material. In one sample from the Gold Run showing, fluid inclusions of analytical quality were found within a few hundred microns of gold or sulfide mineralization; however, in general it was not possible to establish with certainty whether particular inclusions were related to mineralization. In addition, the massive, unbanded, anhedral nature of most of the quartz precluded unequivocal identification of multiple generations, or relative ages, of primary inclusions related to incremental vein growth or crystal growth zones.

Despite these problems, studies of discordant vein paragenesis in the Hunker Dome area indicate that in at least one Au-bearing vein, gold-mineralization is paragenetically early and coeval with quartz formation (Friedrich and Hoymann, 1989). Therefore, for

simplicity, and in the absence of detailed parageneses for all discordant veins, only fluid inclusions which were considered to be primary with respect to the main stage of vein-quartz formation were analyzed. Classification of inclusions as primary, pseudosecondary or secondary is according to the criteria of Roedder (1984) and Shepherd et al. (1985).

Foliaform vein quartz contains far fewer, workable, primary inclusions than discordant Au-bearing vein quartz. As a result, foliaform vein data are biased towards low temperature, low salinity secondary inclusions (see below). Where primary inclusions were identified, textural evidence for re-equilibration and/or leakage of the inclusions was common (e.g., Sterner and Bodnar, 1989).

The effects of post-trapping changes, due to deformation and thermal events such as that associated with the Mt. Burnham orthogneiss (Mortensen, 1990), on inclusions from Au-quartz vein material appear to be negligible. Although most quartz samples show undulose extinction in thin section, phase ratios in fields of primary inclusions are generally constant. Similarly, homogenization temperatures do not show the spread which would be expected if significant stretching or leakage had occurred (Lerrick, 1978).

Results of Fluid Inclusion Study

Fluid Inclusion Types

Classification of fluid inclusion types is based on the number of phases observed at room temperature, and the nature of the phase changes observed during heating and freezing runs. Three compositional types, designated as aqueous (type 1), intermediate X_{CO_2} (type 2), and high X_{CO_2} (type 3), were identified in this study. Inclusions belonging to each compositional type can be primary or secondary with respect to the host material, depending on their relative ages. The compositional designations are relative terms and do not imply an absolute value for X_{CO_2} .

Type 1: Aqueous Inclusions

Aqueous inclusions contain two phases at room temperature (Plates 8e and 8f). Phase changes at low temperatures indicate that the inclusions contain an aqueous low salinity fluid and an aqueous vapor phase. The absence of CO₂-hydrate (clathrate) formation during freezing experiments constrains the concentration of CO₂ (XCO₂) in type 1 inclusion fluids to <0.01 mole fraction (Hedenquist and Henley, 1985).

Type 1 primary inclusions in discordant veins occur predominantly in the northern portion of the field area (e.g., Lone Star, Hilchey, 27 Pup) although some were seen in the Sheba, Mitchell and Hunker Dome veins (Figure 8). Primary inclusions generally range in size from approximately 5 to 20 μm, up to a maximum of 60 to 70 μm in Hunker Dome amethyst samples, and are irregular to negative crystal in shape. The degree of fill (F) of primary inclusions- defined as the volumetric proportion of liquid relative to the total volume of the inclusion (Shepherd et al., 1985)- was determined by visual estimation and varies from approximately 0.90 in inclusions from the Virgin showing to 0.70-0.75 in veins from more southerly showings, e.g., Lone Star and 27 Pup.

Low temperature, type 1 secondary inclusions are common in all vein types and exhibit degrees of fill of between 0.95-0.98. They are usually negative crystal or elongate in shape and average around 5-10 μm or less in size. With two exceptions (see below), all foliaform vein samples contained predominantly secondary, low salinity type 1 inclusions with rare fields of type 1 primary inclusions (Figure 9). Fluid inclusions in foliaform veins tend to be smaller than those in Au-quartz veins.

Type 2: Intermediate XCO₂ Inclusions

Type 2 inclusions are either two phase or three phase at room temperature (Plates 8a to 8d). Two phase inclusions generally nucleate a thin liquid or vapor phase on cooling below room temperature (ca. < 23°C). All type 2 inclusions show low temperature phase changes indicative of the presence of clathrate, and most also contain liquid CO₂ at low

temperatures. The degree of fill of the CO₂ phase (F_{CO_2}) increases from ≈ 0.30 to ≈ 0.40 between the Aime and Mitchell lodes (Table 1). Primary and possible pseudosecondary inclusions from Sheba vein quartz display a range of F_{CO_2} and fluid compositions, from $\approx 100\%$ CO₂ ($\pm CH_4$) to 100% H₂O+NaCl, and at times occur within the same field of inclusions, suggesting that they may have trapped two discrete fluid phases.

Type 2 inclusions are generally between 5-20 μm in size, although inclusions in one sample from the Aime showing were particularly large (ca. 80 μm) (Plates 8a to 8c). Type 2 inclusions occur predominantly as primary and secondary inclusions in discordant veins from the south of the Klondike region, although two clathrate-bearing inclusions were seen in quartz samples from the Violet showing (see below) (Figure 8). Type 2 inclusions can be further subdivided based on the mode of homogenization of the carbonic phases:

Type 2a: These are the most abundant type seen. The carbonic phase homogenizes to liquid; the inner CO₂ vapor bubble shrinks and finally vanishes during gradual heating.

Type 2b: Homogenization of the carbonic phase occurs by expansion of the CO₂ vapor bubble.

Type 2c: CO₂ homogenization occurs by critical or near-critical behavior of the inner vapor bubble, at or below the critical point of pure CO₂

Type 3: High XCO₂ Inclusions

High XCO₂ inclusions contain 1 or 2 phases at room temperature. They homogenize below 31.1°C, generally to the liquid phase, and appear to contain essentially pure CO₂ ($\pm CH_4 \pm N_2$). Single phase, type 3 inclusions nucleate a second phase on cooling to a few degrees below room temperature (ca. 23°C). F_{CO_2} appears to be >0.95 ; no aqueous phase was seen in any type 3 inclusions, but may have been present as a film

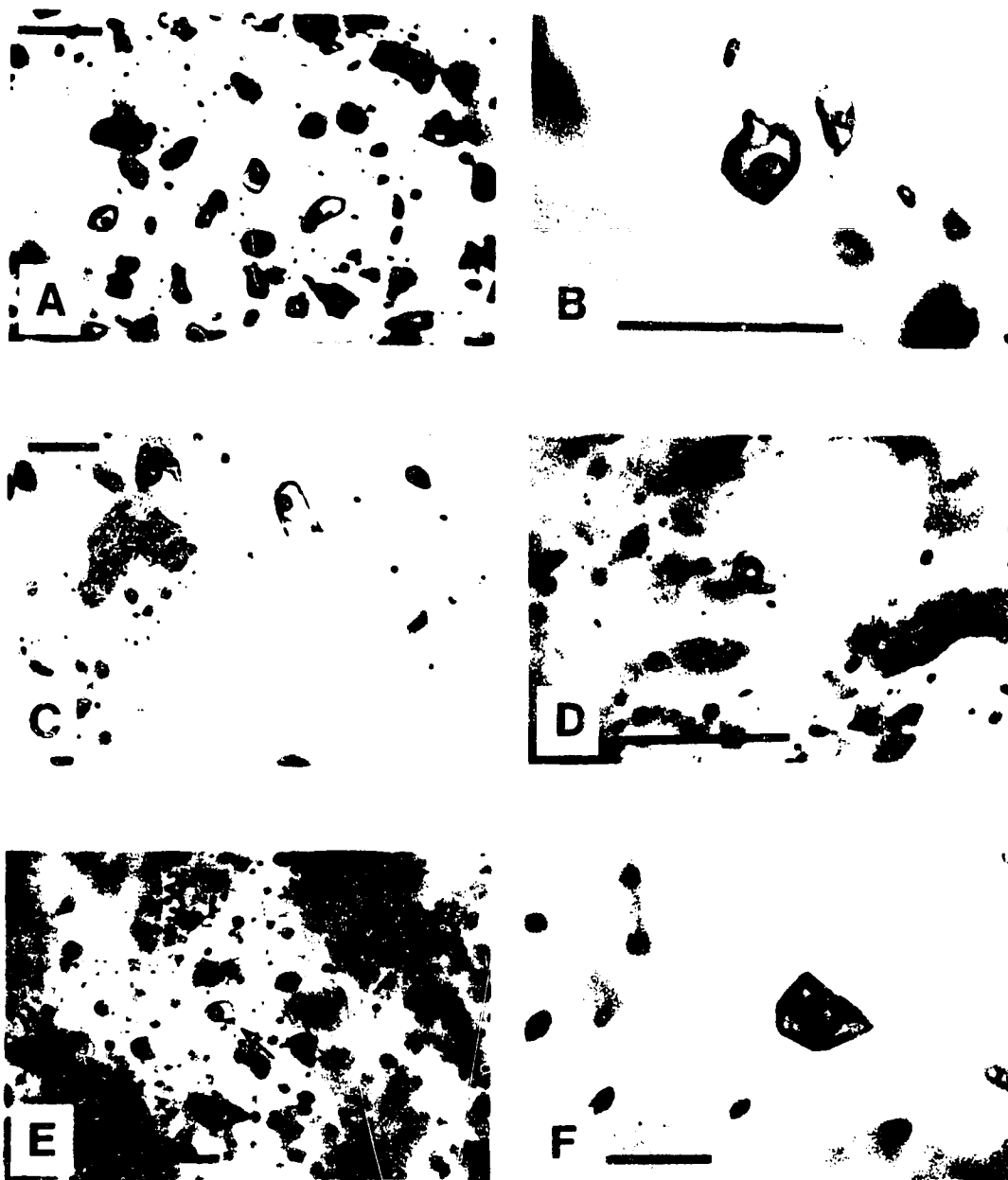


Plate 8. Photomicrographs of type 1 and 2 fluid inclusions in discordant vein quartz, taken at room temperature (ca. 23°C); A. Field of large type 2a inclusions in sample YR64a (NB CO₂-phases have homogenized); B. 3-phase type 2a inclusions, sample YR64a; C. 3-phase type 2a inclusions, sample YR64a (in plates B and C, sample was cooled briefly in liquid nitrogen to nucleate CO₂-vapor phase); D. 3-phase type 2b inclusion in mesothermal quartz, sample RR137; E. Type 1 inclusions (arrowed), sample RR322; F. Type 1 inclusion in amethyst, sample RR137. All scale bars are 100 microns, except plate E (50 microns).

wetting the inclusion walls. These inclusions are interpreted as primary or pseudosecondary in origin. Only 8 type 3 inclusions were seen during this study; 4 in samples from the Sheba vein, and 2 in samples of quartz from the Lloyd vein, and one each from the Gold Run and Violet veins. However, Friedrich and Hoymann (1989), in a detailed study of the Sheba vein, report microthermometric data for 8 "pure" CO₂ (cf. type 3) inclusions from Sheba quartz samples.

The occurrence of CO₂ in primary inclusions from Au-bearing quartz veins defines two geographic populations of veins; "CO₂-absent" veins in the northern portion of the Klondike region in which the primary inclusions are dominated by type 1 aqueous inclusions, and "CO₂-bearing" veins in the south, in which the primary inclusions are dominantly 3-phase, type 2 inclusions (Figure 8).

CO₂-bearing veins occur in the central and south-eastern portion of the Klondike region at the Aime, Gold Run, Lloyd, Hunker, Mitchell and Sheba showings, as well as two other discordant vein occurrences on Dominion Creek (Figure 8). The Mitchell and Sheba occurrences in the King Solomon Dome (KSD) area define the approximate northern limit of CO₂-bearing veins. As well, there appears to be a systematic, regional variation in the abundance of type 2a, 2b and 2c inclusions within CO₂ bearing veins. Primary inclusions from the Aime, Gold Run and Lloyd occurrences are predominantly type 2a with a minor proportion of types 2b and 2c. Veins in the Hunker Dome area contain types 1, 2a, 2b and 2c primaries, whereas type 1 and 2b inclusions are the most common primary inclusions in samples examined from the Mitchell vein system. Sheba vein quartz contains primary and/or pseudosecondary types 1, 2a, 2b and type 3 (see below).

North and north-west of KSD, the Lone Star, Hilchey, Virgin, Violet and 27 Pup discordant vein occurrences contain almost exclusively aqueous type 1 inclusions, with inclusion types 2 and 3 almost entirely absent, although a few were seen in samples from Violet (Figure 8).

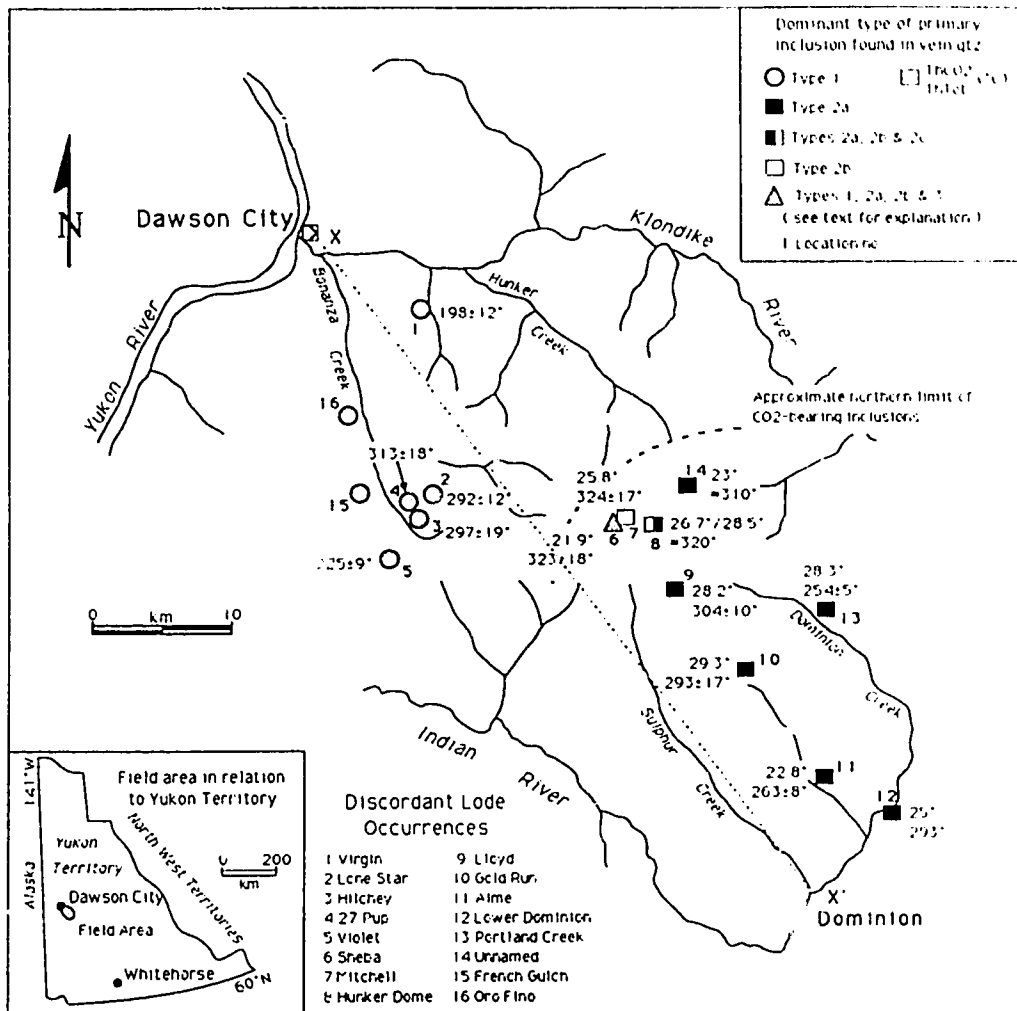


Figure 8. Map of the Klondike District showing the principal Au-quartz vein occurrences examined in this study, the most abundant type of primary inclusion found in quartz from each location, and the average Th_{tot} and Th_{CO_2} for each location.

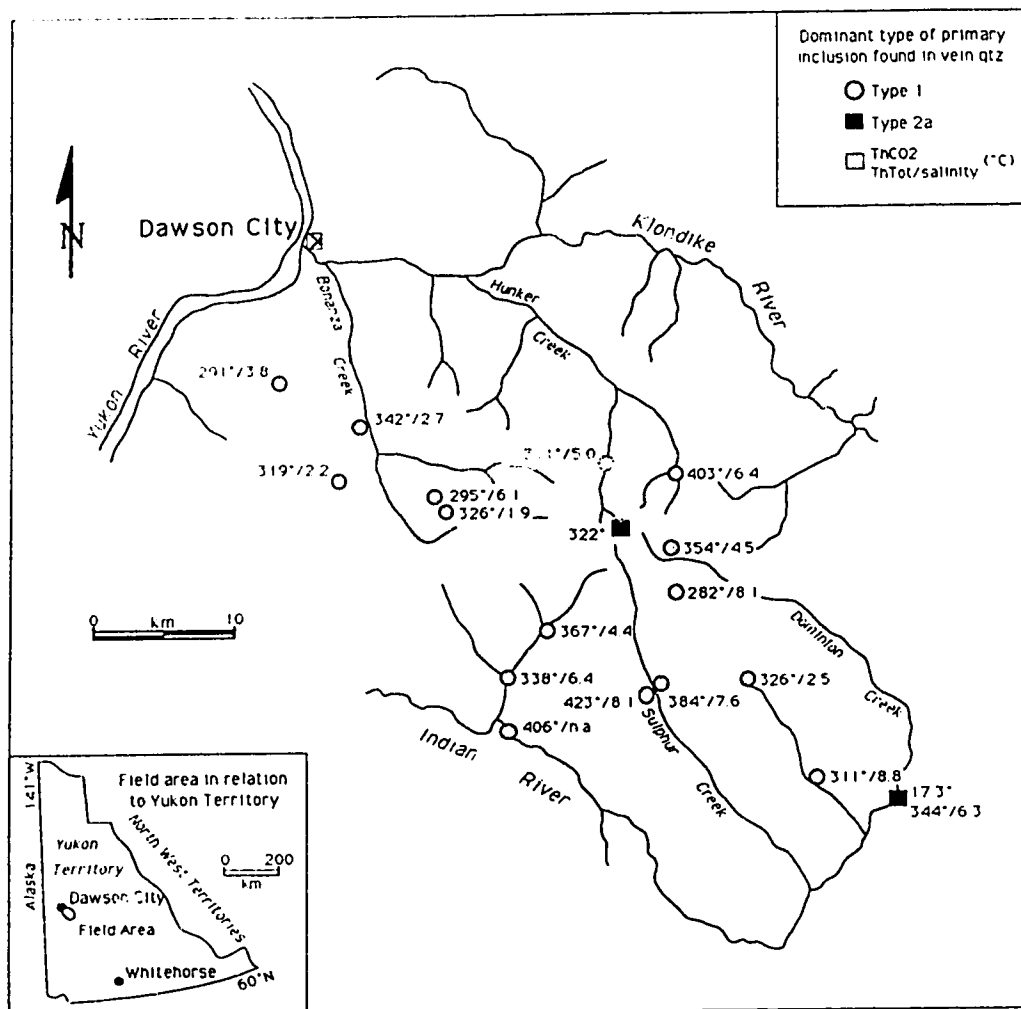


Figure 9. Map of the Klondike District showing the locations of foliaform quartz vein occurrences examined in this study, the most abundant type of primary inclusion found in quartz from each location, and the average Th_{tot} , Th_{CO_2} (where applicable) and fluid salinity for each vein.

The locations of foliaform veins in which primary inclusions were found are shown in Figure 9. The majority of foliaform quartz samples appeared to contain only type 1 inclusions; type 2 inclusions were found in only two samples. No systematic, geographical variations were seen within the distribution of fluid inclusion types in foliaform veins.

The microthermometric data will be presented in three parts: CO₂-absent Au-quartz veins, CO₂-bearing Au-quartz veins, and foliaform vein data. Errors quoted in the following sections represent plus/minus one standard deviation from the average phase change temperature.

Au-Quartz Veins

CO₂-Absent Au-Quartz Veins

Five principal occurrences of CO₂-absent Au-quartz veins were examined in detail, including the Virgin, Lone Star, Hilchey, 27 Pup and Violet occurrences (Figure 8). Detectable levels of CO₂, revealed by the presence of clathrate, were found in approximately half a dozen inclusions. Samples of late stage amethyst from brecciated discordant veins in the Hunker Dome region, were also found to contain only type 1 inclusions. Microthermometric data are shown by location in Table 1, and by sample in Appendix 2.

Final Melting Temperature of Ice: T_{mice}

The average T_{mice}, and calculated fluid salinities (Appendix 3) (Potter et al., 1978) are presented by location in Table 1. Figure 10a shows the total T_{mice} data. The total range in T_{mice} for individual type 1 inclusions is from ca. 0° to approximately -6°C.

Although the absence of clathrate indicates that only low concentrations of CO₂ are present in type 1 inclusions, even low concentrations of dissolved CO₂ can contribute as much as -1.5°C to the total melting point depression (Hedenquist and Henley, 1985). Consequently, salinities calculated from the T_{mice} data must be regarded as maximum

values. Eutectic temperatures, when observed, were generally above -20°C , suggesting that the dissolved salt is predominantly NaCl.

The average $T_{m_{ice}}$ of $-2.6 \pm 1.4^{\circ}\text{C}$ converts to an average salinity of 4.3 ± 2.1 eq.wt.% NaCl. Type 1, secondary inclusions generally exhibit $T_{m_{ice}}$ approaching 0°C , implying very low salinities. Amethyst samples taken from discordant veins in the Hunker Dome area have an average $T_{m_{ice}}$ of $-0.7 \pm 0.4^{\circ}\text{C}$, and calculated fluid salinities of 1.2 ± 0.7 eq.wt.% NaCl (Table 1).

Temperature of Total Homogenization: T_{tot}

All type 1 primary inclusions from northern Au-quartz veins homogenized to liquid on heating, except those which appear to have leaked during heating. Histograms of T_{tot} for CO_2 -absent veins are shown in Figure 11, and the results are tabulated in Table 1. Homogenization temperatures range from 160° to 350°C with two prominent peaks apparent in the histogram (Figure 11). The low temperature peak defines the population of primary type 1 inclusions from the Virgin and Violet veins, and secondary type 1 inclusions from all locations. The higher temperature peak corresponds to primary inclusions from the 27 Pup, Lone Star and Hilchey occurrences, with average homogenization temperatures of 313° , 292° and 297°C respectively (Table 1). Inclusions in Hunker Dome amethyst samples have an average T_{tot} of $341 \pm 11^{\circ}\text{C}$.

CO_2 -Bearing Au-Quartz Veins

The vast majority of samples containing evidence for the presence of a carbonic phase came from the Sheba, Hunker, Mitchell, Lloyd, Gold Run and Aime showings (Figure 8). Dufresne (1987) notes the occurrence of clathrate in inclusions from mesothermal/metamorphic veins from the Dago Hill and Lone Star areas. However, the present study failed to reveal a systematic enrichment of CO_2 in discordant vein inclusion fluids from the north of the field area.

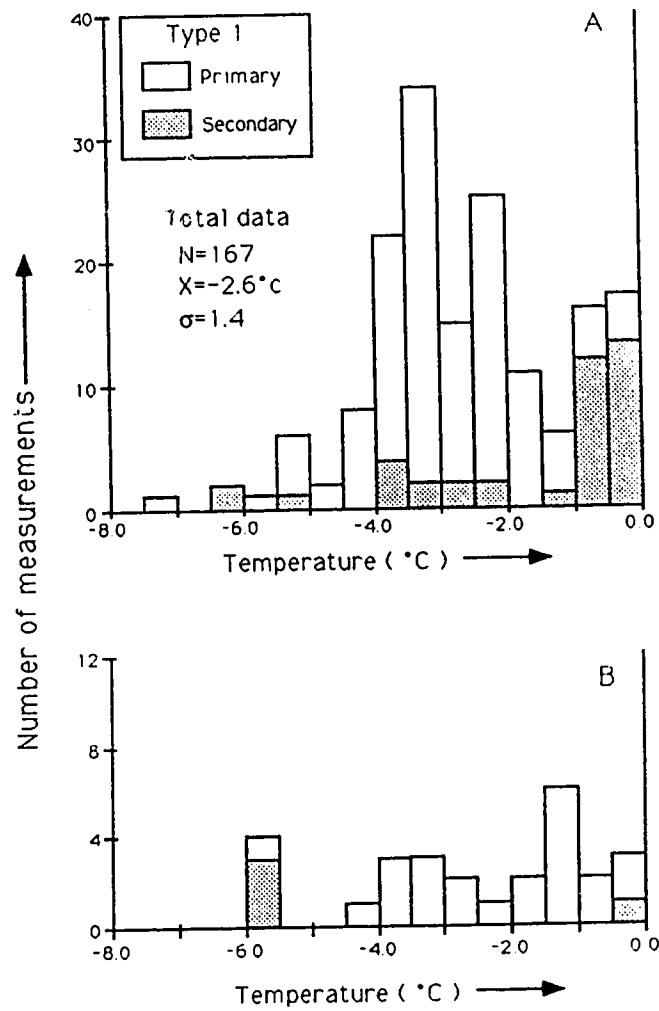


Figure 10. Ice melting temperatures ($T_{m_{ice}}$) for type 1 inclusions in A. CO₂-absent, northern Klondike Au-quartz veins, B. CO₂-bearing Au-quartz veins from the central Klondike, excluding Hunker Dome amethyst.

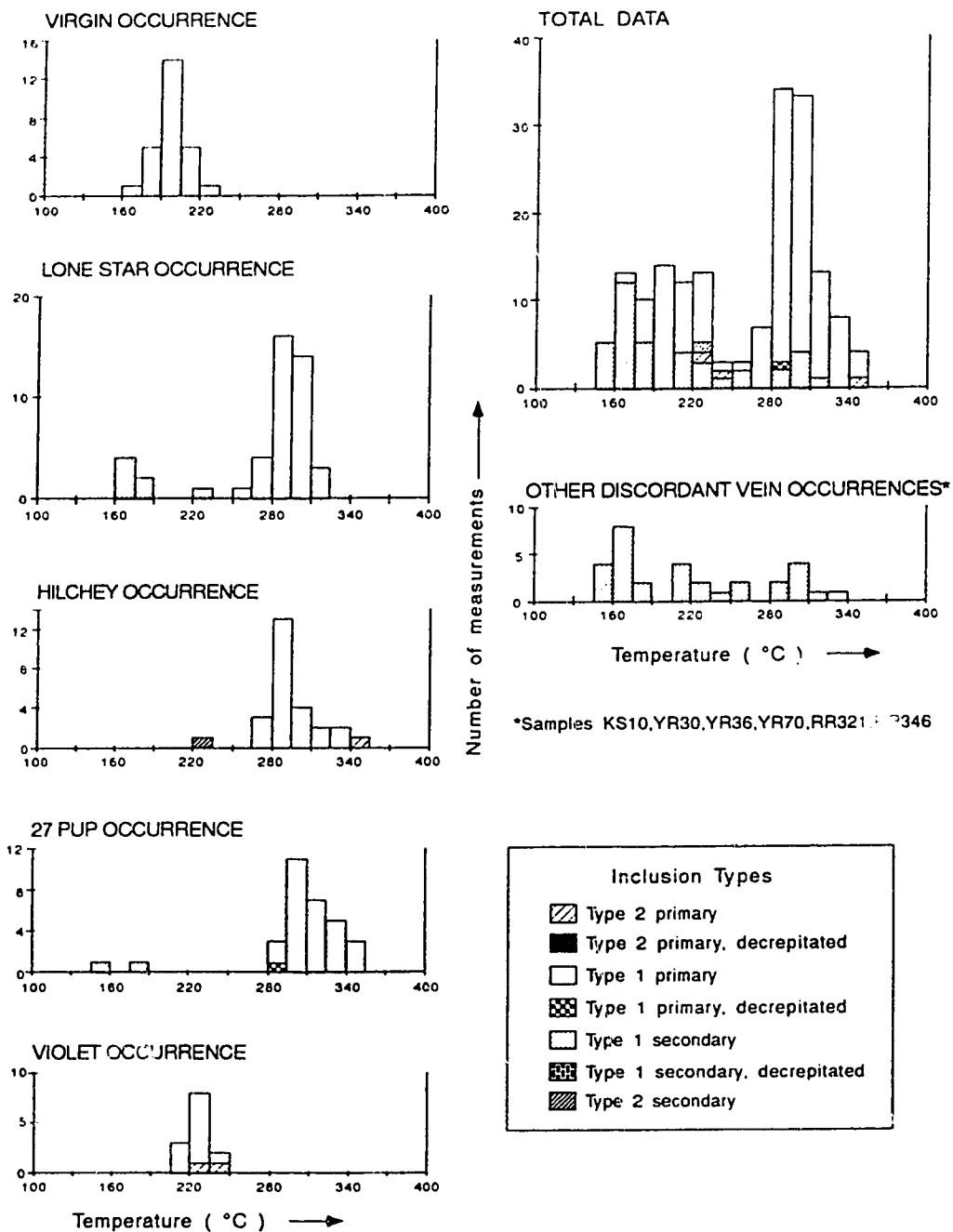


Figure 11. Temperature of total homogenization (Th_{100}) for CO_2 -absent Au-quartz veins, broken down by location (see Figure 8, and Table 1).

Final Melting Temperature of CO₂: T_{mCO2}

The T_{mCO2} data are shown in Figure 12a. The average T_{mCO2} is $-56.7 \pm 0.6^\circ\text{C}$ with a well defined peak at around -56.5° to -57.0°C , indicating that the carbonic phase is essentially pure CO₂ (Donnelly and Katz, 1954). The presence of T_{mCO2} values above -56.6°C is a result of experimental error. The tail off in the data towards -58°C is probably due to the presence of minor amounts of CH₄ or other volatiles such as N₂, although it is not possible to accurately define the mole fraction of CH₄ (or other volatiles) on the basis of T_{mCO2} alone (Buruss, 1981).

Final Melting Temperature of Ice: T_{mice}

Fluid inclusions in vein occurrences south and east of the Mitchell and Hunker lodes are dominated by CO₂-bearing fluids (see earlier discussion) and usually nucleate clathrate on cooling. If both clathrate and ice are observed in the same inclusion, T_{mice} must be ignored, because exclusion of NaCl from the clathrate structure preferentially concentrates NaCl in the residual aqueous fluid. Thus, T_{mice} recorded in the presence of clathrate would give anomalously high aqueous phase salinities (Collins, 1979). Ice melting temperatures for primary type 1 inclusions in the Mitchell, Hunker and Sheba lodes range from 0 to -6°C , approximately the same range as the non-CO₂ bearing lodes (Figure 10b).

Final Melting Temperature of Clathrate: T_{mclath}

The average T_{mclath} for the total data set is $7.8 \pm 0.8^\circ\text{C}$ (Figure 12b, Table 1). There is very little variation in T_{mclath} between vein locations. Averages fall between 6.9° and 8.1°C , although slightly more spread is evident in the data from the Hunker Dome, Mitchell and Sheba veins. Salinities were calculated from T_{mclath} using the equation of Bozzo et al. (1975) (Appendix 3), and are shown in Table 1. The average salinity for the

total data set is 4.3 ± 1.5 eq.wt.% NaCl, in good agreement with the average fluid salinity of 4.3 ± 2.1 eq.wt.% NaCl calculated for type 1 inclusions in the northern, aqueous veins.

Temperature of CO₂ Homogenization: ThCO₂

Histograms of ThCO₂ for each of the CO₂-bearing lodes are shown in Figure 13. The temperature and mode of homogenization of the carbonic phase change systematically from southeast to northwest across the southern portion of the field area. In type 2 inclusions from Aime and Gold Run, the CO₂-phase homogenizes predominantly to the liquid phase, and ThCO₂ increases from $22.8 \pm 3.0^\circ\text{C}$ to $29.1 \pm 1.2^\circ\text{C}$ between the two lodes.

Moving further north from Lloyd to the Hunker Dome veins, an increasing proportion of inclusions homogenize by critical or near critical behavior of CO₂, and ThCO₂ drops slightly from $28.2 \pm 1.7^\circ\text{C}$ to $27.2 \pm 3.1^\circ\text{C}$. In addition, inclusions which homogenize by critical behavior, homogenize below the critical temperature of pure CO₂, indicating the presence of small amounts of CH₄ and/or N₂ dissolved in the CO₂ phase (Swanenberg, 1979).

The largest range in ThCO₂, is seen in samples from the central portion of the region (e.g., Mitchell, Sheba). Type 2b inclusions from samples of Mitchell vein quartz homogenize at between 19 to 31°C. Type 2 inclusions in Sheba quartz homogenize over a similar temperature range of approximately 21-30°C, and both dew- and vapor-curve homogenizations were seen.

High CO₂, type 3 inclusions which are relatively common in the Sheba quartz samples, homogenize to the liquid phase at $21.9 \pm 1.6^\circ\text{C}$. Friedrich and Hoymann (1989) also describe pure CO₂ inclusion from Sheba vein quartz, which homogenized at approximately 23°C. However, they do not report whether these inclusions homogenized to the liquid or vapor phase. Northwest of the Mitchell and Sheba lodes (Figure 8), detectable CO₂ is absent from primary inclusions, with the exception of 3 inclusions from the Violet

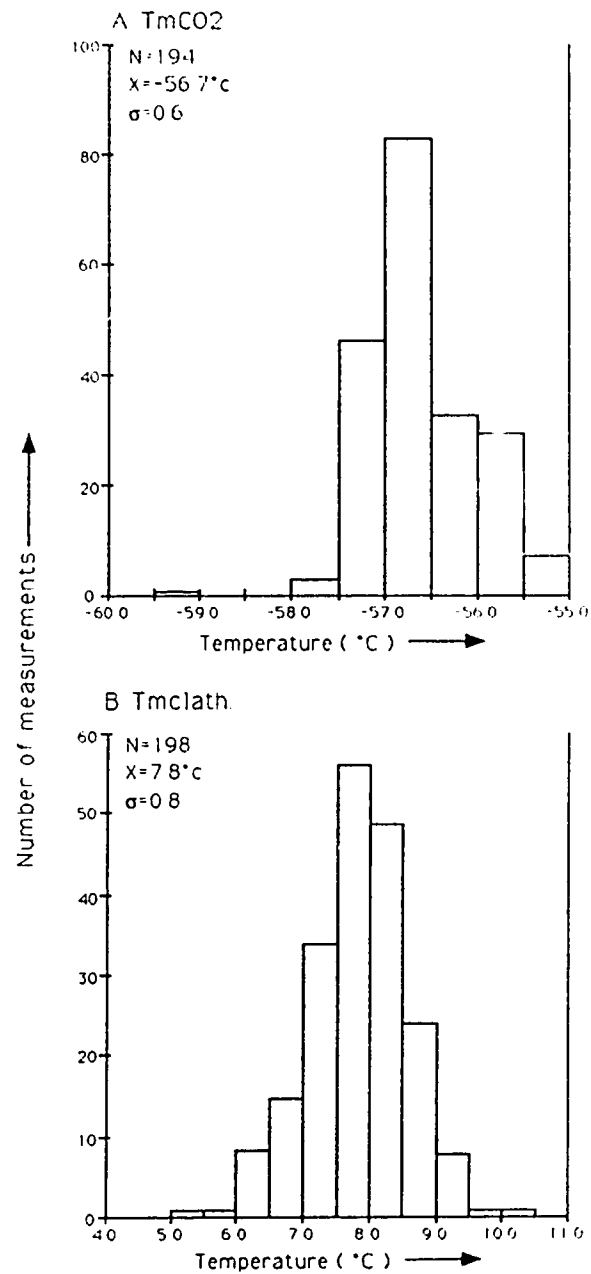


Figure 12. A. Melting temperature of CO_2 (T_{mCO_2}), and B. melting temperature of clathrate (T_{mclath}), for CO_2 -bearing Au-quartz veins in central and southern Klondike.

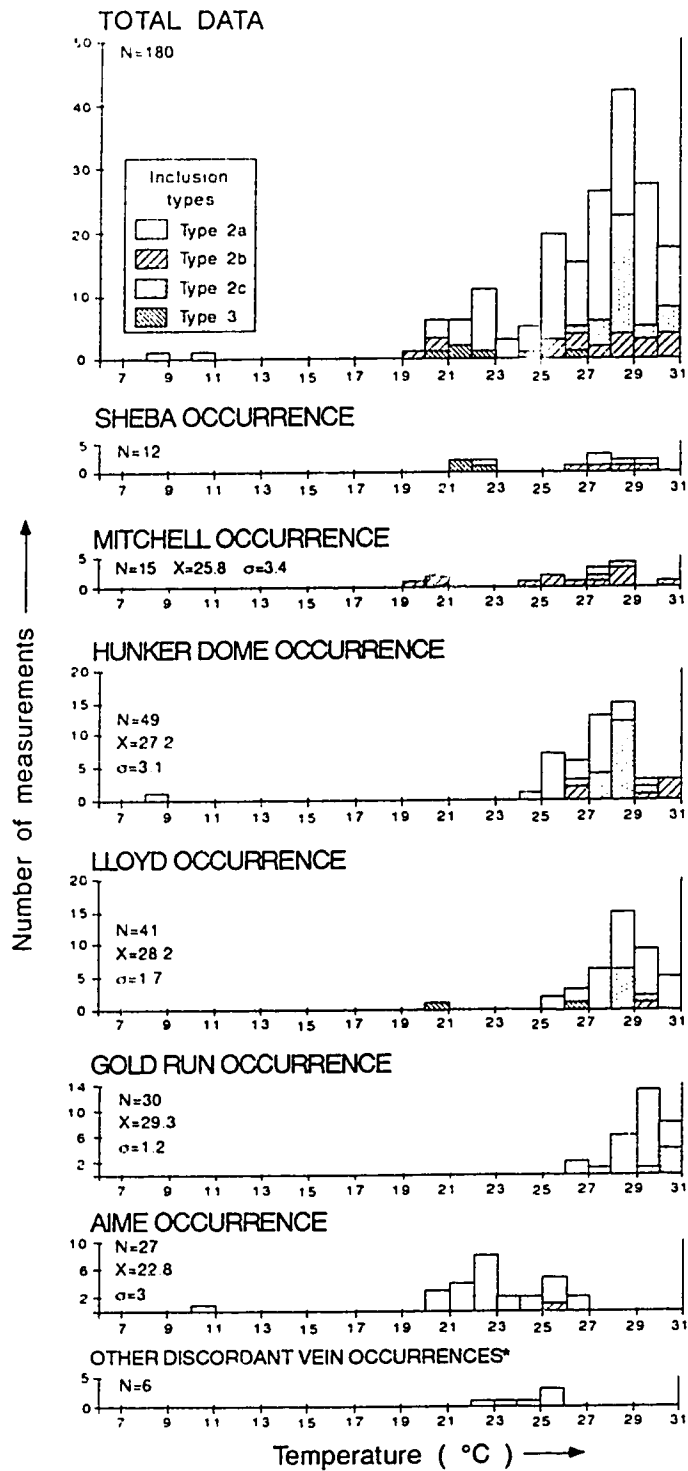


Figure 13. Temperature and mode of homogenization of CO_2 phase (Th_{CO_2}) in CO_2 -bearing, Au-quartz veins, broken down by location.

showing. A single type 3 inclusion, which homogenized to the liquid phase at -33.3°C , was seen in sample RR132, and 2 clathrate-bearing inclusions were also noted in the same sample (Appendix 2). The significance of the low Th_{CO_2} in sample RR132 is uncertain.

Temperature of Total Homogenization: Th_{TOT}

Histograms of Th_{TOT} are shown in Figure 14 and results are summarized in Table 1. Figure 15 is a plot of the average temperature of total homogenization for the principal discordant veins (CO_2 -absent and CO_2 -bearing) against distance along a section line extending southeast from Dawson City through Dominion. Homogenization temperatures peak in the central Klondike region. In the south, Th_{TOT} gradually increases from $263 \pm 8^{\circ}\text{C}$ at Aime to approximately $300\text{-}350^{\circ}\text{C}$ for type 2 inclusions in the Sheba, Hunker and Mitchell veins. This increase is accompanied by a decrease in the proportion of type 2 inclusions which decrepitated during heating (Figure 14), and also by a change in the mode of homogenization of the CO_2 phase (Figure 13). This suggests that the temperature decrease southwards may actually be a function of an increase in the internal pressure of the fluid inclusions (see below). Type 1 inclusions from Mitchell and Sheba, have slightly lower homogenization temperatures than type 2 inclusions from the same samples. A small proportion of the total number of inclusions analyzed homogenized to the vapor phase.

Foliaform Veins

With the exception of samples YR24 and RR262, foliaform vein quartz contained predominantly secondary type 1 inclusions, with rare primaries (Figure 9). YR24 and RR262 were unusual and contained apparently primary, type 2a inclusions. Evidence of re-equilibration of inclusions is seen in many samples. The occurrence of swarms of tiny ($<1\ \mu\text{m}$) satellite inclusions surrounding many primary(?) inclusions indicates that the microthermometric data in Appendix 2 should be regarded with caution (Stern and Bodnar, 1989).

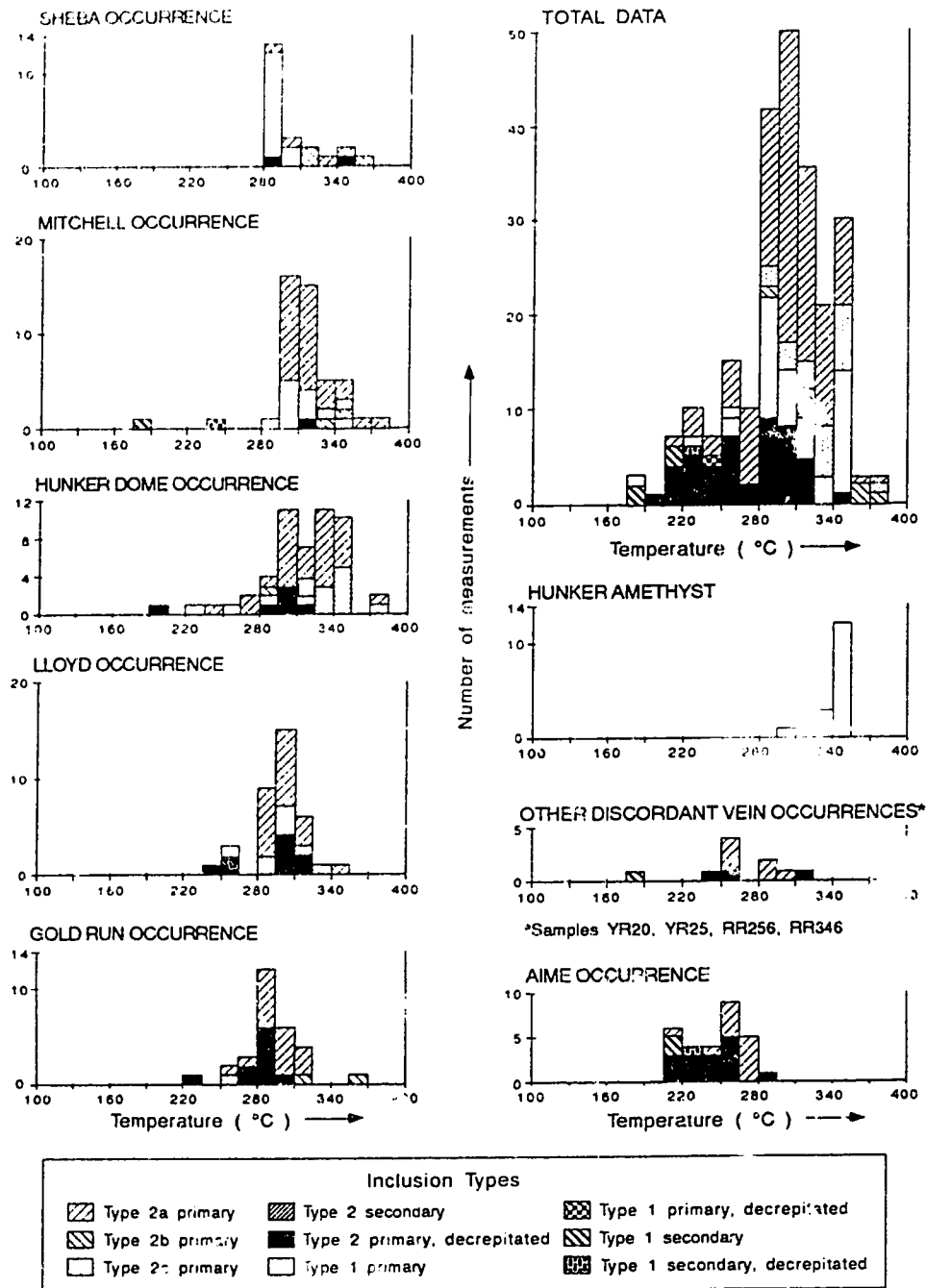


Figure 14. Temperature of total homogenization (T_{htot}) for CO_2 -bearing Au-quartz veins, broken down by location (see Figure 8, and Table 1).

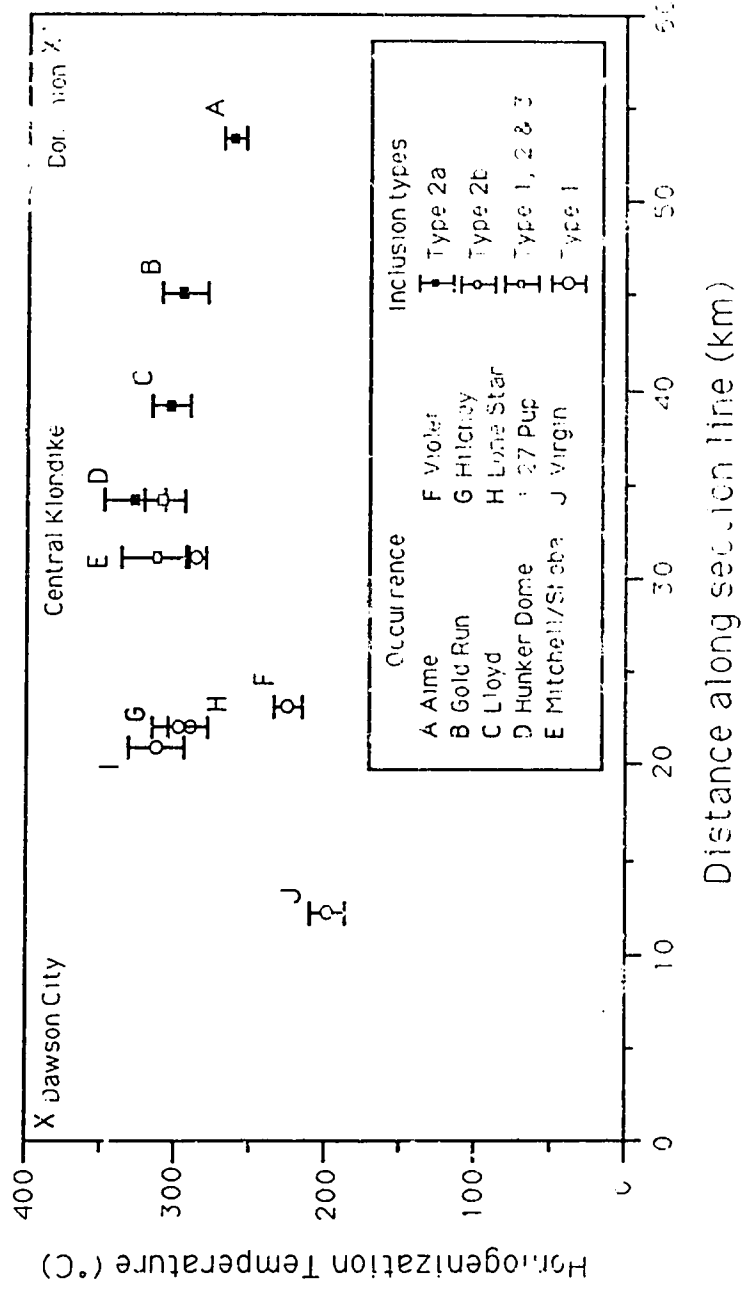


Figure 15. Plot of Throt of primary inclusions in Au-quartz veins, against distance along section line X-X' (see Figure 8).

T_{mice} for all type 1 primary inclusions range from -10° to 0°C (Figure 16a). Calculated salinities range from 0 to 14 eq.wt.% NaCl and average 5.3 ± 2.2 eq.wt.% NaCl. Fluid salinities from southern veins are slightly higher on average than those in the north (Figure 9).

Homogenization temperatures for primary inclusions are shown in Figure 16b. Temperatures range from 110° - 420°C , and appear to increase southwards (Figure 9). Secondary inclusions produce a broad, low-temperature peak on the histogram, between 100° - 270°C , with a maxima at $\approx 200^{\circ}\text{C}$.

Type 2a primary inclusions contain liquid CO_2 which melts at between -56.8° to -57.5°C . Clathrate melts at around 6.0° to 6.6°C , giving salinities of approximately 6 eq.wt.% NaCl. The average $T_{h\text{CO}_2}$, seen only in sample YR24, was $17.3 \pm 4.8^{\circ}\text{C}$. Total homogenization of Type 2a inclusions occurred at approximately 344°C .

Fluid Composition and Density

CO_2 -Absent Au-Quartz Vein Fluids

P-V-T-X data for the H_2O -NaCl system (e.g., Haas, 1976; Potter and Brown, 1977; Knight and Bodnar, 1989) adequately describe the phase changes seen within type 1 inclusions in CO_2 -absent veins. For simplicity, in all calculations using data from type 1 inclusions, the CO_2 ($+\text{CH}_4+\text{H}_2\text{S}+\text{N}_2$) content of the liquid and vapor phases was assumed to be negligible. Inclusion fluid densities for primary type 1 inclusions were calculated from the data of Haas (1976). Isochore P/T coordinates for the calculated densities were taken from Potter and Brown (1977).

Isochores calculated for type 1 inclusion fluids in discordant, Au-quartz lode occurrences, including the Sheba and Mitchell veins and amethyst samples from Hunker Dome are shown in Figure 17a. Average type 1 fluid densities range from 0.73 ± 0.04 to 0.90 ± 0.01 g/cc, and increase towards the north from the central part of the field area (Table 1). Fluid densities in primary type 1 inclusions from the Mitchell and Sheba veins

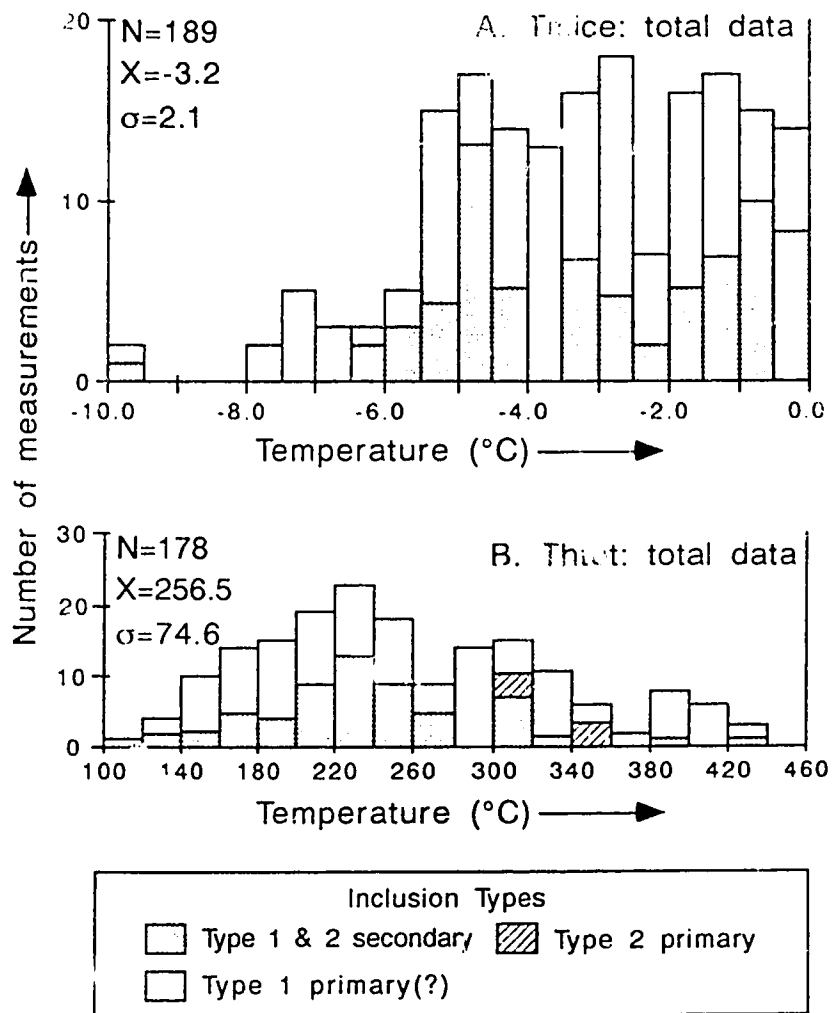


Figure 16. A. Total $T_{m_{ice}}$ data, and B. total $T_{h_{tot}}$ data, for foliaform vein quartz samples.

Table 1. Summary of Microthermometric and Inclusion Fluid Composition Data for the Principal Au-quartz Vein Occurrences*

¹ Local/ Occurrence	² Inc Type	Volume % CO ₂	Corrected ³ volume % CO ₂	TmCO ₂ (°C)	Tm _{ice} (°C)	Tm _{clath} (°C)	ThCO ₂ (°C)	Th _{total} (°C)	Salinity ⁴ (eq.wt% NaCl)	³ Corrected XCO ₂	Bulk fluid ³ Density (g/cc)
Alme	2a	31 ±6	31 ±6	-57.0 ±0.3	-	7.5 ±0.5	22.8 ±3.0	263 ±5	4.9 ±0.9	0.10-0.15	0.91-0.96
Gold Run	2a	34 ±10	32	-56.7 ±0.2	-	7.8 ±0.5	29.3 ±1.2	293 ±17	4.3 ±0.9	0.12 ±0.04	0.90 ±0.05
Lloyd	2a	34 ±8	36	-56.2 ±0.6	-	8.1 ±0.4	28.2 ±1.7	304 ±10	3.8 ±0.8	0.13 ±0.04	0.88 ±0.04
Hunker	2a	39 ±9	45	-56.6 ±0.8	-	8.0 ±0.8	26.7 ±1.3	310 ±14	4.0 ±1.5	0.18 ±0.03	0.86 ±0.03
Doms	2c(2b)	39 ±9	42	-57.0 ±0.7	-	7.4 ±1.1	28.5 ±1.2	332 ±22	5.0 ±2.0	0.14 ±0.03	0.81 ±0.04
Mitchell	2b	40 ±8	39	-56.8 ±0.8	-	7.9 ±0.9	25.3 ±3.5	324 ±17	4.1 ±1.7	0.09 ±0.02	0.75 ±0.06
	1	-	-	-	-3.0 ±0.8	-	-	309 ±13	4.6 ±1.5	<0.01	0.74 ±0.03
Sheba	3	>95	-	-56.9 ±0.4	-	-	21.9 ±0.6	-	-	~1.00	0.74 ±0.01
	2a	53 ±15	?	-56.5 ±0.3	-	6.8 ±0.4	27.9 ±0.9	323 ±18	6.1 ±0.7	0.19 ±0.03	0.87 ±0.02
	2b	39 ±9	?	-53.4 ±0.5	-	7.7 ±0.9	27.9 ±1.1	323 ±18	4.5 ±1.6	0.09 ±0.02	0.76 ±0.07
	1	-	-	-	-2.3 ±0.5	-	-	286 ±5	4.8 ±1.6	<0.01	0.79 ±0.01
Lone Star	1	-	-	-	-2.0 ±0.4	-	-	292 ±12	3.4 ±2.2	<0.01	0.77 ±0.02
Hilchey	1	-	-	-	-0.6 ±1.6	-	-	297 ±19	5.8 ±2.3	<0.01	0.76 ±0.03
27 Pup	1	-	-	-	-2.1 ±0.8	-	-	313 ±18	3.5 ±1.3	<0.01	0.73 ±0.04
Violet	1	-	-	-	-3.8 ±0.4	-	-	225 ±9	6.1 ±0.6	<0.01	0.87 ±0.01
Virgin	1	-	-	-	-3.4 ±0.4	-	-	198 ±12	5.5 ±0.6	<0.01	0.90 ±0.01
Amethyst	1	-	-	-	-0.7 ±0.4	-	-	341 ±11	1.2 ±0.7	<0.01	0.66

* All errors quoted represent ± 1 standard deviation.

1 See Figure 3 for locations 2 See text for explanation

3 See Appendix 1 for explanation of correction procedure.

4 Salinity calculated from the equations of Bozzo et al., 1975 (clathrate) and Potter et al., 1978 (ice). See Appendix 3.

average 0.74 ± 0.01 and 0.79 ± 0.01 g/cc, respectively. Further north, average inclusion fluid densities from the Hilchey, Lone Star and 27 Pup veins cluster around 0.73-0.78 g/cc. Inclusion fluids from the Virgin showing have an average density of approximately 0.90 ± 0.01 g/cc. Data from the Violet lode indicate fluid densities as high as 0.87 ± 0.01 g/cc. Fluids trapped in primary inclusions in Hunker amethyst samples have the lowest density, 0.66 g/cc.

CO₂-Bearing Au-Quartz Vein Fluids

Bulk fluid compositions and densities were calculated using a simplification of the method presented by Diamond (1986). Quantitative estimates are made of the mole fractions of each component in the aqueous and carbonic phases at the homogenization temperature of the carbonic phase. Molar volumes are calculated for each phase and then combined using visual estimates of F_{CO_2} to obtain the density of the trapped fluids. The averaged F_{CO_2} estimates plus/minus one standard deviation were used in all density calculations.

Although the technique is still reliant upon the visual estimates of F_{CO_2} as a variable during calculations, which is probably the largest source of error in bulk-density calculations, an iterative procedure is used to reduce F_{CO_2} to a dependent variable and thereby reduce much of the associated error (Diamond, 1986) (Appendix 1).

Microthermometric data and phase ratios for Aime, Gold Run and Lloyd are internally fairly homogeneous (Table 1, Appendix 2). However, the observed variation between these locations and veins in the central part of the area (Table 1) suggests that although each vein system trapped an homogeneous fluid, the P-T-X conditions at trapping differed between locations. Due to the homogeneity in the microthermometric data for individual lodes, and to minimize the error introduced by the use of visual estimations of phase volumes, the averaged data for each lode system were used in all density calculations. As well, the data from the Hunker Dome, Mitchell and Sheba occurrences

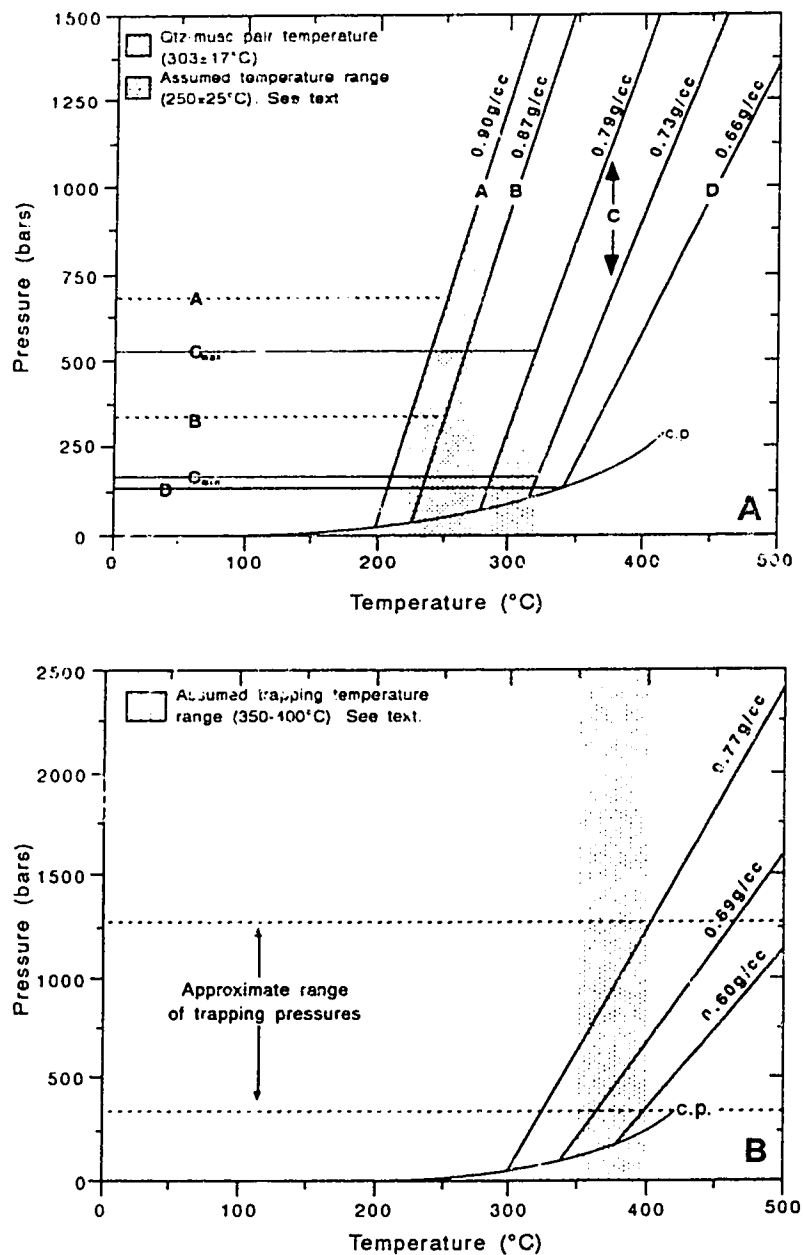


Figure 17. A. Isochores and estimated trapping pressures for fluids in type 1 primary inclusions in CO₂-absent Au-quartz veins. Explanation: A. Virgin, B. Violet, C. range of isochores for 27 Pup, Lone Star, Hilchey, Sheba and Mitchell veins, D. Hunker amethyst. Boiling curve calculated for ≈4 eq. wt.% NaCl. B. Isochores for type 1 inclusion fluids in foliaform vein quartz, calculated for ≈5 eq. wt.% NaCl and T_{tot} ± 1 st.dev. (data from Haas, 1976; Potter and Brown, 1977; Knight and Bodnar, 1989).

were separated into aqueous (type 1 inclusions), intermediate- X_{CO_2} (type 2a,b and c inclusions), and high- X_{CO_2} (type 3 inclusions), categories. The assumptions made in estimating fluid/vapor compositions are discussed briefly below.

Vapor Phase Composition

The slight depression of T_{mCO_2} evident in both the Aime and Hunker showings is indicative of the presence of minor amounts of other volatiles such as CH_4 or N_2 (Swanenberg, 1979). Maximum concentrations of approximately 4 mole % CH_4 in the carbonic phase were estimated for the Aime and Hunker data (Heyen et al., 1982). The concentration of other volatiles, specifically H_2S , is unknown.

A number of type 2 inclusions from the Hunker Dome, Gold Run and Lloyd veins contained CO_2 phases which homogenized by critical, or near critical, behavior below $31.1^\circ C$. Addition of CH_4 (or N_2) to CO_2 lowers the temperature of the critical point with respect to the pure CO_2 system (Swanenberg, 1979). The average temperature of critical homogenization for Hunker inclusions (ca. $28^\circ C$) corresponds to an $X_{CH_4} \approx 0.02$ in the CO_2 phase (Donnelly and Katz, 1941). Thus, an average value of 2 mole % CH_4 (or N_2) in the carbonic phase was included in the fluid composition calculations. The net effect on the bulk fluid density is negligible.

The molar volumes of the CO_2 ($\pm CH_4$) mixture for the observed temperature and mode of T_{hCO_2} , were obtained by interpolation of the data of Arai et al. (1971). The mole fraction of H_2O dissolved in the carbonic phase was assumed to be zero (Diamond, 1986; Wiebe and Gaddy, 1941).

Aqueous Phase Composition

The salinity of the aqueous phase in clathrate-bearing systems can be determined from the equations of Bozzo et al. (1975) (Appendix 3). The molar volume of the H_2O - $NaCl$ solution was assumed to be the same for each data set, despite salinity differences.

Variation in the molar volume of the H₂O-NaCl solution over the temperature and compositional range of interest (i.e., ≈20-31°C, 3-5 eq.wt.% NaCl) is less than 1%, which is minimal compared to the other potential sources of error (e.g., F_{CO₂}) (Rogers and Pitzer, 1982). The contribution of the molar volume of dissolved CO₂ in the aqueous phase to the total molar volume of the fluid is also minor due to the low mole fraction of dissolved CO₂ (ca. X_{CO₂} <0.02), and has been ignored.

Bulk Fluid Density and Composition

Corrected fluid densities and compositions are presented in Table 1. 2-phase curves were constructed from this data by interpolation and extrapolation of the results of Takenouchi and Kennedy (1965). P/T coordinates for fluid isochores were calculated from the data of Bowers and Helgeson (1983).

Fluid densities in CO₂-bearing veins appear to decrease northwards from the Aime lode towards the Mitchell and Sheba veins. Calculated densities for type 2a inclusions from Aime, Gold Run and Lloyd are 0.91-0.96, 0.90 ±0.05 and 0.88 ±0.03 g/cc respectively. The calculated bulk fluid CO₂ concentrations for the same veins are in rough agreement at 0.13 ±0.02, 0.12 ±0.04, and 0.13 ±0.04 mole fraction CO₂, respectively. The slight decrease in average bulk fluid density, moving northwest across the southern portion of the Klondike, is a consequence of progressively lower CO₂ densities.

Contrasting fluid densities and compositions are observed in inclusions from the Hunker, Mitchell and Sheba veins (Table 1). High X_{CO₂} (X_{CO₂} ≈1.0), type 3 inclusions from Sheba have a bulk fluid density of 0.74 g/cc. Intermediate X_{CO₂} fluids trapped in type 2a inclusions from Hunker and Sheba quartz samples, have average densities of 0.86 ±0.03 g/cc and 0.90 ±0.02 g/cc, and CO₂ concentrations of 0.18 ±0.03 and 0.19 ±0.03 mole fraction respectively. Type 2b and 2c inclusions in all three vein systems, trapped fluids with CO₂ concentrations which range from 0.09 to 0.14 mole fraction, and average

bulk fluid densities of between 0.76 and 0.81 g/cc (Table 1). Values for X_{CO_2} calculated from Schwartz (1989) are in good agreement with the results presented above.

Aqueous type 1 inclusions from Sheba and Mitchell vein quartz contain fluids with low CO_2 concentrations ($X_{CO_2} < 0.01$) and bulk densities of between 0.74 and 0.79 g/cc, which are in the same range as primary type 1 inclusions from the Lone Star/27 Pup area (Table 1). Calculated average salinities for all veins are approximately 4-5 eq.wt.% NaCl, relative to $H_2O+NaCl$.

Foliaform Vein Fluids

Isochores calculated for primary(?) type 1 inclusion fluids from foliaform veins are shown in Figure 17b. P/T coordinates for the isochores were calculated assuming an average salinity of ≈ 5 eq.wt.% NaCl at the average homogenization temperature of $342 \pm 40^\circ C$.

Fluid densities range from approximately 0.60 g/cc to 0.77 g/cc. The bulk fluid density of the CO_2 -bearing fluids in sample YR24 lies in the range 0.95 ± 0.04 g/cc with a CO_2 concentration of 0.165 ± 0.05 mole fraction. The mole fraction CO_2 estimated for the same sample from Schwartz (1989), assuming an aqueous phase salinity of ≈ 6 eq.wt.% NaCl for YR24, is 0.175 ± 0.05 .

Pressure calculations

Pressure at Total Homogenization: P_{Thtot}

Au-Quartz Veins

Fluid pressures within type 2 fluid inclusions at the temperature of total homogenization (P_{Thtot}) (Table 2), were determined from Schwartz (1989), the graphical construction method of Brown and Lamb (1989) (Appendix 7), and from the pressure coordinates of isochore origins on 2-phase curves (Appendix 7) constructed from the

compositional data in Table 1, using the data of Bowers and Helgeson (1983), and Takenouchi and Kennedy (1965).

Pressures obtained by the method of Brown and Lamb (1989), are higher than those obtained from the other two methods, and decrease from approximately 2.3 to 1.5 kbars between Aime and the Mitchell and Sheba veins. The method of Schwartz (1989) indicates that $P_{T_{tot}}$ dropped from ≈ 1.3 kbars for type 2a inclusions in Aime vein quartz, to approximately 600 bars in type 2b inclusions in the Mitchell and Sheba veins. Pressures calculated from isochore origin coordinates are in rough agreement with those from Schwartz (1989), and appear to decrease from approximately 1 kbar to 500 bars across the same area.

Significant ranges in $P_{T_{tot}}$ are implied for data from the Mitchell, Sheba and Hunker vein systems. Values for $P_{T_{tot}}$, calculated from type 2a and type 2b inclusions in these veins differ by as much as 1 kbar, in some cases within the same sample (Table 2).

Foliaform Veins

The calculated pressure at T_{tot} of type 2 inclusions from sample YR24 is 1400 \pm 400 bars. The construction method from Brown and Lamb (1989) indicates that the pressure at T_{tot} was significantly higher, in the region of 2.3-2.5 kbars.

Pressure at Trapping: P_t

Fluid pressures estimated at the temperature of total homogenization (previous section), can be used as trapping pressure estimates only if it is assumed that the inclusions were trapped on the 2-phase curve (Shepherd et al., 1985). If, however, the fluid was trapped as one homogeneous phase within the single-phase region, it is impossible to fix the exact P/T coordinates of the point on the isochore at which trapping occurred without an independent estimate of the trapping pressure or temperature (Roedder, 1984; Shepherd et al., 1985). Thus, to calculate the approximate trapping pressure for each lode, an

Table 2. Inclusion Fluid Pressures for Principal Au-Quartz Veins, Calculated at the Temperature of Homogenization and the Estimated Temperature of Trapping (see Table 1 for Fluid Compositions)

Location/ Occurrence	Inc. Type ¹	Pressure at homogenization (Bars) ⁴			Pressure at trapping (Bars) ⁴	
		Isochore origin ³	Brown and Lamb (1989)	Schwartz (1989)	Isochore intercept ⁴	Brown and Lamb (1989)
Aime	2a	(750-1125)	1925 ±175	1260	[2070 ±420]	[2250 ±250]
Gold Run	2a	760 ±200	1600 ±200	1160	[1875 ±675]	[1650 ±250]
Lloyd	2a	860 ±170	1900 ±200	1160	[1625 ±375]	[1900 ±300]
Hunker Dome	2a	1200 ±200	1675 ±225	1030	[1600 ±200]	[1650 ±250]
	2c(2b)	730 ±130	1725 ±325	690	>625	[1550 ±250]
Mitchell	2b	450 ±60	1525 ±275	590	[500]	1525 ±275
	1	<100	-	-	[300 ±200]	-
Sheba	3	<100	-	-	[1375 ±75]	[1375 ±75]
	2a	1350 ±250	-	1400	1350 ±250	-
	2b	470 ±70	-	620	750	-
	1	<100	-	-	[300 ±200]	-
Lone Star	1	<100	-	-	[300 ±200]	-
Hilchey	1	<100	-	-	[300 ±200]	-
27 Pup	1	<100	-	-	[300 ±200]	-
Violet	1	<100	-	-	340 ±260	-
Virgin	1	<100	-	-	700 ±250	-

¹ See text for explanation of inclusion types.

² See text and appendices for explanation of methods used and assumptions made in calculations.

³ Values in (parentheses) represent pressure ranges.

⁴ Pressures in [parentheses] calculated using the average quartz-muscovite stable isotope temperature (303±17°C) (Chapter VI). All other pressure are calculated from fluid inclusion homogenization temperatures (Table 1).

independent temperature estimate is required, for example from mineral-pair, stable isotope geothermometry; the point at which the calculated fluid isochore and the independent temperature line intersect on a P/T diagram, defines the approximate pressure of trapping (P_T) (Figure 17) (Shepherd et al., 1985).

For the Au-quartz lodes, an average temperature of $303 \pm 17^\circ\text{C}$, calculated from $\delta^{18}\text{O}$ analyses of two quartz-muscovite mineral pairs from the Sheba vein (Chapter VI), was used as an independently derived trapping temperature estimate. The foliaform veins appear to have formed under lower greenschist facies P - T conditions (Mortensen, 1990). Therefore, trapping pressures were calculated for type 1 and type 2 inclusions in foliaform vein quartz using an assumed temperature range of 350 - 400°C (Essene, 1988).

Au-Quartz Veins in the Central Klondike

Estimated trapping pressures for the main Au-bearing lodes in the central Klondike are given in Table 2. Using the quartz-muscovite temperature, type 2a inclusion fluids in Hunker vein quartz yield corrected pressures of 1600 ± 200 bars. For type 2a inclusions in Sheba vein quartz, the pressure at total homogenization (ca. 1350 ± 250 bars) has been taken as the trapping pressure, because the quartz-muscovite temperature is in good agreement with fluid inclusion homogenization temperatures and no pressure correction could be applied to the data from type 2a inclusions in these samples. Also, evidence presented below suggests that the fluid trapped in type 2a inclusions in the Sheba and Mitchell veins, was at, or was approaching, a state of immiscibility. Therefore, as the fluid was apparently trapped close to the 2-phase curve, the temperatures and pressures at homogenization closely approximate the P/T conditions at trapping.

For type 1, 2b and 2c inclusions from the Hunker, Mitchell and Sheba veins, the pressure at which the upper limit of the quartz-muscovite temperature (ca. 320°C) intersects the fluid isochores was taken as the trapping pressure. The upper temperature limit was used because it yields the maximum possible pressure estimate which can be made using

this method. The trapping pressures of 400-750 bars calculated for these inclusions, are substantially lower than the trapping pressures for type 2a and type 3 inclusions (see below) from the same veins.

To estimate the possible trapping pressure of type 3 inclusions, it was assumed that they were trapped at approximately the same temperatures as other inclusion types within the same samples. The type 3 fluid isochore was projected until it intersected the temperature range defined by the stable isotope pair ($303 \pm 17^\circ\text{C}$). The corresponding pressure range is 1375 ± 75 bars, which strongly suggests that type 2a and type 3 inclusions in Sheba vein quartz, although compositionally distinct, were trapped under very similar P-T conditions.

Au-Quartz Veins in the Southern Klondike

The quartz-muscovite mineral pair temperature was also applied to the CO₂-bearing veins in the southern part of the field area (e.g., Lloyd, Gold Run, Aime). Although homogenization temperatures decrease southwards from Hunker Dome (Figure 13), the decrease is probably a product of the increasing bulk fluid and CO₂-phase densities, in response to increasing total pressure within the original fluid system.

For southern veins, estimates of the pressure at total homogenization increase southwards with increasing CO₂-phase density (Table 2), which implies increasing depth within the system. For a fixed fluid composition, an increase in bulk density with pressure forces the fluid isochore origin coordinates towards higher pressures and lower temperatures, despite the fact that the true trapping temperature may actually be increasing (Bowers and Helgeson, 1983). Therefore, a correction factor (the pressure correction) must be applied to the average homogenization temperatures to revise them upwards, closer to the true fluid temperature at the time of trapping.

Two additional lines of evidence suggest that the decrease in mineralizing fluid temperature is only apparent: (1) $\delta^{18}\text{O}$ values of discordant vein quartz from Gold Run and

Aime do not increase towards the south, which would be expected if fluid temperatures were decreasing (assuming that the fluid had a uniform isotopic composition) (Chapter VI), (2) Mortensen (1990) reports an increase in the metamorphic grade of the country rocks towards lower Dominion Creek, implying that deeper structural levels are exposed in the south of the area. Consequently, it is concluded that the true trapping temperatures for the Aime and Gold Run lodes were probably equal to, or greater than, the homogenization temperatures of 300-350°C measured in the Hunker Dome region.

By again using the upper limit of the quartz-muscovite temperature, a pressure correction of 60°C can be applied to the Aime data, and 20°C for Gold Run (for most locations, the lower isotopic temperature limit (286°C) is either below the lower limit of the average $T_{H_{tot}}$, or does not intersect any of the calculated isochores). Corrected trapping pressures for Aime, Gold Run and Lloyd are 2070 ±420 bars, 1875 ±657 bars and 1625 ±375 bars respectively. Because the true magnitude of the required pressure correction is uncertain, and the calculations are necessarily constrained by the stable isotope temperature, these trapping pressures can probably be regarded as minimum estimates.

Trapping pressure estimates obtained through Brown and Lamb's (1989) construction method, are in reasonable agreement with the values reported above (Table 2).

Au-Quartz Veins in the Northern Klondike

The quartz-muscovite mineral pair temperature was also applied to the Lone Star, 27 Pup and Hilchey data, from the north of the area. Average fluid inclusion homogenization temperatures and $\delta^{18}O_{\text{quartz}}$ values from these veins, are similar to those from the Hunker Dome area, implying that the temperature of formation of veins from the two regions is similar (Table 2). Estimated trapping pressures from these veins are in the range 300 ±200 bars, which is slightly lower than pressures estimated from type 1 inclusions in the northernmost CO₂-bearing veins.

The Violet and Virgin lodes, and three other minor occurrences at French Gulch, Oro Fino and Bear Creek (Figure 8) have the lowest observed homogenization temperatures (ca. 190-230°C). Also, with the exception of the Virgin and Violet claims, $\delta^{18}\text{O}_{\text{quartz}}$ values of these samples are 2-3 ‰ heavier than average implying that fluid temperatures in this area were lower than those estimated for veins in the central Klondike region. In the absence of an acceptable mineral pair stable isotope temperature from any of the northern veins, an arbitrary trapping temperature of $250 \pm 25^\circ\text{C}$ has been assumed, which falls roughly between the northern fluid inclusion homogenization temperatures and the estimated trapping temperatures for the central Klondike veins. Using this temperature, trapping pressure estimates for the northern lodes range from 300 ± 200 to 750 ± 500 bars, which are in rough agreement with pressures estimated for type 1 fluids in the Sheba and Mitchell lodes.

Foliaform Veins

The upper limit of the assumed temperature range (see above) intersects the isochores in Figure 17b between 380 to 1250 bars. Over the same temperature range, using data from type 2 inclusions in sample YR24, the method of Brown and Lamb (1989) yields trapping temperatures of 2.3 to 3 kbars, for a volume % CO_2 estimate of 38 ± 8 %.

The true trapping temperature for foliaform vein fluids probably lies between the two extremes given above. However, given that the foliaform veins are probably older than the discordant lodes, one constraint which can be placed on the minimum pressure of formation of the foliaform veins is the maximum trapping pressure calculated for the younger, discordant veins in the south of the field area (i.e., ca. 2 kbars calculated for the Aime lode data).

Interpretation of Discordant Vein Data

Despite the large errors inherent in estimating P-X conditions from fluid inclusion data, there are significant regional trends apparent in the Au-quartz vein pressure and compositional data across the field area. Although the relative timing of vein formation in the southern, central and northern vein systems is uncertain, it is clear that the bulk fluid compositions and trapping pressures recorded by inclusions in the three areas differ significantly. Also, the central lodes appear to have trapped at least three different fluids, one of which (type 2b) appears to be transitional in composition and pressure between the southern CO₂-rich, and the northern CO₂-absent, fluids.

Type 2a inclusions in the Aime, Gold Run and Lloyd veins contain fluids with CO₂ concentrations in the range 0.10 to 0.15 mole fraction. Estimated trapping pressures for these veins decrease progressively northwards between the Aime and Lloyd veins. In the Hunker, Mitchell and Sheba veins, contrasting fluid compositions and pressures are seen. Pressures calculated from type 1, 2b and 2c inclusion fluids in these veins indicate that there was a drop in trapping pressure of approximately 800 to 1000 bars relative to type 2a inclusions from the same veins, and from veins further to the southeast. This pressure drop was accompanied by a reduction in the bulk fluid XCO₂, from between 0.15 to 0.20 mole fraction in Hunker/Sheba type 2a fluids, through intermediate concentrations of 0.09 mole fraction in type 2b inclusions, to <0.01 mole fraction in type 1 inclusions from central and northern veins.

Effervescence of CO₂

To account for the loss of CO₂ from the mineralizing fluid, effervescence of a CO₂-rich fluid from the type 2a fluid is interpreted to have occurred as the P-T path of the type 2a fluid passed through the solvus in the H₂O-CO₂-NaCl system. Although unmixing of CO₂ can occur due to a reduction in the temperature of the mineralizing fluid (Robert and Kelly, 1987; Bowers and Helgeson, 1983), the similarity in the homogenization

temperatures of all types of primary inclusions from veins in the central region argue against temperature loss as the dominant driving force behind CO₂ effervescence. Thus, unmixing probably occurred in response to the large pressure drop noted between type 2a and type 1 inclusions in the central region.

Mechanisms which may have caused effervescence to occur include a) loss of CO₂ in a response to a rapid pressure drop caused by a transition from suprahydrostatic or lithostatic, to hydrostatic fluid pressure conditions (e.g., the fault-valve mechanism of Sibson (1990)), or b) regional uplift and mineralization over an extended time period, allowing for gradual pressure reduction and loss of CO₂ from the fluid system (e.g. Diamond, 1990). These models will be discussed further in Chapter VII.

The end products of effervescence of CO₂ from a H₂O-CO₂-NaCl (\pm CH₄) fluid will be coexisting, but immiscible, CO₂-rich and H₂O-rich fluids (Ramboz et al., 1982). The likelihood that both of these fluids will be trapped as inclusions in the growing quartz crystals depends on a number of factors, such as the different wetting properties of H₂O and CO₂ liquids, and whether or not the system is open and allows removal of the CO₂ phase as it exsolves (Roedder, 1984).

Figures 18a, b, and c show the position of the solvus in the H₂O-CO₂-NaCl system, calculated for 6 wt.% NaCl in the aqueous phase, at pressures of 2.0, 1.5 and 0.5 kbars. Figure 18a shows the shape of the solvus at the approximate trapping pressure of type 2a inclusion fluids from the Aime lode (ca. 2 kbars). The stippled rectangle in Figure 18a is the area in T-X space occupied by the Aime, Gold Run, Lloyd and Hunker type 2a fluids (fluid temperatures have been corrected to the range 300-350°C). At a pressure of 2.0 kbars, only the most CO₂-rich fluid compositions lie on the solvus. In fact, the slightly lower calculated salinities of type 2a fluids (ca. 4-5 eq.wt.% NaCl), mean that the solvus position should actually be slightly lower than that shown, bringing the T-X rectangle further into the single phase region. Similarly, the temperature range used (ca. 300-350°C)

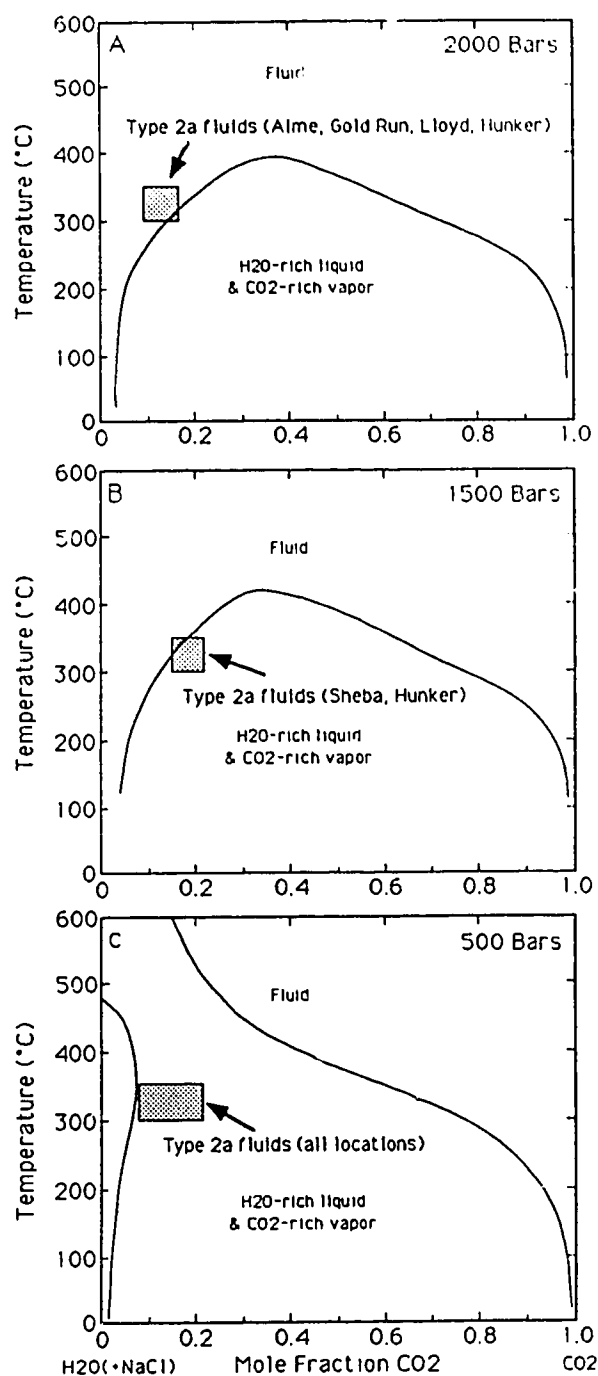


Figure 18. The shape of the solvus in the $\text{H}_2\text{O}-\text{CO}_2$ -NaCl system, at 6 wt.% NaCl and varying pressures. Modified from Bowers and Helgeson (1983). Stippled rectangle represents the T-X area occupied by type 2a inclusion fluids in CO_2 -bearing Au-quartz veins (see text).

is probably a minimum estimate. Therefore, although fluids trapped in the southern veins plot close to the solvus, it is likely that they were trapped as a single, homogeneous fluid.

Figure 18b shows the same system at 1500 bars, approximating the conditions calculated for type 2a fluids from Sheba and Hunker Dome. The T-X rectangle now clearly straddles the solvus. Any further reduction in pressure (such as that recorded between type 2a and 2b inclusions) will force the fluid into the 2-phase field as the area beneath the solvus expands, and a CO₂-rich phase will unmix from the parent fluid.

Although the pressure drop appears to have induced separation of a CO₂-rich phase, it was apparently not sufficient to cause the loss of significant amounts of H₂O_{vapor} by boiling. If an appreciable amount of steam was lost from the system, the residual fluid temperature would drop because of the high enthalpy of exsolution of steam (Lynch, 1989). Fluid inclusion homogenization temperatures, and $\delta^{18}\text{O}_{\text{quartz}}$ values from veins between the Lloyd and Lone Star showings are similar and argue against a significant temperature drop. Also, the average salinity of the residual H₂O_{liquid} phase, which should increase as H₂O_{vapor} is lost, does not change significantly across the area.

Criteria for Demonstrating Immiscibility

In order to demonstrate if any of the inclusions trapped in the Hunker Dome, Sheba, or Mitchell veins represent the exsolved CO₂-rich and H₂O-rich fluids, or perhaps the parent fluid, a number of criteria must be satisfied (Ramboz et al., 1982).

Firstly, if the presence of coexisting but immiscible fluids is inferred, the two fluids must be trapped in inclusions which are contemporaneous and preferably spatially related. Unfortunately, the milky, anhedral nature of the Au-bearing vein quartz, and the large number of primary and secondary inclusions present, rules out unequivocal satisfaction of this criterion (see above). However, type 1, 2 and 3 inclusions are commonly found within a few tens of microns of each other, and at times within the same field of inclusions, and may be contemporaneous.

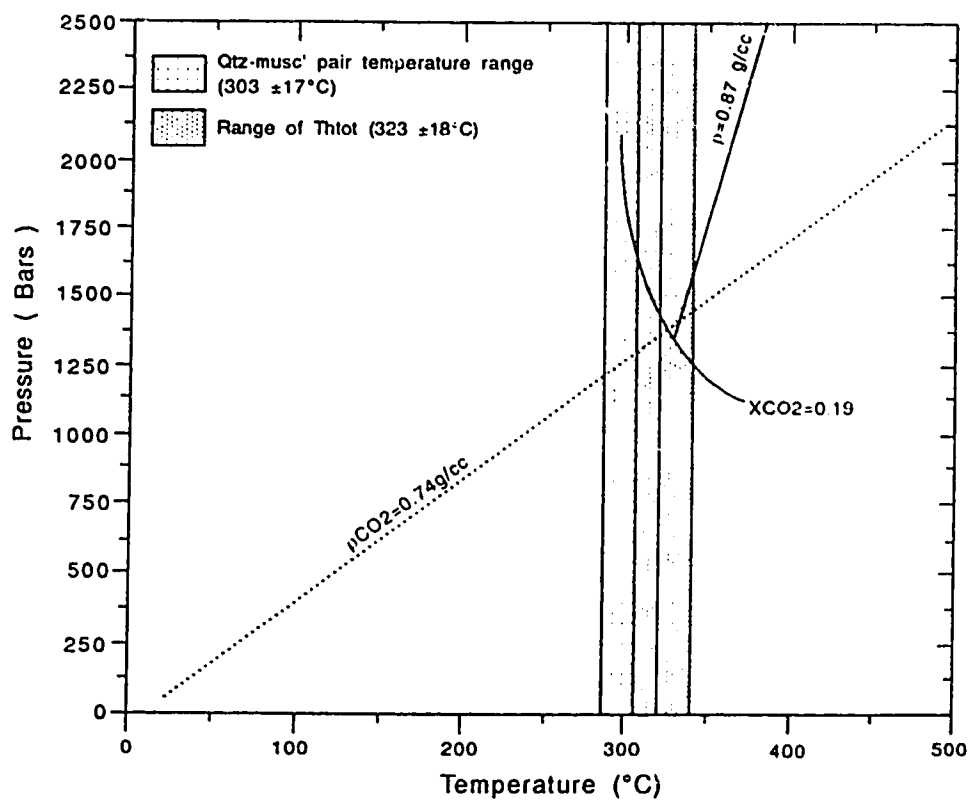


Figure 19. Isochores for type 2a and type 3 fluids from the Sheba vein. The estimated pressure at the intersection of the type 2a inclusion homogenization temperature range with the type 3 fluid isochore, and the pressure at the origin of the type 2a fluid isochore, are in close agreement. Isochores constructed from the data of Angus et al. (1976) and Bowers and Helgeson (1983). 2-phase curve constructed from the data of Takenouchi and Kennedy (1965).

Secondly, total homogenization of coexisting inclusion types must be in the same temperature range, at approximately equal internal pressures, one to the liquid phase and one to the vapor phase. Although type 1 inclusions homogenize at roughly the same temperature as type 2a inclusions, the estimated pressures at homogenization for the two types are roughly 1.0 kbar apart. However, the internal pressures of type 2a and 3 inclusions from Sheba vein quartz are approximately equal over the quartz-muscovite pair temperature range ($303 \pm 17^\circ\text{C}$) (Chapter VI). The type 3 fluid isochore intersects the projected temperature line at approximately 1350 ± 75 bars, whereas isochores calculated for the type 2a fluids intersect the 2-phase curve at approximately 1350 ± 250 bars (Figure 19).

Although type 2a and type 3 inclusions appear to have disparate homogenization temperatures (Table 1), only ThCO_2 was measured for type 3 inclusions, and it is not certain that they contain fluids which are comprised of 100 % CO_2 . A small proportion of H_2O within CO_2 -rich inclusions (ca. 5-10 vol.% H_2O) is easily overlooked (Goldfarb et al., 1989) and if H_2O is present, the homogenization temperature of type 3 inclusions will be much higher, and they will homogenize to the vapor phase. Therefore, type 2a and type 3 inclusions satisfy criterion 2, at least in part.

Nevertheless, despite the similarity in trapping pressures between the two inclusion types, the dominance of primary, type 2a inclusions in quartz from southern veins which apparently trapped an homogeneous, single phase fluid (see above), suggests that the type 2a fluid is actually the parent fluid from which the immiscible phases were exsolved, rather than an exsolved end-member fluid.

Generation of the observed compositional and P-T trends through mixing of two chemically distinct fluids is thought unlikely for a number of reasons: (1) inclusion fluid temperatures and salinities show very little variation across the transition zone between aqueous and CO_2 -bearing veins, and no mixing trends can be discerned within the data, (2) stable isotope data from northern, central and southern discordant veins indicate that the

fluids responsible for formation of the veins were isotopically similar, and again, no obvious mixing trends were seen (see below).

Thus, it is suggested that type 1 primary inclusions in central and northern veins (and possibly type 1 secondary inclusions in southern veins) probably trapped the late, residual, CO₂-depleted, aqueous fluid, whereas type 3 inclusions from the Sheba vein trapped the exsolved, CO₂-rich fluid phase. Type 2a fluids represent the parent fluid, and type 2b fluids may represent the parent fluid which has been partially depleted in CO₂.

VI. LIGHT STABLE ISOTOPE STUDY

Introduction

In conjunction with the fluid inclusion study, a regional stable isotope study of foliaform and Au-quartz vein minerals (quartz, carbonate and muscovite), was carried out in order to investigate the origin, isotopic nature, and the degree of chemical evolution of the fluids responsible for vein formation. Also, with the emergence of regional P-T-X trends in the Au-bearing vein fluid inclusion data (Chapter V), it was hoped that parallel enrichment/depletion trends would be discernible within the stable isotope data. In addition, samples of calcite from ultramafic-hosted carbonate veins, and from epithermal veins of possible Eocene age (J. Mortensen, pers. comm.) in the Germaine Creek area, were also analyzed.

Silicate samples were analyzed using the standard BrF_5 technique of Clayton and Mayeda (1963). Carbonates were reacted with phosphoric acid according to the method of McCrea (1951). Inclusion fluids from quartz, and two samples of hydrothermal muscovite, were analyzed for their deuterium/hydrogen ratios. Quartz samples were coarsely crushed, acid washed and then heated under vacuum to decrepitate fluid inclusions and liberate their contents. Muscovite samples were first degassed at 150°C , and then dehydrated at $\approx 1100^\circ\text{C}$ under vacuum. Water released from fluid inclusions and muscovite, was reduced with zinc metal to generate H_2 for analysis (Coleman et al., 1982). All isotopic data are reported in the conventional δ notation, relative to SMOW standard for oxygen and hydrogen, and PDB for carbon isotopes. Uncertainties on $\delta^{18}\text{O}$ and $\delta^{13}\text{C}$ analyses are $\pm 0.1\text{‰}$, and $\pm 3.0\text{‰}$ for δD (Nesbitt et al., 1989).

Results

The $\delta^{18}\text{O}$, δD and $\delta^{13}\text{C}$ values of mineral separates and inclusion fluids are presented in Table 3, and by sample location in Figures 20 and 21. Errors quoted below represent plus/minus one standard deviation.

Oxygen and Carbon Isotopes

$\delta^{18}\text{O}$ values of Au-bearing vein quartz range from 11.1 to 19.3 ‰, and average 14.9 ± 1.6 ‰, with a median value of ca. 15-16 ‰ (Figure 22). Discordant veins in the far northwest of the Klondike region appear to have heavier $\delta^{18}\text{O}_{\text{quartz}}$ values than veins further southeast, consistent with the lower fluid inclusion homogenization temperatures recorded in this area (Figure 8, Chapter V).

In contrast, foliaform quartz samples have a wider spread of $\delta^{18}\text{O}$ values and range from 7.4 to 18.7 ‰ (Figure 22a), also with a higher proportion of heavy values towards the northwest. Mortensen et al. (in press) note that there is no consistent pattern of enrichment or depletion of ^{18}O between foliaform and Au-quartz veins. However, although the average $\delta^{18}\text{O}$ for foliaform vein quartz of 13.1 ± 3.2 ‰ overlaps the Au-quartz vein average (ca. 14.9 ± 1.6 ‰), it is evident from Figure 22a, that there is a greater degree of heterogeneity within the foliaform data. When the oxygen isotope data for foliaform veins are broken down by host lithology (Figure 23), there appears to be a greater spread in the $\delta^{18}\text{O}$ ratios of quartz veins hosted by rocks with sedimentary protoliths: i.e., the carbonaceous quartz-muscovite schist, and micaceous/chloritic quartzite. Discordant veins, which are hosted predominantly by the chloritic schist and the quartz-augen schist, appear to show much less variation with host lithology.

Two samples of amethyst, RR287B and RR137B, which were collected from vugs in mesothermal veins in the Hunker Dome area (Chapter IV) yielded $\delta^{18}\text{O}_{\text{quartz}}$ values of -4.4 and -6.7 ‰ respectively, whereas the host mesothermal quartz veins yielded significantly heavier values of 12.4 and 13.8 ‰, respectively (Table 3).

$\delta^{18}\text{O}_{\text{calcite}}$ values from Au-quartz veins range from 4.3 to 15.9 ‰ (Table 3). $\delta^{13}\text{C}_{\text{calcite}}$ and $\delta^{13}\text{C}_{\text{CO}_2}$ from the same veins range from -1.2 to -21 ‰, with an average value of -8.2 ± 2.3 ‰. Calcite samples from foliaform veins have $\delta^{18}\text{O}$ values of 10.6 to 16.1 ‰, and $\delta^{13}\text{C}_{\text{calcite}}$ and $\delta^{13}\text{C}_{\text{CO}_2}$ values which range from -5.4 to -16.7 ‰, and average -11.4 ± 3.5 ‰. Calcite from two samples of Eocene epithermal veins, collected

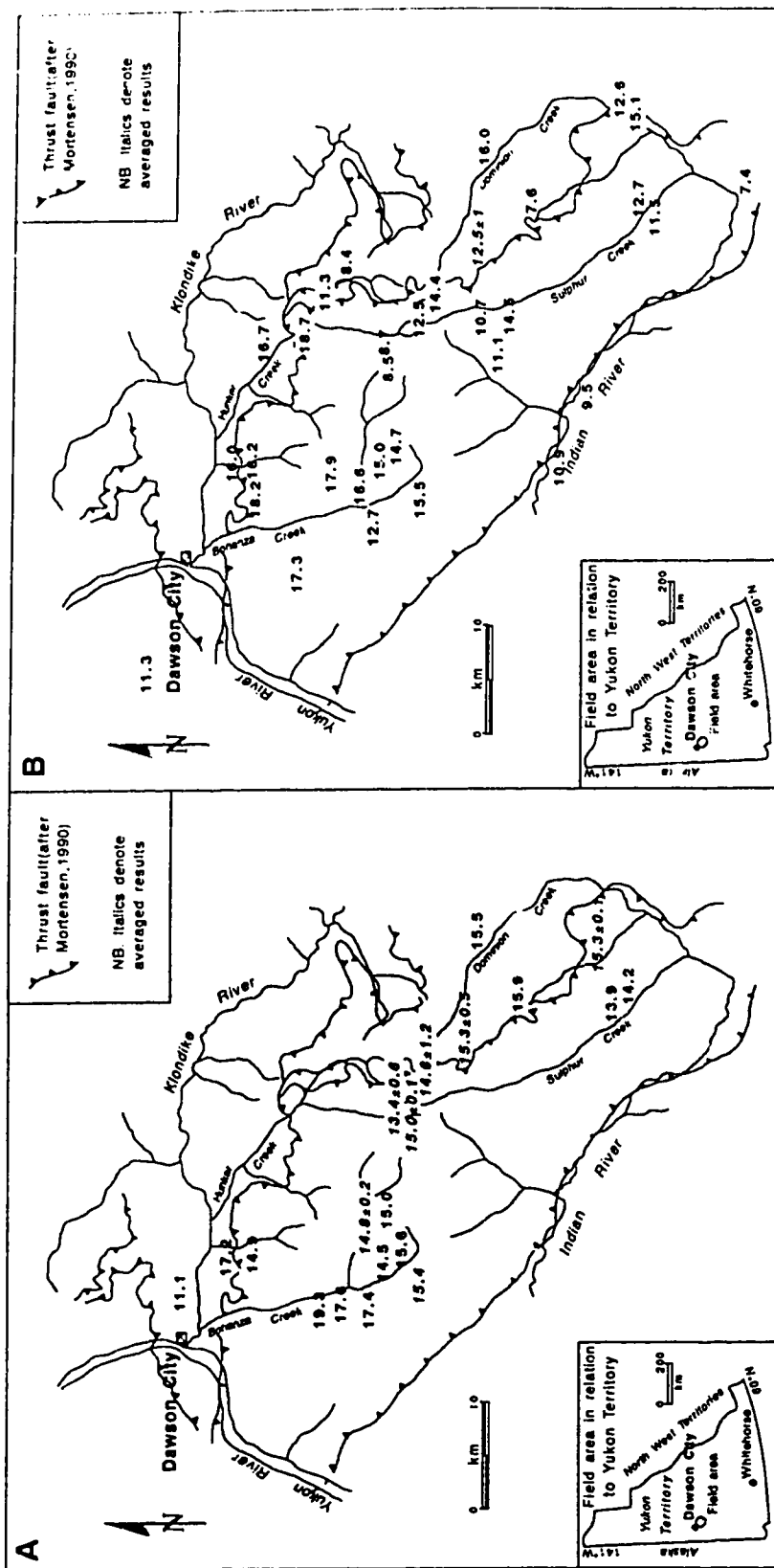


Figure 20. Oxygen isotope analyses of quartz from: A. Au-bearing, mesothermal veins, B. unmineralized, foliaform veins ($\delta^{18}\text{O}\text{‰ SMOW}$). See also Table 3.

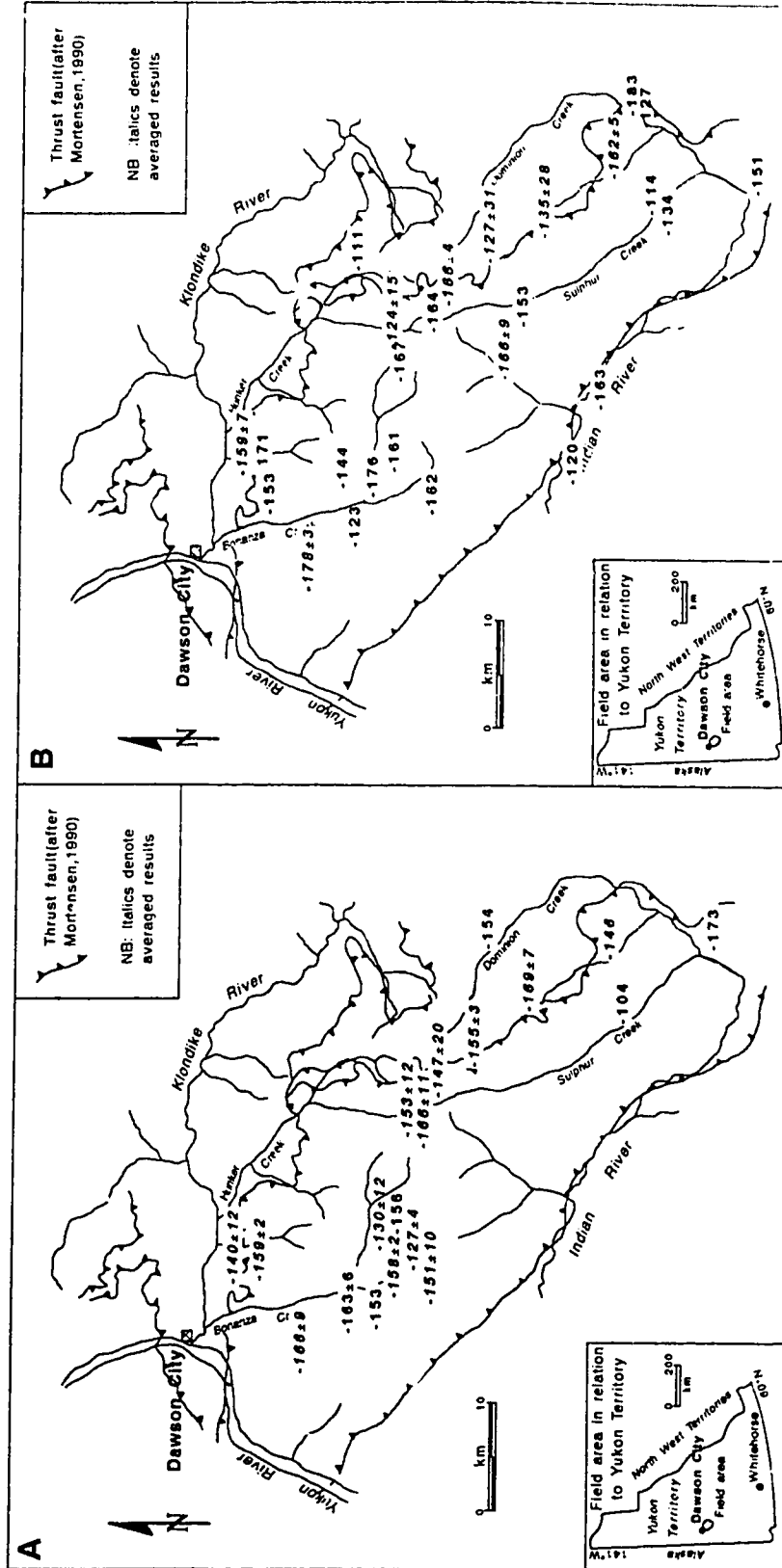


Figure 21. Hydrogen isotope analyses of inclusion fluids in quartz from: A. Au-bearing, mesothermal veins, B. unmineralized, foliaform veins ($\delta D\text{‰ SMOW}$). See also Table 3.

Table 3. Light Stable Isotope Analyses of Vein Minerals from Au-quartz and Foliiform Veins, Klondike District (see Appendix 5 for detailed sample locations).

Location/ Occurrence	Sample Number ¹	Mineral ¹	$\delta^{18}\text{O}$ ‰ (SMOW)	δD^2 ‰ (SMOW)	$\delta^{13}\text{C}^3$ ‰ (PDB)	Fluid ⁴ Temp. (T°C)	$\delta^{18}\text{O}_{\text{Fluid}}^5$ ‰ (SMOW)
<i>Au-quartz veins</i>							
EUREKA Ck	RR69	Cc	9.5		-7.8	303±17 [†]	-4.0±0.5
AIME	YR64	Qtz	15.2			303±17 [†]	8.4±0.6
	YR66	Qtz	15.4	-146		303±17 [†]	8.6±0.6
DOMINION	YR20	Qtz	15.5	-154		303±17 [†]	8.7±0.6
SULPHUR	YR28	Qtz	14.2			303±17 [†]	7.4±0.6
	YR30	Qtz	13.9	-104		303±17 [†]	7.1±0.6
	YR63	Qtz		-173			
GOLD RUN	RR95	Qtz	15.7	-163		303±17 [†]	8.9±0.6
	rep.	Qtz	15.9			303±17 [†]	9.1±0.6
	RR96	Qtz		-179			
	rep.	Qtz		-166			
LLOYD	KS6	Qtz	14.8	-151	-14.7 [‡]	304±10 [*]	8.0±0.6
	YR31 rep.	Qtz	15.8	-154		304±10 [*]	9.0±0.6
		Qtz		-159			
HUNKER DOME	KS1	Qtz	15.3	-161	-10.7 [‡]	318±30 [*]	9.0±0.9
	rep.	Qtz		-155			
	KS2	Qtz	15.4	-160	-12.3 [‡]	318±30 [*]	9.1±0.9
	YR17 YR18	Qtz	15.0	-113		318±30 [*]	8.7±0.9
		Qtz	15.7			318±30 [*]	9.4±0.9
	RR137A	Qtz	13.8			318±30 [*]	7.5±0.9
	RR287A	Qtz	12.4			318±30 [*]	6.1±0.9
RR287B	Am	-4.4			341±11 [*]	-9.9±0.2	
RR137B	Am	-6.7	-134		341±11 [*]	-12.2±0.2	
MITCHELL	KS4	Qtz	12.9	-143	-7.2 [‡]	324±17 [*]	6.8±0.6
	rep.	Qtz		-138			
	KS5	Qtz	13.1	-169		324±17 [*]	7.0±0.6
	rep.	Qtz	14.3	-164		324±17 [*]	8.2±0.6
	RR143	Qtz		-150			
SHEBA	RR272	Qtz	14.9	-155		303±17 [†]	8.1±0.6
	rep.	Qtz	15.1			303±17 [†]	8.3±0.6
	RR274	Qtz	15.1	-177		303±17 [†]	8.3±0.6
	rep.	Qtz	14.7			303±17 [†]	7.9±0.6
	MLB-89- 263	Musc Musc	10.1	(-178) (-185)		303±17 [†]	6.8±0.4

Table 3 continued

Location/ Occurrence	Sample Number ¹	Mineral ¹	$\delta^{18}\text{O}$ ‰ (SMOW)	δD^2 ‰ (SMOW)	$\delta^{13}\text{C}^3$ ‰ (PDB)	Fluid ⁴ Temp. (°C)	$\delta^{18}\text{O}_{\text{Fluid}}^5$ ‰ (SMOW)
<i>Au-quartz veins cont.d</i>							
Sheba Cont.d	MLB-89- 264	Musc Musc	9.2	(-186) (-192)		303±17 [†]	5.9±0.4
LONE STAR	KS8 rep.	Qtz Qtz	14.4	-124 -140	-21 [‡]	292±12*	7.3±0.5
	RR322 rep.	Qtz Qtz	15.1	-131 -110		292±12*	7.9±0.5
	RR326	Qtz	14.8	-145		292±12*	7.6±0.5
PIONEER ADIT	KS10	Qtz	15.0	-156		292±12*	7.8±0.5
27 PUP	RR283 rep.	Qtz Qtz	14.5	-157 -159		313±18*	8.1±0.6
HILCHEY	RR135 RR312	Qtz Qtz		-123 -131		297±19*	8.6±0.7
FRENCH GULCH	RR302	Qtz	17.4	-153		303±17 [†]	10.6
VIOLET	RR131 RR132 RR128	Qtz Qtz Qtz	15.4	-162 -137 -153		225±9* 225±9*	5.2±0.5 5.2±0.5
PLINK	YR67 YR69	Qtz Qtz		-157 -175			
VIRGIN	YR9 rep. YR60 rep.	Qtz Qtz Cc Cc Qtz		-156 -156			
	RR114 rep. rep.	Qtz Qtz Qtz	14.9	-117 -119 -159		198±12*	3.2±0.7
BEAR CK	YR5 rep. rep.	Qtz Qtz Qtz Cc	17.2	-152 -127 -143		198±12*	5.5±0.7
			16.2		-11.3	198±12*	6.6±0.6
ADAMS CK	YR70 rep.	Qtz Qtz	17.6	-157 -169		238*	8.1
OROFINO	YR36 rep.	Qtz Qtz	19.3	-146 -172	-6.6 [‡]	238*	9.8

Table 3 continued

Location/ Occurrence	Sample Number ¹	Mineral ¹	$\delta^{18}\text{O}$ ‰ (SMOW)	δD^2 ‰ (SMOW)	$\delta^{13}\text{C}^3$ ‰ (PDB)	Fluid ⁴ Temp. (T°C)	$\delta^{18}\text{O}_{\text{Fluid}}^5$ ‰ (SMOW)
DOMERd	YR1	Qtz	11.1	-164	-8.3 [‡]		
<i>Foliaform Veins</i>							
AIME	YR65	Qtz		-167			
	rep.	Qtz		-157			
EUREKA CK	RR66	Qtz	7.4	-151		350	2.1
DOMINION	YR22	Qtz	12.6	-183	-10.7 [‡]	350	7.3
DOMINION	YR24	Qtz	15.1	-127	-5.2 [‡]	350	9.8
CK	YR61	Qtz	16.0			350	10.7
SULPHUR	YR27	Qtz	11.3			350	6.0
CK.	YR29	Qtz	12.7	-114		350	7.4
	RR37	Qtz	10.7			350	5.4
	RR56	Qtz		-145		350	7.4
		Cc	11.7		-9.7		
	RR187	Qtz	14.5	-153		350	9.2
	RR253	Qtz	11.5	-134		350	6.2
GOLD RUN	RR84	Qtz		-175			
	RR85	Qtz		-157			
	RR89	Qtz	7.6	-114		350	2.3
	rep	Qtz		-151			
LLOYD	KS7	Qtz	13.8	-132		350	8.5
	YR32	Qtz	12.5	-171		350	7.2
	YR33	Qtz	11.2	-102	-4.7 [‡]	350	5.9
INDIAN	RR165	Qtz	9.5	-163		350	4.2
	RR299	Qtz	10.9	-120		350	5.6
QUARTZ CK	RR18	Qtz	11.1	-160		350	5.8
	rep.	Qtz		-173			
HUNKER	KS3	Qtz	14.4	-169		350	9.1
DOVE	rep.	Qtz		-163			
	RR288	Qtz		-130			
SHEBA	RR262	Qtz	12.5	-164		350	7.2
PIONEER	KS11	Qtz	14.7			350	9.4
ADIT							
LONE STAR	KS9	Qtz	15.0	-161		350	9.7
FRENCH Gch	RR301	Qtz	12.7			350	7.4

Table 3 continued

Location/ Occurrence	Sample Number ¹	Mineral ¹	$\delta^{18}\text{O}$ ‰ (SMOW)	δD^2 ‰ (SMOW)	$\delta^{13}\text{C}^3$ ‰ (PDB)	Fluid ⁴ Temp. (T°C)	$\delta^{18}\text{O}_{\text{Fluid}}^5$ ‰ (SMOW)
<i>Foliaform Veins cont.d</i>							
FRENCH GULCH	RR301	Cc	12.1		-11.8	350	7.8
UPPER BONANZA	RR32	Qtz	8.5	-167		350	3.2
	RR306	Qtz	17.9	-144		350	12.6
	RR171	Qtz	16.6	-171		350	11.3
HUNKER Ck	YR11	Qtz	16.7			350	11.4
	YR12	Qtz	11.3			350	6.0
	YR14	Qtz	8.4	-111		350	3.1
	RR155	Qtz	18.7			350	13.4
GOLD BOTTOM	RR151	Qtz	8.7	-109		350	3.4
	rep.	Qtz		-139			
VIRGIN & BEAR Ck	YR4	Qtz	16.0	-154		350	10.7
	rep.	Qtz		-164		350	11.8
		Cc	16.1		-10.9		
	YR7	Qtz	16.2	-171		350	10.9
		Cc	11.0		-5.4	350	6.7
TRAIL HILL	YR38	Qtz	18.2	-153		350	12.9
YUKON RIV.	YR35	Qtz	18.8	-112		350	13.5
PLINK RIDGE	YR68	Qtz	17.3	-175		350	12.0
	rep.	Qtz		-180			
ADAMS Ck	YR71	Qtz		-123	-16.7 [‡]		
VIOLET	RR124	Qtz	15.5	-162		350	10.2
CULLEN	RR120	Cc	10.6		-13.6	350	6.3
	RR122	Qtz		-161			
<i>Carbonate (\pmquartz) veins in greenstone/ultramafic host rocks</i>							
BEN LEVY	YR10	Cc	11.6		-0.8	300 \pm 50	6.0 \pm 1.3
	KS12	Cc	10.8		-0.9		5.2 \pm 1.3
YUKON R.	YR34	Cc	7.6		-1.1	300 \pm 50	2.0 \pm 1.3
		Qtz	11.2	-105			4.3 \pm 1.6
	rep.	Qtz		-106			
ROCK Ck	RR160	Cc	14.2		-6.7	300 \pm 50	8.6 \pm 1.3
HUNKER DOVE	RR370	Cc	18.3		-6.6	300 \pm 50	12.7 \pm 1.3

Table 3 continued

Location/ Occurrence	Sample Number ¹	Mineral ¹	$\delta^{18}\text{O}$ ‰ (SMOW)	δD^2 ‰ (SMOW)	$\delta^{13}\text{C}^3$ ‰ (PDB)	Fluid ⁴ Temp. (T°C)	$\delta^{18}\text{O}_{\text{Fluid}}^5$ ‰ (SMOW)
<i>Epithermal veins, Germaine Creek</i>							
GERMAINE	RR247	Cc	6.7		-4.8	250 ±50	-0.6±2.0
CREEK	RR249	Cc	6.8		-4.8	250 ±50	-0.5z±2.0

¹ Abbreviations, rep.=Repeat analysis, Cc=Calcite, Qtz=Quartz, Musc=Muscovite, Am=Amethyst

² D/H analyses of inclusion fluids except results in parentheses, which are uncorrected D/H analyses of muscovite separates.

³ All samples analysed are calcite, except ‡ analyses of CO₂ from inclusion fluids

⁴ All temperatures are assumed ranges (see text for explanation) except, * fluid inclusion homogenization temperature, † stable isotope quartz-muscovite mineral pair temperature.

⁵ See Appendix 4 for equilibrium fractionation equations used in calculations.

from the Germaine Creek prospect, gave $\delta^{18}\text{O}_{\text{calcite}}$ values of 6.7 and 6.8 ‰ respectively, and identical $\delta^{13}\text{C}_{\text{calcite}}$ values of -4.7 ‰ for both samples.

Four samples of vein calcite were also analyzed from veins hosted within greenstones or ultramafic rocks. Sample YR10 from the Ben Levy vein (Figure 2), which is a 5 m thick, finely banded carbonate vein hosted by carbonate-silica altered serpentinite (Mortensen et al., in press), gave $\delta^{13}\text{C}_{\text{calcite}}$ values of -0.8 to -0.9 ‰, and a $\delta^{18}\text{O}_{\text{calcite}}$ value of 11.2 ± 0.4 ‰. A second serpentinite-hosted calcite sample (RR370) was collected from a thrust plane in the Hunker Dome area (Figure 6), and gave $\delta^{13}\text{C}_{\text{calcite}}$ and $\delta^{18}\text{O}_{\text{calcite}}$ values of -6.6 ‰ and 18.3 ‰, respectively. Finally, 2 calcite samples from veins hosted by greenstones (YR34 and RR160) had $\delta^{13}\text{C}_{\text{calcite}}$ values of -1.1 ‰ and -6.7 ‰, and $\delta^{18}\text{O}_{\text{calcite}}$ values of 7.6 ‰ and 14.2 ‰, respectively.

Hydrogen Isotopes

Deuterium analyses were performed on inclusion fluids from a number of quartz samples, as well as two samples of hydrothermal muscovite from the Sheba vein. δD values of Au-quartz vein inclusion fluids range from -104 to -179 ‰, and average -150 ± 18 ‰ (Figure 22). Fluids from foliaform vein quartz have a range of -102 to -183 ‰, and have a similar average of -150 ± 22 ‰. As with the $\delta^{18}\text{O}_{\text{quartz}}$ values, the Au-quartz vein deuterium data appear to show a greater degree of homogeneity between locations. There are no apparent geographical enrichment or depletion trends in the deuterium data. Muscovite samples MLB-89-263 and MLB-89-264, from the Sheba vein, yielded average δD values of -182 and -189 ‰ respectively. Inclusion fluids in quartz from the same sample locations have δD values of -155 and -177 ‰, respectively.

Mineral Pair Geothermometry

The simple vein mineralogy, encountered in foliaform and Au-quartz veins, limited the applicability of mineral pair, isotope geothermometry. However, fluid temperatures

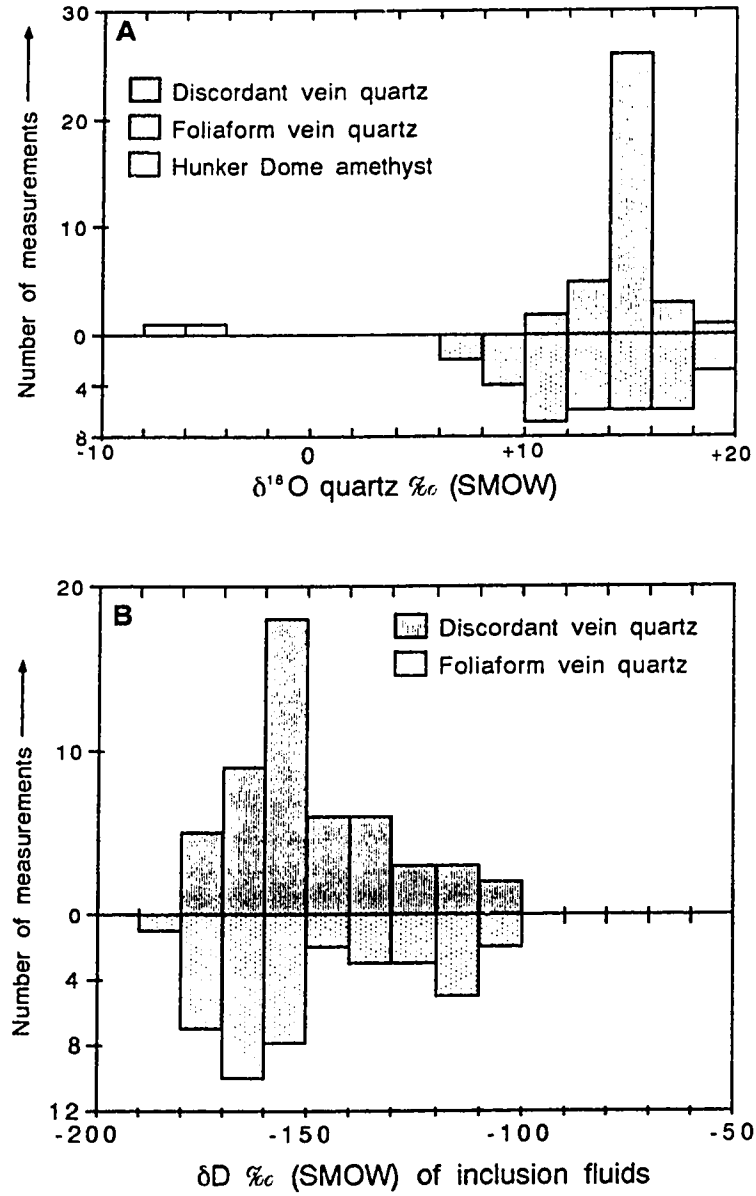


Figure 22. A. Comparison of $\delta^{18}\text{O}_{\text{quartz}}$ analyses, and B. comparison of δD analyses of inclusion fluids, from Au-bearing and foliaform vein quartz samples.

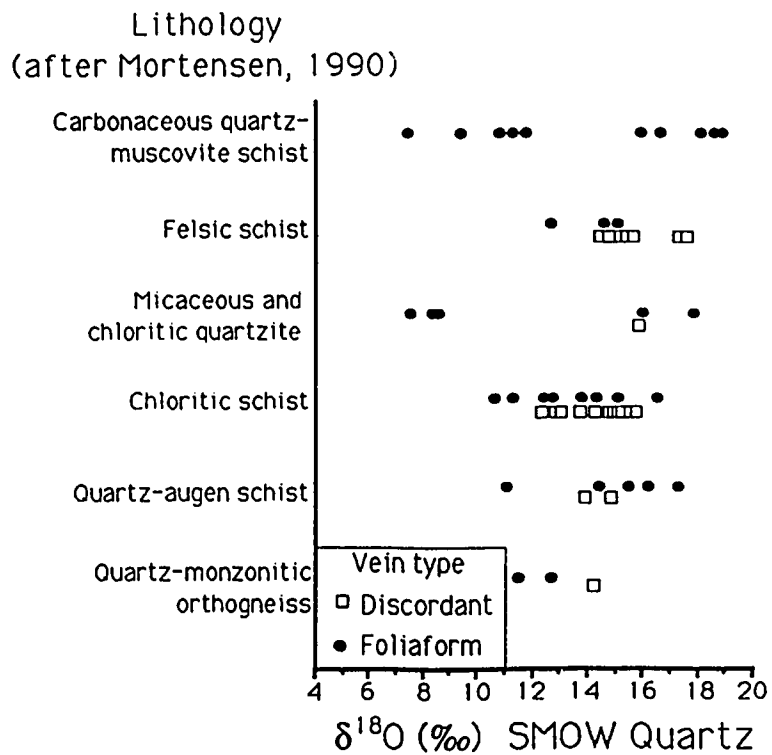


Figure 23. $\delta^{18}\text{O}_{\text{quartz}}$ of Au-bearing and foliaform vein quartz, against vein host lithology.

were calculated from two quartz-muscovite, and six quartz-calcite pairs, for comparison with temperature estimates derived from fluid inclusion evidence and metamorphic mineral assemblages (e.g., Mortensen, 1990).

Two quartz-muscovite mineral separates were obtained from samples collected from the Sheba claim group; one pair from the largest quartz vein exposed in trenching at the prospect, and the second pair from a minor discordant vein approximately 50 m south of the first. Textural evidence suggests that the micas are coeval with the main stage of quartz formation.

$\delta^{18}\text{O}$ values for the muscovite samples are 10.1 and 9.2 ‰, respectively. $\delta^{18}\text{O}$ values for the corresponding quartz samples (RR272 and RR274) averaged 15.0 and 14.9 ‰ respectively, yielding $\Delta_{\text{qtz-musc}}$ values of 4.9 and 5.7 ‰ respectively. When the fractionation values are plotted on an isotope exchange equilibrium diagram (Figure 24), tie lines for both mineral pairs are approximately parallel to the calculated equilibrium tie lines (over the temperature range 275-350°C), indicating that both pairs approached, or attained, isotopic equilibrium at around this temperature range.

Temperatures were calculated for the quartz-muscovite fractionations using an unpublished, experimentally derived fractionation expression (T. Chacko, pers. comm., Appendix 4). Calculated temperatures for the pairs are 315° and 290°C, respectively. The average for both pairs, when errors are taken into account, is $303 \pm 17^\circ\text{C}$ which is in good agreement with the average fluid inclusion T_{tot} of $323 \pm 18^\circ\text{C}$, obtained from the same vein system (Table 1).

In addition to the quartz-muscovite pairs, a number of quartz-calcite pairs were available from foliaform and Au-quartz veins. However, the use of quartz-calcite pairs in geothermometry can be hampered by oxygen isotope exchange between calcite and later fluids, and compositional variations within calcite which have a significant effect on the $\delta^{18}\text{O}$ values (Kyser, 1987).

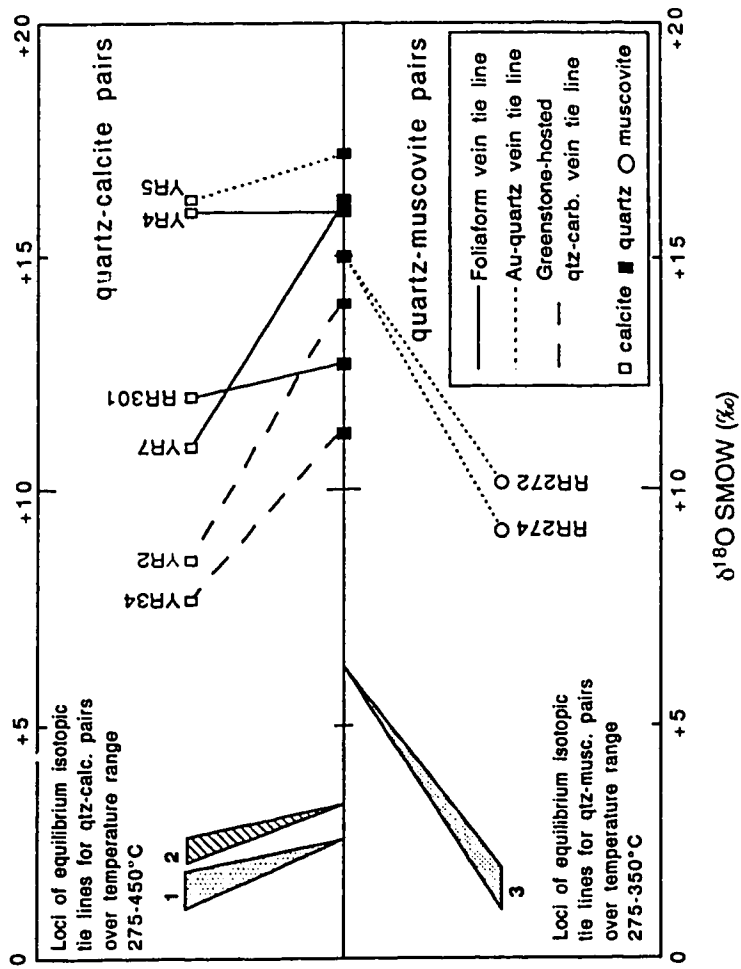


Figure 24. Exchange equilibrium diagram for quartz-calcite, and quartz-muscovite mineral pairs from Au-bearing and foliiform vein quartz. Only two quartz-calcite pairs are approaching isotopic equilibrium over the estimated temperature range. Loci of tie lines calculated from equilibrium fractionation expressions of 1. Matsuhisa et al. (1979) and O'Neil et al. (1969), 2. Clayton et al. (1989), 3. unpublished quartz-muscovite fractionation expression (T. Chacko, pers. comm.). Diagram adapted from Rumble (1978).

Figure 24 demonstrates that only two of the quartz-calcite pairs- YR5 (from a vein in the northern Klondike), and RR301 (from a foliaform vein)- approach isotopic equilibrium over the temperature range 275-450°C. Temperatures obtained for these pairs are 355°C and 468°C respectively. On the basis of fluid inclusion evidence (Chapter V), the temperatures calculated for both pairs are considered to be erroneously high. Calculated temperatures for the remaining pairs fall outside the range of geologically reasonable temperatures, and are thought not to be equilibrium temperatures.

Fluid Isotopic Signature

If the temperature of a hydrothermal fluid is known, or can be inferred, the isotopic signature of the fluid can be calculated from oxygen and hydrogen isotope analyses of minerals precipitated from the fluid. Such data reveals much about the ultimate genesis/source of the fluids, its degree of interaction with the country rocks and mechanisms of vein formation. In the following discussion, $\delta^{18}\text{O}_{\text{fluid}}$ and $\delta\text{D}_{\text{fluid}}$ refer to the aqueous phase of the $\text{H}_2\text{O}-\text{CO}_2-\text{NaCl} (\pm\text{CH}_4)$ bulk fluid.

Choice of Equilibrium Fractionation Expressions

For $\delta^{18}\text{O}_{\text{quartz}}$ analyses, the quartz-water fractionation factor of Matsuhisa et al. (1979) was used to calculate the $\delta^{18}\text{O}$ value of equilibrated fluids (Appendix 4). The δD value of the fluids in equilibrium with muscovite samples from the Sheba vein, can be calculated using the factor from Suzuoki and Epstein (1976), however the validity of extrapolating this expression below 400°C is questionable (Bowers and Taylor, 1985). Therefore, in this study, the "best fit" calibration of Bowers and Taylor (1985) (Appendix 4) has been used in conjunction with the expression of Suzuoki and Epstein (1976) for comparison. The $\delta^{18}\text{O}$ values of fluids in equilibrium with the muscovite samples were calculated using O'Neil and Taylor's (1969) fractionation expression. The equation of

O'Neil et al. (1969) was used to calculate $\delta^{18}\text{O}_{\text{fluid}}$ values from calcite analyses.

Calculation of $\delta^{13}\text{C}_{\text{CO}_2}$ in equilibrium with calcite used the calibration of Bottinga (1968).

Fluid temperature

Au-Quartz Veins

The choice of temperature used in $\delta^{18}\text{O}_{\text{fluid}}$ and $\delta\text{D}_{\text{fluid}}$ calculations varied across the field area. Evidence for effervescence of CO_2 in the central part of the vein system (Chapter V) means that the fluid inclusion homogenization temperatures recorded from these veins are probably close to the fluid temperature at the time of trapping. Also, the fluid inclusion study indicates that paleodepths increase towards the southeast from the central region, and that homogenization temperatures obtained from Au-quartz veins in the southeastern part of the Klondike (e.g., Gold Run, Aime) require the addition of a pressure correction to bring them closer to the trapping temperature (Chapter V). The only available independent temperature estimate available in this study is the average quartz-muscovite mineral pair temperature calculated for the Sheba vein system (see above).

In Chapter V it was suggested that fluid temperatures for Au-quartz veins in the southeast of the region were at least equal to, or greater than, those calculated for the central locations. Therefore, the quartz-muscovite temperature ($303 \pm 17^\circ\text{C}$) has been used for Au-quartz vein locations southeast of Sheba, where the measured Th_{TOT} is below ca. 303°C . For CO_2 -bearing veins which yielded homogenization temperatures equal to, or greater than 303°C , the fluid inclusion homogenization temperature has been used in all calculations.

North and northwest of the central lodes (e.g., Lone Star, Hilchey), $\delta^{18}\text{O}_{\text{quartz}}$ and Th_{TOT} values suggest that fluid trapping temperatures were slightly lower than those from central and southern regions. No independent temperature estimates were available for these veins, thus the uncorrected fluid inclusion temperatures have been used in the

calculations. By not applying a pressure correction to these temperatures, the resulting $\delta^{18}\text{O}_{\text{fluid}}$ values will be somewhat lower than the true values.

Folliciform Veins

The calculation of $\delta^{18}\text{O}_{\text{fluid}}$ values for foliaform quartz data was problematical because of much poorer control over fluid temperature estimates. Fluid inclusion homogenization temperatures, which range from 100-450°C, are biased by a high proportion of secondary inclusions and evidence for leakage of primary inclusions (Chapter V). Mortensen et al. (in press) suggest that the foliaform veins are syn-F2 and were formed during lower-greenschist metamorphism. Therefore, assuming a temperature range of 300-500°C for greenschist facies metamorphism (Essene, 1988), a temperature of 350°C was used in all foliaform $\delta^{18}\text{O}_{\text{fluid}}$ calculations, which does not account for the presence of thermal gradients across the area, or for local thermal perturbations.

Mesothermal Vein Fluid Composition

Au-Quartz Veins

The calculated $\delta^{18}\text{O}_{\text{fluid}}$ of Au-quartz veins range from 3.2 to 10.6 ‰ and average 7.8 ± 1.5 ‰. Despite the range in $\delta^{18}\text{O}_{\text{fluid}}$ values, the average values for each location show much less variability, falling between 7 to 10 ‰ (Table 4). $\delta\text{D}_{\text{fluid}}$ values of inclusion fluids and calculated from δD analyses of muscovite (see below), range from -104 to -179 ‰, with an average of -150 ± 18 ‰.

The trend towards heavier $\delta^{18}\text{O}_{\text{quartz}}$ values in the northwest of the field area is consistent with either a decrease in the mineralizing fluid temperature, or a decrease in the $\delta^{18}\text{O}$ value of the fluid. On the basis of the fluid inclusion study (Chapter V), the first explanation is preferred here. Average homogenization temperatures appear to decrease significantly to the north and northwest of the Lone Star area, and although the magnitude of the pressure correction which must be applied to these temperatures is uncertain, the

Table 4. Summary of Fluid Isotopic Compositions from the Principal Discordant, Au-Quartz veins, Klondike Region.

Location/ Occurrence	Mineral	$\delta^{18}\text{O}_{\text{fluid}}\text{‰ (SMOW)}^1$			$\text{dD}_{\text{fluid}}\text{‰ (SMOW)}^2$		
		No. of analyses	Mean	Standard deviation ³	No. of analyses	Mean	Standard deviation
Aime	Quartz	2	8.5	0.6	1	-146	
Gold Run	Quartz	2	9.0	0.6	3	-169	7
Lloyd	Quartz	2	8.5	0.6	3	-155	3
Hunker Dome	Quartz	6	8.3	1.2	4	-147	20
	Amethyst	2	-11.1	1.2	1	-134	
Mitchell	Quartz	3	7.3	0.6	5	-153	12
Sheba	Quartz	4	8.2	0.6	2	-166	11
	Muscovite	2	6.4	0.5	4	-174*	4
	Muscovite				4	-138†	4
Lone Star	Quartz	3	7.6	0.5	5	-130	12
27 Pup	Quartz	1	8.1	0.6	2	-158	2
Hilchey	Quartz	1	8.6	0.7	2	-127	4
Violet	Quartz	2	5.2	0.5	3	-151	10
Virgin	Quartz	1	3.2	0.7	6	-145	19

¹ See Appendix 4 for equilibrium fractionation equations used in calculations.

² δD analyses of inclusion fluids, except where indicated.

³ Calculated from standard deviation of temperature estimates, or from standard deviation of fluid compositions, whichever is largest.

* Calculated from the empirical quartz-muscovite calibration of Bowers and Taylor (1985).

† Calculated from the quartz-muscovite calibration of Suzuoki and Epstein (1976).

decrease in homogenization temperatures is thought to be a reflection of a real drop in the trapping temperatures, relative to more southerly veins.

The $\delta^{18}\text{O}_{\text{quartz}}$ values do not show a noticeable trend towards lighter values to the southeast of the Hunker Dome area, implying that fluid temperatures in the deeper parts of the mineralizing system did not significantly exceed those recorded in veins in the central region (ca. 300-350°C).

The loss of CO_2 from the Au-quartz vein fluids during effervescence was apparently accompanied by minimal loss of $\text{H}_2\text{O}_{\text{vapor}}$, because (1) the salinity of the aqueous phase in the northern and southern veins is essentially the same within error, and (2) the bulk fluid temperature does not appear to have dropped significantly during exsolution of the CO_2 phase (Chapter V). Similarly, effervescence of CO_2 apparently had no obvious effect on the $\delta^{18}\text{O}_{\text{fluid}}$ value, because calculated fluid values for the Lloyd, Hunker Dome, Sheba and Lone Star veins are in agreement, within error (Table 4). The loss of CO_2 by exsolution has little effect on the $\delta^{18}\text{O}_{\text{fluid}}$ of the residual water, because exsolved CO_2 is isotopically very similar to the CO_2 dissolved in the aqueous phase (Vogel et al., 1970). Therefore, since only CO_2 ($\pm\text{CH}_4$ $\pm\text{N}_2$ $\pm\text{H}_2\text{S}$) was lost in appreciable amounts from the bulk fluid, the calculated $\delta^{18}\text{O}_{\text{fluid}}$ remained essentially the same across the zone of CO_2 loss. The limited $\delta^{13}\text{C}_{\text{CO}_2}$ and $\delta^{13}\text{C}_{\text{calcite}}$ data, do not allow for a meaningful analysis of the effects of CO_2 loss on the $\delta^{13}\text{C}_{\text{fluid}}$ values across the area.

Fluids in equilibrium with the Sheba muscovite had an average $\delta^{18}\text{O}_{\text{fluid}}$ of 6.4 ± 0.5 ‰. Quartz analyses from the same samples gave an average $\delta^{18}\text{O}_{\text{fluid}}$ value of 8.2 ± 0.6 ‰. The close agreement between the average mineral pair temperature, and the average fluid inclusion homogenization temperatures implies that the quartz and muscovite $\delta^{18}\text{O}$ values are close to equilibrium values. The ca. 2 ‰ difference between the $\delta^{18}\text{O}_{\text{fluid}}$ values calculated from the quartz and muscovite analyses may be a product of the different fractionation equations which have been used in the calculations. The $\delta^{18}\text{O}$ values of fluids in equilibrium with the muscovite samples, were calculated using the equation of O'Neil

and Taylor (1969). Derivation of an alternative muscovite-water calibration by subtraction of the quartz-water calibration of Matsuhisa et al. (1979) from the experimental quartz-muscovite calibration used to calculate mineral pair temperatures, may produce better agreement between fluid values, but was considered invalid due to the different experimental techniques used in the derivation of the calibrations (T. Chako, pers.comm.).

δD values of fluids in equilibrium with the Sheba muscovite samples were calculated at the quartz-muscovite temperature of $303 \pm 17^\circ\text{C}$ and are in close agreement with δD analyses of inclusion fluids from the corresponding quartz samples (Table 4). The equation of Suzuoki and Epstein (1976) yields δD_{fluid} values of -134 ± 4 ‰ and -141 ± 4 ‰, for Sheba muscovite samples, which are isotopically heavier than the inclusion fluids. At $\approx 300^\circ\text{C}$, the graphical calibration of Bowers and Taylor (1985) predicts a muscovite-water fractionation of approximately -12 ‰, yielding δD_{fluid} values of -170 and -177 ‰ for Sheba muscovite samples MLB-89-263 and MLB-89-264, respectively. These results are the same, within error, as δD values of inclusion fluids in Sheba vein quartz (Tables 3 and 4).

The $\delta^{18}\text{O}_{\text{fluid}}$ values calculated from $\delta^{18}\text{O}$ analyses of discordant vein calcite, are in general somewhat lighter than the fluids in equilibrium with coexisting quartz (Table 3). The limited data base precludes a meaningful discussion of these results. Also, the small $\delta^{13}\text{C}$ data base prohibits a meaningful speculation on the source of the carbon. However, the average $\delta^{13}\text{C}_{\text{CO}_2}$ value of -5.5 ± 2.3 ‰ for CO_2 in equilibrium with discordant vein calcite at $\approx 300^\circ\text{C}$ (Bottinga, 1968) is similar to $\delta^{13}\text{C}$ values reported from other mesothermal gold camps in the Cordillera (Nesbitt and Muehlenbachs, 1989).

Foliaform Veins

$\delta^{18}\text{O}$ values of foliaform vein fluids range from 2.1 to 14 ‰, with an average value of 7.9 ± 3.3 ‰. The average $\delta^{18}\text{O}_{\text{fluid}}$ value is similar to that of the Au-bearing veins, however more spread is evident in the foliaform data (Table 3). The average $\delta^{13}\text{C}_{\text{CO}_2}$

values for CO₂ in equilibrium with carbonate is -8.7 ± 3.5 ‰. As with the Au-quartz vein data, the small data base limits the interpretation of these values.

Hunker Dome Amethyst

Using the uncorrected fluid inclusion homogenization temperature of 341 ± 11 °C, an average $\delta^{18}\text{O}_{\text{fluid}}$ value of -11.0 ± 1.2 ‰ was calculated for amethyst samples from Hunker Dome. This is substantially lighter than the $\delta^{18}\text{O}_{\text{fluid}}$ values of 6.1 to 7.5 ‰ calculated for the host quartz veins. The $\delta\text{D}_{\text{fluid}}$ of inclusion fluids from one amethyst sample was -134 ‰, which is approximately 15 to 20 ‰ heavier than the average $\delta\text{D}_{\text{fluid}}$ of the Au-bearing, mesothermal veins.

Eocene(?) Epithermal Veins

Two $\delta^{18}\text{O}_{\text{fluid}}$ values were calculated from analyses of calcite from the Germaine Creek epithermal deposit (Figure 2). Although an attempt was made to obtain fluid inclusion homogenization temperatures, no workable inclusions were found in the ten chips examined during the study. Therefore, an arbitrary temperature range of 200-300 °C was assumed in all calculations, which is typical of other epithermal deposits in the Canadian Cordillera (Nesbitt et. al., 1986). $\delta^{18}\text{O}_{\text{fluid}}$ values average -0.8 ± 2.0 ‰. No δD analyses of inclusion fluids were available to better constrain the fluid source.

Ultramafic-Hosted Carbonate Veins

The small amount of data available from these veins is presented in Table 3. Using an arbitrary fluid temperature of 300 ± 50 °C, $\delta^{18}\text{O}_{\text{fluid}}$ calculations for 4 carbonate samples indicate fluid compositions of between 2.1 ± 1.3 to 12.7 ± 1.3 ‰. $\delta^{13}\text{C}_{\text{calcite}}$ analyses, yield values for $\delta^{13}\text{C}_{\text{CO}_2}$ which range from -4.0 to 2.0 ‰.

Discussion of Mesothermal Vein Data

Reliability of Deuterium Analyses

Pickthorn et al., (1987) raised a number of points concerning the validity of the bulk decrepitation method of D/H analyses. They maintain that the released fluids most likely represent late-stage, easily decrepitated secondary inclusions which are unrepresentative of the mineralizing fluids, and suggest that ore-phase hydrous silicates should also be analyzed for comparison with the inclusion fluid analyses. The problem of incorporation of secondary inclusion fluids during decrepitation was addressed by Nesbitt and Muehlenbachs (1987). They argue that if the extracted fluids are a mixture of, for example, heavy metamorphic fluids in primary inclusions, and light meteoric waters in secondary inclusions, the δD_{fluid} results should reflect variable mixtures of the two endmember fluids, depending on the proportion of primary and secondary inclusions in the sample. Nesbitt and Muehlenbachs (1987) also suggest that many secondary inclusions are actually late stage fluids, and are therefore representative of the mineralizing event. In apparent support of this argument, Goldfarb et al. (1989) report that microthermometric data from secondary fluid inclusions in Au-bearing quartz from the Juneau Au-belt in Alaska, are consistent with data from primary inclusions, and probably represent the ore-forming fluid. Similarly, Robert and Kelly (1987), in a study of the Sigma mine in Canada, describe gold mineralization which formed during brittle fracturing of vein minerals, coeval with the trapping of fluid inclusions along fracture planes, and note the coincidence of gold deposition with entrapment of secondary inclusions.

Thus, it is simplistic to argue that *only* primary or *only* secondary inclusion fluids, from a particular deposit, will yield δD_{fluid} analyses which are representative of the mineralizing fluids. Pending the development of easily applicable techniques for analysis of individual inclusions, and in the absence of unequivocal textural evidence for the relative ages of the inclusion types, the best interpretation of the deuterium data from the Au-quartz veins is that *some* of the decrepitate analyses probably reflect the deuterium composition of

the ore-forming fluid, which lay in the range of -104 to -179 ‰. The high proportion of apparent primary inclusions in some Au-bearing vein quartz samples increases the likelihood that the range of δD values encompasses the actual mineralizing fluid values. Greater uncertainty exists in interpretation of the foliaform data because of the lack of observed primary inclusions.

δD_{fluid} values calculated from micas (Table 4), are in good agreement with the inclusion fluid values, and appear to satisfy the criterion of Pickthorn et al. (1987). Although hydrogen isotope exchange between mica and coexisting hydrous fluids can continue to temperatures of $<100^{\circ}\text{C}$ (Graham, 1981), D/H isotope studies of mica separates from a number of ore-deposits indicate that calculated δD_{fluid} values are generally representative of the ore-forming fluid values, and have not been reset by later, deuterium-depleted secondary fluids (e.g., Pickthorn et al., 1987; Bowman et al., 1985; Peters et al., 1990; Böhlke and Kistler, 1986). Therefore, the δD_{fluid} values of inclusion fluids in Au-bearing quartz (see above), and of fluids in equilibrium with hydrothermal muscovite (ca. -134 to -177 ‰ depending on the choice of calibration), are considered to be representative of the primary, mesothermal δD_{fluid} signature.

Compositional Range of Klondike Mesothermal Fluids

The calculated foliaform and Au-quartz vein fluid compositions occupy overlapping areas on a δD vs. $\delta^{18}\text{O}$ plot (Figure 25). Also shown for reference are the regions occupied by metamorphic and magmatic waters (Sheppard, 1986), as well as the results from a number of other isotopic studies of mesothermal veins.

The use of $\delta^{18}\text{O}_{\text{quartz}}$ analyses alone, is not sufficient to constrain the origin of the mineralizing fluid; the calculated Au-quartz vein $\delta^{18}\text{O}_{\text{fluid}}$ values fall within the range of magmatic, metamorphic and evolved meteoric waters. In combination with deuterium analyses, however, the range of discordant vein fluid compositions ($\delta^{18}\text{O}_{\text{fluid}} \approx 3.2$ to 9.8 ‰, and $\delta D \approx -104$ to -179 ‰; average values, $\delta^{18}\text{O}_{\text{fluid}} 7.8 \pm 1.5$ ‰, $\delta D 150 \pm 18$ ‰)

clearly lies outside of the metamorphic and magmatic water fields. The measured range in δD_{fluid} values is roughly equivalent to present day, meteoric waters in Yukon (Sheppard, 1986), although the $\delta^{18}O_{\text{fluid}}$ values are 25 to 30 ‰ enriched relative to the meteoric water line. The foliaform fluid compositional range occupies a similar region to that of the Au-quartz vein fluids, although a slightly greater range is evident in the deuterium and oxygen data. The implications of these observations are discussed below.

VII. DISCUSSION AND CONCLUSIONS

Au-Quartz Veins

The results of the fluid inclusion and stable isotope study presented above, are summarized in Table 5 with the results of a number of other studies of mesothermal Au-quartz vein systems for comparison.

Nesbitt et al. (1989) define mesothermal lode Au deposits as lode deposits mined primarily for Au, formed at temperatures of 250° to 350°C and pressures greater than 600 bars. Typically, the mineralizing fluids have a CO₂ content of >4 mol %, and salinities of approximately 0 to 4 eq.wt.% NaCl. Fluid pressures are generally greater than 1 kbar, and evidence for unmixing of immiscible aqueous and CO₂-bearing fluid phases is common. Calculated $\delta^{18}\text{O}_{\text{fluid}}$ values range between 4 to 10 ‰. δD values of inclusion fluids, and fluids in equilibrium with hydrothermal micas, lie in the range -160 to -10 ‰ (Nesbitt, 1988). It is clear from this definition, from Table 1, and from comparison with the other deposits listed in Table 5, that the geochemical and stable isotopic characteristics of the Klondike discordant Au-quartz veins are typically mesothermal in nature.

However, the Klondike veins differ in two aspects from generally accepted empirical and genetic models of Phanerozoic and Archean mesothermal vein systems (e.g., Kerrich and Wyman, 1990; Groves and Foster, 1991). Firstly, the stable isotope data suggest that the Klondike mineralizing fluids were compositionally similar to meteoric fluids, whereas most workers favor involvement of metamorphic fluids in the mineralizing processes (e.g., Kerrich and Fyfe, 1981). Secondly, the common association of quartz vein systems with major crustal structures (Kerrich and Wyman, 1990) is absent in the Klondike (see below) (Chapter IV).

Regional Structural Relationships

A feature common to many Phanerozoic and Archean mesothermal vein systems is their association with major shear zones or strike slip faults (Kerrich and Wyman, 1990;

Table 5. Comparison of Some Geochemical Characteristics of Inclusion Fluids and Mineral Separates from Phanerozoic, Mesothermal Au-deposits.

Deposit/ Area	Principal reference	Age of deposit (Ma)	T_{tot}^1 (fluid temp) (°C)	CO ₂ mol. %	NaCl eq. wt. %	Evidence for immisc'	P _{trap} (Kbars)	$\delta^{18}\text{O}_{\text{Qtz}}$ ($\delta^{18}\text{O}_{\text{fluid}}$) (‰ SMOW)	$\delta\text{D}_{\text{inc. fluid}}$ ($\delta\text{D}_{\text{silicate}}$) (‰ SMOW)
Phanerozoic (general)	Nesbitt, 1991	-	(250 to 350)	5 to 20	<5	Common	>1.0	+12 to +19	-160 to -30
Archean (general)	Groves & Foster, 1991	-	(200 to 450)	3 to 25 10 to 15	<6	Common	1.0 to 4.5	+8 to +16 (≈+3 to +10)	-86 to +6 (-87 to -50)
Alaska-Juneau Alaska	Goldfarb et al., 1989	≈55	150 to 300	<10	<5	Local	>1 to 1.5	+15.7 to +18.5 (8 to 12)	(≈-60)
Klondike Yukon	This study	140-135†	200 to 330	1 to 20	<6	Probable (see text)	0.5 to 2.1	≈+11 to +19 (≈+3 to +10)	-104 to -179 (-138 to -179)
Snowbird B.C.	Madu et al., 1990	N/A	200 to 260	≈10	≈3	-	>0.8	+22.6 ±1.2 (+13.2 ±1.5)	-139 ±2.5 N/A
Mother Lode California	Wier & Kerrick, 1987	≈115*	150 to 200	<10	<2	-	1.0 to 2.0	≈+12 to +20 (+6 to +15)	-40 to -100 (-40 to -60)
Jungwon Korea	Shelton et al., 1988	156-146	290 to 375	15 to 25	≈4	Yes	1.2 to 1.5	≈+11 to +15 (+5 to ≈+8)	-110 to -80 N/A
Hodgkinson Australia	Peters et al., 1990	≈300#	170 to 305	<<4	3 to 11	-	1.0	+16.6 ±0.9 (+10 ±2)	-84 to -115 (-106 ±7)

¹ Temperatures in parentheses estimated from fluid inclusion and/or stable isotopic and geologic evidence.

† J. Mortensen (pers. comm.).

* Böhle and Kistler (1986).

Morrison (1988).

Nesbitt, 1991). Frequently, the major structure is barren, and mineralization is hosted by secondary structures related to the major fault(s) (Nesbitt and Muehlenbachs, 1989). The major faults, and their secondary splays, are believed by most authors to have acted as channels or zones of enhanced permeability through which the Au-transporting, mineralizing fluids flowed (e.g., Böhlke and Kistler, 1986; Nesbitt et al., 1986; Goldfarb et al., 1989; Kerrich and Wyman, 1990).

The significant vertical and lateral extent of many of the vein systems is probably a result of this association, which is particularly apparent in mesothermal vein systems of the North American Cordillera. For example, veins of the Mother Lode system in California are hosted by structures related to the Melones fault zone, a major structure which ranges from a 3.5 km wide tectonic melange to a 1 km wide mylonite zone (Landefeld, 1988). Similarly, the Bralorne-Pioneer vein system in British Columbia, which is approximately 6 km in strike length and has a depth of at least 2 km, is associated with a major strike-slip fault system, trending northwest and extending for about 100 km (Leitch, 1990).

A similar structural association has not been noted in the Klondike. Although mapping of the area has revealed two distinct, regional scale structural features- the Tintina fault, and the major assemblage-bounding thrust faults- neither structure appears to have had any significant influence on the location of the vein-hosting structures.

The Tintina fault zone defines the northeastern margin of the field area (Figure 1). Significant movement along the fault zone is believed to have taken place between mid-Cretaceous to Eocene/Oligocene times, and may have persisted up to the Pliocene (Gabrielse, 1985; Templeman-Kluit, 1981). Two lines of evidence suggest that the vein-hosting structures are unrelated to this feature. Firstly, K-Ar ages of hydrothermal muscovite indicate that the veins are Earliest Cretaceous in age (see above), and are therefore substantially older than the Tintina fault. Secondly, there are no obvious splays or secondary structures associated with the Tintina fault outcropping within the field area (Mortensen, 1990).

Structures Related to Thrusting

An alternative explanation is that the vein-hosting structures are genetically related to the regional-scale thrust sheets recognized by Debicki (1984, 1985) and Mortensen (1990). Recent mapping by these workers has indicated a possible relationship between the trace of the thrust faults (see above) and a number of the discordant quartz vein occurrences (Figure 2). In the southeast and central parts of the Klondike, Au-quartz veins occur in both the hangingwall and footwall of the regional thrust faults (Figures 1 and 2), but almost invariably occur within a few hundreds of meters of a thrust fault. This relationship is illustrated on a smaller scale by trench mapping in the Hunker Dome area, where discordant veins occur in the footwall and hanging wall of a splay from the main thrust fault, and strike roughly parallel to the trace of the thrust (Figure 6). Thus it is possible that the vein-hosting structures may be minor, steeply-dipping brittle faults associated with thrust faulting, analogous to Au-quartz veins hosted by thrust-related faults in the Hyde-Macraes shear zone, Otago Schist, New Zealand, described recently by Teagle et al. (1990). However, in the northern part of the field area, the association is less obvious and with the exception of the Virgin showing, none of the veins occur in close proximity to a thrust fault (Figure 2). Thus, the exact role of thrust deformation in the siting of Au-quartz veins remains speculative at best.

Structures Related to Regional Uplift

Au-quartz veining, unrelated to major crustal structures, have been studied at the Erickson gold mine in the Cassiar district of British Columbia where Au-quartz veins cut oceanic rocks of the Slide Mountain Terrane. These rocks were structurally emplaced during the Mid Jurassic over miogeoclinal rocks of the NACM (Anderson and Hodgson, 1989). There are no obvious major crustal structures exposed in the area, and the veins are hosted by relatively minor, extensional faults (Anderson and Hodgson, 1989). Mineralization has been dated at approximately 130 Ma, and it was suggested by Anderson

and Hodgson (1989) that Early Cretaceous extensional faults developed during the isostatic rise of the Orogenic belt following thrust-induced crustal-thickening during the Mid Jurassic collisional events.

Diamond (1986, 1990) describes a similar structural setting for Au-quartz veins located at Brusson in central Val d'Ayas in the Northwest Italian Alps, where veins occupy steeply dipping extensional faults and joints within rocks of the Piemonte ophiolite nappe and the Pennine Monte Rosa nappe. The peak of Meso-Alpine metamorphism took place at approximately 40 to 36 Ma. A K-Ar age of approximately 32 Ma for vein muscovites constrains vein formation to a period of post-metamorphic extensional tectonics during rapid uplift and cooling of the Western Alps (Diamond, 1990).

A similar structural model might account for the formation of the structures which host the Klondike Au-quartz vein system. Thrust deformation in the region has been constrained to between 190 to 180 Ma (J. Mortensen, pers. comm.). Metamorphic cooling ages across the Klondike generally fall between Middle to Late Jurassic, indicating that uplift began shortly after thrust imbrication (Mortensen, in press). However, regional variations in the ages suggest that uplift rates may have varied somewhat across the area (see above). Widespread uplift and erosion is believed to have taken place across most of the western Cordillera between approximately 145 to 125 Ma (Gabrielse and Yorath, 1989) broadly coincident with the magmatic lull reported by Armstrong (1988), and the Early Cretaceous (140 to 135 Ma) age range obtained for the discordant veins.

It is suggested that during uplift of the Klondike region, extensional faults developed within the schist complex as a result of extensional collapse, although the exact timing of extensional deformation is uncertain (Norris and Henley, 1976; Dewey, 1988). These faults then acted as the fluid conduits and host structures for Au-quartz mineralization (see below). This model does not rule out the possibility that some veins may also be hosted by extensional structures developed during thrust deformation. Further work is required to better determine the precise structural controls on vein location.

Au-Quartz Vein Fluid Source

The cluster of $\delta^{18}\text{O}_{\text{quartz}}$ values of Au-quartz veins between 15 to 16 ‰ (average 14.9 ± 1.6 ‰), and the calculated average $\delta^{18}\text{O}_{\text{fluid}}$ value of 7.8 ± 1.5 ‰ ($\delta^{18}\text{O}_{\text{fluid}}$ range $\approx +3$ to $+10$), are typical of most mesothermal vein systems, which generally display regional homogeneity in $\delta^{18}\text{O}_{\text{quartz}}$ values (Nesbitt and Muehlenbachs, 1989; Kerrich, 1989). There is no obvious correlation between host lithology and $\delta^{18}\text{O}_{\text{quartz}}$ values, and although veins hosted by felsic schist have heavier average $\delta^{18}\text{O}_{\text{quartz}}$ values (Figure 23), the enrichment is attributable to lower fluid temperatures, rather than host rock control (Chapter VI).

The high degree of uniformity in the discordant vein data implies that the vein system was fluid dominated (Kerrich, 1989), and that the fluids responsible for formation of individual veins either (a) had a common source, or (b) underwent similar processes/degrees of evolution prior to vein formation, or both. The presence of wallrock alteration around the veins demonstrates that the fluids were not in chemical or thermal equilibrium with the host rocks.

Models of Mesothermal Fluid Genesis

Mechanisms which have been invoked to account for the generation of the mineralizing fluids involved in mesothermal vein genesis include (a) lateral secretion (Boyle, 1979), (b) mantle degassing-granulitization (Colvine et al., 1984; Cameron, 1988), (c) meteoric water circulation (Nesbitt et al., 1986; Shelton, 1988) and (d) metamorphic devolatilization (Kerrich and Fyfe, 1981; Goldfarb et al., 1989).

The genetic model which has enjoyed greatest acceptance amongst geologists working on mesothermal veins, is the generation of H_2O and CO_2 during prograde metamorphism under greenschist to amphibolite facies P-T conditions (e.g., Kerrich and Fyfe, 1981). The fluids are focussed along, and channelled into, major crustal structures, for example terrane-boundary faults, and migrate upwards along the structures losing CO_2

($\pm\text{CH}_4 \pm\text{N}_2$) and precipitating ore and gangue minerals (Nesbitt and Muehlenbachs, 1989; Kyser and Kerrich, 1990). A similar mechanism has been proposed for the formation of Phanerozoic mesothermal lode deposits in the Canadian Cordillera: In a study of the Juneau gold belt in Alaska, Goldfarb et al. (1988) suggested that the hydrothermal fluids were generated during prograde metamorphic devolatilization of subducted sediments and igneous rocks.

Recently, however, the general applicability of the metamorphic devolatilization model to all mesothermal Au-quartz lode deposits has been questioned (e.g., Nesbitt et al., 1986; Nesbitt, 1990; Shelton et al., 1988). Based primarily on the interpretation of stable isotope data acquired during studies of Canadian and Korean lode-Au systems, Nesbitt et al. (1986) and Shelton et al. (1988) proposed that the mineralizing fluids responsible for lode formation are not metamorphic in origin, but rather deeply convecting, chemically evolved meteoric waters (see below).

Arguments for and against both the metamorphic and evolved meteoric fluid models are partly dependent on the interpretation of stable isotope data from vein and wallrock minerals, particularly deuterium analyses of inclusion fluids and micas (see Chapter VI, and discussion in Nesbitt et al., 1986; Pickthorn et al., 1987).

The meteoric water model was proposed to account for the common observation in Cordilleran lode deposits, that δD values of inclusion fluids are extremely depleted in deuterium relative to the magmatic and metamorphic water fields. Also, the $\delta\text{D}_{\text{fluid}}$ values demonstrate an apparent systematic latitudinal dependence, in that they appear to become progressively more depleted in deuterium at higher latitudes. This observation is not readily explainable by the metamorphic dehydration model. More recently, independent evidence in support of meteoric water involvement has come from a study of noble gas and halogen isotope ratios of inclusion fluids (see below) (e.g., Böhlke et al., 1989).

Klondike Au-Quartz Vein Fluid Source

Metamorphic/Magmatic Fluids

Although the $\delta^{18}\text{O}_{\text{fluid}}$ values of the Klondike Au-quartz vein fluids are compatible with either a metamorphic or a magmatic fluid source (Figure 25), the range of $\delta\text{D}_{\text{fluid}}$ values from the principal Au-quartz vein locations (ca. -104 to -179 ‰) lie outside of the metamorphic and magmatic water fields, and could only be derived from these fluids through a significant negative shift in the $\delta\text{D}_{\text{fluid}}$ values. It is highly unlikely that metamorphic or magmatic fluids would become depleted in deuterium as a result of interaction with rock, because most mineral-water deuterium fractionations are negative, and the fluid becomes enriched in deuterium as a result of fluid-mineral interaction (Field and Fifarek, 1985). Thus, the depletion of the $\delta\text{D}_{\text{fluid}}$ values relative to the metamorphic or magmatic water fields (see above) would appear to rule out derivation of the Klondike mineralizing fluids from these sources.

Also, it is difficult to reconcile the age of the Klondike veins (ca. 140-135 Ma) with a metamorphic fluid origin. The discordant veins apparently post-date the main mid-Permian to late Triassic prograde metamorphic event by as much as 60 Ma (Mortensen, 1990; Mortensen et al., in press). As the highest level of metamorphic fluid generation generally precedes peak metamorphism (Nesbitt, 1990) it is highly unlikely that the mineralization is related to prograde metamorphism, unless metamorphic fluids were retained at depth for a considerable time.

The apparent time-lag between peak metamorphism and the onset of mineralization is a feature common to many mesothermal deposits and is a potential problem for adherents to the metamorphic dehydration model (Nesbitt, 1991; Kyser and Kerrich, 1990). To account for this discrepancy, Kyser and Kerrich (1990) suggest that in collisional belts which have experienced significant crustal thickening, peak metamorphism at depth may post-date peak metamorphism at shallower levels by up to tens of millions of years, thus accounting for the apparent discrepancy in age between mineralization and metamorphism.

However, theoretical modelling by Connolly and Thompson (1989) suggests that much of the fluid generated by prograde reactions at depth is probably consumed by retrograde hydration reactions in the overlying, dehydrated rocks. Also, their model suggests that the amount of silica transported by metamorphic fluids is insufficient to explain the volume quartz veining seen in metamorphic terranes, unless significant convective recirculation of fluids occurs (see below).

A variation of the metamorphic dehydration model has recently been proposed by Peters et al. (1990), in a study of the Hodgkinson goldfields in Australia. They suggest that deuterium-depleted fluids can be generated by exchange reactions between metamorphic fluids and organic matter in metasediments, or reduced gas species. These reactions deplete the fluid in deuterium and shift the composition to progressively more negative values. Peters et al. (1990) argue that interaction between the metamorphic fluids and organic-rich rocks was sufficient to shift the δD_{fluid} from an original metamorphic signature, to the observed, "organic" (cf. meteoric) values (ca. $-100 \pm 20 \text{‰}$). In the Klondike region, with the exception of carbonaceous metasediments in Assemblage I (which do not host significant mineralization), the Au-quartz vein host rocks appear to be devoid of organic material, and this model will not be discussed further.

A direct magmatic source for the mineralizing fluids can be ruled out on the basis of geochronological evidence. Although volcanic activity and plutonism were widespread across the Yukon-Tanana Terrane between the Jurassic and the Tertiary, there was a period of quiescence across most of the Cordillera between 155 to 125 Ma (Armstrong, 1988; J. Mortensen, pers.comm.). K-Ar dates reported earlier for hydrothermal muscovites from the Sheba vein (ca. 140-135 Ma) fall during the magmatic lull and appear to preclude a magmatic fluid source (J. Mortensen, pers.comm.).

Meteoric Fluids

An alternative explanation for the observed fluid compositions, which has recently been proposed by Nesbitt et al (1986), Shelton et al. (1988) and Böhlke (1989), involves isotopic and chemical evolution of deeply convecting meteoric fluids through interaction with rock at fairly high temperatures (ca. 300-350°C), and low water/rock (w/r) ratios.

According to this model, crustal permeabilities are sufficiently high to allow convection of meteoric water to the brittle-ductile transition, which marks an abrupt decrease in the permeability of the rock. During its passage through the rock-mass, and if w/r ratios are fairly low, significant positive shifts can occur in the $\delta^{18}\text{O}$ composition of the fluid, due to the high oxygen content of the rocks in comparison to that of the relatively limited volume of fluid (Nesbitt and Muehlenbachs, 1989). However, the $\delta\text{D}_{\text{fluid}}$ changes very little due to the high ratio of hydrogen in water, compared to rock. Transported solutes and dissolved volatiles may also be acquired as a result of chemical interaction with the rock (Nesbitt and Muehlenbachs, 1989). At some point in the system, the fluids are channelled into suitable conduits, such as faults, shear zones, bedding planes etc., begin to migrate upwards through the fracture system, and under the right conditions, Au-quartz vein deposits may be formed.

This model predicts that the $\delta\text{D}_{\text{fluid}}$ values should retain much of their original meteoric signature, while the $\delta^{18}\text{O}_{\text{fluid}}$ values will reflect equilibration with the bulk of the host rock mass (although at very low w/r ratios, and high degrees of fluid evolution, the δD signature will also reflect equilibration with the rock). The fluid composition is shifted along a path similar to the solid curve shown in Figure 25. The exact position of the curve is dependent on the w/r ratio, fluid temperature and the isotopic composition of the rock type involved. At high to moderate w/r ratios, the fluid undergoes a large shift in $\delta^{18}\text{O}$, and follows a horizontal evolution path (Figure 25). At low ratios, the evolution path eventually curves towards the vertical as the $\delta\text{D}_{\text{fluid}}$ begins to evolve towards that of the rock (Field and Fifarek, 1985; Kerrich, 1987; Nesbitt and Muehlenbachs, 1989). It should be noted

that this model does not preclude the incorporation of metamorphic or magmatic waters into the fluid system.

The involvement of meteoric fluids can only be demonstrated using hydrogen isotopes in areas where a significant difference existed between the δD signature of the convecting meteoric water and the range of values defined by metamorphic water field, at the time of mineralization. Thus, areas at high (paleo-) latitudes or high elevations, with highly D-depleted meteoric fluid signatures, are ideally suited to allow detection of meteoric fluid involvement during lode-formation; it is relatively easy to distinguish isotopically between meteoric, or evolved meteoric waters, and other types of fluids in these areas (e.g., metamorphic and/or magmatic waters). Conversely, in areas with heavier meteoric water signatures (e.g., low latitudes), which overlap or coincide with the magmatic and metamorphic fields, this distinction is virtually impossible, and considerable ambiguity exists in these regions in the interpretation of fluid origin based solely on oxygen and hydrogen stable isotope data.

Yukon Meteoric Waters

The deuterium and oxygen compositions of present day meteoric waters in Yukon are approximately $\delta D \approx -150$ to -170 ‰, and $\delta^{18}O \approx -20$ to -23 ‰ (Taylor, 1979). Unfortunately, the precise isotopic composition of Yukon meteoric waters in the Cretaceous is unknown, due to a lack of data on the paleolatitude and altitude. However, Dagenais (1984) estimated the meteoric $\delta^{18}O_{\text{fluid}}$ value at approximately -16 ‰ for central and southern Yukon, during Cretaceous and Tertiary times. The equivalent deuterium value (ca. -120 ‰) can be calculated from the $\delta^{18}O_{\text{fluid}}$ value, using the standard meteoric water line equation (Craig, 1961). Thus, the meteoric water composition during the Cretaceous probably lay somewhere between the values estimated by Dagenais (1984), and present day values, i.e. $\delta D \approx -120$ to -170 ‰, and $\delta^{18}O \approx -16$ to -23 ‰.

The observed discordant vein fluid composition can be derived from the Cretaceous meteoric fluid by a shift of between +24 to +31 ‰ in the $\delta^{18}\text{O}_{\text{fluid}}$ composition, and up to +90 ‰ in the $\delta\text{D}_{\text{fluid}}$ value. At a temperature of ca. 300°C, positive isotopic shifts of this magnitude require water/rock ratios in the order of 0.1 to 0.01 (Field and Ficarek, 1985). It is suggested therefore, that the discordant vein fluids are of meteoric origin, perhaps incorporating a metamorphic fluid component, and that the observed fluid composition was derived by substantial interaction of this fluid with the rock mass.

D-depleted Fluids: Other Examples

Depleted $\delta\text{D}_{\text{fluid}}$ values have been reported in a number of studies of mesothermal lodes (Shelton et al., 1988; Madu et al., 1990; Nesbitt and Muehlenbachs, 1989; Nesbitt et al., 1989; Shaw et al., 1991; Peters et al., 1990; Rushton et al., 1990; this study).

Shelton et al. (1988), in a study of the Jungwon deposits in Korea, report inclusion fluids from late Jurassic Au-quartz veins which have a $\delta\text{D}_{\text{fluid}}$ range of -78 to -113 ‰. Modern Korean groundwaters have a $\delta\text{D}_{\text{fluid}}$ range of between -42 to -73 ‰ which cannot be explained by entrapment of modern groundwater in fluid inclusions, or by mixing of meteoric and magmatic/metamorphic waters. However, studies of plate movements (Uyeda and Miyashiro, 1974, in Shelton et al., 1988) have indicated that the Korean Peninsula was at higher latitudes in the Jurassic than at present, suggesting that the $\delta\text{D}_{\text{fluid}}$ values represent involvement of Jurassic meteoric waters during mineralization.

Recent studies of Cordilleran Au-quartz mineralization by Madu et al. (1990), and Shaw et al. (1991), have added weight to the concept of meteoric fluid involvement in mesothermal processes. Madu et al. (1990), in a study of the Snowbird mesothermal deposit of central British Columbia, report hydrothermal fluids with calculated $\delta^{18}\text{O}_{\text{fluid}}$ and $\delta\text{D}_{\text{fluid}}$ values of 13.2 ± 1.5 ‰ and -139 ± 2.5 ‰, respectively. They suggest that the deposit formed from evolved meteoric water at a temperature of 240°C and a depth of at least 8 km. Similarly, Shaw et al. (1991) report $\delta\text{D}_{\text{fluid}}$ values which range from -105 to -

124 ‰, from inclusion fluids in Au-quartz veins hosted by low-grade metasediments in the Central Rocky Mountains, Canada. The results of the present study are therefore consistent with a growing body of evidence in support of meteoric water involvement in mesothermal mineralizing processes.

Additional geochemical evidence for meteoric water involvement has come from recent work by Böhlke et al. (1989). They analyzed halogen and noble gas isotopes in CO₂-bearing primary fluid inclusions in vein quartz from the Alleghany district of California, and concluded that the measured isotopic ratios of Ar, Kr and Xe isotopes have an atmospheric signature, which is best explained by either (1) formation of the veins from ascending fluids which originated at the surface, or (2) mixing between ascending magmatic or metamorphic fluids and descending meteoric waters at the site of mineralization.

Depth of Au-Mineralization: Hydrostatic vs. Lithostatic Fluid Pressures

In Chapter V, it was shown that fluid trapping pressures were as high as 2 kbars during formation of discordant veins in the south of the field area. In order to make a meaningful estimate of the depth of mineralization, it is necessary to decide whether these pressures represent lithostatic, hydrostatic or perhaps intermediate pressure conditions within the mineralizing system. If bulk densities of 2.75 to 3.00 g/cc and 0.90 to 1.00 g/cc are assumed for lithostatic and hydrostatic pressure gradients respectively, disparate estimates of the depth of formation of the discordant veins are obtained from the calculated trapping pressures given in Table 3.2. Assuming a hydrostatic gradient, the data imply formation depths of greater than 20 km in the southeast, decreasing to between 4 to 16 km in the central and northern parts of the region. Assuming a lithostatic gradient these estimates drop from approximately 7 km in the southeast, to between 1 to 5 km in the northern and central Klondike.

Effervescence of CO₂

Although detailed textural evidence for CO₂ effervescence is generally equivocal or circumstantial, the regional (and temporal?) fluid composition trends documented in this study are fairly compelling evidence in favour of effervescence of CO₂ from the mineralizing fluids; it is clear that the vein fluid underwent a substantial chemical evolution during formation of the Klondike veins. Effervescence of CO₂ may have occurred either during regional uplift, as the fluid was forced through the solvus in the H₂O+CO₂+NaCl system, or in response to a switch from lithostatic to hydrostatic fluid conditions (see below). Thus, the transition from apparent high pressures in the south of the field area to low pressures in the northeast can be interpreted in several ways:

(a) All discordant veins exposed within the field area are approximately coeval, and the pressure reduction across the central Klondike represents a transition from lithostatic (suprahydrostatic?) to hydrostatic conditions, at approximately the same depth within the fluid system (Figure 26). Abrupt reductions in fluid pressure can occur in vein systems as a consequence of, for example, fault-valve activity (Sibson, 1990).

The pressure estimates of between 1400 to 1600 bars obtained from type 2a fluids in Hunker and Sheba vein quartz, suggest a depth of formation of approximately 5 to 6 km under lithostatic conditions. If hydrostatic conditions are assumed, similar depths of 5 to 7 km are obtained for the type 2b and type 1 inclusion fluid pressures from the same veins and from those further northwest (ca. 500 to 700 bars). A reduction in pressure of this magnitude would be sufficient to induce effervescence of a CO₂-rich phase from the vein forming fluid (see above). This model implies that the Klondike Au-quartz veins represent an oblique section through a mesothermal vein system, with deeper structural levels exposed in the southeast, and is in agreement with the known occurrence of higher grade metamorphic rocks in the southeast.

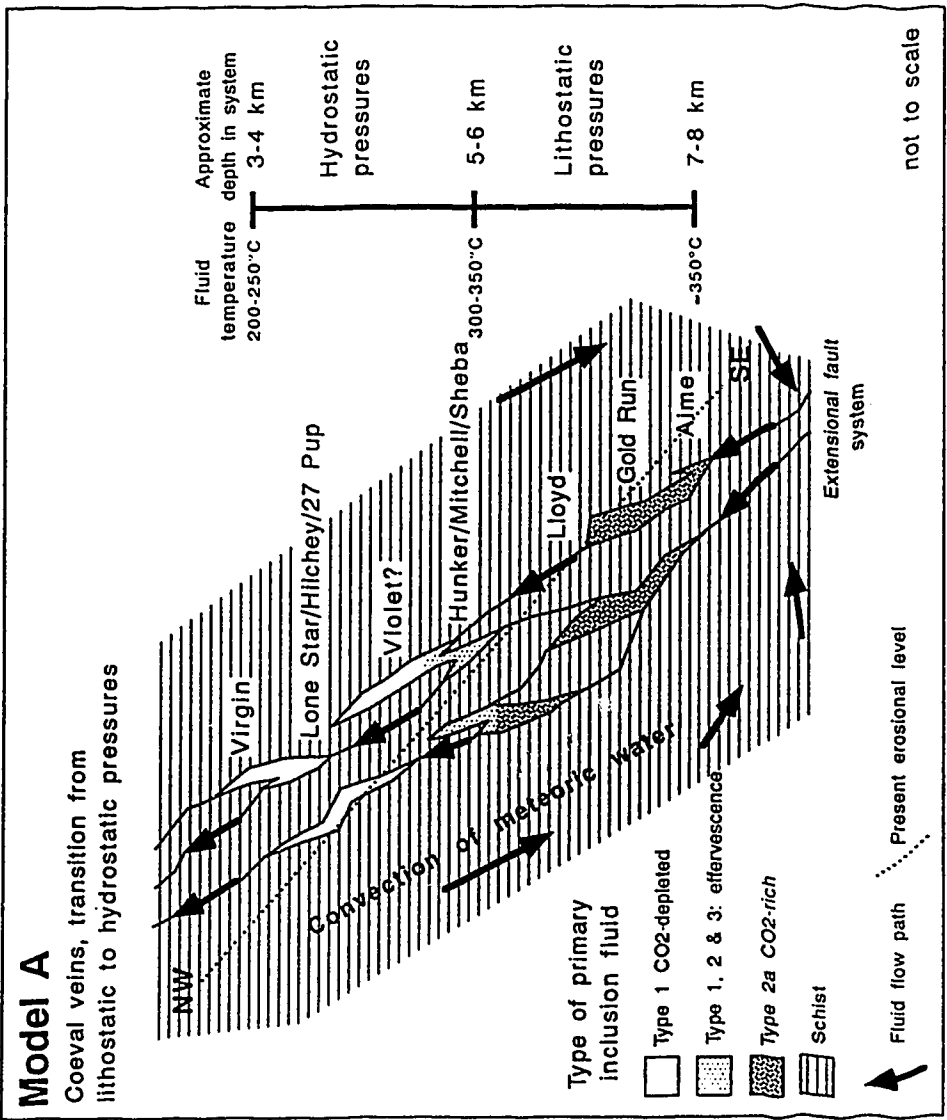


Figure 26. Schematic section through the Klondike Au-quartz vein system at the time of formation of the veins. In this model, the veins are coeval. The loss of CO₂ from the mineralizing fluid occurs at the transition from lithostatic or supralithostatic, to hydrostatic fluid pressures, at a depth of approximately 5-6 km within the fluid system (See text).

Note that if the pressures estimated for the Aime lode (ca. 2 kbars) are regarded as hydrostatic pressures, and if the veins are in fact coeval, the central pressure reduction becomes difficult to explain by the above model. The observed pressure reduction would require a switch from hydrostatic to *sub*hydrostatic conditions at depths of around 14 to 16 km. It is hard to envisage a mechanism which could sustain subhydrostatic fluid pressures at these depths, over a significant period of time.

(b) Mineralization occurred over an extended time period, under a relatively uniform pressure gradient, during regional uplift (Figure 27). In this model, mineralization in the Hunker Dome/Sheba area occurred while the region experienced between 3 to 10 km of uplift (depending on whether fluid pressures are regarded as hydrostatic or lithostatic). For type 2a inclusion fluid compositions, this degree of uplift and pressure reduction is sufficient to induce effervescence of CO₂ (Figure 18) and accounts for the observed P-X evolution of the inclusion fluids. In this model, veins in the far northwest and southeast can be the same age, and would represent exposure of different structural levels within the system. Veins in the northern part of the field area formed above the zone of fluid immiscibility, from CO₂-depleted fluids.

Diamond (1990) described the progressive P-T-X evolution of inclusion fluids trapped over a time span of approximately 2.2 Ma, in quartz from mesothermal veins at Brusson in the Northwestern Italian Alps. The fluids were interpreted to have been trapped over a P-T gradient, which changed from 300°C at 1300 bars, to 240 °C at 650 bars, during regional uplift of the Alps during the Oligocene. Uplift was rapid enough to force the fluids through the immiscibility boundary at approximately 600 bars, and 230°C. The endmember fluid products of immiscibility were then trapped along fractures of similar ages within vein quartz.

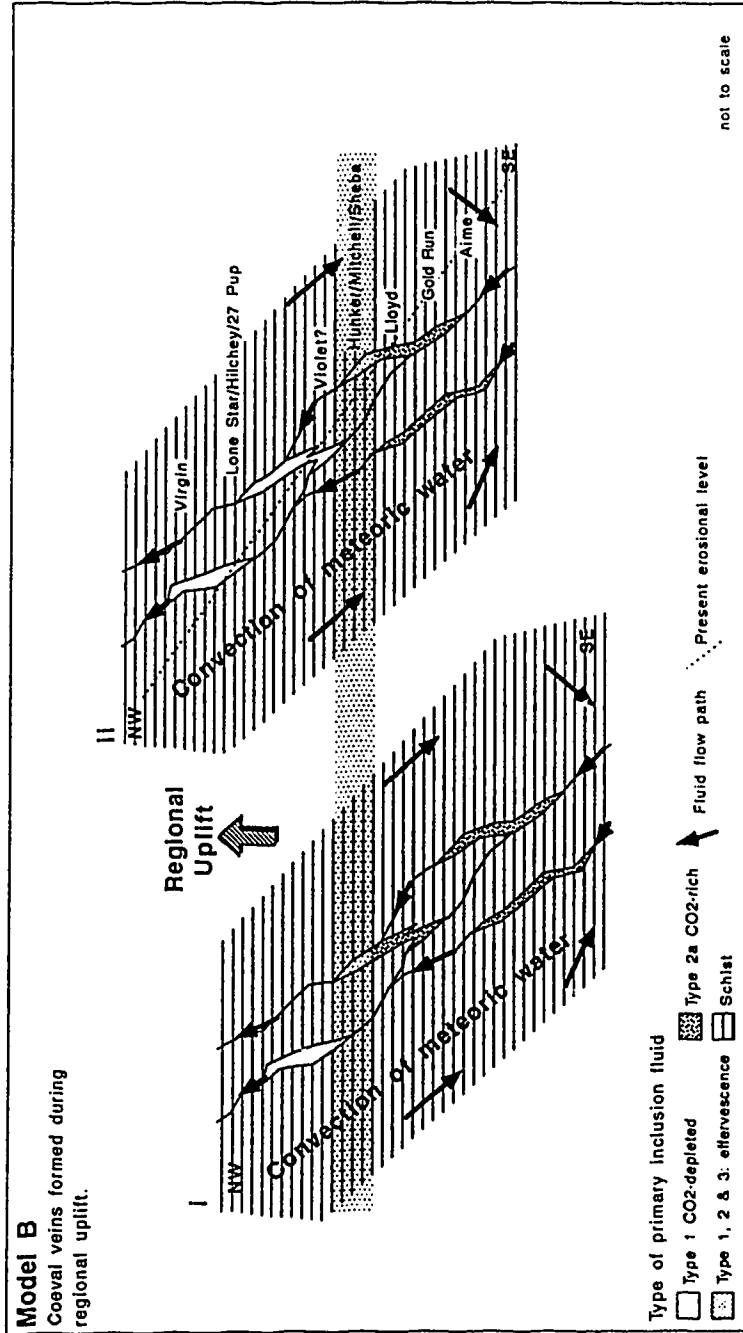


Figure 27. Schematic section through the Klondike Au-quartz vein system at the time of formation of the veins. The veins are coeval, and loss of CO₂ occurs as regional uplift forces the fluid system through the solvus in the H₂O-CO₂-NaCl system (See text).

(c) The veins in the southeast and northwest Klondike are of different ages, becoming progressively younger towards the northwest, with significant uplift occurring in the intervals between formation of individual veins (Figure 28). Although the veins now occupy a similar structural level, they formed at progressively shallower paleodepths during uplift of the Klondike region, from a chemically evolving fluid. If the veins formed from fluids under hydrostatic conditions, approximately 10 to 15 km of uplift must have occurred between the onset and culmination of mineralization. Veins in the central Klondike were trapped as immiscibility/effervescence occurred within the fluid system.

This model has been invoked in studies of vein systems in New Zealand (e.g., McKeag and Craw, 1989). McKeag and Craw (1989) describe four vein systems- the Macreas, Barewood, Bonanza and Nenthorn systems- which are exposed in east Otago on South Island, New Zealand. Fluid pressures, estimated from fluid inclusion studies, show a progressive decrease from approximately 3 kbars for Macreas, to near surface conditions (<300 bars) at Nenthorn. As the veins are all exposed at surface at the same level, they are interpreted to have formed at different times (and different paleodepths) during regional uplift of Otago during the Jurassic and Cretaceous (McKeag and Craw, 1989).

In the absence of K-Ar ages for the southern and northern Klondike veins, and given the poor state of knowledge of the regional geological history of the area (e.g., uplift rates etc.), it is difficult to assess the relative merits of each of the above models further. However, the general lack of banded, breccia and ribbon textures which would provide evidence for repeated crack-seal events and transient lithostatic pressures, and the regional nature of the fluid P-T-X trends, suggest that model (a) is probably the least applicable. Evolution of the mineralizing fluids in response to uplift of this area of the YTT (e.g., mechanisms (b) and (c)) is therefore the preferred mechanism to account for the regional P-T-X trends described in Chapter V, although the true mechanism probably incorporates aspects of all three models.

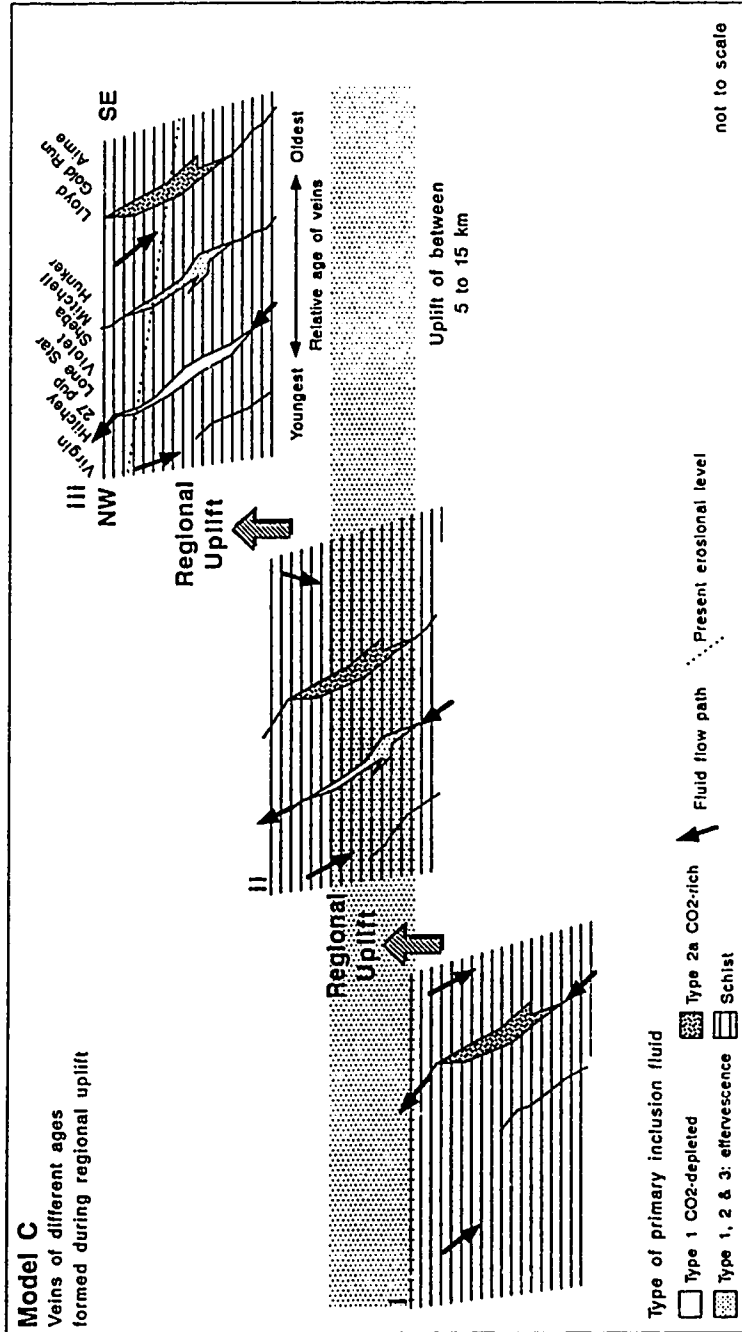


Figure 28. Schematic section through the Klondike Au-quartz vein system at the time of formation of the veins. The veins are of different ages, with the youngest veins now exposed in the northwestern Klondike. Significant uplift occurred between episodes of vein formation. Regional uplift forces the fluid system through the solvus in the H₂O-CO₂-NaCl system, and the youngest veins formed from a CO₂-depleted hydrothermal fluid.

Heat Source

Uplift rates in some metamorphic belts have been shown to be very high. For example, Craw (1988) notes that uplift rates in the Alpine Schists in New Zealand were as high as 10 km per million years, approximately equal to removal of the entire greenschist facies. In such areas, crustal geotherms tend to curve upwards towards the surface. Theoretical modelling of the thermal state of high uplift regions by Craw and Koons (1988) indicates that uplift rates of greater than 2 mm per year result in temperatures of greater than 300°C at depths of less than 5 km.

In this type of system, fluid flow is initiated by buoyancy effects because of the high heat flow, and also probably as a result of topographic effects due to uplift. Also, hydrothermal fluid systems in these areas are likely to be longer lasting than, say, pluton-related systems, as the heat source is a regional feature (Nesbitt, 1990; Norris and Henley, 1976). Thus it is conceivable that the Klondike system was of sufficient duration to allow mineralization to occur during significant vertical uplift; perhaps as much as 10 to 15 km (assuming hydrostatic pressures) during the life of the hydrothermal system, if uplift rates were high enough. Perturbation of the normal geothermal gradient caused by uplift would probably be sufficient to drive convection of meteoric fluids in the rock mass.

Gold Transport and Deposition Mechanisms

Gold has been reported from all of the principal discordant vein occurrences examined in the current study (e.g., Figure 2) (Mortensen et al., in press; this study). The occurrence of Au within veins containing predominantly type 2a primary fluid inclusions (e.g., Aime, Gold Run), as well as veins containing predominantly type 1 inclusions (e.g., Lone Star, 27 Pup), suggests that the loss of CO₂ from the mineralizing fluid in the central Klondike region was probably not a major controlling factor on gold deposition. Also, lithological control on gold deposition was probably subordinate to other processes; gold has been found in veins hosted by felsic-, chloritic- and quartz-augen-schists.

Geochemical studies have shown that Au in mesothermal fluids is probably transported as the bisulfide complex $\text{Au}(\text{HS})_2^-$ (Seward, 1989). The stability of the $\text{Au}(\text{HS})_2^-$ complex is controlled primarily by the concentration of HS^- in the hydrothermal solution. Removal of HS^- by the loss of H_2S from solution, during boiling or effervescence of volatiles, will decrease the solubility of Au and induce precipitation. Alternatively, loss of HS^- as a result of base metal sulfide precipitation is also a viable mechanism for inducing Au precipitation (Seward, 1989).

Figure 29, constructed from the data of Takenouchi and Kennedy (1965), illustrates the solubility of CO_2 in a 6 wt.% NaCl solution, as a function of pressure and temperature. At a fixed temperature, as a hydrothermal solution moves up through the mineralizing system the fluid pressure will progressively decrease. Under ideal circumstances (e.g., an open system) the solubility of CO_2 in the solution will decrease as the pressure is reduced, and the solution will constantly lose CO_2 . It was demonstrated in Chapter V that type 2a Au-quartz vein inclusion fluids recorded a progressive decrease in fluid pressures from southeast to northwest. Thus, loss of H_2S *accompanying* the progressive loss of CO_2 and thereby reducing the solubility of Au is the most likely mechanism to explain the occurrence of Au throughout the Klondike vein system (Seward, 1989).

In the central Klondike, the loss of volatiles was more pronounced as the fluid system passed through the 2-phase curve in the $\text{H}_2\text{O}+\text{CO}_2 (\pm\text{CH}_4 \pm\text{H}_2\text{S})+\text{NaCl}$ system, and slightly higher Au concentrations might be expected in this region. In the north of the field area, the hydrothermal fluids appear to have lost much of the dissolved volatile content. Gold precipitation in these veins may have resulted from a number of mechanisms including: (a) continued loss of H_2S , which being slightly more soluble in water than CO_2 (Seward, 1989) might be expected to persist within the fluid system for slightly longer than CO_2 , or (b) a reduction in fluid temperature (e.g., such as that noted between Lone Star and Virgin) which may lead to precipitation of small quantities of Au (Seward, 1989).

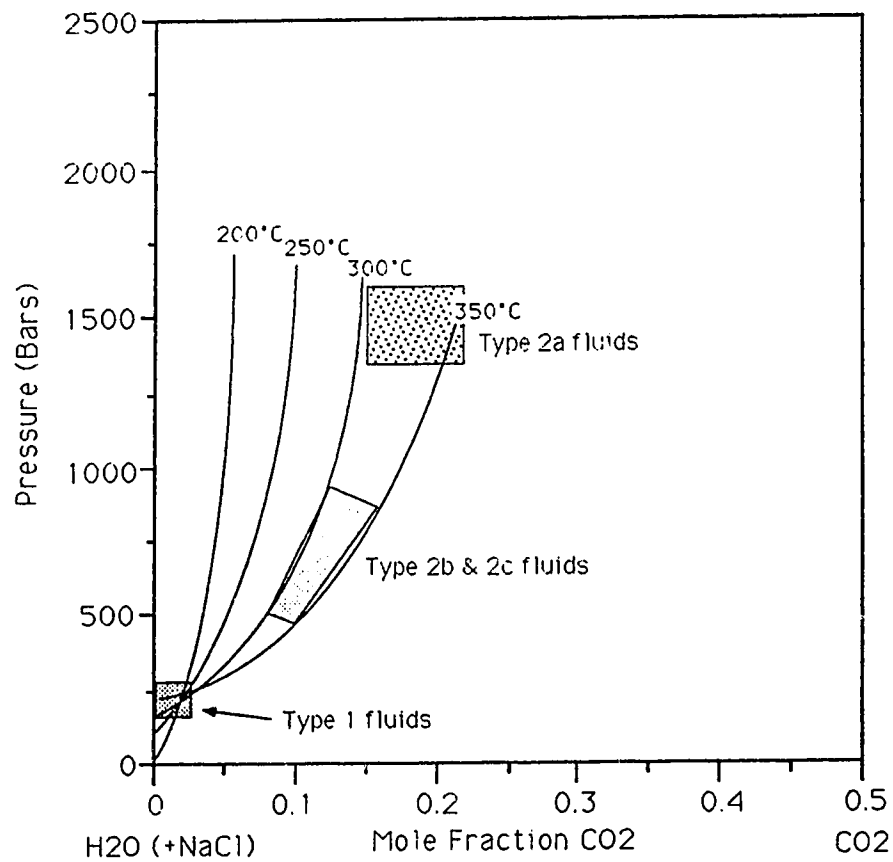


Figure 29. The solubility of CO₂ in a 6 wt.% NaCl solution, at varying pressure and temperature. The shaded boxes represent the approximate P-T-X areas occupied by primary inclusion fluids in the Klondike Au-bearing veins, and illustrate the loss of CO₂ with decreasing fluid pressure. Diagram constructed from the data of Takenouchi and Kennedy (1965).

Origin of Gangue Barite in the Violet Lode

Loss of H₂S, CH₄ and H₂ during separation of volatiles will tend to oxidize the residual fluid and any volatiles which remain in solution (Kerrick, 1989). H₂S will be oxidized to SO₄²⁻, and precipitation of barite may result. This suggests that the Violet lode may have formed either from an oxidized fluid immediately above the zone of CO₂ immiscibility and volatile loss, or immediately after loss of CO₂ from the system. The presence of clathrate in some inclusions indicates that the CO₂ content of primary inclusion fluids in Violet quartz is slightly higher than fluids from other northern lodes, and supports the aforementioned mechanisms.

The lower homogenization temperatures recorded from fluid inclusions in Violet samples (ca. ±200°C vs. ±300°C for Lone Star, 27 Pup etc.) are not supported by the δ¹⁸O_{quartz} values of vein quartz from the lode, which are the same within error as samples from more southerly veins (Figure 20), and therefore argue against a significant fluid temperature difference between these locations. The low Th_{tot} values (in comparison to other lodes in the same area) may be due to inadequate pressure correction of the homogenization temperatures, or alternatively a statistically unrepresentative data set.

Foliaform Veins

δ¹⁸O values of foliaform vein quartz show a greater degree of heterogeneity, and a larger range, than discordant vein quartz values (Table 3, Figure 20), probably as a result of host rock control of the δ¹⁸O signature of the mineralizing fluid (Kyser and Kerrich, 1990). If the observed variations were merely a function of local changes in the fluid temperature acting on an isotopically homogeneous fluid, large fluid temperature variations would have to have existed between closely spaced veins to account for the differences in δ¹⁸O_{quartz} values between adjacent veins (Figure 20). Alternatively, if the vein fluid components were locally derived, for example in response to pressure solution, then the isotopic composition of the mineralizing fluid should reflect a high degree of isotopic

equilibration with the host rocks, and variations in the $\delta^{18}\text{O}$ values of the host rocks will be echoed by the $\delta^{18}\text{O}_{\text{quartz}}$ values of the foliaform veins (Kyser and Kerrich, 1990).

The largest range in $\delta^{18}\text{O}_{\text{quartz}}$ is seen in veins hosted by metasedimentary rocks; the quartz-carbonate-muscovite schist and the micaceous-chloritic quartzite units of Mortensen (1990). Metavolcanic units host veins with a more restricted isotopic range (Figure 23). This variation would be expected if the vein components were derived locally, as igneous rocks generally have a smaller range of whole rock $\delta^{18}\text{O}$ values in comparison to sedimentary rocks (Taylor et al., 1986). The lack of isotopic analyses of host-rock minerals precludes detailed discussion of the effects of host-rock isotopic composition on the vein ^{18}O signature. However, a number of general comments on the probable mechanisms of foliaform vein genesis can be made.

Although Mortensen et al. (in press) suggest that the foliaform and discordant veins may be contemporaneous, it is apparent from their respective geometries that the two vein types formed in response to different stress regimes. Foliaform veins invariably occupy fractures/openings which are parallel to the F1 foliation, and discontinuous (see above). They are also probably coeval with thrusting and F2 fold development (Mortensen et al., in press). These observations suggest that at the time of formation of the foliaform veins, the least principal stress was probably vertical, and fluid pressures within the veins were lithostatic to supralithostatic (Sibson, 1990). This contrasts markedly with the extensional setting described previously for the Au-quartz veins. In addition, the marked similarity locally between foliaform vein and host rock mineralogy, the apparent scatter in the stable isotope data, and the lack of wall rock alteration (cf. discordant veins) all suggest that vein forming fluids were thermally and chemically equilibrated with the host rocks.

Mechanisms of vein formation in metamorphic rocks have been studied by a number of workers (e.g., Yardley, 1975, 1983, 1986; Kerrich et al., 1978; Vidale, 1974). Two end-member mechanisms have been proposed to explain how these veins form; (1) transfer of mineral species into veins from the adjacent rocks by diffusion through an

essentially static pore fluid, in response to a chemical potential gradient between minerals in the host rock and those in the vein (Yardley, 1975; Kerrich, 1978), and (2) deposition of minerals from hydrothermal solutions migrating through a network of fractures/conduits, in response to simple cooling or pressure reduction (Holland, 1967 *in* Kerrich et al., 1978). In some areas, the large mass of vein quartz which is present cannot be explained simply by consideration of mineral solubilities and fluid volumes alone (i.e., mechanism (2)), suggesting that diffusional transfer is probably the dominant vein forming mechanism in these regions (Kerrich et al., 1978).

Yardley (1975) described quartz-plagioclase "segregation" veins in the Connemara schists, Ireland, which share a number of similarities with the Klondike foliaform veins; (1) the veins are parallel to schistosity, (2) the vein mineralogy reflects the mineralogy of the host rocks, and (3) the vein margins are frequently depleted in the vein minerals, suggesting that the veins withdrew material from the wallrocks. He proposed a mechanism for vein formation, whereby hydraulic fracturing or dilation during metamorphism initiates a fluid-filled fracture along the plane of greatest weakness (i.e., parallel to foliation, or in fold hinges), and the vein constituents are transported into the vein from the wallrocks by diffusion of material through the static pore fluid. Kerrich et al. (1978), in a similar study of mineralization in tectonic veins and pressure shadows, also suggested that vein formation occurred by diffusional mass transfer of material. It is suggested that a similar mechanism may account for the formation of foliaform veins in the Klondike metamorphic rocks.

Foliaform Vein Fluid Source

The source of the foliaform vein fluids remains equivocal. Figure 16 shows the total homogenization temperature data for foliaform quartz samples. It was argued previously (see above) that a high proportion of the analyses probably represent data from secondary inclusions; proportionately fewer primary inclusions were seen in foliaform

quartz in comparison to Au-bearing vein material in the course of the fluid inclusion study, which casts some doubt on the interpretation of the δD values of extracted fluids as being representative of the primary vein-forming fluids. The lack of primary inclusions in foliaform quartz may be a result of deformation and recrystallization after formation of the veins (Kerrick, 1978). Alternatively, significant overpressures may have developed within primary inclusions in foliaform vein quartz during regional uplift, resulting in autodecrepitation of many of the inclusions (Sterner and Bodnar, 1989). The deuterium data can therefore be interpreted in two ways:

(a) The inclusion fluid deuterium data are unreliable because of the apparent lack of primary fluid inclusions, and the δD values in Table 3 are unrepresentative of the foliaform vein mineralizing fluid, whose isotopic composition remains unknown. The range of values in Table 3 represent mixtures of varying proportions of primary and secondary fluids.

(b) The δD_{fluid} values are representative of the mineralizing fluids, which must have had a meteoric source, although the heterogeneity apparent in the δD data would seem to imply a degree of mixing/incorporation of heavier (metamorphic?) fluids.

For structural reasons, the last model is problematical. The inferred age of the veins (syn- to late-F2) implies that they formed during, or towards the end of thrust faulting (Mortensen, 1990). Middle to Late Jurassic cooling ages reported by Mortensen (in press) suggest that the Klondike schists had not cooled below $\approx 300\text{-}400^\circ\text{C}$ before thrusting occurred (based on biotite and muscovite closure temperatures quoted in Sevigny et al., 1990). Rheologically, rocks at these temperatures are likely to be approaching the transition from brittle to quasi-plastic behaviour, and would therefore be fairly impermeable to the convective movement of fluids. Furthermore, recent work by Nesbitt (1989) suggests that

the fluid regime in thrust faulted regions of the Canadian Cordillera is dominated by metamorphic fluids (cf. areas of extensional faulting where stable isotope evidence suggests that meteoric waters dominate). Thus, the age and probable tectonic/rheological setting of the foliaform veins would seem to argue against the possibility of significant meteoric water involvement, and imply that the D-depleted inclusion fluids are secondary in origin. It is felt, therefore, that the origin of the foliaform vein fluids is equivocal at best.

Recommendations for further work to better constrain the fluid origin would be (a) δD analysis of hydrous silicates paragenetically coeval with foliaform vein quartz, (b) stable isotope analysis of mineral separates from foliaform vein host rocks to demonstrate whether vein minerals are in isotopic equilibrium/disequilibrium with the surrounding rocks.

Hunker Dome Amethyst Fluid Source

The calculated fluid composition for the Hunker Dome amethyst samples ($\delta^{18}O_{\text{fluid}} -11.1 \pm 1.2 \text{ ‰}$, $\delta D_{\text{fluid}} -134 \text{ ‰}$) differs significantly from that of the host mesothermal veins. The fluid was clearly meteoric in origin, and substantially less evolution of the oxygen isotopic signature occurred prior to mineralization, in comparison to the mesothermal fluids. At temperatures of greater than 300°C, the amethyst fluid composition can be generated from Yukon meteoric water at a water/rock ratio of between 10 and 1 (Field and Fifarek, 1985). It is also conceivable that the fluid composition lies on a mixing line between a magmatic and meteoric fluid (Figure 25).

Textural evidence has shown that the amethyst is paragenetically late in comparison to the host veins. Thus, the calculated fluid composition and the fluid inclusion data (Chapter V) are unequivocal evidence for a late stage influx of hot, meteoric fluid along at least some of the Hunker Dome vein structures. In this regard, it is interesting to note that these late stage fluids have a heavier deuterium signature than the majority of the discordant vein inclusion fluids, including those calculated from mica analyses (Table 4). If this fluid

were trapped as secondary inclusions within the host mesothermal quartz veins (e.g., Pickthorn et al., 1987), or if substantial resetting of the primary Sheba muscovite signature had occurred due to interaction with the amethyst-forming fluid, calculated δD_{fluid} values for the mesothermal veins would be enriched in deuterium relative to fluids from uncontaminated/unreset quartz (cf. Pickthorn et al., 1987).

The exact age of amethyst formation is unknown. Thus it is uncertain whether the amethyst formed at a late stage of regional uplift towards the end of the mesothermal mineralizing event (see below), or is perhaps related to Eocene age quartz-feldspar porphyry intrusives which are known to occur within the field area (Mortensen, 1990).

Eocene Epithermal Vein Fluid Source

On the basis of the $\delta^{18}\text{O}_{\text{fluid}}$ value alone, the mineralizing fluid appears to have been isotopically similar to fluids from other epithermal deposits in the Cordillera, although a substantial range of values exists in the literature (Nesbitt et al., 1986). Walton (1987) reports $\delta^{18}\text{O}_{\text{fluid}}$ values of +2.4 to +6.4 ‰, calculated for the Venus mine, Yukon Territory. Zhang (1986) reports a range of $\delta^{18}\text{O}$ values between -7.0 to -9.0 ‰ for the Dusty Mac mine in south-central British Columbia, and Nesbitt et al., (1986) report $\delta^{18}\text{O}_{\text{fluid}}$ values of -14 to -11 ‰ for the Mt. Skukum epithermal gold vein in Yukon. The $\delta^{13}\text{C}_{\text{calcite}}$ value of -4.8 ‰ falls within the range of carbonate analyses from epithermal and geothermal systems reported by Field and Fifarek (1985), but is insufficient to unequivocally constrain the source of the carbon.

A Model for Foliaform and Au-Quartz Vein Formation

The structural settings and the likely mechanisms of foliaform and discordant vein formation have been described above. In addition, the most likely fluid sources for each vein type have been identified. Despite the poor time constraints on thrusting and uplift of the Klondike region, an attempt has been made to place the formation of each vein type into

a coherent geological model in which formation of both vein types occurred in response to different episodes of an extended, regional tectonic event.

1) Thrusting and Subsidence of the Klondike Region

Thrusting and crustal thickening in the Klondike is believed to have occurred sometime in the Early to Middle Jurassic (ca. 190-180 Ma; J. Mortensen, pers. comm.), probably in response to the amalgamation of other terranes on the western margin of the YTT (Mortensen, 1990; in press). During, and immediately post-thrusting, the lower portions of the imbricated, thickened rock mass will be cool relative to the "normal" geothermal gradient in the area, and the initial effects of thrusting will be to increase rock and pore fluid pressures rapidly, but essentially isothermally (Norris and Henley, 1976; Dewey, 1988).

Thermal reequilibration occurs during a return to a "normal" geothermal gradient, and the rock temperature increases, as will the temperature of any pore-fluids trapped within the rock mass (Norris and Henley, 1976). These fluids may be remnant metamorphogenic fluids related to F1 prograde metamorphism, or alternatively deeply circulating meteoric waters which penetrated to deep levels prior to the onset of thrust deformation(?): thrusting would effectively prevent further convection of meteoric fluids (Nesbitt and Muehlenbachs, 1989b). Low permeabilities within the warm, ductile/quasi plastic rock mass restrict fluid movement and allow chemical and thermal equilibration of fluids with the surrounding rocks. Retrograde metamorphism occurs at this time.

2) Formation of Foliaform Veins

Thermal expansion of the trapped fluids leads to a further increase in fluid pressure to lithostatic or supralithostatic levels, and hydraulic fracturing/dilation is initiated along the planes of greatest weakness (i.e., parallel to foliation) (Norris and Henley, 1976). Pressure solution and diffusion of mineral components through the pore fluids, leading to the

formation of the foliaform veins, occurs at this stage (Yardley, 1975; Kerrich, 1978). The timing of formation of the foliaform veins was probably towards the latter stages of, or immediately post thrusting (Mortensen et al., in press). Vein quartz precipitated from these fluids is isotopically equilibrated with the immediate host rocks, hence the heterogeneity in $\delta^{18}\text{O}_{\text{quartz}}$ values of foliaform veins (Chapter VI).

3) Uplift of the Klondike Region

The structurally imbricated rock mass heats up further, rock densities decrease and the Klondike begins to uplift during the Middle to Late Jurassic. Uplift rates in orogenic belts may reach as high as 3-6 mm per year (Dewey, 1988). Erosion and removal of material at surface further unloads the imbricate stack and may increase the uplift rate. Extensional structures develop within the crust as the uprising region collapses (Norris and Henley, 1976; Dewey, 1988). If the uplift rate is rapid enough, over-pressures may develop within fluid inclusions hosted by foliaform vein quartz, causing them to decrepitate (Sterner and Bodnar, 1989).

4) Convection of Meteoric Water

In the portion of the crust which has entered the brittle rheological regime, rock permeabilities increase to values above those required for convection of fluids ($>10^{-17}\text{m}^2$) (Nesbitt and Muehlenbachs, 1989). Continued (extensional?) deformation further enhances rock permeabilities, and downflow of meteoric waters is initiated. Convection of these fluids, driven by the now elevated regional geothermal gradient, begins. The fluids acquire volatiles and other transported components as a result of chemical interaction with the host rocks, and undergo substantial isotopic evolution, but not equilibration.

5) Discordant Vein Formation

Convection continues and the uprising fluids, predominantly of meteoric origin but probably including a component of metamorphic fluid, are channelled into the extensional structures. Ore and gangue minerals are deposited in response to changes in the P-T state of the fluids, and as volatiles are lost from the fluid. Wallrock alteration assemblages develop in response to chemical and thermal disequilibrium between the fluid and the vein walls. Uniformity of $\delta^{18}\text{O}$ values of discordant vein quartz imply that the vein system is fluid dominated. Convection and channelling of fluids probably occur over an extended time period, and as uplift continues, pressures within the fluid system decrease initiating effervescence of CO_2 .

At a late stage of uplift (or during an Eocene intrusive event?), hot isotopically light fluids are introduced into the vein system precipitating amethyst in brecciated mesothermal vein quartz.

Implications

The results and interpretations of the fluid inclusion and stable isotope study presented above, have a number of implications for genetic and exploration models of mesothermal vein systems, both in the Cordillera and other regions:

(1) Economic Au-quartz mineralization may develop in any actively uplifting area of regionally metamorphosed rocks in which, (a) suitable shear zones or fault structures develop to act as fluid channels, (b) rock permeabilities are high enough to permit deep penetration and convection of meteoric fluids, and (c) geothermal gradients are high enough to drive convection of the fluids: major crustal scale structures are not necessarily a prerequisite for development of mesothermal vein systems in such a tectonic environment. The bulk of the Yukon-Tanana terrane has suffered a very similar deformational and metamorphic history to the Klondike region (Mortensen, in press). Thus, it is probable that

similar, but as yet undiscovered, Au-mineralization is developed in other parts of the terrane.

(2) A growing body of evidence, collected from a number of Cordilleran vein deposits, suggests that chemically evolved meteoric fluids play a much greater role in mesothermal systems than more generally accepted genetic models allow. Depleted δD_{fluid} values from Klondike Au-quartz veins, obtained from primary inclusion-rich vein quartz *and* mica analyses, add further weight to models which favor meteoric fluid involvement in deep hydrothermal systems within permeable rocks.

(3) Although it is uncertain whether all of the veins exposed within the field area are coeval, it is clear that the Klondike offers a rare opportunity to examine a regional scale mesothermal vein system at a number of different structural levels, and to observe the progressive chemical evolution of the mineralizing fluids as they moved up through the system. The P-T-X trends described in the fluid inclusion study may have developed in response to either regional uplift of the entire system, or a transition from lithostatic to hydrostatic fluid pressures within the system. Also, estimates of fluid pressures indicate that a potentially significant portion of the vein system may have been eroded from the southern Klondike region (e.g., Aime, Gold Run), and that only the deeper roots of the system are exposed in this area.

(4) It is unlikely that any single discordant vein in the Klondike region can be considered the "Mother Lode" placer-Au source, *per se*. Given the abundance of Au-bearing discordant veins across the region, and the degree and duration of weathering (in the absence of glaciation) which has affected the area, it is not unreasonable to speculate that the placer gold was derived by erosion of numerous, low-grade mesothermal veins

rather than a single major Au-rich lode (an hypothesis which is presently being tested through geochemical comparison of placer and hardrock gold [Knight et al., in prep.]).

REFERENCES

- Aleinikoff, J. N., Dusel-Bacon, C., and Foster, H. L., 1986, Geochronology of augen gneiss and related rocks, Yukon-Tanana terrane, east-central Alaska: *Geol. Soc. America Bull.*, v. 97, p. 626-637.
- Alldrick, D. J., 1983, The Mosquito Creek Mine, Cariboo gold belt: *B.C. Min. of Ener. Mines and Petrol. Res.*, Paper 1983-1, p. 99-112.
- Anderson, P. G., and Hodgson, C. J., 1989, The structure and geological development of the Erickson gold mine, Cassiar District, British Columbia, with implications for the origin of mother-lode-type gold deposits: *Canadian Jour. Earth Sci.*, v. 26, p. 2645-2660.
- Angus, S., Armstrong, B., and de Reuck, K. M., 1976, International thermodynamic tables of the fluid state, v. 3, carbon dioxide: Pergamon Press, Oxford, England, 385 p.
- Arai, Y., Kaminishi, G., and Saito, S., 1971, The experimental determination of the P-V-T-X relations for the carbon dioxide-nitrogen and the carbon dioxide-methane systems: *Jour. Chem. Eng. Japan*, v. 4, p. 113-122.
- Armstrong, R. A., 1988, Mesozoic and early Cenozoic magmatic evolution of the Canadian Cordillera: *Geol. Soc. America Spec. Paper* 218, p. 55-92.
- Böhlke, J. K., and Kistler, R. W., 1986, Rb-Sr, K-Ar, and stable isotope evidence for the ages and sources of fluid components of gold-bearing quartz veins in the northern Sierra Nevada foothills metamorphic belt, California: *Econ. Geol.*, v. 81, p. 296-322.
- Böhlke, J. K., Kirschbaum, C., and Irwin, J., (in press), Simultaneous analyses of noble gas isotopes and halogens in fluid inclusions in neutron-irradiated quartz veins a laser microprobe noble gas mass spectrometer: *in* Shanks, W.G., and Criss, R.E. eds., *Frontiers in stable isotope research: Laser probes, Ion probes and Small Sample Analysis*, U. S. Geol. Survey. Bull. 1890.
- Bostock, H. S., 1942, Ogilvie map-sheet; Canada Geol. Survey Map 711A.
- Bostock, H. S., 1957, Yukon Territory: Selected field reports of the Geological Survey of Canada, 1898-1933: *Canada Geol. Survey Mem.* 284, 650 p.
- Bottinga, Y., 1968, Calculation of fractionation factors for carbon and oxygen isotope exchange in the system calcite-carbon dioxide-water: *J. Phys. Chem.*, v. 72, p. 296-322.
- Bowers, T. S., and Helgeson, H. C., 1983, Calculation of the thermodynamic and geochemical consequences of nonideal mixing in the system H_2O-CO_2-NaCl on phase relations in geologic systems: Equation of state for H_2O-CO_2-NaCl fluids at high pressures and temperatures: *Geochem. et Cosmochim. Acta*, v. 47, p. 1247-1276.
- Bowers, T. S., and Taylor, H. P. Jr., 1985, An integrated chemical and stable-isotope model of the origin of Mid-ocean Ridge hot spring systems: *Jour. of Geophys. Research*, v. 90, p. 12583-12606.

- Bowman, J. R., Covert, J. J., Clark, A. H., and Mathieson, G. A., 1985, The CanTung E Zone scheelite skarn orebody, Tungsten, Northwest Territories: Oxygen, hydrogen, and carbon isotope studies: *Econ. Geol.*, v. 80, p. 1872-1895.
- Bozzo, A. T., Chen, H-S., Kass, J. R., and Barduhn, A. J., 1975, The properties of the hydrates of chlorine and carbon dioxide: *Desalination*, v. 16, p. 303-320.
- Brock, R. W., 1909, Yukon Territory: Geological Survey of Canada Summary Report for 1909, *in* Bostock, H.S., 1957, ed., Yukon Territory: Selected field reports of the Geological Survey of Canada, 1898-1933: Canada Geol. Survey Mem. 284, 650 p.
- Brown, P. E., and Lamb, W. M., 1989, P-V-T properties of fluids in the system $H_2O \pm CO_2 \pm NaCl$: New graphical presentations and implications for fluid inclusion studies: *Geochim. Cosmochim. Acta*, v. 53, p. 1209-1222.
- Burrus, R. C., 1981, Analysis of phase equilibria in C-O-H-S fluid inclusions: Mineralog. Assoc. Canada Short Course Handbook, v. 6, p. 39-74.
- Cameron, E. M., 1988, Archean gold: relation to granulite formation and redox zoning in the crust: *Geology*, v. 16, p. 109-112.
- Christie, A. B., Duke, J. L., and Rushton, R. W., in press, Grew Creek epithermal gold-silver deposit, Tintina Trench, Yukon: *in* Yukon Exploration and Geology; Exploration and Geological Services Division, D.I.A.N.D., Yukon,
- Clayton, R. N., and Mayeda, T. K., 1963, The use of bromine pentafluoride in the extraction of oxygen from oxides and silicates for isotopic analysis: *Geochim. Cosmochim. Acta*, v. 27, p. 43-52.
- Coleman, M. L., Shepherd, T. J., Durham, J. J., Rouse, J. E., and Moore, G. R., 1982, Reduction of water with zinc for isotopic analysis: *Analytical Chem.*, v. 54, p. 993-995.
- Collins, P. L. F., 1979, Gas hydrates in CO_2 -bearing fluid inclusions and the use of freezing data for estimation of salinity: *Econ. Geol.*, v. 74, p. 1435-1444.
- Colvine, A. C., Andrews, A. J., Cherry, M. E., Durocher, M. E., Fyon, A. J., Lavigne, M. J., Macdonald, A. J., Marmont, S., Poulsen, K. H., Springer, J. S., and Troop, D. G., 1984, An integrated model for the origin of Archean lode gold deposits: Ontario Geol. Survey, Open File Report 5524, 98 p.
- Connolly, J. A. D., and Thompson, A. B., 1989, Fluid enthalpy and production during regional metamorphism: *Contr. Mineralogy Petrology*, v. 102, p. 347-366.
- Craig, H., 1961, Standard for reporting concentrations of deuterium and oxygen-18 in natural waters: *Science*, v. 133, p. 1833-1834.
- Craw, D., and Koons, P. O., 1988, Tectonically induced gold mineralisation adjacent to major fault zones: *Geol. Soc. Australia Abstracts*, no. 22, p. 338-343.
- Craw, D., 1988, Shallow-level metamorphic fluids in a high uplift rate metamorphic belt; Alpine Schist, New Zealand: *Jour. Metamorph. Geology*, v. 6, p. 1-16.

- Dagenais, G. R., 1984, The oxygen isotope geochemistry of granitoid rocks from the southern and central Yukon: Unpub. M.Sc. thesis, Univ. Alberta, 168 p.
- Debicki, R. L., 1984, Bedrock geology and mineralization of the Klondike area (west), 115 0/14,15 and 16 B/2,3, Open File, 1:50,000 scale map with marginal notes; Exploration and Geological Services Division, D.I.A.N.D., Yukon.
- _____, 1985, Bedrock geology and mineralization of the Klondike area (east), 115 0/9,10, 11, 14, 15, 16, and 16 B/2, Open File, 1:50,000 scale map with marginal notes; Exploration and Geological Services Division, D.I.A.N.D., Yukon.
- Dewey, J. F., 1988, Extensional collapse of orogens: *Tectonics*, v. 7, p. 1123-1139.
- Diamond, L. W., 1986, Hydrothermal geochemistry of late-metamorphic gold-quartz veins at Brusson, Val D'Ayas, Pennine Alps, NW. Italy: Unpub. Ph.D thesis, Swiss Federal Institute of Technology, Zurich, Switzerland, 256 p.
- _____, 1990, Fluid inclusion evidence for P-V-T-X evolution of hydrothermal solutions in Late-Alpine gold-quartz veins at Brusson, Val d'Ayas, N.W. Italian Alps: *Am. Jour. Sci.*, v. 290, p. 912-958.
- Donnelly, H. B., and Katz, D. L., 1954, Phase equilibria in the carbon dioxide-methane system: *Indust. Eng. Chem.*, v. 46, p. 511-517.
- Dowling, K., and Morrison, G., 1989, Application of quartz textures to the classification of gold deposits using North Queensland examples: *Econ. Geol. Mon.* 6, p. 342-355
- Dufresne, M. B., 1987, Origin of gold in the White Channel sediments of the Klondike region, Yukon Territory: Unpub. M.Sc. thesis, Univ. of Alberta, 181 p.
- Dusel-Bacon, C. and Aleinikoff, J. N., 1985, Petrology and tectonic significance of augen gneiss from a belt of Mississippian granitoids in the Yukon-Tanana terrane, east-central Alaska: *Geol. Soc. America Bull.*, v. 96, p. 411-425.
- Essene, E. J., 1988, The current status of thermobarometry in metamorphic rocks: *in* Daly, J.S., Cliff, R.A., and Yardley, B.W.D., eds, *Evolution of metamorphic belts*: *Geol. Soc. London Special Publication* No. 43, 566 p.
- Field, C. W and Ficarek, R. H., 1985, Light stable isotope systematics in the epithermal environment. *Rev. Econ. Geology*, v. 2, p. 99-128.
- Friedrich, F. G., and Hoymann, K. H., 1989, Litho-geochemistry, ore mineralization and alteration of bedrock and auriferous quartz veins, Hunker Dome, Mitchell Vein and Sheba Vein, Klondike area, Yukon Territory, Canada: Preliminary report, Institute für Mineralogie und Lagerstättenlehre, Aachen, West Germany, 45 p.
- Fyfe, W. S., Price, N. J., and Thompson, A. B., 1978, *Fluids in the Earth's crust*: Amsterdam-Oxford-New York, Elsevier Scientific Publishing Company, 383 p.
- Gabrielse, H., 1985, Major dextral transcurrent displacements along the Northern Rocky Mountain Trench and related lineaments in north-central B.C.: *Geol. Soc. Amer. Bull.*, v. 96, p. 1-14.

- Gabrielse, H., and Yorath, C. J., 1989, DNAG #4. The Cordilleran Orogen in Canada: Geoscience Canada. v. 16, p. 67-83.
- Gleeson, C. F., 1970, Heavy mineral studies in the Klondike area, Yukon Territory: Canadian Geol. Survey Bull. 173, 63 p.
- Goldfarb, R. J., Leach, D. L., Pickthorn, W. J., and Paterson, C. J., 1988, Origin of lode-gold deposits of the Juneau gold belt, southeastern Alaska: Geology, v. 16, p. 440-443.
- Goldfarb, R. J., Leach, D. L., Rose, S. C., and Landis, G. P., 1989, Fluid inclusion geochemistry of gold-bearing quartz veins of the Juneau Gold Belt, Southeastern Alaska: Implications for ore genesis: Econ. Geol. Mon. 6, p. 363-375.
- Graham, C. M., 1981, Experimental hydrogen isotope studies III: Diffusion of hydrogen in hydrous minerals, and stable isotope exchange in metamorphic rocks: Contr. Mineralogy Petrology, v. 76, p. 216-227.
- Green, L. H., 1972, Geology of Nash Creek, Larson Creek and Dawson map-areas, Operation Ogilvie: Canadian Geol. Survey Mem. 364, 156 p.
- Groves, D. I., and Phillips, G. N., 1987, The genesis and tectonic control on Archean gold deposits of the Western Australian Shield- a metamorphic replacement model: Ore Geology Rev., v. 2, p. 287-322.
- Groves, D. I., and Foster, R. P., 1991, Archean lode gold deposits: in Foster, R. P., ed., Gold metallogeny and exploration: Glasgow, Blackie Sons Ltd., p. 63-103.
- Haas, J. L. Jr., 1976, Physical properties of the coexisting phases and thermochemical properties of the H₂O component in boiling NaCl solutions: U.S. Geol. Survey Bull. 1421-A, 73 p.
- Hansen, V. L., 1988, A model for terrane accretion: Yukon-Tanana and Slide Mountain terranes, northwest North America: Tectonics, v. 7, No.6, p.1167-1177.
- Hansen, V. L., Mortensen, J. K., and Armstrong, R. L., 1989, U-Pb, Rb-Sr, and K-Ar isotopic constraints for ductile deformation and related metamorphism in the Teslin suture zone, Yukon-Tanana terrane, south-central Yukon: Canadian Jour. Earth Sci., v. 26, p. 2224-2235.
- Hansen, V. L., 1990, Yukon-Tanana terrane: a partial acquittal: Geology, v. 18, p. 365-369.
- Hedenquist, J. W., and Henley, R. W., 1985, The importance of CO₂ on freezing point measurements of fluid inclusions: Evidence from active geothermal systems and implications for epithermal ore deposition: Econ. Geol., v. 80, p. 1379-1406.
- Heyen, G., Ramboz, C., and Dubessy, J., 1982, Simulation des equilibres de phases dans le systeme CO₂-CH₄ en dessous de 50° et de 100 bar. Application aux inclusions de fluides: Acad. Sci. (Paris) Comptes Rendus, v. 294, sér. 2, p. 203-206.
- Kerrick, R. W., 1978, Some effects of tectonic recrystallisation on fluid inclusions in vein quartz: Contr. Mineralogy Petrology, v. 59, p.195-202.

- Kerrich, R. W., 1987, The stable isotope geochemistry of Au-Ag vein deposits in metamorphic rocks: Mineralog. Assoc. Canada Short Course Handbook, v. 13, p. 287-336.
- Kerrich, R. W., 1989, Geochemical evidence on the sources of fluids and solutes for shear zone hosted mesothermal Au deposits: Geol. Assoc. Canada, Short Course Notes, v. 6, p.129-198.
- Kerrich, R. W., and Fyfe, W. S., 1981, The gold-carbonate association: source of CO₂ and CO₂-fixation reactions in Archean lode gold deposits: Chem. Geology. v. 33, p. 265-294.
- Kerrich, R. W., and Wyman, D. 1990, Geodynamic setting of mesothermal gold deposits: an association with accretionary tectonic regimes: Geology v. 18, p. 882-885.
- Knight, C. L., and Bodnar, R. J., 1989, Synthetic fluid inclusions: IX. Critical PVTX properties of NaCl-H₂O solutions: Geochim. Cosmochim. Acta, v. 53, p. 3-8.
- Kyser, T. K., 1987, Equilibrium fractionation factors for stable isotopes: Mineralog. Assoc. Canada Short Course Handbook, v. 13, p. 1-76.
- Kyser, T. K., and Kerrich, R., 1990, Geochemistry of fluids in tectonically active regions: Mineralog. Assoc. Canada Short Course Handbook, v. 18, p. 133-215.
- Landefeld, L. A., 1988, The geology of the Mother Lode gold belt, Sierra Nevada Foothills metamorphic belt, California (abs.): Geol. Soc. Australia Abstracts, no. 22, p. 167-172.
- LeBarge, W., and Bremner, T., 1991, Lone Star: *in* Yukon Exploration 1990, Part C: Geological Descriptions of Selected Properties, Indian and Northern Affairs Canada, 64 p.
- Leitch, C. H. B., 1990, Bralorne: a mesothermal, shield-type vein gold deposit of Cretaceous age in southwestern British Columbia: Canadian Inst. Mining Metal. Bulletin, v. 83, No. 941, p. 53-80.
- Lynch, J. V. G., 1989, Hydrothermal zoning in the Keno Hill Ag-Pb-Zn vein system: A study in structural geology, mineralogy, fluid inclusions and stable isotope geochemistry: Unpub. PhD. thesis, Univ. Alberta, 217 p.
- MacLean, T. A., 1914, Lode mining in the Yukon: An investigation of quartz deposits in the Klondike division: Canada Dep.t. Mines, Mines Branch, Publication 222, 205 p.
- Madu, B. E., Nesbitt, B. E., and Muehlenbachs, K., 1990, A mesothermal gold-stibnite-quartz vein occurrence in the Canadian Cordillera: Econ. Geol., v. 85, p. 1260-1268.
- Maheux, P. J., 1989, A fluid inclusion and light stable isotope study of antimony-associated gold mineralization in the Bridge River District, British Columbia, Canada: Unpub. M.Sc. thesis, Univ. of Alberta, 159 p.

- Matsuhisa, Y., Goldsmith, J. R., and Clayton, R. N., 1979, Oxygen isotopic fractionations in the system quartz-albite-anorthite-water: *Geochim. Cosmochim. Acta*, v. 43, p. 1131-1140.
- McConnell, R. G., and Tyrrell, J. B., 1898, Preliminary note on the gold deposits and gold mining in the Klondike region: *in* Bostock, H. S., 1957, ed., Yukon Territory: Selected field reports of the Geological Survey of Canada, 1898-1933: Canada Geol. Survey Mem. 284, 650 p.
- McConnell, R. G., 1905, Report on the Klondike gold fields: *in* Bostock, H. S., 1957, ed., Yukon Territory: Selected field reports of the Geological Survey of Canada, 1898-1933: Canada Geol. Survey Mem. 284, 650 p.
- McCrea, J. M., 1950, On the isotopic chemistry of carbonates and a paleotemperature scale: *J. Chem. Physics*, v. 18, p. 849-857.
- McKeag, S. A., and Craw, D., 1989, Contrasting fluids in gold-bearing quartz vein systems formed progressively in a rising metamorphic belt: Otago Schist, New Zealand: *Econ. Geol.*, v. 84, p. 22-33.
- Metcalf, P., 1981, Petrogenesis of the Klondike Formation, Yukon Territory: Unpub. M Sc. thesis, Univ. Manitoba, 103 p.
- Milner, M. W., 1976, Geomorphology of the Klondike placer goldfields: Final Report, Contract OSV 5-0047, Exploration and Geological Services Division, D.I.A.N.D., Yukon, 157 p.
- Monger, J. W. H., Price, R. A., and Templeman-Kluit, D. J., 1982, Tectonic accretion and the origin of the two major metamorphic and plutonic belts in the Canadian Cordillera: *Geology*, v. 10, p. 70-75.
- Monger, J. W. H., 1984, Cordilleran tectonics: a Canadian perspective; *Bull. Soc. Géol. France*, 1984, no. 2, p. 255-278.
- Morison, S. R., and Hein, F. J., 1987, Sedimentology of the White Channel Gravels, Klondike area, Yukon Territory: Fluvial deposits of a confined valley: *in* Society of Economic Paleontologists and Mineralogists, Special Publication 39, p. 205-216.
- Morrison, G. W., 1988, Paleozoic gold deposits in Northeast Queensland: *Geol. Soc. Australia Abstracts*, no. 22, p. 91-101.
- Mortensen, J. K. and Jilson, G. A., 1985, Evolution of the Yukon-Tanana terrane: Evidence from southeastern Yukon Territory: *Geology*, v. 13, p. 806-810.
- Mortensen, J. K., 1990, Geology and U-Pb Geochronology of the Klondike District, west-central Yukon Territory: *Canadian Jour. Earth Sci.*, v. 27, p. 903-914.
- in press, Pre-Mid-Mesozoic tectonic evolution of the Yukon-Tanana terrane, Yukon and Alaska: *Tectonics*.
- Mortensen, J. K., Nesbitt, B. E., and Rushton, R. W., in press, Preliminary observations on the geology and geochemistry of quartz veins in the Klondike District, West-Central Yukon: *in* Yukon Exploration and Geology; Exploration and Geological Services Division, D.I.A.N.D., Yukon.

- Mortensen, J. K., in press, *in* Hunt, P. A., and Roddick, J. C., Radiogenic age and isotopic studies, Report 5, Canada Geol. Survey Paper 91-2.
- Nesbitt, B. E., Murowchick, J. B., and Muehlenbachs, K., 1986, Dual origins of lode gold deposits in the Canadian Cordillera: *Geology*, v. 14, p. 506-509.
- _____ 1987, Reply to a comment on "Dual origins of lode gold deposits in the Canadian Cordillera": *Geology*, v. 15, p. 472-473.
- Nesbitt, B. E., Muehlenbachs, K., and Murowchick, J. B., 1989, Genetic implications of stable isotope characteristics of mesothermal Au deposits and related Sb and Hg deposits in the Canadian Cordillera: *Econ. Geol.*, v. 84, p. 1489-1506.
- Nesbitt, B. E., 1988, The gold deposit continuum: A genetic model for lode gold mineralisation in the continental crust: *Geology*, v. 16, p. 1044-1048.
- Nesbitt, B. E., 1990, Fluid flow and chemical evolution in the genesis of hydrothermal ore deposits: *Mineralog. Assoc. Canada Short Course Handbook*, v. 18, p. 261-292.
- Nesbitt, B. E., and Muehlenbachs, K., 1989a, *Geology, geochemistry and genesis of mesothermal lode gold deposits of the Canadian Cordillera: Evidence for ore formation from evolved meteoric water: Econ. Geol. Mon.* 6, p. 553-563.
- _____ 1989b, Origins and movement of fluids during deformation and metamorphism in the Canadian Cordillera: *Science*, v. 245, p. 733-736.
- _____ 1991, Comment on "Mélange- and Sediment-Hosted Gold-Bearing Quartz Veins, Hodgkinson Gold Field, Queensland, Australia": *Econ. Geol.*, v. 86, p. 195-197.
- Nesbitt, B. E., 1991, Phanerozoic gold deposits in tectonically active continental margins, *in* Foster, R. P., ed., *Gold metallogeny and exploration: Glasgow, Blackie Sons Ltd.*, p. 104-132.
- Norris, R. J., and Henley, R. W., 1976, Dewatering of a metamorphic pile: *Geology*, v. 4, p. 333-336.
- Northern Cordillera Mineral Inventory: Unpublished company report, Archer, Cathro and Associates (1981) Ltd.
- O'Neil, J. R., and Taylor, H. P., Jr., 1969, Oxygen isotope equilibrium between muscovite and water: *Jour. of Geophys. Research*, V. 74, p. 6012-6022.
- O'Neil, J. R., Clayton, R. N., and Mayeda, T. K., 1969, Oxygen isotope fractionation in divalent metal carbonates: *Jour. Chem. Phys.*, v. 51, p. 5547-5558.
- Peters, S. G., and Golding, S. D., and Dowling, K., 1990, Mélange- and Sediment-Hosted Gold-Bearing Quartz Veins, Hodgkinson Gold Field, Queensland, Australia: *Econ. Geol.* v. 85, p. 312-327.
- _____ 1991, Reply to a comment on "Mélange- and Sediment-Hosted Gold-Bearing Quartz Veins, Hodgkinson Gold Field, Queensland, Australia": *Econ. Geol.*, v. 86, p. 197-200.

- Phillips, G. N., and Groves, D. I., 1983, The nature of Archean gold-bearing fluids as deduced from gold deposits of Western Australia: *Geol. Soc. Australia Jour.*, v. 30, p. 25-39.
- Pickthorn, W. J., Goldfarb, R. J., and Leach, D. L., 1987, Comment on "Dual origins of lode gold deposits in the Canadian Cordillera": *Geology*, v. 15, p. 471-472.
- Potter, R. W. II, and Brown, D. L., 1977, The volumetric properties of aqueous sodium chloride solutions from 0° to 500° C at pressures up to 2000 bars based on a regression of available data in the literature: *U.S. Geol. Survey. Bull.* 1421-C, 36 p.
- Potter, R. W. II, Clyne, M. A., and Brown, D. L., 1978, Freezing point depression of aqueous sodium chloride solutions: *Econ. Geol.*, v. 73, p. 284-285.
- Ramboz, C., Pichavant, M., and Weisbrod, A., 1982, Fluid immiscibility in natural processes: Use and misuse of fluid inclusion data II. Interpretation of fluid inclusion data in terms of immiscibility: *Chem. Geology*, v. 37, p. 29-48.
- Robert, F., and Kelly, W. C., 1987, Ore-forming fluids in Archean gold-bearing veins at the Sigma mine, Abitibi Greenstone belt, Quebec, Canada: *Econ. Geol.*, v. 82, p. 1464-1482.
- Roedder, E., 1984, Fluid Inclusions: *Rev. Mineralogy*, v. 12, 644 p.
- Rogers, P. S. Z., and Pitzer, K. S., 1982, Volumetric properties of aqueous sodium chloride solutions: *Jour. Phys. Chem. Ref. Data*, v. 11, p. 15-81.
- Rumble, D., 1978, Mineralogy, petrology, and oxygen isotopic geochemistry of the Clough Formation, Black Mountain, western New Hampshire, U.S.A.: *J. Petrol.*, v. 19, p. 317-340.
- Rushton, R. W., Nesbitt, B. E., and Mortensen, J. K., 1990, Fluid inclusion and stable isotope study of mesothermal Au-quartz veins in the Klondike schist, Klondike District, Yukon Territory: *Geol. Assoc. Canada, Program with Abstracts*, v. 15, p. A115.
- Schwartz, M. O., 1989, Determining phase volumes of mixed CO₂-H₂O inclusions using microthermometric measurements: *Mineralium Deposita*, v. 24, p.43-47.
- Sevigny, J. H., Parrish, R. R., Donelick, R. A., and Ghent, E. D., 1990, Northern Monashee Mountains, Omineca Crystalline belt, British Columbia: Timing of metamorphism, anatexis, and tectonic denudation: *Geology*. v. 18, p. 103-106.
- Seward, T. M., 1989, The hydrothermal geochemistry of gold and its implications for ore formation: boiling and conductive cooling as examples: *Econ. Geol. Mon.* 6, p. 398-404.
- Shaw, R. P., Morton, R. D., Gray, J., and Krouse, H. R., 1991, Origins of metamorphic gold deposits: Implications of stable isotope data from the central Rocky Mountains, Canada: *Mineralogy and Petrology*, v. 43, p. 193-209.

- Shelton, K. L., So, C. -S., and Chang, J. -S., 1988, Gold-rich mesothermal vein deposits of the Republic of Korea: Geochemical studies of the Jungwon gold area: *Econ. Geol.*, v. 83, p. 1221-1237.
- Shepherd, T. J., Rankin, A. H., and Alderton, D. H. M., 1985, A practical guide to fluid inclusion studies: Glasgow, Blackie and Son Limited, 293 p.
- Sheppard, S. M. F., 1986, Characterization and isotopic variations in natural waters: *Rev. Mineralogy*, v. 16, p. 165-183.
- Sibson, R. H., 1990, Faulting and fluid flow: *Mineralog. Assoc. Canada Short Course Handbook*, v. 18, p. 93-129.
- Sketchley, D. A., Sinclair, A. J., and Godwin, C. I., 1986, Early Cretaceous gold-silver mineralization in the Sylvester allochthon, near Cassiar, north central British Columbia: *Canadian Jour. Earth Sci.*, v. 23, p. 1455-1458.
- Sterner, S. M., and Bodnar, R. J., 1989, Synthetic fluid inclusions-VII. Re-equilibration of fluid inclusions in quartz during laboratory-simulated metamorphic burial and uplift: *Jour. Met. Geology*, v. 7, p. 243-260.
- Suzuoki, T., and Epstein, S., 1976, Hydrogen isotope fractionation between OH-bearing minerals and water: *Geochem. et Cosmochim. Acta*, v. 40, p. 1229-1240.
- Swanenberg, H. E. C., 1979, Phase equilibria in carbonic systems and their application to freezing studies of fluid inclusions: *Contr. Mineralogy Petrology*, v. 68, p. 303-306.
- Takenouchi, S., and Kennedy, G. C., 1965, The solubility of carbon dioxide in NaCl solutions at high temperatures and pressures: *Am. Jour. Sci.*, v. 263, p. 445-454.
- Taylor, H. P., Jr., and Sheppard, S. M. F., 1986, Igneous rocks: I. Processes of isotopic fractionation and isotope systematics: *Rev. Mineralogy*, v. 16, p. 227-272.
- Teagle, D. A. H., Norris, R. J., and Craw, D., 1990, Structural controls on gold-bearing quartz mineralization in a duplex thrust system, Hyde-Macraes shear zone, Otago Schist, New Zealand: *Econ. Geol.*, v. 85, p. 1711-1719.
- Templeman-Kluit, D., 1976, The Yukon Crystalline Terrane: enigma in the Canadian Cordillera: *Geol. Soc. America Bull.*, v. 87, p. 1343-1357.
- Templeman-Kluit, D., 1979, Transported cataclasite, ophiolite and granodiorite in Yukon: evidence for arc-continent collision: *Canada Geol. Survey Paper 79-14*, 27 p.
- Templeman-Kluit, D., 1982, White Chanel gravel of the Klondike: *Yukon Exploration and Geology 1981*; Exploration and Geological Services Division, D.I.A.N.D., p. 74 -79.
- Tyrrell, J. B., 1912, The Gold of the Klondike: *Transcripts Roy. Soc. Canada, Third Series, Section IV*, v. 6, p. 29-59.
- Van Angeren, P., 1989, The Lone Star Property. A new assesment of the Boulder Lode: Unpublished company report, Dawson Eldorado Mines Ltd.

- Vidale, R. J., 1974, Vein assemblages and metamorphism in Dutchess County, New York: Geol. Soc. America Bull., v. 85, p. 303-306.
- Vogel, J. C., Grootes, P. M., and Mook, W. G., 1970, Isotopic fractionation between gaseous and dissolved carbon dioxide: Zeit. Physik. v. 230, p. 225-238.
- Walton, L. A., 1987, Geology and geochemistry of the Venus Au-Ag-Pb-Zn vein deposit, Yukon Territory: Unpub. M.Sc. thesis, Univ. of Alberta, 113 p.
- Weir, R. H. Jr., and Kerrick, D. M., 1987, Mineralogic, fluid inclusion and stable isotope studies of several gold mines in the Mother Lode, Tuolumne and Mariposa counties, California: Econ. Geol., v. 82, p. 328-344.
- Whelan, B. L., and Meixner, H. M., 1989, Review of the lode gold potential on eleven claim blocks of the Hughes-Lang Klondike project, Dawson Mining District, Yukon Territory: Unpublished company report, Adventure Exploration, 40 p.
- Wiebe, R., and Gaddy, V. L., 1941, Vapor phase composition of carbon dioxide-water mixtures at various temperatures and pressures to 700 atm.: American Chemical Society Journal, v. 63, p.475-477.
- Yardley, B. W. D., 1975, On some quartz veins in the Connemara schists, Ireland: Geological Magazine, v. 112(2), p. 183-190.
- Yardley, B. W. D., 1983, Quartz veins and devolatilization during metamorphism: Journal of the Geol. Soc. of London, v. 140, p. 657-663.
- Yardley, B. W. D., 1986, Fluid migration and veining in the Connemara Schists, Ireland: *in* Walther, J.V., and Wood, B.J., (Eds), Fluid-rock interactions during metamorphism, 218 p.
- Zhang, X., Nesbitt, B. E., and Muehlenbachs, K., 1989, Gold mineralization in the Okanagan Valley, Southern British Columbia: Fluid inclusion and stable isotope studies: Econ. Geol., v. 84, p. 410-424.

Appendices

Appendix 1

Correction of F_{CO_2} and X_{CO_2} using the procedure of Diamond (1986)

Despite the large error introduced into fluid-composition calculations through the use of visual F_{CO_2} estimates, it is possible to partially correct for these errors using an iterative technique described by Diamond (1986).

For each CO_2 -bearing vein set, three pairs of 2-phase curves and fluid isochores were calculated on the basis of estimated $F_{CO_2} \pm 1$ standard deviation. For example, using data from the Gold Run lode (Figure A), the average F_{CO_2} estimate is 0.34 ± 0.10 . Using the minimum, average and maximum values of F_{CO_2} , three values for X_{CO_2} ($X_{CO_2} \approx 0.09, 0.12$ and 0.165) of the inclusion fluids were calculated. Three 2-phase curves were then constructed for these compositions from the data of Takenouchi and Kennedy (1965), with corresponding fluid isochores for fluid densities of 0.94, 0.89 and 0.84 g/cc respectively calculated from Bowers and Helgeson (1983). If this range of visual estimates encompasses the true F_{CO_2} , the origin of one of the fluid isochores at the appropriate 2-phase curve should approximately correspond to the intersection of the known average Th_{TOT} line with the same 2-phase curve.

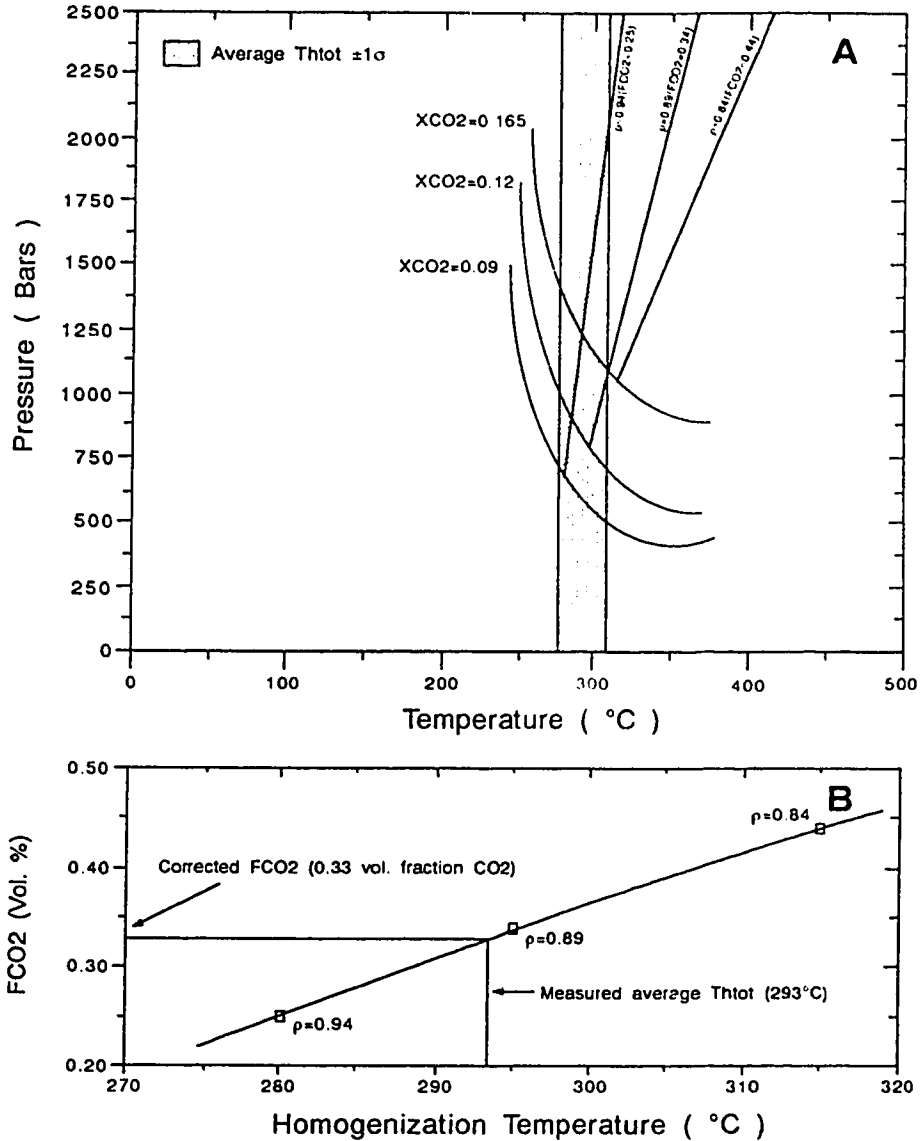
For the Gold Run data, it can be seen from Figure A that the origins of all three isochores fall within, or close to, the projected temperature range of $293 \pm 17^\circ C$. However, the temperature at the origin of the 0.89 g/cc isochore with the $X_{CO_2} = 0.12$, 2-phase boundary curve is closest to the mean temperature line. This suggests that the visual F_{CO_2} estimate of 0.34 is fairly close to the true value, and that the fluid contains approximately 0.12 mole fraction CO_2 .

This technique can be refined further. For each of the calculated isochores, the temperature coordinate of the isochore origin should correspond to the theoretical homogenization temperature of inclusions containing fluid with that specific composition and density. Therefore, by graphically comparing the three values of F_{CO_2} and the corresponding predicted homogenization temperatures, the value of F_{CO_2} which corresponds to the *known* Th_{TOT} can be obtained from the graph (Figure B) (Diamond, 1986). The corrected F_{CO_2} value can then be used to graphically fix the fluid density and X_{CO_2} .

For the Gold Run data, the homogenization temperature of $293^\circ C$ gives a corrected F_{CO_2} of 0.33, and $X_{CO_2} = 0.12$. The corrected values of X_{CO_2} and F_{CO_2} derived in this way agree well with values derived using the graphical technique of Schwartz (1989).

It is noteworthy that none of the isochore origins calculated from the Aime lode data lay within the range of measured homogenization temperatures. From isochore origins, the

predicted homogenization temperature range for the compositional estimate is 280-300°C, approximately 20°C above the average T_{tot} (a similar temperature of 286°C was obtained graphically from Schwartz (1989) using the known CO_2 density and the calculated X_{CO_2}). The reasonable agreement between predicted and measured homogenization temperatures from other locations suggests that the *average* visual estimates of F_{CO_2} are fairly precise. Therefore, the temperature discrepancy for the Aime data is best explained if the average homogenization temperature is low. Because of the relatively high CO_2 densities encountered in the Aime inclusions (Table 1), small variations in F_{CO_2} and/or the CO_2 phase density within individual inclusions, will have a large effect on the CO_2 concentration and the pressure at total homogenization. Inclusions containing fluids with high X_{CO_2} will have lower bulk fluid densities, and higher isochore-origin P/T coordinates than the average inclusion population. As a result, they will tend to decrepitate before total homogenization occurs, and bias the T_{tot} histogram towards a low average temperature. If the F_{CO_2} estimates were 100% precise, this effect could be demonstrated by graphically comparing X_{CO_2} with the frequency of decrepitation/homogenization for the measured temperatures. However, the large error inherent in *individual* F_{CO_2} estimates precludes using the calculated X_{CO_2} values of single inclusions for precise graphical comparison. The temperature and frequency of fluid inclusion decrepitations is also greatly dependent on the strength of the host mineral, but no attempt was made in this study to account for this because of the complexities involved.



Appendix 1, Figure A. Example of construction of three sets of 2-phase curves and matching fluid isochores, based on the average volume percent CO_2 estimate plus/minus 1 standard deviation from the Gold Run, Au-quartz vein data (see text). Figure B. Graphical correction procedure, using known and predicted homogenization temperatures, to correct the visual estimate of volume percent CO_2 (see text). 2-phase curves constructed from the data of Takenouchi and Kennedy (1965). Isochores coordinates calculated from the data of Bowers and Helgeson (1983). Construction method in Figure B from Diamond (1986).

Appendix 2. Microthermometric data for Au-bearing and foliaform vein quartz.

Sample/ location ¹	Vein type	Inc. origin	Phase assem ²	Vol.% H ₂ O ³	T _{mCO2}	T _{mice}	T _{mclath}	T _{hCO2} ⁴	T _{htot} T _{dec} ⁵	Eq.Wt. % NaCl
<i>RB4-29-5 ch 1</i> Aime	Disc	P	L-V	60	-56.6	-	7.8	24.2	260.0	4.3
		P	L-V	70	-56.7	-	8.1	24.0	250.0	3.8
		P	L-V	60	-56.6	-	8.0	23.9	255.0	4.0
		P	L-V	-	-56.6	-	7.9	22.8	228.0	4.1
<i>RB4-29-5 ch 2</i>	P?	L-V	90	not seen	-	5.1	not seen	207.0	8.9	
		L-L-V	80	-56.7	-	7.8	25.2	273.2	4.4	
		L-L-V	80	-56.6	-	7.3	26.4	280.0	5.2	
		L-L-V	60	-56.9	-	8.1	22.0	249.0	3.9	
<i>KS2 ch 1</i> Hunker Dome <i>KS2 ch 3</i>	Disc	P/PS	L-L-V	60	-56.6	-	7.5	27.5	304.1	5.0
		P/PS	L-L-V	65	-57.1	-	6.9	25.7	280.0	5.9
		P	L-L-V	80	-58.0	-	9.0	26.3	272.7	2.0
		P	L-V	90	-	-0.8	-	-	229.5	1.4
		P	L-L-V	70	-57.7	-	8.8	26.3	274.0	2.4
		P	L-L-V	80	-57.7	-	8.5	27.2	283.0	3.1
<i>KS3A ch 1</i> Hunker Dome <i>KS3A ch 2</i>	Ffm	P/PS	L-V	95	-	-2.1	-	-	150.9	3.5
		P/PS	L-V	90	-	-3.4	-	-	228.0	5.5
		P	L-V	70	-	not seen	-	-	278.3	-
		P	L-V	70	-	not seen	-	-	278.4	-
		P	L-V	70	-	-1.9	-	-	245.0	3.1
		PS/S	L-V	90	-	-2.4	-	-	236.5	4.0
<i>KS4 ch 1</i> Mitchell <i>KS4 ch 2</i>	Disc	P	L-L-V	50	-56.9	-	6.9	(28.3)	335.2	5.9
		P?	L-L-V	50	-56.9	-	6.5	(28.0)	341.6	6.6
		P?	L-L-V	50	-57.0	-	6.6	27.1	319.0	6.5
		PS	L-L-V	50	-56.7	-	6.9	28.4	328.7	5.9
		P?	L-L-V	65	-56.8	-	6.1	28.3	319.9	7.3
		S?	L-V	60	-56.7	-	6.0	not seen	307.8	7.5
<i>KS4 ch 3</i>	S	L-V	80	-	-2.8	-	-	315.4	4.6	
		L	100	-	-0.3	-	-	240.0	0.5	
		L-V	60	-	-1.5	-	-	340.2	2.6	
		L-V	60	-	-3.2	-	-	304.2	5.2	
<i>KS7A ch 1</i> Lloyd <i>KS7A ch 2</i>	Ffm	S	L-V	85	-	-4.7	-	-	244.2	7.4
		S	L-V	80	-	-4.3	-	-	242.7	6.9
		S	L-V	90	-	-4.4	-	-	240.2	7.0
		S	L-V	80	-	-4.4	-	-	235.3	6.9
		S	L-V	80	-	-4.3	-	-	238.4	6.8
		S	L-V	90	-	-4.6	-	-	241.6	7.3
<i>KS7A ch 2</i>	Ffm	S	L-V	90	-	-4.8	-	-	239.5	7.6
		S	L-V	90	-	-4.6	-	-	238.3	7.2
		S	L-V	90	-	-4.6	-	-	233.1	7.3
		S	L-V	90	-	-4.6	-	-	250.6	7.2
		S	L-V	85	-	-4.6	-	-	237.4	7.2
		S	L-V	90	-	-4.6	-	-	231.3	7.2
<i>KS 7A ch 3</i>	Ffm	P?	L-V	70	-	-5.5	-	-	312.2	8.5
		S	L-V	80	-	-5.2	-	-	274.0	8.1
		P?	L-V	70	-	-5.2	-	-	273.8	8.1
		P?	L-V	70	-	-5.0	-	-	266.9	7.9

Appendix 2 continued

Sample/ location ¹	Vein type	Inc. origin	Phase assem ²	Vol.% H ₂ O ³	TmCO ₂	Tmice	Tmclath	ThCO ₂ ⁴	T _{htot} T _{dec} ⁵	Eq.Wt. % NaCl
<i>KS8 ch 1</i> Lone Star	Disc	P?	L-V	90	-	-3.1	-	-	296.2	5.0
		P?	L-V	70	-	-3.1	-	-	not seen	5.1
		P?	L-V	80	-	not seen	-	-	311.2	-
		P?	L-V	70	-	-3.8	-	-	310.2	6.1
		P?	L-V	65	-	-3.5	-	-	298.0	5.6
<i>KS9 ch 1</i> Lone Star	Ffm	P/PS	L-V	80	-	-3.2	-	-	290.4	5.2
		P/PS	L-V	85	-	-3.0	-	-	297.5	4.9
		P/PS	L-V	80	-	-3.1	-	-	not seen	5.1
		P/PS	L-V	80	-	not seen	-	-	283.9	-
		P/PS	L-V	80	-	-3.0	-	-	280.8	4.9
<i>KS9 ch 2</i>	P/PS	L-V	80	-	-2.8	-	-	292.0	4.6	
		L-V	60	-	-5.2	-	-	291.6	8.1	
		L-V	70	-	-5.0	-	-	313.1	7.8	
		L-V	70	-	-5.1	-	-	311.5	8.0	
		L-V	70	-	-5.1	-	-	311.5	8.0	
<i>KS10 ch 1</i> Pioneer Adit	Disc	P/PS	L-V	90	-	-0.4	-	-	218.3	0.7
		P/PS	L-V	80	-	-0.4	-	-	205.3	0.7
		P/PS	L-V	90	-	-0.4	-	-	215.7	0.7
		P/PS	L-V	80	-	-0.3	-	-	230.0	0.4
		P/PS	L-V	60	-	-0.8	-	-	296.2	1.4
		P/PS	L-V	80	-	-0.9	-	-	300.2	1.5
<i>KS 11 ch 1</i> Pioneer Adit	FFm	PS	L-V	90	-	-0.9	-	-	248.3	1.5
		PS	L-V	60	-	-1.2	-	-	281.4	2.1
		PS	L-V	95	-	-0.7	-	-	261.7	1.1
<i>KS11 ch 2</i>	S/PS	L-V	60	-	-1.6	-	-	323.4	2.7	
		L-V	60	-	-1.5	-	-	319.8	2.5	
		L-V	70	-	-0.7	-	-	325.7	1.2	
		L-V	60	-	-0.8	-	-	329.5	1.3	
		L-V	70	-	-1.0	-	-	331.8	1.7	
<i>YR7 ch 1</i> Bear Ck.	Ffm	P	L-V	90	-	-1.9	-	-	137.5	3.2
		P	L-V	95	-	-0.1	-	-	134.5	0.2
		P	L-V	90	-	-0.7	-	-	140.0	1.2
<i>YR9 ch 1</i> Virgin	Disc	P	L-V	90	-	-2.9	-	-	201.0	4.8
		P	L-V	90	-	-2.7	-	-	202.2	4.5
		P	L-V	90	-	-3.4	-	-	198.5	5.5
		P	L-V	80	-	-3.4	-	-	not seen	5.5
		P	L-V	80	-	-3.2	-	-	200.7	5.2
<i>YR9 ch 2</i>	P	L-V	95	-	-2.7	-	-	175.5	6.0	
		L-V	90	-	-3.1	-	-	191.0	5.0	
		L-V	90	-	-3.2	-	-	182.8	5.2	
<i>YR9 ch 3</i>	P/PS	L-V	80	-	-2.9	-	-	212.5	4.8	
		L-V	85	-	-3.4	-	-	204.8	5.5	
		L-V	85	-	-2.9	-	-	200.8	4.8	
		L-V	90	-	-3.2	-	-	197.7	5.2	
		L-V	95	-	-3.3	-	-	204.7	5.4	
<i>YR14 ch 1</i> Hunker Ck.	Ffm	P	L-V	90	-	-5.5	-	-	232.5	8.5
		P	L-V	70	-	-3.7	-	-	207.3	5.9

Appendix 2 continued

Sample/ location ¹	Vein type	Inc. origin	Phase assam ²	Vol.% H ₂ O ³	T _{mCO2}	T _{mice}	T _{mclath}	ThCO ₂ ⁴	T _{htot} T _{dec} ⁵	Eq.Wt. % NaCl
YR14 ch 1 cont.d	Ffm	P	L-V	90	-	-4.0	-	-	193.4	6.4
		P	L-V	85	-	-4.3	-	-	189.0	6.9
		P	L-V	80	-	-4.3	-	-	209.7	6.9
		P	L-V	90	-	-4.5	-	-	206.7	7.1
YR14 ch 2	PS/P	L-V	50	-	-4.1	-	-	409.0	6.5	
		L-V	60	-	-3.9	-	-	397.0	6.2	
		L-V	60	-	not seen	-	-	380.0	-	
YR15 ch 1 Hunker Dome	Disc	PS/P	L-V	92	-59.3	-	8.4	8.7	203.0	3.2
		PS/P	L-L-V	60	-57.5	-	7.2	(27.1)	320.9	5.5
		PS/P	L-L-V	50	-57.5	-	8.5	26.0	[336.5]	3.1
		PS/P	L-L-V	50	-57.4	-	7.0	27.2	-	5.9
		PS/P	L-L-V	60	-	-	-	(27.3)	-	-
YR15 ch 2	PS/P	L-L-V	60	-57.1	-	7.0	27.6	323.7	5.8	
		L-L-V	60	-57.4	-	6.1	(27.0)	[380.6]	7.3	
		L-L-V	60	-57.2	-	5.8	(26.7)	not seen	7.9	
		L-L-V	60	-57.4	-	6.4	27.0	340.0	6.8	
YR18 ch 1 Hunker Dome	Disc	P	L-L-V	70	-56.5	-	8.3	25.4	310.0	3.4
		P	L-L-V	60	-56.5	-	7.9	25.6	not seen	4.2
		P	L-L-V	60	-56.6	-	7.8	25.2	325.0	4.3
		P	L-L-V	55	-56.6	-	8.1	25.8	305.8	3.8
		P	L-L-V	70	-55.5	-	7.8	28.1	326.1	4.3
YR18 ch 2	P	L-V	80	-	-5.8	-	-	254.8	6.9	
		L-V	80	-	-	-	-	243.8	-	
		L-V	70	-55.8	-	7.0	27.5	301.0	5.8	
		L-L-V	60	-56.1	-	8.0	24.2	not seen	3.9	
		L-L-V	60	-55.6	-	6.8	25.6	309.5	6.1	
		L-L-V	60	-56.0	-	7.9	25.4	303.0	4.2	
YR20 ch 1 Dominion Ck.	Disc	P	L-V	70	-56.8	-	8.0	28.6	250.6	4.0
		P	L-V	70	-56.7	-	7.9	27.5	259.2	4.1
		P	L-V	60	-55.8	-	7.9	not seen	250.3	4.1
		P	L-V	70	-56.7	-	8.0	28.2	248.0	4.0
		S	L-V	95	-	-0.6	-	-	not seen	1.0
YR24 ch 1 Dominion Ck.	Ffm	P	L-V	60	-57.9	-	6.6	-	341.2	6.5
		P	L-V	60	-57.3	-	6.8	-	335.5	6.1
		F	L-V	70	-57.7	-	6.7	-	355.5	6.4
YR24 ch 2	S/PS	L-V	70	-57.4	-	not seen	-	300.0	-	
		L-V	50	not seen	-	not seen	-	not seen	-	
		L-V	80	not seen	-	not seen	-	246.5	-	
		L-V	50	-57.4	-	not seen	-	280.0	-	
YR25 ch 1 Dominion Ck.	Disc	P/PS	L-L-V	60	-56.0	-	7.9	25.4	303.0	4.2
		P/PS	L-L-V	60	-56.3	-	9.0	25.8	291.3	2.0
		P/PS	L-L-V	60	not seen	-	8.1	24.8	250.0	3.8
		P/PS	L-L-V	60	-56.4	-	8.3	25.0	293.2	3.4
		P/PS	L-V	95	-	-1.6	8.3	-	189.6	2.7
YR27 ch 1 Sulphur Ck.	Ffm	PS/S	L-V	80	-	-5.0	-	-	245.4	7.8
		PS/S	L-V	70	-	-6.1	-	-	460.0	9.3
		PS/S	L-V	-	-	not seen	-	-	348.0	-

Appendix 2 continued

Sample/ location ¹	Vein type	Inc. origin	Phase assem ²	Vol.% H ₂ O ³	T _{mCO2}	T _{mice}	T _{mclath}	T _{hCO2} ⁴	T _{htot} T _{dec} ⁵	E.Q.Wt. % NaCl
YR29 ch 1 Sulphur Ck.	Ffm	P?	L-V	80	-	-3.0	-	-	171.7	4.9
YR30 ch 1 Sulphur Ck.	Disc	P?	L-V	80	-	-5.4	-	-	203.8	8.3
YR30 ch 2		P?	L-V	90	-	-6.6	-	-	272.6	9.9
		P?	L-V	95	-	-6.2	-	-	154.1	9.5
		P?	L-V	95	-	-6.3	-	-	160.0	9.5
YR31 ch 1 Lloyd	Disc	P/PS	L-L-V	60	-56.9	-	7.9	26.1	256.0	4.2
		P/PS	L-L-V	60	-57.0	-	8.2	27.6	240.0	3.6
		P/PS	L-L-V	60	-56.9	-	8.0	27.3	256.0	3.9
YR31 ch 2		P/PS	L-L-V	90	-	-1.8	-	-	251.3	3.1
		P/PS	L-L-V	80	-57.2	-	8.4	27.7	318.0	3.2
		P/PS	L-L-V	80	-57.3	-	7.7	28.2	284.0	4.6
YR32 ch 1 Lloyd	Ffm	P/PS	L-V	90	-	-5.2	-	-	252.3	8.1
		P/PS	L-V	80	-	-5.1	-	-	249.3	8.0
		P/PS	L-V	85	-	-4.9	-	-	250.0	7.7
		P/PS	L-V	85	-	-5.9	-	-	267.3	9.1
YR36 ch 1 Oro Fino	Disc	P	L-V	95	-	-0.7	-	-	169.9	1.2
		P	L-V	90	-	-1.0	-	-	160.2	1.7
		P	L-V	90	-	-0.5	-	-	164.9	0.9
YR36 ch 2		P?	L-V	55	-	-2.5	-	-	528.6	4.1
		S	L-V	95	-	-4.0	-	-	210.0	6.4
YR36 ch 3		P/PS	L-V	90	-	-5.3	-	-	250.6	8.3
YR38 ch 1 Trail Hill	Ffm	P?	L-V	95	-	-0.4	-	-	150.7	0.7
		P?	L-V	95	-	-0.9	-	-	153.9	1.6
		P?	L-V	95	-	-0.2	-	-	171.5	0.3
		P?	L-V	95	-	-2.6	-	-	185.0	4.2
YR38 ch 2		S/PS	L-V	60	-	-4.7	-	-	251.9	7.4
		S/PS	L-V	90	-	-3.4	-	-	202.3	5.5
YR60 ch 1 Virgin	Disc	P	L-V	90	-	-3.1	-	-	198.5	5.1
		P	L-V	90	-	-3.4	-	-	194.5	5.5
		P	L-V	90	-	-4.6	-	-	170.9	7.2
		P	L-V	90	-	-3.5	-	-	208.6	5.7
YR60 ch 2		P	L-V	90	-	-3.0	-	-	203.8	4.9
		P	L-V	90	-	-4.2	-	-	211.9	6.7
		P	L-V	90	-	-4.1	-	-	199.0	6.5
YR61 ch 1 Dominion Ck.	Ffm	P	L-V	70	-	-5.5	-	-	231.7	8.5
		P	L-V	70	-56.4	-4.4	-	-	306.4	7.0
		S/P?	L-V	90	-	-4.0	-	-	234.6	6.4
		S/P?	L-V	90	-	-4.2	-	-	198.0	6.7
YR61 ch 2		P	L-V	75	-	-2	-	-	220.7	4.6
		P	L-V	80	-	-2.9	-	-	215.3	4.8
		S	L-V	90	-	-2	-	-	169.6	4.4
YR61 ch 3		P	L-V	70	-	-5.8	-	-	278.6	8.9
		P	L-V	70	-	-5.1	-	-	257.0	13.6
		S	L-V	95	-	-3.0	-	-	170.7	13.9

Appendix 2 continued

Sample/ locator, ¹	Vein type	Inc. origin	Phase assem ²	Vol.% H ₂ O ³	TmCO ₂	Tmice	Tmclath	ThCO ₂ ⁴	T _{htot} T _{dec} ⁵	Eq.Wt. % NaCl
YR64 ch 1 Aime	Disc	P	L-V	70	-57.2	-	7.8	-	not seen	4.4
		P	L-L-V	80	-57.3	-	7.3	25.7	244.0	5.2
		P	L-L-V	70	-57.3	-	7.9	25.2	not seen	4.2
		P	L-L-V	70	-57.0	-	7.1	25.8	242.0	5.6
		P	L-L-V	70	-57.2	-	7.4	25.4	260.0	5.1
YR64 ch 2		P	L-L-V	80	-57.0	-	7.3	26.3	261.0	5.2
		P	L-V	90	-	-6.0	-	-	234.0	9.1
		P	L-V	80	-	-5.7	-	-	218.1	8.8
		P	L-V	90	-	-6.0	-	-	not seen	9.1
YR64a ch 1 Aime	Disc	PS/P	L-V	70	-57.3	-	7.8	20.7	261.1	4.4
		P/P	L-V	75	-57.2	-	7.7	20.6	261.0	4.6
		PS/P	L-V	70	-57.4	-	7.4	22.6	270.7	5.1
		PS/P	L-V	75	-57.3	-	7.8	21.3	219.7	4.4
		PS/P	L-V	75	-57.4	-	7.7	22.2	251.0	4.5
YR64a ch 2		P?	L-V	70	-57.1	-	7.7	22.8	266.2	4.5
		P?	L-V	70	-57.2	-	7.5	20.6	233.2	5.0
		P?	L-V	70	-57.3	-	7.6	21.4	268.5	4.8
		P?	L-V	70	-57.3	-	7.4	22.3	266.8	5.1
		P?	L-V	60	-57.3	-	7.6	21.5	264.1	4.7
YR65 ch 1 Aime	Ffm	P	L-V	95	-	-7.1	-	-	175.1	10.6
		P	L-V	95	-	-7.2	-	-	223.2	10.7
		P	L-V	93	-	-7.5	-	-	205.6	11.0
		P	L-V	95	-	-6.5	-	-	174.7	9.8
YR65 ch 2		P	L-V	95	-	-1.1	-	-	not seen	1.9
		P	L-V	95	-	-4.0	-	-	173.3	6.4
		P	L-V	70	-	-3.8	-	-	181.0	6.1
YR65 ch 3		P/PS	L-V	95	-	-4.0	-	-	189.1	6.4
		P/PS	L-V	95	-	-7.0	-	-	not seen	10.5
		P	L-V	90	-	-6.7	-	-	190.6	10.0
		P	L-V	95	-	-7.2	-	-	159.4	10.7
		P	L-V	95	-	-6.8	-	-	188.2	10.2
		P/PS	L-V	95	-	-7.7	-	-	185.0	11.4
		P?	L-V	95	-	-8.0	-	-	169.4	11.7
YR65 ch 4		P?	L-V	95	-	-7.1	-	-	188.0	10.6
		PS?	L-V	80	-	-5.8	-	-	304.7	8.9
		PS?	L-V	80	-	-5.2	-	-	not seen	8.1
		PS?	L-V	80	-	-6.2	-	-	286.5	9.4
		PS?	L-V	60	-	not seen	-	-	341.5	-
YR66 ch 1 YR66 ch 2 Aime	Disc	P?	L-L-V	75	-56.5	-	7.1	24.7	210.0	5.6
		P?	L-V	60	-57.1	-	7.8	10.8	210.0	4.3
		P/PS	L-L-V	70	-56.5	-	7.4	22.3	239.0	5.1
		P/FS	L-L-V	70	-56.9	-	8.0	22.2	216.0	3.9
YR66 ch 3		P	L-V	60	-57.2	-	7.1	22.1	224.0	5.6
YR68 ch 1 Plink	Ffm	P	L-V	85	-	-2.3	-	-	291.4	3.8
		P	L-V	80	-	-2.3	-	-	290.8	3.8
YR68 ch 2		S/PS	L-V	90	-	-1.1	-	-	207.4	1.9
		S/PS	L-V	90	-	-1.1	-	-	207.3	1.8
		S/PS	L-V	90	-	-1.1	-	-	208.4	1.8

Appendix 2 continued

Sample/ location ¹	Vein type	Inc. origin	Phase assem ²	Vol.% H ₂ O ³	T _{mCO2}	T _{mice}	T _{mclath}	T _{hCO2} ⁴	T _{htot} T _{dec} ⁵	Eq.Wt. % NaCl
YR68 ch 2 cont.d	Ffm	S/PS	L-V	90	-	-1.0	-	-	212.7	1.6
YR70 ch 1 Adams Ck.	Disc	P	L-V	90	-	-2.1	-	-	148.3	3.5
		P	L-V	90	-	-2.3	-	-	149.4	3.9
		P	L-V	90	-	-2.6	-	-	158.5	4.3
		P	L-V	70	-	-2.9	-	-	248.6	4.8
YR71 ch 1 Adams Ck.	Ffm	P	L-V	45	-	-2.0	-	-	392.0	3.4
		P	L-V	80	-	-1.5	-	-	293.3	2.6
		P	L-V	95	-	0.0	-	-	155.3	0.0
		P	L-V	70	-	-1.5	-	-	289.9	2.6
		P	L-V	97	-	-1.4	-	-	159.2	2.4
YR71 ch 2	Ffm	P	L-V	92	-	-1.6	-	-	174.3	2.7
		P	L-V	95	-	-1.5	-	-	154.4	2.5
		P	L-V	95	-	-1.6	-	-	202.5	2.7
YR71 ch 3		P?	L-V	50	-	-1.8	-	-	398.0	3.1
		P?	L-V	70	-	-1.2	-	-	338.1	2.1
YR72 ch 1 Clinton Ck.	Ffm	PS	L-V	90	-	-0.2	-	-	199.5	0.4
		PS	L-V	90	-	-0.3	-	-	217.6	0.4
		S/PS	L-V	90	-	-0.3	-	-	not seen	0.5
		S/PS	L-V	95	-	-0.4	-	-	199.4	0.6
YR72 ch 2		P/PS	L-V	90	-	-0.3	-	-	198.2	0.5
		P/PS	L-V	90	-	-0.5	-	-	212.2	0.8
		P/PS	L-V	92	-	-0.4	-	-	197.9	0.7
RR18 ch 1 Blanche Ck.	Ffm	P?	L-V	70	-	-4.0	-	-	296.6	6.4
		P?	L-V	60	-	-	-	-	380.0	-
RR23 ch 1 Hunker Dome	Ffm	P?	L-V	70	-	-3.2	-	-	253.9	5.2
		P?	L-V	75	-	-3.3	-	-	259.5	5.4
		P?	L-V	80	-	-1.8	-	-	212.8	3.0
RR23 ch 2		P?	L-V	80	-	-5.8	-	-	251.8	8.9
		S/PS	L-V	70	-	-5.3	-	-	244.5	8.9
		S/PS	L-V	80	-	-0.3	-	-	229.5	0.4
RR24 ch 1 Hunker Dome	Disc	P?	L-L-V	70	-56.0	-	7.9	28.1	325.2	4.2
		P?	L-L-V	60	-56.1	-	8.4	26.4	300.0	3.2
		P?	L-L-V	60	-55.9	-	8.4	27.6	300.5	3.2
RR24 ch 2		P?	L-L-V	60	-56.3	-	8.6	26.4	302.7	2.8
		P?	L-V	60	-56.0	-	8.6	25.6	302.8	2.8
		P?	L-L-V	50	-56.0	-	7.5	27.1	314.1	4.9
RR27 ch 1 French Gulch	Ffm	P	L-V	60	-	-1.5	-	-	317.7	2.5
		P	L-V	70	-	-1.2	-	-	320.5	2.0
		P	L-V	60	-	-0.8	-	-	leaked	-
RR37 ch 1 Sulphur Ck.	Ffm	P/PS	L-V	90	-	-3.7	-	-	218.7	5.9
		P/PS	L-V	95	-	-3.5	-	-	206.9	5.7
		P/PS	L-V	90	-	-3.7	-	-	211.7	6.0
RR39 ch 1 Sulphur Ck.	Ffm	P	L-V	95	-	-4.0	-	-	153.4	6.4
		P?	L-V	97	-	-4.2	-	-	152.0	6.7

Appendix 2 continued

Sample/ location ¹	Vein type	Inc. origin	Phase assem ²	Vol.% H ₂ O ³	T _{mCO2}	T _{mice}	T _{mclath}	T _{hCO2} ⁴	T _{htot} T _{dec} ⁵	Eq.Wt. % NaCl
RR39 ch 2	FIm	P?	L-V	97	-	-2.4	-	-	175.6	3.9
RR39 ch 2		P?	L-V	70	-	-5.4	-	-	419.3	8.4
		P?	L-V	70	-	-4.3	-	-	392.7	6.8
		P?	L-V	70	-	not seen	-	-	340.7	-
RR43 ch 1	FIm	P	L-V	90	-	not seen	-	-	403.7	-
Esperanza		PS?	L-V	90	-	not seen	-	-	427.4	-
		PS?	L-V	90	-	not seen	-	-	392.5	-
		PS?	L-V	90	-	not seen	-	-	401.8	-
RR71 ch 1	FIm	P?	L-V	50	-	-5.4	-	-	≈395.0	8.4
Dominion Ck.		P?	L-V	50	-	-5.0	-	-	≈400.0	7.9
		P?	L-V	50	-	not seen	-	-	377.0	-
RR89 ch 1	FIm	P?	L-V	70	-	-1.6	-	-	326.8	2.7
Gold Run		P?	L-V	80	-	-1.0	-	-	229.0	1.7
RR89 ch 2		P	L-V	60	-	-1.4	-	-	325.3	2.3
RR94 ch 1	Disc	P	L-L-V	80	-56.8	-	7.7	29.9	287.5	4.5
Gold Run		P	L-L-V	70	-56.9	-	7.9	30.4	not seen	4.2
		P	L-L-V	70	-56.9	-	7.9	not seen	not seen	4.2
		P	L-L-V	70	-56.9	-	7.9	30.5	283.0	4.1
		P	L-L-V	70	-56.9	-	7.6	29.3	283.0	4.7
		P	L-L-V	70	-56.9	-	7.8	29.1	315.0	4.3
RR94 ch 2	Disc	P	L-L-V	70	-56.9	-	7.9	28.7	[320.0]	4.1
Gold Run		P	L-L-V	60	-56.9	-	8.0	29.6	290.0	4.0
400 μm from galena		P?	L-L-V	80	-56.8	-	7.8	(30.4)	254.5	4.3
		P	L-L-V	70	-56.9	-	7.7	(30.6)	295.0	4.5
RR95 ch 1	Disc	P?	L-L-V	80	-56.5	-	8.5	(30.7)	283.0	5.1
Gold Run		P?	L-L-V	80	-56.6	-	7.3	30.4	286.0	5.2
		P?	L-L-V	70	-56.7	-	9.2	not seen	300.0	1.6
		P?	L-V	90	-56.4	-		26.2	26.2	-
RR95 ch 2	Disc	S/PS	L-L-V	80	-56.4	-	8.1	29.5	264.5	3.8
		P	L-L-V	80	-56.5	-	8.2	30.8	288.0	3.6
		P	L-V	80	-56.2	-	not seen	not seen	270.7	-
RR95 ch 3		P	L-L-V	50	-56.4	-	7.8	29.6	leaked	4.4
		P	L-L-V	60	-56.5	-	7.9	(30.1)	not seen	4.1
		P	L-L-V	50	-56.3	-	7.4	29.9	[314.0]	5.1
		P	L-L-V	60	-56.5	-	7.9	not seen	311.0	4.1
RR96 ch 1	Disc	P	L-L-V	60	-56.8	-	7.6	29.8	[366.8]	4.7
Gold Run		P	L-L-V	65	-56.7	-	8.1	not seen	299.8	3.8
Quartz in pyrite		P	L-L-V	50	-56.8	-	7.6	29.8	not seen	4.7
		P	L-L-V	70	-57.0	-	8.2	29.8	298.2	3.6
		P	L-L-V	60	-56.7	-	8.1	not seen	297.6	3.9
		P	L-L-V	50	-56.9	-	8.0	29.0	not seen	3.9
		P	L-L-V	60	-56.8	-	8.1	29.6	not seen	3.8
		P	L-L-V	50	-56.8	-	8.6	29.9	not seen	2.9
		P	L-L-V	70	-56.8	-	8.2	not seen	293.5	3.6
RR97a ch 1	Disc	P?	L-L-V	60	-56.4	-	7.5	28.2	288.0	5.0
Gold run		P?	L-L-V	70	-56.5	-	7.4	28.5	278.0	5.1

Appendix 2 continued

Sample/ location ¹	Vein type	Inc. origin	Phase assem ²	Vol.% H ₂ O ³	T _{mCO2}	T _{mice}	T _{mclath}	ThCO ₂ ⁴	T _{htot} T _{dec} ⁵	Eq.Wt. % NaCl		
RR97a ch 1 cont.d	Disc	P?	L-L-V	60	-56.6	-	7.4	28.7	280.0	5.1		
		P?	L-L-V	60	-56.6	-	6.7	27.5	278.0	6.3		
RR97b ch 1 Gold Run	Disc	P	L-L-V	70	-56.8	-	8.1	not seen	286.0	3.9		
		P	L-L-V	60	-56.8	-	6.9	28.7	306.5	5.9		
		P	L-L-V	60	-56.6	-	7.9	28.0	230.0	4.1		
		P	L-L-V	60	-56.7	-	7.1	26.6	280.0	5.7		
RR101 ch 1 Lloyd	Disc	P	L-L-V	10	-55.9	-	7.9	28.0	not seen	4.1		
		P	L-V	50	-56.0	-	8.2	not seen	340.0	3.7		
		P	L-L-V	5	-55.7	-	not seen	25.4	not seen	-		
		P	L-V	5	-55.8	-	not seen	26.7	26.7	-		
RR101 ch 2	Disc	P	L-L-V	60	-55.8	-	8.2	28.5	307.2	3.0		
		P	L-L-V	60	-55.5	-	7.6	(28.8)	318.5	4.7		
		P	L-L-V	60	-55.8	-	8.3	28.7	311.6	3.5		
		P	L-L-V	70	-55.9	-	7.6	(29.1)	329.5	4.7		
RR102 ch 1 Lloyd	Disc	P	L-L-V	60	-56.0	-	8.4	30.2	not seen	3.3		
		P	L-L-V	60	-55.4	-	9.2	28.9	301.6	1.6		
		P	L-L-V	70	-55.4	-	8.2	29.3	313.3	3.7		
		P	L-L-V	70	-55.2	-	7.8	29.3	314.5	4.3		
RR102 ch 2	Disc	P	L-L-V	70	-55.8	-	8.7	28.2	310.3	2.6		
		P	L-L-V	70	-55.7	-	8.5	28.0	296.4	3.0		
		P	L-L-V	60	-56.0	-	8.7	28.7	300.9	2.7		
		P	L-L-V	60	-55.8	-	8.2	27.0	309.7	3.7		
RR104 ch 1 Lloyd	Disc	P/PS	L-L-V	80	-55.7	-	8.0	(29.2)	not seen	4.0		
		P	L-L-V	60	not seen	-	8.5	30.2	308.5	3.0		
		P	L-L-V	65	-55.7	-	8.6	30.0	293.0	2.8		
		P	L-L-V	65	-56.6	-	8.6	30.2	305.0	2.8		
		P	L-L-V	60	-55.5	-	8.3	30.0	307.6	3.4		
		P/PS	L-L-V	70	-56.7	-	8.2	(29.0)	293.0	3.7		
		P/PS	L-L-V	70	-56.6	-	7.9	(28.6)	301.9	4.1		
		P/PS	L-L-V	60	-56.7	-	7.8	(29.0)	307.7	4.3		
RR105 ch 1 Lloyd	Disc	P	L-L-V	70	-56.0	-	8.1	27.8	293.5	3.8		
		P	L-L-V	75	-55.8	-	8.4	28.4	289.5	3.2		
		P	L-L-V	70	-56.1	-	8.1	28.1	293.8	3.8		
		P	L-L-V	70	-56.1	-	8.3	28.4	290.5	3.5		
		RR105 ch 2	Disc	P	L-L-V	60	-56.3	-	8.1	29.0	308.0	3.9
				P	L-L-V	40	-56.4	-	8.2	25.7	301.6	3.7
				P/S	L-L-V	50	-56.3	-	7.9	30.0	not seen	4.1
				P	L	-	-56.6	-	-	20.2	20.2	-
RR106 ch 1 Lloyd	Disc	P	L-L-V	80	-56.9	-	7.3	29.3	307.5	5.3		
		P	L-L-V	70	-56.8	-	7.2	29.2	291.2	5.4		
		P	L-L-V	70	-56.9	-	7.2	(28.9)	291.3	5.5		
		P	L-L-V	70	-56.9	-	7.5	27.8	315.0	5.0		
RR106 ch 2	Disc	P	L-L-V	70	not seen	-	not seen	28.7	-	-		
RR112 ch 1 Virgin	Disc	P?	L-V	70	-	not seen	-	-	386.3	-		
		P?	L-V	45	-	not seen	-	-	(440.0)	-		
		P?	L-V	50	-	not seen	-	-	400.7	-		

Appendix 2 continued

Sample/ location ¹	Vein type	inc. origin	Phase assem ²	Vol.% H ₂ O ³	T _{mCO2}	T _{mice}	T _{mclath}	T _{hCO2} ⁴	T _{htot} T _{dec} ⁵	Eq.Wt. % NaCl
RR113 ch 1 Virgin	Disc	P?	L-V	50	-	-4.4	-	-	-	7.0
		P?	L-V	40	-	-5.3	-	-	380.0	8.3
RR114 ch 1 Virgin	Disc	P?	L-V	80	-	-3.9	-	-	216.8	6.2
		P?	L-V	90	-	-3.9	-	-	220.0	6.3
		P?	L-V	90	-	-3.4	-	-	not seen	5.5
		P?	L-V	90	-	-3.2	-	-	not seen	5.2
RR114 ch 2		P/PS	L-V	85	-	-3.4	-	-	205.0	5.5
		P/PS	L-V	90	-	-3.0	-	-	181.6	4.9
		P/PS	L-V	70	-	-3.1	-	-	185.2	5.1
		P/PS	L-V	85	-	-3.3	-	-	189.4	5.4
RR132 ch 1 Violet	Disc	P	L-V	80	-	-3.9	-	-	225.0	6.2
		P	L-V	90	-	-3.2	-	-	216.1	5.2
		P	L-V	90	-	-3.3	-	-	218.4	5.3
		P	L-V	90	-	-3.2	-	-	212.6	5.2
		P	L-V	90	-	-3.5	-	-	228.8	5.6
RR132 ch 2		P	L-V	80	-	-4.4	-	-	226.3	6.9
		P	L-V	75	-58.1	-4.0	8.8	-	245.5	6.4
		P	L-V	80	-	-4.5	-	-	221.1	6.1
		P	L-V	80	-58.2	-4.1	8.8	-	239.6	6.6
		P	L-V	90	-	-4.3	-	-	223.2	6.8
RR132 ch 3		P	L-V	-	-57.3	-	-	-33.3	-33.3	-
		P?	L-V	90	-	-3.7	-	-	225.6	6.0
		P?	L-V	90	-	-3.8	-	-	226.3	6.1
		P?	L-V	80	-	-3.7	-	-	222.0	5.9
		P?	L-V	80	-	-3.6	-	-	225.8	6.1
RR135 ch 2 Hilchey	Disc	S/PS	L-V	80	-	-5.0	-	-	284.3	7.8
		S/PS	L-V	70	-	-4.4	-	-	291.9	6.9
		S/PS	L-V	80	-	-5.2	-	-	287.4	8.1
		S/PS	L-V	80	-	-5.2	-	-	284.9	8.1
RR135 ch 3		P	L-V	80	-	-1.9	-	-	273.1	3.2
		P	L-V	80	-	-1.7	-	-	270.4	2.9
RR137 ch 1 Hunker Dome Amethyst	Disc	PS	L-V	65	-	-1.1	-	-	342.1	1.8
		PS	L-V	70	-	-1.0	-	-	340.2	1.6
		PS	L-V	70	-	-1.0	-	-	339.9	1.6
		PS	L-V	70	-	-1.0	-	-	343.3	1.7
		PS	L-V	65	-	-1.1	-	-	347.9	1.9
RR137 ch 2		PS/P	L-V	70	-	-0.9	-	-	342.0	1.5
		PS/P	L-V	60	-	-1.0	-	-	344.4	1.6
		PS/P	L-V	70	-	-0.8	-	-	345.5	1.3
		PS/P	L-V	60	-	-1.0	-	-	342.5	1.6
RR137a ch 1 Hunker Dome Milky quartz	Disc	P	L-L-V	-	-57.4	-	6.6	(28.6)	337.0	5.5
		P	L-L-V	-	-57.2	-	6.2	(28.5)	337.3	7.1
		P	L-L-V	-	-57.4	-	8.0	(27.8)	not seen	3.9
		P	L-L-V	-	-57.3	-	7.1	(28.2)	340.0	5.6
		P	L-L-V	-	-57.4	-	6.8	(28.4)	341.4	6.1
RR137a ch 2		P	L-L-V	60	-57.1	-	6.2	(28.9)	334.0	7.2
		P	L-L-V	80	-57.2	-	6.7	(28.9)	322.7	6.4
		P	L-L-V	70	-57.2	-	6.0	(28.8)	345.5	7.5

Appendix 2 continued

Sample/ location ¹	Vein type	Inc. origin	Fracture assem ²	Vol.% H ₂ O ³	TmCO ₂	Tm _{ice}	Tm _{clath}	ThCO ₂ ⁴	T _{htot} <i>dec</i> ⁵	Eq.Wt. % NaCl
RR137a ch 1 cont.d		P	L-L-V	70	-57.1	-	6.5	(28.6)	341.9	6.6
		P	L-L-V	60	-57.1	-	6.9	(28.7)	341.7	5.9
RR142 ch 1 Mitchell	Disc	P	L-V	70	-	-2.2	-	-	298.5	3.6
		P	L-V	60	-	-2.0	-	-	323.2	3.4
		P	L-V	60	not seen	-	9.1	not seen	308.9	1.8
		P	L-V	60	-56.0	-	9.2	not seen	325.3	1.6
		P	L-V	70	-56.0	-	9.1	not seen	321.3	1.8
RR142a ch 1 Mitchell	Disc	P	L-V	60	-56.9	-	8.5	19.2	318.2	3.0
		P	L-V	70	-56.9	-	8.5	20.1	322.0	3.0
		P	L-V	70	-56.9	-	8.5	not seen	301.0	3.0
		P	L-V	60	-57.2	-	8.7	20.5	334.3	2.7
		P	L-V	70	-56.9	-	8.8	not seen	317.0	2.4
RR142a ch 2		P/PS	L-L-V	40	-57.3	-	8.2	30.2	not seen	3.6
		P/PS	L-L-V	60	-57.3	-	not seen	28.3	(340.0)	-
		P/PS	L-L-V	60	-57.3	-	8.4	25.0	342.2	3.3
		P/PS	L-L-V?	60	not seen	-	not seen	not seen	326.6	-
RR142a ch 3		P/PS	L-L-V	60	-57.1	-	8.7	not seen	321.4	2.6
		P	L-V	60	-56.9	-	8.7	not seen	306.0	2.7
		P	L-V	70	-56.8	-	8.4	not seen	310.8	3.2
		P	L-V	50	-56.5	-	8.5	not seen	307.1	3.0
RR143 ch 1 Mitchell	Disc	P	L-V	70	-	-3.3	-	-	304.3	5.3
		P	L-V	75	-	-3.7	-	-	300.8	6.0
		P	L-V	70	-	-3.9	-	-	312.5	6.2
		P	L-V	75	-	-4.1	-	-	304.1	6.5
RR143 ch 2		P?	L-V	70	-	-	7.2	-	305.9	5.4
		P?	L-V	60	-	-	7.0	-	306.0	5.8
		P?	L-V	80	-	-0.3	-	-	288.5	0.4
		P?	L-V	90	-	-0.2	-	-	188.2	0.4
		P?	L-V	60	-	-	7.1	-	307.4	5.6
		P?	L-V	60	-	-	7.1	-	310.1	5.6
RR143a ch 1 Mitchell	Disc	P	L-L-V	70	not seen	-	8.4	not seen	320.7	3.2
		P	L-L-V?	70	-56.8	-	8.8	24.3	303.5	2.4
		P	L-L-V	60	-56.6	-	8.8	25.5	309.5	2.5
		P	L-L-V	75	-56.8	-	7.2	not seen	341.1	5.5
RR143a ch 2		P	L-V	-	-57.0	-	8.3	not seen	321.5	3.4
		P	L-V	-	-	-3.7	-	-	305.0	6.0
		P	L-L-V	-	-56.9	-	7.0	26.9	355.5	5.8
RR151 ch 1 Gold Bottom Ck.	Ffm	PS?	L-V	70	-	-3.4	-	-	314.6	5.5
		PS?	L-V	70	-	-3.4	-	-	309.5	5.5
		PS?	L-V	70	-	-2.9	-	-	309.8	4.8
		PS?	L-V	70	-	-2.9	-	-	313.5	4.8
RR151 ch 2		PS?	L-V	70	-	-3.5	-	-	321.0	5.7
		PS?	L-V	70	-	-2.6	-	-	304.3	4.2
		PS?	L-V	70	-	-3.0	-	-	310.6	4.9
RR151 ch 2		PS?	L-V	70	-	-2.6	-	-	307.6	4.3

Appendix 2 continued

Sample/ location ¹	Vein type	Inc. origin	Phase assem ²	Vol.% H ₂ O ³	TmCO ₂	Tmice	Tmclath	ThCO ₂ ⁴	Thtot Tdec ⁵	Eq.Wt. % NaCl
RR187 ch 1 Sulphur Ck.	Fim	P	L-V	50	-	-5.4	-	-	419.0	8.4
		P	L-V	50	-	-5.2	-	-	{423.0}	8.1
		S	L-V	50	-	-4.7	-	-	[439.5]	7.4
		P	L-V	50	-	-5.5	-	-	410.0	8.5
RR187 ch 2	S/PS	L-V	60	-	not seen	-	-	390.0	-	
		L-V	90	-	-4.2	-	-	278.4	6.7	
		P	L-V	92	-	-3.4	-	-	193.6	5.5
RR187 ch 3		P?	L-V	75	-	-3.1	-	274.7	5.1	
RR187 ch 4	P/S?	L-V	90	-	-1.4	-	-	215.1	2.3	
		L-V	95	-	-2.5	-	-	not seen	4.1	
RR1/251 ch 1 Quartz Ck.	Fim	P?	L-V	95	-	-2.7	-	-	122.9	4.5
		P?	L-V	95	-	-4.3	-	-	126.1	6.9
		P?	L-V	95	-	-3.9	-	-	116.7	6.2
RR256 ch 1 Sulphur Ck.	Disc	P	L-V	50	-	-7.1	-	-	not seen	10.6
RR262 ch 1 Sheba	Fim	P?	L-V	5	-56.8	-	-	-	355.9	-
		P?	L-V	80	-	-1.5	-	-	309.3	2.6
		P?	L-V	5	-56.8	-	6.0	-	not seen	7.5
		P?	L-V	80	-	-2.1	-	-	300.0	3.5
RR266 ch 1 Sheba	Disc	P/PS	L-V	70	-	-3.4	-	-	294.4	5.5
		P/PS	L-V	0	-57.4	-	not seen	21.5	21.5	-
		P/PS	L-V	70	-	-	6.0	-	309.0	7.5
		P/PS	L-L-V	50	-57.2	-	6.5	27.4	not seen	6.6
		P/PS	L-L-V	60	-57.2	-	6.3	-	327.0	7.0
RR266 ch 2	P	L-L-V	50	-56.3	-	6.3	27.4	280.0	7.0	
		-	-	-	-	-	-	290.0	-	
		L-L-V	70	-56.2	-	7.2	(28.0)	340.0	5.4	
		L-L-V	75	-55.8	-	7.1	28.2	314.0	5.6	
		L-V	70	-	-	-	-	290.0	-	
RR266 ch 3	P	L-V	80	-	-1.6	-	-	295.0	2.7	
		S/PS	L-V	80	-	-1.8	-	-	281.2	3.1
		S/PS	L-L-V	30	-57.0	-	-	29.3	[290.0]	-
RR273 ch 1 Sheba	Disc	PS	L-V	70	-	-2.3	-	-	284.3	3.9
		PS	L-V	70	-	-1.8	-	-	286.1	3.0
		PS	L-V	60	-	-2.4	-	-	281.9	4.0
		PS	L-V	60	-	-2.4	-	-	285.0	3.9
		PS	L-V	60	-	-2.3	-	-	287.0	3.8
RR273 ch 2	P	L-V	60	-	-2.4	-	-	284.0	4.0	
		L-V	0	-56.4	-	-	22.9	22.9	-	
		L-V	75	-	-2.5	-	-	281.0	4.2	
		L-V	70	-	-2.8	-	-	286.4	4.6	
		L-V	60	-56.1	-	8.6	29.5	316.0	-	
RR273 ch 3	PS	L-L-V	40	-56.4	-	7.0	27.0	[340.0]	5.8	
		L-L-V	60	-56.6	-	8.5	26.4	[356.0]	3.0	
		L-V	0	-56.8	-	-	22.0	22.0	-	
		L-V	70	-	-	6.0	-	300.0	7.5	
		L-V	0	-56.8	-	-	21.3	21.3	-	

Appendix 2 continued

Sample/ location ¹	Vein type	Imp origin	Phase assem ²	Vol.% H ₂ O ³	TmCO ₂ ⁴	Tmice	Tmclath	ThCO ₂ ⁴	Thtot T _{dec} ⁵	Eq.Wt. % NaCl
RR283 ch 1 27 Pup	Disc	P	L-V	80	-	-2.4	-	-	304.5	4.0
		P	L-V	80	-	-3.1	-	-	297.8	5.0
		PS	L-V	80	-	-2.6	-	-	291.9	4.2
		PS	L-V	70	-	-2.6	-	-	289.0	4.2
RR283 ch 2		P	L-V	70	-	-2.3	-	-	321.7	3.9
		P/PS	L-V	70	-	-2.2	-	-	326.2	3.7
		P/PS	L-V	60	-	-2.3	-	-	280.0	3.8
		P/PS	L-V	70	-	-2.3	-	-	324.5	3.9
RR283 ch 3		P/PS	L-V	70	-	-2.5	-	-	325.1	4.1
		S/PS	L-V	75	-	-2.0	-	-	306.5	3.3
		S/PS	L-V	75	-	-1.8	-	-	not seen	3.1
		S/PS	L-V	80	-	-2.1	-	-	307.2	3.5
RR286 ch 1 27 Pup	Disc	P/PS	L-V	80	-	0.1	-	-	303.6	-
		P/PS	L-V	70	-	not seen	-	-	311.1	-
		P/PS	L-V	70	-	not seen	-	-	326.8	-
		P	L-V	70	-	-2.4	-	-	327.0	4.0
RR286 ch 2		P	L-V	60	-	-1.7	-	-	350.0	2.9
		P	L-V	60	-	-2.0	-	-	352.0	3.4
		P	L-V	65	-	-2.4	-	-	337.5	3.9
		P	L-V	65	-	-2.2	-	-	344.0	3.7
RR287 ch 1 Hunker Dome Amethyst RR287 ch 2	Disc	P	L-V	60	-	-0.9	-	-	332.3	1.5
		P	L-V	65	-	-0.9	-	-	331.4	1.5
		PS?	L-V	70	-	0.0	-	-	308.2	0.0
		P/PS	L-V	70	-	0.0	-	-	350.9	0.0
		P/PS	L-V	70	-	-0.1	-	-	351.9	0.2
		P/PS	L-V	70	-	-0.1	-	-	351.1	0.1
RR292 ch 1 Hunker Dome RR292 ch 2	Disc	PS?	L-L-V	50	-56.9	-	7.9	(28.2)	{340.0}	4.2
		PS?	L-L-V	60	-57.0	-	7.9	(28.4)	{334.9}	4.2
		P?	L-V	75	-	-0.7	-	not seen	312.7	-
		P?	L-L-V	70	-57.0	-	8.4	not seen	304.1	3.2
		PS/S	L-L-V	60	-55.8	-	8.7	29.9	{354.0}	2.7
		PS/S	L-L-V	60	-56.4	-	10.4	28.6	{303.5}	-
RR295 ch 1 Hunker Dome RR295 ch 3	Disc	PS/S	L-L-V	60	-56.2	-	9.7	(28.2)	{329.5}	0.6
		P	L-L-V	50	-55.6	-	7.4	not seen	{378.0}	5.1
		P	L-L-V	50	-55.7	-	7.8	30.4	{351.3}	4.3
		P	L-L-V	50	-55.6	-	8.3	30.7	327.3	3.4
		P	L-L-V	60	-55.2	-	8.4	29.3	334.4	3.3
		P	L-L-V	70	-57.0	-	6.2	not seen	348.1	7.1
RR301 ch 1 French Gulch	Disc	P	L-V?	80	-	-1.5	-	not seen	283.1	2.6
		P	L-L-V	40	-57.0	-	9.0	29.9	{285.0}	2.0
		P	L-L-V	50	-56.9	-	8.7	(30.3)	{314.0}	2.7
		P/PS	L-V	-	-	-3.7	-	-	241.9	6.0
RR301 ch 1 French Gulch	Disc	P/PS	L-V	-	-	-5.0	-	-	229.2	7.9
		P/PS	L-V	-	-	-2.8	-	-	239.4	4.6
		P/PS	L-V	-	-	-2.8	-	-	235.2	4.6
		P/PS	L-V	-	-	-2.9	-	-	239.1	4.7

Appendix 2 continued

Sample/ location ¹	Vein type	Inc. origin	Phase assem ²	Vol.% H ₂ O ³	TmCO ₂	Tnl _{ice}	Tm _{clath}	ThCO ₂ ⁴	T _{htot} T _{dec} ⁵	Eq.Wt. % NaCl
RR304 ch 1 27 Pup	Disc	P?	L-V	90	-	-0.4	-	-	155.8	0.7
		P?	L-V	95	-	-0.7	-	-	180.3	1.1
RR304 ch 2		P/PS	L-V	90	-	-2.1	-	-	298.9	3.5
		P/PS	L-V	80	-	-2.4	-	-	300.4	3.9
		P/PS	L-V	80	-	-2.2	-	-	297.1	3.7
		P/PS	L-V	70	-	-2.3	-	-	298.0	3.9
		P/PS	L-V	70	-	-3.1	-	-	292.1	5.1
RR304 ch 3		P	L-V	80	-	-0.9	-	-	297.5	1.6
		S	L-V	60	-	-1.7	-	-	295.8	2.9
		S/P?	L-V	70	-	-4.4	-	-	311.8	7.0
RR305 ch 1 27 pup	Disc	P	L-V	80	-	-2.6	-	-	319.8	4.3
		P	L-V	60	-	-2.2	-	-	312.2	3.6
RR312 ch 1 Hilchey	Disc	PS/P	L-V	80	-	-5.7	-	-	287.7	8.8
		PS/P	L-V	80	-	-5.4	-	-	285.3	8.3
		PS/P	L-V	90	-	-7.5	-	-	289.9	11.1
		PS/P	L-V	60	-	-2.2	-	-	284.1	3.7
RR312 ch 2		PS/P	L-V	70	-	-2.6	-	-	293.7	4.3
		PS/P	L-V	80	-	-3.5	-	-	294.5	5.7
		PS/P	L-V	70	-	-2.1	-	-	293.1	3.9
		PS/P	L-V	80	-	-2.7	-	-	272.6	4.5
RR312 ch 3		PS/P	L-V	70	-	-2.5	-	-	304.0	4.1
		PS/P	L-V	70	-	-2.6	-	-	323.6	4.3
		PS/P	L-V	60	-	-2.5	-	-	337.0	4.2
		PS/P	L-V	60	-	-2.1	-	-	319.5	3.5
RR321 ch 1 Lone Star	Disc	S	L-V	80	-	-3.9	-	-	256.4	6.2
		S	L-V	80	-	-0.4	-	-	224.2	0.6
		S	L-V	60	-	-3.5	-	-	288.9	5.6
		S	L-V	70	-	-3.7	-	-	313.3	6.0
		S	L-V	70	-	-3.3	-	-	301.8	5.4
RR321 ch 2		P	L-V	70	-	-3.8	-	-	295.2	6.1
		S	L-V	60	-	-0.4	-	-	288.4	0.7
		S	L-V	95	-	-1.5	-	-	179.5	2.5
RR321 ch 3		S	L-V	95	-	-0.6	-	-	161.6	1.0
		S	L-V	95	-	-0.5	-	-	172.4	0.8
		S	L-V	95	-	-0.8	-	-	162.4	1.4
		S	L-V	95	-	-1.0	-	-	185.6	1.6
		S	L-V	95	-	-1.0	-	-	not seen	1.7
		S	L-V	95	-	-0.5	-	-	169.2	0.8
RR322 ch 1 Lone Star	Disc	P/PS	L-V	80	-	-1.4	-	-	277.6	2.3
		P/PS	L-V	60	-	-0.5	-	-	274.6	0.8
		P/PS	L-V	70	-	not seen	-	-	279.6	-
		P	L-V	70	-	-0.8	-	-	286.9	1.4
		P	L-V	60	-	-3.6	-	-	283.2	5.8
RR322 ch 2		P/S	L-V	70	-	-0.2	-	-	291.6	0.4
		P/S	L-V	70	-	-0.5	-	-	not seen	0.8
		P/S	L-V	70	-	-1.6	-	-	289.3	2.7
RR324 ch 1 Lone Star	Disc	P?	L-V	70	-	-0.8	-	-	307.3	1.3
		P?	L-V	80	-	-1.3	-	-	298.5	2.2
		P?	L-V	60	-	-0.7	-	-	311.9	1.2

Appendix 2 continued

Sample/ location ¹	Vein type	Inc. origin	Phase assem ²	Vol.% H ₂ O ³	T _{mCO₂}	T _{mice}	T _{mclath}	ThCO ₂ ⁴	T _{htot} T _{dec} ⁵	Eq.Wt. % NaCl
<i>RR324 ch 1</i>	Disc	P?	L-V	75	-	-1.1	-	-	306.6	1.8
<i>RR324 ch 2</i>		P	L-V	70	-	-3.7	-	-	304.3	5.9
		P	L-V	70	-	-3.7	-	-	288.0	5.9
		P	L-V	80	-	-3.4	-	-	285.4	5.5
		P	L-V	70	-	-3.1	-	-	297.0	5.1
<i>RR326 ch 1</i>	Disc	P	L-V	70	-	not seen	-	-	295.1	-
Lone Star		P	L-V	70	-	not seen	-	-	291.7	-
		P	L-V	70	-	not seen	-	-	294.6	-
		P	L-V	70	-	not seen	-	-	297.3	-
		P	L-V	70	-	not seen	-	-	285.4	-
<i>RR326 ch 2</i>		P	L-V	70	-	not seen	-	-	290.0	-
		P	L-V	80	-	not seen	-	-	293.6	-
		P	L-V	80	-	-1.2	-	-	267.4	2.1
		P	L-V	80	-	not seen	-	-	299.2	-
<i>RR327a ch 1</i>	Disc	PS/P	L-V	-	-	not seen	-	-	327.9	-
Hilchey		PS/P	L-V	-	-	-5.1	-	-	294.8	8.0
Au-bearing		PS/P	L-V	-	-57.4	not seen	4.8	-	341.0	-
vein		PS/P	L-V	-	-	not seen	6.3	-	225.8	-
<i>RR327 ch 1</i>		PS/P	L-V	70	-	-2.5	-	-	291.9	4.2
		PS/P	L-V	80	-	-5.4	-	-	297.0	8.3
		PS/P	L-V	80	-	-2.4	-	-	302.4	3.9
		PS/P	L-V	70	-	-3.1	-	-	296.4	5.1
<i>RR333 ch 1</i>	Ffm	S	L-V	95	-	-2.0	-	-	148.8	3.3
TOTW		S	L-V	90	-	-1.9	-	-	202.3	3.1
Highway*		S	L-V	90	-	-1.9	-	-	207.4	3.2
		S	L-V	80	-	-1.9	-	-	207.9	3.2
		S	L-V	80	-	-2.0	-	-	242.8	3.4
		S	L-V	90	-	-2.0	-	-	210.4	3.3
<i>RR333 ch 2</i>		S/PS	L-V	95	-	-0.2	-	-	170.3	0.4
		S/PS	L-V	90	-	-0.2	-	-	197.7	0.4
		S/PS	L-V	75	-	-0.2	-	-	197.9	0.3
		S/PS	L-V	90	-	-0.2	-	-	207.7	0.3
		S/PS	L-V	90	-	-0.1	-	-	208.5	0.1
<i>RR342 ch 1</i>	Ffm	S	L-V	90	-	-1.4	-	-	178.9	2.4
King Solomon		S	L-V	90	-	-1.0	-	-	180.6	1.6
Dome		S	L-V	90	-	-1.1	-	-	175.3	1.5
		S	L-V	92	-	-1.0	-	-	173.8	1.7
		S	L-V	90	-	-1.0	-	-	175.2	1.7
<i>RR342 ch 2</i>		P?	L-V	92	-	-0.8	-	-	181.0	1.4
		S	L-V	92	-	-0.9	-	-	183.1	1.6
		PS?	L-V	92	-	-3.3	-	-	212.2	5.4
		PS?	L-V	92	-	-3.4	-	-	206.5	5.5
<i>RR345 ch 1</i>	Ffm	P	L-V	60	-	-2.9	-	-	371.6	4.8
Quartz Ck.		P	L-V	60	-	-2.0	-	-	349.6	3.4
		P	L-V	50	-	-3.1	-	-	380.0	5.0

Appendix 2 continued

Sample/ location ¹	Vein type	Inc. origin	Phase assem ²	Vol.% H ₂ O ³	T _{mCO2}	T _{mice}	T _{mclath}	T _{hCO2} ⁴	T _{htot} T _{dec} ⁵	Eq.Wt. % NaCl
<i>RR346 ch 1</i> Hunker Ck.	Disc	P	L-L-V	60	-56.3	-	7.0	23.2	<i>~310.0</i>	5.9
		P	L-L-V	60	-56.6	-	6.7	22.7	not seen	6.3
<i>RR349 ch 1</i> Dominion Ck.	Ffm	S	L-V	90	-	0.0	-	-	213.7	0.0
		S	L-V	92	-	0.0	-	-	213.3	0.0
		S	L-V	92	-	0.0	-	-	201.6	0.0
		S	L-V	90	-	0.0	-	-	224.1	0.0
		P/S	L-V	90	-	0.0	-	-	229.4	0.0
		P/S	L-V	90	-	0.0	-	-	220.3	0.0
<i>RR349 ch 2</i>	Ffm	S	L-V	80	-	-4.6	-	-	194.2	7.3
		S/PS	L-V	60	-	-2.5	-	-	379.0	4.1
		S/PS	L-V	70	-	-3.1	-	-	328.6	5.0
<i>RR361 ch 1</i> Lone Star	Ffm	P?	L-V	70	-	-1.6	-	-	299.6	2.7
		P?	L-V	50	-	-1.9	-	-	not seen	3.2
<i>RR361 ch 2</i>		P?	L-V	75	-	-3.6	-	-	288.0	5.8
		P	L-V	60	-	-3.9	-	-	291.1	6.2
		P?	L-V	70	-	-2.6	-	-	280.9	4.2

* All measurements in °C.

¹ For detailed sample locations see Appendix X.

² Phase assemblage observed at room temperature (≈23°C). Abbreviations: L= liquid, V= vapour.

³ Volume percent aqueous phase from visual estimation.

⁴ All inclusions exhibit CO₂ homogenization to liquid phase, except: *italics*, homogenization to vapour, (parentheses) homogenization by critical behaviour.

⁵ All inclusions homogenize to liquid phase, except: *italics*, inclusion decrepitated before homogenization, [300] homogenized to vapour phase, {300} homogenized by critical or near critical behaviour. Temperatures in bold type denote "pure"-CO₂ inclusions (see text).

Appendix 3

Salinity Calculations

a) Calculation of fluid salinity in H₂O-NaCl bearing inclusions, from the freezing point depression of ice:

$$\text{Salinity} = 0.00 + 1.76958 \theta - 4.2384 \times 10^{-2} \theta^2 + 5.2778 \times 10^{-4} \theta^3$$

Potter et al., 1978

where,

salinity is expressed as weight percent equivalent NaCl in solution (± 0.028)

θ = the freezing point depression of ice in °C

b) Calculation of fluid salinity in H₂O-CO₂-NaCl bearing inclusions, from the freezing point depression of CO₂-hydrate (clathrate):

$$\text{Salinity} = 15.52023 - 1.02342 (T_{m\text{clath}}) - 0.05286 (T_{m\text{clath}})^2$$

Bozzo et al., 1973

where,

salinity is expressed as weight percent equivalent NaCl in solution

$T_{m\text{clath}}$ = the final melting temperature of clathrate in °C

Critical point pressure-temperature calculations

a) Calculation of the critical temperature of H₂O-NaCl fluids:

$$T = 374.1 + 8.800\phi + 0.1771\phi^2 - 0.02113\phi^3 + 7.334 \times 10^{-4}\phi^4$$

Knight and Bodnar, 1989

where,

T = critical temperature in °C ($\pm 4^\circ\text{C}$)

ϕ = fluid salinity in weight percent NaCl

b) Calculation of the critical pressure of H₂O-NaCl fluids:

$$P = 2094 - 20.56T + 0.06896T^2 - 8.903 \times 10^{-5}T^3 + 4.214 \times 10^{-8}T^4$$

Knight and Bodnar, 1989

where,

P = critical pressure in bars (± 21 bars)

T = critical temperature in °C

Appendix 4

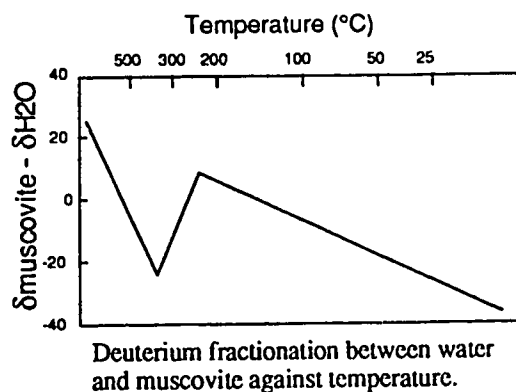
Equilibrium fractionation expressions used in isotope geothermometry and fluid isotopic composition calculations (see Chapter VI):

a) Oxygen isotopes

$\Delta_{\text{quartz-water}} = 3.34 (10^6/T^2) - 3.31$	Matsuhisa et al., 1979
$\Delta_{\text{muscovite-water}} = 2.38 (10^6/T^2) - 3.89$	O'Neil and Taylor, 1969
$\Delta_{\text{calcite-water}} = 2.78 (10^6/T^2) - 2.89$	O'Neil et al., 1969
$\Delta_{\text{quartz-muscovite}} = 1.9924 (10^6/T^2) - 0.79364$	Chako et al., pers. comm.

b) Hydrogen isotopes

$\Delta_{\text{muscovite-water}} = - 22.1 (10^6/T^2) - 19.1$	Suzuoki and Epstein, 1976
Empirical equilibrium hydrogen isotope curve	Bowers and Taylor, 1985.



c) Carbon isotopes

$$\Delta_{\text{CO}_2\text{-calcite}} = - 2.988 (10^6/T^2) + 7.6663 (10^6/T^2) - 2.4612$$

Bottinga, 1968

Where:

T = temperature in °Kelvin,

$\Delta_{\text{A-B}} = \delta R_{\text{A}} - \delta R_{\text{B}}$ where R_{A} is the ($^{18}\text{O}/^{16}\text{O}$, D/H or $^{13}\text{C}/^{12}\text{C}$) isotopic ratio of sample A.

Appendix 5 Location and description of vein quartz and host rock samples from the Klondike.

Sample no.	Approximate location	1: 50,000 map sheet	UTM* grid ref.	Sample description ¹	Vein Type
RR Samples					
RR15	Base of Midnight Dome Rd	116 B/3	778 030	Qtz vein	Disc
RR16	As above	116 B/3	778 030	Altered schist	-
RR17	As above	116 B/3	778 030	Chloritic schist	-
RR18	Mouth of Blanche Creek	115 0/14	954 776	Qtz-carb vein	Ffm
RR19	Mouth of Blanche Creek	115 0/14	954 776	Qtz-carb vein	Ffm
Hunker Adit, Hunker Dome					
RR20	Hunker adit, tailings pile	115 0/15	030 825	Fe-stained qtz vein	Disc
RR21	As above	115 0/15	030 825	Pyritised schist	-
RR22	As above	115 0/15	030 825	Altered schist	-
RR23	As above	115 0/15	030 825	Qtz vein margin	Disc
RR24	Hunker adit, access road	115 0/15	028 833	Qtz-gal float	Disc
RR25	Near Little Skukum Creek	115 0/14	814 898	Pyritic qtz vein	Ffm
RR26	French Gulch, Ur Eldorado	115 0/14	829 865	Qtz vein	Disc
RR27	French Gulch, Ur Eldorado	115 0/14	829 865	Qtz vein	Ffm
Boxcar Claim Group					
RR28	Boxcar claim	115 0/14	963 874	Qtz-musc schist	-
RR29	As above	115 0/14	963 874	Qtz-musc schist	-
RR30	As above	115 0/14	963 874	Oxidised breccia	-
RR31	As above	115 0/14	963 874	Mineralised breccia	-
RR32	As above	115 0/14	963 874	Qtz lens	Ffm
RR33	As above	115 0/14	963 874	Qtz vein float	?
RR34	Boxcar approach road	115 0/14	961 873	Qtz vein	?
RR35	2.3 km north of Boxcar	115 0/14	949 895	Schist with qtz vein	Disc
RR36	200 m south of Boxcar	115 0/14	958 870	Milky qtz vein	?
Sulfur Creek Road					
RR37	Road Cut	115 0/15	020 790	Qtz vein	Ffm
RR38	Road Cut	115 0/15	020 790	Schist	-
RR39	6.5 km from Lloyd turn-off	115 0/15	029 750	Qtz vein	Ffm?
Esperanza Claim, Indian River Valley					
RR40	Esperanza Claim	115 0/11	945 696	Schist	-
RR41	As above	115 0/11	945 696	Qtz vein	Ffm
RR42	As above	115 0/11	945 696	Schist	-
RR43	As above	115 0/11	945 696	Qtz vein	Ffm
RR44	As above	115 0/11	945 696	Minerals	-
RR45	As above	115 0/11	945 696	As above	-
RR46	As above	115 0/11	945 696	As above	-
RR47	As above	115 0/11	945 696	As above	-

Appendix 5 continued

Sample no.	Approximate location	1: 50,000 map sheet	UTM* grid ref.	Sample description	Vein Type
RR48	3.45 km NW. of Dominion	115 0/10	132 633	Calcite mass	?
RR49	As above	115 0/10	132 633	Qtz vein	Ffm
RR50	As above	115 0/10	132 633	Schist	-
RR51	8.6 km NW of Dominion	115 0/10	095 661	Schist	-
RR52	As above	115 0/10	095 661	Minor: qtz vein	Disc
RR53	As above	115 0/10	095 661	Milky qtz vein	Disc
RR54	As above	115 0/10	095 661	Milky qtz vein	Disc
RR55	13 km NW of Dominion	115 0/10	068 690	Schist	-
RR56a	As above	115 0/10	068 690	Qtz-carb vein	Ffm
RR56b	As above	115 0/10	068 690	Qtz-carb vein	Ffm
RR57	As above	115 0/10	068 690	Qtz-carb vein	Ffm
<i>Eureka Creek, south of Dominion</i>					
RR58	Ur Eureka Placer Camp	115 0/10	064 527	Banded calc-silicate	-
RR59	As above	115 0/10	064 527	Calc-silicate	-
RR60	As above	115 0/10	064 527	Qtz-vein with pyrite	?
RR61	As above	115 0/10	064 527	Pink phyllosilicate	-
RR62	As above	115 0/10	064 527	Calc-silicate	-
RR63	As above	115 0/10	064 527	Carbonate Vein	?
RR64	Eureka Creek Road	115 0/10	072 523	Qtz lens/boudin	Ffm
RR65	Eureka Creek Road	115 0/10	072 523	Schist	-
RR66	Eureka Creek Road	115 0/10	134 561	Qtz buodin	Ffm
RR67	Eureka Creek Road	115 0/10	134 561	Qtz-fspar-bi schis:	-
RR68	Eureka Creek Road	115 0/10	138 573	Orthogneiss	-
RR69	Eureka Creek Road	115 0/10	138 573	Qtz-carb vein	Disc
<i>Dominion Road</i>					
RR70	Quartz Strike adit	115 0/10	191 625	Qtz-musc schist	-
RR71	Quartz Strike adit	115 0/10	191 625	Qtz vein float	?
RR72	7.3 km NE of Dominion	115 0/10	200 664	Qtz vein on fault plane	Disc
RR73	7.3 km NE of Dominion	115 0/10	200 664	Qtz-musc schist	-
RR74	7.8 km NE of Dominion	115 0/10	206 666	Qtz-carb-hem vein	Disc
RR75	As above	115 0/10	206 666	Qtz-pyrite vein	?
RR76	As above	115 0/10	206 666	Qtz vein	?
RR77	As above	115 0/10	206 666	Schist	-
RR78	As above	115 0/10	206 666	Qtz-carb vein	Disc
RR79	As above	115 0/10	206 666	Qtz-carb vein	Disc
RR80	25 km NE of Dominion	115 0/15	157 785	Qtz vein float	?
RR81	27.3 km NE of Dominion	115 0/15	140 798	Schist	-
RR82	27.3 km NE of Dominion	115 0/15	140 798	Qtz vein	Disc
<i>Gold Run Claims, Lloyd Road</i>					
RR83	Trenches, Lloyd road	115 0/15	107 748	Qtz-musc schist	-
RR84	As above	115 0/15	107 748	Qtz lens	Ffm
RR85	Summit, Gold Run test pits	115 0/15	100 750	Milky vein qtz	Disc
RR86	As above	115 0/15	100 750	Milky vein qtz	Disc
RR87	As above	115 0/15	100 750	Milky vein qtz	Disc
RR88	As above	115 0/15	100 750	Qtz vein	Disc
RR89	As above	115 0/15	100 750	Qtz lens	Ffm

Appendix 5 continued

Sample no.	Approximate location	1: 50,000 map sheet	UTM* grid ref.	Sample description	Vein Type
RR90	As above	115 0/15	100 750	Pyritised schist	-
RR91	As above	115 0/15	100 750	Vuggy qtz	Ffm
RR92	As above	115 0/15	100 750	Schist	-
RR94	Gold Run adits on north slope	115 0/15	097 752	Qtz-gal vein	Disc
RR95	As above	115 0/15	097 752	Qtz-py vein	Disc
RR96	As above	115 0/15	097 752	Qtz vein+ schist	Disc
RR97	As above	115 0/15	097 752	Vein margin	Disc
RR98	As above	115 0/15	097 752	Schist	-
<i>Lloyd Claims</i>					
RR100	Trench on road to creek	115 0/15	049 792	Wall rock schist	-
RR101	As above	115 0/15	049 792	Qtz vein+ schist	Disc
RR102	As above	115 0/15	049 792	Qtz vein	Disc
RR103	Trench east of cabin	115 0/15	058 793	Schist wall rock	-
RR104	As above	115 0/15	058 793	Vuggy qtz	Disc
RR105	As above	115 0/15	058 793	Vuggy qtz breccia	Disc
RR106	As above	115 0/15	058 793	Vuggy qtz	Disc
RR107	As above	115 0/15	058 793	Minor qtz stringer	Disc
<i>Virgin occurrence</i>					
RR108	Virgin dump	116 B/3	862 982	Qtz-carb vein	Disc
RR109	As above	116 B/3	862 982	Qtz-carb vein margin	Disc
RR110	As above	116 B/3	862 982	Augen schist	-
RR111	As above	116 B/3	862 982	Minor qtz vein	Disc
RR112	As above	116 B/3	862 982	Vein margin	Disc
RR113	As above	116 B/3	862 982	Disc vein merging with Ffm vein?	-
RR114	As above	116 B/3	862 982	Vein qtz with pyrite	Disc
<i>Lloyd Road</i>					
RR117	Trenches at start of road	115 0/15	035 810	Qtz vein in schist	Disc
RR118	As above	115 0/15	035 810	Qtz vein	Disc
RR119	As above	115 0/15	035 810	Qtz vein	Disc
<i>Cullen Claim, near the Violet Shaft</i>					
RR120	Overgrown Adit	115 0/14	848 828	Qtz-carb vein	Ffm
RR121	As above	115 0/14	848 828	Schist	-
RR122	As above	115 0/14	848 828	Qtz vein	Ffm
RR123	As above	115 0/14	848 828	Qtz vein float	?
<i>Violet Shaft</i>					
RR124	Spoil Heap and Ore stockpile	115 0/14	847 819	Qtz lens	Ffm
RR125	As above	115 0/14	847 819	Qtz-carb vein	-
RR126	As above	115 0/14	847 819	Breccia	Disc
RR127	As above	115 0/14	847 819	Barite with boxwork	Disc
RR128	As above	115 0/14	847 819	Sulfides in qtz	Disc
RR129	As above	115 0/14	847 819	Vein margin	Disc
RR130	As above	115 0/14	847 819	Massive vein qtz	Disc
RR131	As above	115 0/14	847 819	Qtz vein	Disc

Appendix 5 continued

Sample no.	Approximate location	1: 50,000 map sheet	UTM* grid ref.	Sample description	Vein Type
RR132	As above	115 0/14	847 819	Qtz-bar vein	Disc
RR133	As above	115 0/14	847 819	Qtz-bar-gal vein	Disc
RR134	As above	115 0/14	847 819	Qtz-bar-gal vein	Disc
<i>Visible Gold Specimens</i>					
RR135	Hilchey Trenches	115 0/14	853 844	Au on qtz	Disc
RR136	Hunker Dome Trench	115 0/15	030 835	Au(?) in limonite?	Disc
RR137	Hunker Dome Trench	115 0/15	025 855	Zoned Amethyst	Disc
RR138	Lone Star, Boulder Lode	115 0/15	025 855	Brecciated qtz?	Disc
<i>Mitchell Vein, Old Shaft</i>					
RR139	Trench next to old shaft	115 0/15	010 856	Chloritic schist	-
RR140	Trench next to old shaft	115 0/15	010 856	Pyritised vein margin	Disc
RR141	Trench next to old shaft	115 0/15	010 856	Magnetite in schist	-
RR142	Trench next to old shaft	115 0/15	010 856	Banded qtz	Disc
RR143	Trench next to old shaft	115 0/15	010 856	Banded qtz	Disc
RR144	Trench next to old shaft	115 0/15	010 856	Altered schist	-
RR145	Brandon Claim, near hut	115 0/15	023 893	Qtz float	?
RR146	Near Alphonse Lode	115 0/15	019 874	Qtz float	?
RR147	Near Alphonse Lode	115 0/15	019 874	Chloritic schist	-
RR148	Fox showing, Mint Gulch	115 0/15	027 914	Qtz vein float	?
RR149	As above	115 0/15	027 914	Qtz-musc schist	-
RR150	As above	115 0/15	027 914	Qtz float	?
<i>Gold Bottom Creek, Near Bum Claim Group</i>					
RR151	Near Bum claim	115 0/15	989 895	Qtz vein in fold hinge	Ffm
RR152	Near Bum claim	115 0/15	989 895	Schist	-
RR153	Near Bum claim	115 0/15	989 895	Milky qtz vein	Ffm?
RR154	Near Bum claim	115 0/15	989 895	Milky qtz vein	Ffm?
RR155	Marguerita shaft,	115 0/15	979 959	Qtz lens	Ffm
RR156	Near Fraser showing	115 0/15	031 929	Milky qtz float	?
<i>Rock Creek Quarry on main Whitehorse Rd</i>					
RR157	Quarry	116 B/3	041 051	Greenstone	Ffm
RR158	Quarry	116 B/3	041 051	Minor vein	Disc
RR159	Quarry	116 B/3	041 051	Qtz-carb vein	Disc
RR160	Quarry	116 B/3	041 051	Carbonate vein	Disc
RR161	Quarry	116 B/3	041 051	Carbonate vein	Disc
<i>Near Arlington</i>					
RR162	SW of Australia Hill	116 B/3	898 102	Vein qtz float	Ffm
RR163	SW of Australia Hill	116 B/3	896 100	Vein qtz float	Ffm

Appendix 5 continued

Sample no.	Approximate location	1: 50,000 map sheet	UTM* grid ref.	Sample description	Vein Type
<i>Indian River</i>					
RR164	Esperanza	115 0/11	945 696	Altered schist	-
RR165	600m SE of Esperanza	115 0/11	950 694	Qtz-fspar lens	Ffm
RR166	600m SE of Esperanza	115 0/11	950 694	Biotite orthogneiss	-
<i>Quartz Creek</i>					
RR167	1.9km N of dredge	115 0/14	931 725	Pyritic schist	-
RR168	As above	115 0/14	931 725	Metachert?	-
RR169	As above	115 0/14	931 725	Vein in chert?	Disc
<i>Bonanza Road</i>					
RR170	SE of Grand Forks	115 0/14	825 895	Schist	-
RR171	As above	115 0/14	825 895	Qtz vein	Ffm
RR172	As above	115 0/14	825 895	Qtz-carb vein	Disc
RR173	As above	115 0/14	825 895	Massive carbonate	Disc
RR174	As above	115 0/14	825 895	Qtz lens	Ffm
RR175	As above	115 0/14	825 895	Syn F1 qtz vein?	Ffm
RR176	6.7 km SE of Grand Forks	115 0/14	875 886	Qtz vein in schist	Disc
RR177	6.7 km SE of Grand Forks	115 0/14	875 886	Schist	Ffm
RR178	Bend above Dam	115 0/14	900 883	Dyke	Disc
RR179	As above	115 0/14	900 883	Quartzite	-
RR180	As above	115 0/14	900 883	Folded chloritic schist	-
RR181	As above	115 0/14	900 883	Qtz-carb vein	Ffm
RR182	As above	115 0/14	900 883	Qtz-carb vein	Ffm
RR183	As above	115 0/14	900 883	Breccia?	Disc
RR184	Bend in road	115 0/14	934 867	Milky qtz float	Ffm
<i>Sulfur Creek, bedrock tailings in dredge pile</i>					
RR185	Dredge Pile	115 0/15	025 750	Qtz-augen schist	-
RR186	As above	115 0/15	025 750	Qtz lens	Ffm
RR187	As above	115 0/15	025 750	Qtz-carb lens	Ffm
RR188	As above	115 0/15	025 750	Breccia	-
RR189	As above	115 0/15	025 750	Breccia	-
RR190	As above	115 0/15	025 750	Qtz-carb vein	Disc
RR191	50m south	115 0/15	025 750	Unaltered schist	-
RR192	As above	115 0/15	025 750	Altered schist	-
RR193	As above	115 0/15	025 750	Altered schist	-
RR194	As above	115 0/15	025 750	Sericitised schist	-
<i>Bonanza Creek</i>					
RR195	Near California Gulch	116 B/3	791 005	Qtz-augen schist	-
RR196	As above	116 B/3	791 005	Folded ffm qtz vein	Ffm
RR197	As above	116 B/3	791 005	Folded ffm qtz vein	Ffm
RR198	South of Cripple Gulch	116 B/3	801 983	Pyritic qtz schist	-
RR199	South of Cripple Gulch	116 B/3	801 983	Qtz-augen schist	-
RR200	Bench slope, W of road	115 0/14	818 908	Felsic augen schist	-
RR201	Bench slope, W of road	115 0/14	818 908	Qtz vein	Ffm
RR202	Sourdough Gulch	115 0/14	801 970	Cherty QFP	-
RR203	As above	115 0/14	801 970	Pyritic quartzite	-

Appendix 5 continued

Sample no.	Approximate location	1: 50,000 map sheet	UTM* grid ref.	Sample description	Vein Type
RR204	As above	115 0/14	801 970	Pyritic vein	Disc
RR205	As above	115 0/14	801 970	Pyrite vein	Disc
RR206	As above	115 0/14	801 970	Pyritic qtz vein	?
RR207	As above	115 0/14	801 970	Altered schist	-
RR208	As above	115 0/14	801 970	Schist	-
RR209	"Claim 33"	115 0/14	809 938	Pyritic qtz vein	?
RR210	As above	115 0/14	809 938	Folded pyritic schist	-
RR211	As above	115 0/14	809 938	Qtz-carb vein	Disc
RR212	As above	115 0/14	809 938	As above	Disc
RR213	As above	115 0/14	809 938	As above	Disc
RR214	As above	115 0/14	809 938	As above	Disc
<i>Dominion Road</i>					
RR215	Dominion Road	115 0/15	043 842	Micaceous schist	-
RR216	Dominion Road	115 0/15	074 818	Chloritic felsic schist	-
RR217	Dominion Road	115 0/15	126 804	Chloritic felsic schist	-
RR218	Dominion Road	115 0/15	157 785	Quartzite	-
RR219	Dominion Road	115 0/15	157 785	Garnet-mica schist	-
RR220	Dominion Road	115 0/15	182 771	Marble	-
RR221	Dominion Road	115 0/15	182 771	Marble	-
RR222	Dominion Road	115 0/15	227 726	Qtz-gnt-mica schist	-
RR223	Dominion Road	115 0/15	227 726	Foliated quartzite	-
<i>Sulfur Creek Road</i>					
RR224	Sulfur Creek Road	115 0/10	108 646	Qtz-augen schist	-
RR225	19km N of Dominion	115 0/15	038 728	Qtz vein in schist	Ffm
RR226	As above	115 0/15	038 728	Qtz-carb vein	Disc
RR227	As above	115 0/15	038 728	Qtz-augen schist	-
RR228	As above	115 0/15	038 728	Qtz-augen schist	?
RR229	As above	115 0/15	038 728	Qtz-carb veins in qtz-augen schist	Disc
RR230	As above	115 0/15	038 728	Qtz-augen schist	-
RR231	As above	115 0/15	038 728	Qtz-augen schist	-
RR235	Road to Unexpected Claims	116 B/3	059 985	Qtz vein	Ffm
<i>Ben Levy</i>					
RR236	Ben Levy Adit	116 B/3	945 986	Carb vein	Disc
RR237	As above	116 B/3	945 986	Weathered vein	Disc
RR238	As above	116 B/3	945 986	Banded qtz-carb vein	Disc
RR239	As above	116 B/3	945 986	Vuggy vein	Disc
RR240	As above	116 B/3	945 986	Serpentinite	-
RR241	As above	116 B/3	945 986	Brecciated vein	Disc
RR242	As above	116 B/3	945 986	Fuchsite on schist	-
RR243	As above	116 B/3	945 986	Veinlet in schist	Disc
<i>Germaine Creek epithermal Showing</i>					
RR244	Germaine Creek	116 B/2	025 029	Qtz vein in serp.	Disc
RR245	As above	116 B/2	021 029	Chalcedony vein	Disc

Appendix 5 continued

Sample no.	Approximate location	1: 50,000 map sheet	UTM* grid ref.	Sample description	Vein Type
RR246	As above	116 B/2	021 029	Chalcedony vein	Disc
RR247	As above	116 B/2	014 036	Qtz-chal vein	Disc
RR248	As above	116 B/2	014 036	Qtz-chal vein	Disc
RR249	As above	116 B/2	014 036	Qtz-chal vein	Disc
RR250	As above	116 B/2	014 036	Silicified breccia	-
RR251	As above	116 B/2	014 036	QFP	-
RR1/246	Sulfur Creek dredge tailings	115 0/15	025 750	Qtz-carb vein	Disc
RR1/247	Sulfur Creek dredge tailings	115 0/15	025 750	Qtz-augen schist	-
RR1/248	Sulfur Creek road,	115 0/15	038 728	Qtz-augen schist	-
RR1/250	Qtz Creek dredge tailings	115 0/14	933 739	Qtz vein in schist	Disc
RR1/251	As above	115 0/14	933 739	Qtz lens	Ffm
RR252	As above	115 0/14	933 739	Pyritic schist	-
<i>Sulfur Creek Road</i>					
RR253	Bedrock in dredge tailings	115 0/10	103 654	Qtz lens	Ffm
RR254	As above	115 0/10	103 654	Qtz-py vein	Disc
RR255	As above	115 0/10	103 654	Qtz vein	Disc
RR256	As above	115 0/10	103 654	As above	Disc
RR257	As above	115 0/10	103 654	Qtz-sph-gal vein	Disc
RR258	As above	115 0/10	103 654	Qtz vein	Disc
<i>Dave Johnston's Claim, French Gulch</i>					
RR259	Trench, 27 Pup bench	115 0/14	842 853	Visible Au on limonite	Disc
RR260	As above	115 0/14	842 853	Visible Au on limonite	Disc
<i>Sheba Vein, Mitchell Claim group</i>					
RR262	Sheba claim	115 0/15	011 846	Qtz lens	Ffm
RR263	Sheba claim	115 0/15	011 846	Calcite in minor vein	Disc
RR264	Sheba claim	115 0/15	011 846	Chloritic schist	-
RR265	Sketch 1, location 1	115 0/15	011 846	Pyritised schist	-
RR266	Sketch 1, Pt A	115 0/15	011 846	Vein margin	Disc
RR267	Sketch 1	115 0/15	011 846	Wall rock inclusion	-
RR268	Sketch 1, Pt A	115 0/15	011 846	Wallrock, vein margin	-
RR269	Vug, sketch 1	115 0/15	011 846	Qtz crystals from Vug	Disc
RR270	Sketch 1	115 0/15	011 846	Vein qtz breccia	-
RR271	Sketch 1	115 0/15	011 846	Vein-qtz breccia	-
RR272	Sketch 1, Pt D	115 0/15	011 846	Massive vein qtz	Disc
RR273	Sketch 1, Pt A	115 0/15	011 846	Vein qtz below HW contact	Disc
RR274	Sketch 2,	115 0/15	011 846	Qtz-gal vein	Disc
RR275	See sketch map	115 0/15	011 846	Qtz vein	Disc
RR276	See sketch map	115 0/15	011 846	Wall rock to RR275	-
RR277	Float	115 0/15	011 846	Pb-Cu min's in float	Disc
RR278	Float	115 0/15	011 846	Pb-Cu min's in float	Disc
RR279	Eureka Creek	115 0/10	077 559	Qtz-carb vein	Ffm
RR280	Hunker trenches, trench 1	115 0/15	026 848	Schist	-

Appendix 5 continued

Sample no.	Approximate location	1: 50,000 map sheet	UTM* grid ref.	Sample description	Vein Type
<i>Dave Johnstons Claim, 27 Pup</i>					
RR281	Trench, 27 Pup bench	115 0/14	842 853	Qtz vein with lim.	Disc
RR282	As above	115 0/14	842 853	High grade lim.	Disc
RR283	As above	115 0/14	842 853	High grade qtz vein	Disc
RR284	As above	115 0/14	842 853	High grade qtz vein	Disc
RR285	27 Pup bench Sluice trench	115 0/14	842 853	Qtz vein	Disc
RR286	As above	115 0/14	842 853	Qtz vein	Disc
<i>Hunker Dome trenches</i>					
RR287	Sketch map, Trench 4	115 0/15	026 848	Brecciated qtz vein	Disc
RR288	Sketch map, Trench 5	115 0/15	026 848	Qtz lens	Ffm
RR289	Sketch map, Trench 5	115 0/15	026 848	Chl-musc-qtz schist	-
RR290	Sketch map, Trench 5	115 0/15	026 848	Calcite vein in breccia	Disc
RR291	Sketch map, Trench 4	115 0/15	026 848	Micaceous qtzite	-
RR292	Sketch map, Trench 4	115 0/15	026 848	Banded qtz vein	Disc
RR293	Sketch map, Trench 4	115 0/15	026 848	Qtz-musc schist	-
RR294	Sketch map, Trench 4	115 0/15	026 848	Qtz-gal vein	Disc
RR295	Sketch map, Trench 4	115 0/15	026 848	Brecciated qtz vein	Disc
<i>Boxcar Road</i>					
RR296	Boxcar Road, heading NW	115 0/14	939 904	Qtz vein float	?
RR297	Boxcar Road, heading NW	115 0/14	926 932	Qtz lens	Ffm
RR298	Boxcar Road, heading NW	115 0/14	880 928	Qtz lens	Ffm
<i>Indian River</i>					
RR299	W of Quartz Creek	115 0/14	885 714	Qtz lens	Ffm
RR300	W of Quartz Creek	115 0/14	836 726	Qtz lens/Orthoqtzite?	Ffm
<i>French Gulch Trenches</i>					
RR301	Trenches	115 0/14	805 865	Qtz-carb lens	Ffm
RR302	Trenches	115 0/14	805 865	Qtz with limonite	Disc
RR303	Trenches	115 0/14	805 865	Pyritised schist	-
<i>Dave Johnsons Claim, 27 Pup</i>					
RR304	27 Pup bench	115 0/14	842 853	Au-qtz vein	Disc
RR305	27 Pup bench	115 0/14	842 853	Vuggy qtz-vein	Disc
RR306	Road from Grand Forks	115 0/14	855 934	Qtz vein in schist	Ffm
RR307	Road from Grand Forks	115 0/14	855 934	Chloritic schist	-
RR308	South end of Hill	115 0/14	893 832	Qtz-musc schist	-
RR309	South end of Hill	115 0/14	893 832	Qtz(-carb) vein	Ffm
<i>Parnell Showing</i>					
RR310	Parnell trenches	115 0/14	887 844	Qtz-musc schist float	-
RR311	Parnell trenches	115 0/14	887 844	Qtz-Vein float	Disc
<i>Hilchey Trenches</i>					
RR312	Hilchey Trench	115 0/14	857 846	Vuggy vein qtz	Disc
RR313	Hilchey Trench	115 0/14	857 846	Qtz-Carb lens	Ffm

Appendix 5 continued

Sample no.	Approximate location	1: 50,000 map sheet	UTM* grid ref.	Sample description	Vein Type
RR314	88 Tr08	115 0/14	857 846	Qtz-musc schist	-
RR315	88 Tr08	115 0/14	857 846	Qtz-py vein in schist	Disc
<i>Amanda Showing</i>					
RR316	Amanda adit	115 0/14	839 867	Milky qtz vein	Disc
<i>Lone Star Mine</i>					
RR317	88 Tr 17, assay Pt 0.093oz	115 0/14	872 859	Musc-qtz schist	-
RR320	88 Tr 17, assay Pt 0.093oz	115 0/14	872 859	Pyritic schist	-
RR321	88 LS3	115 0/14	872 859	Mn-stained qtz vein	Disc
RR322	Boulder Lode	115 0/14	872 859	Milky qtz vein	Disc
RR323	Boulder Lode	115 0/14	872 859	Milky Au-qtz vein	Disc
RR324	Boulder Lode	115 0/14	872 859	Milky qtz vein	Disc
RR325	Boulder Lode	115 0/14	872 859	Pyritised schist	Disc
RR326	By Chateau Lonestar	115 0/14	872 859	Qtz-gal vein	Disc
RR327	Hilchey Trenches	115 0/14	857 846	Au-qtz vein	Disc
<i>Top Of The World Highway, west of Dawson City</i>					
RR328	Below Summit 4113	116B- 116CE1/2	485 119	Milky Qtz vein	Disc
RR329	Below Summit 4113	As above	485 119	Host schist	-
RR330	Near BM3534	As above	585 245	Qtz-carb vein	Ffm
RR331	Near BM3534	As above	585 245	Calc-silicate	-
RR332	Near BM3253	As above	685 130	Qtz-augen schist	-
RR333	Near BM3253	As above	685 130	Qtz lens	Ffm
RR334	Corner overlooking Yukon R.	As above	745 165	Qtz-carb vein	Disc
RR335	Ferry approach road	As above	760 140	Qtz vein	Ffm
RR336	Ferry approach road	As above	760 140	Chloritic schist	-
<i>Midnight Dome Road</i>					
RR337	Dome Road	116 B/3	793 053	Carbonaceous schist	-
RR338	As above	116 B/3	793 053	Qtz vein	Disc
RR339	As above	116 B/3	793 053	Qtz lens	Ffm
<i>King Solomon Dome</i>					
RR340	Trenches	115 0/15	011 831	Qtz vein	Disc
RR341	As above	115 0/15	011 831	Qtz-musc schist	-
RR342	As above	115 0/15	011 831	Qtz lens	Ffm
RR343	As above	110 0/15	011 831	Chloritic schist	-
RR344	As above	110 0/15	011 831	Qtz vein	Disc
RR345	Quartz Creek road	115 0/14	974 810	Qtz lens	Ffm
<i>Upper Hunker Road</i>					
RR346	Hunker Rd	115 0/15	046 882	Qtz-gal-py vein	Disc
RR347	Hunker Rd	115 0/15	046 882	Qtz-gal-py vein	Disc

Appendix 5 continued

Sample no.	Approximate location	1: 50,000 map sheet	UTM* grid ref.	Sample description	Vein Type
RR348	Dominion Rd	115 0/15	040 852	Qtz lens	Ffm
RR349	Dominion Rd	115 0/15	046 832	Qtz lens	Ffm
RR350	Sulphur Ck Rd	115 0/15	038 728	Qtz lens	Ffm
<i>Hunker Dome trenches</i>					
RR351	Trench	115 0/15	026 853	Qtz vein in quartzite	Disc
RR352	Trench	115 0/15	026 853	Qtz-carb vein	Disc
RR353	Trench MAC 88-10	115 0/15	026 853	Qtz vein	Disc
RR354	Trench MAC 88-10	115 0/15	026 853	Margin of qtz vein	Disc
RR355	Trench MAC 88-10	115 0/15	026 853	Host schist	-
RR356	Trench MAC 88-9	115 0/15	027 853	Qtz vein	Disc
RR357	See RR294	115 0/15	026 848	Qtz vein	Disc
<i>Hunker Dome Shaft</i>					
RR358	Trench by shaft	115 0/15	033 830	Limonite vein	Ffm?
RR359	Trench by shaft	115 0/15	033 830	As above	Ffm?
RR360	Trench by shaft	115 0/15	033 830	Qtz vein	Disc
RR370	Hunker Dome trenches	115 0/15	033 830	Carb-talc in serp	-
RR380	Right limit, Oro Grande	115 0/14	830 850	Amethyst	Disc
<i>MLB-88 samples</i>					
-160	Germaine Creek	116 B/2	020 030	Qtz-chal in serp.	-
-159	Germaine Creek	116 B/2	020 030	Qtz vein	-
-153	Germaine Creek	116 B/2	020 030	Chalcedony in QFP	-
-101	Hunker Creek	N/A	N/A	Flourite in QFP	-
<i>KS Samples</i>					
KS 1	King Solomon Dome	115 0/15	030 835	Qtz-galena vein	Disc
KS2	king Solomon Dome	115 0/15	030 835	Qtz-galena vein	Disc
KS3	King solomon Dome	115 0/15	030 835	Qtz lens in schist	Ffm
KS4	Mitchell lode	115 0/15	010 856	Qtz-galena vein	Disc
KS5	Orekon lode	115 0/15	016 845	Qtz-galena vein	Disc
KS6	Lloyd	115 0/15	058 793	Qtz vein	Disc
KS7	Lloyd	115 0/15	058 793	Qtz lens in schist	Ffm
KS8	Lone Star, Boulder lode	115 0/14	872 859	Au-qtz vein	Disc
KS9	Lone Star	115 0/14	872 859	Qtz lens in schist	Ffm
KS10	Pioneer adit	115 0/14	877 850	Au-qtz vein	Disc
KS11	Pioneer adit	115 0/14	877 850	Qtz lens in schist	Ffm
KS12	Ben Levy adit	116 B/3	945 986	Carbonate vein	Disc
<i>YR Samples</i>					
<i>Midnight Dome road</i>					
YR 1	Midnight Dome road	116 B/3	N/A	Qtz vein	?
YR2	Midnight Dome road	116 B/3	N/A	Carb. vein	Disc
YR3	Midnight Dome road	116 B/3	N/A	Greenstone	-
<i>Bear Creek Road</i>					
YR4	Bear Creek road	116 B/3	N/A	Qtz lens	Ffm

Appendix 5 continued

Sample no.	Approximate location	1: 50,000 map sheet	UTM* grid ref.	Sample description	Vein Type
YR5	Bear Creek road	116 B/3	N/A	Qtz vein	Disc
YR6	Bear Creek road	116 B/3	N/A	Chlorite-biotite schist	-
YR7	Bear Ck-Discovery Pup	116 B/3	868 982	Qtz lens	Ffm
YR8	Bear Ck-Discovery Pup	116 B/3	868 982	Schist	-
YR9	Virgin prospect	116 B/3	862 982	Qtz vein	Disc
YR10	Ben Levy prospect	116 B/3	945 986	Banded carb vein	Disc
<i>Hunker Creek road</i>					
YR11	Hunker Creek road	115 0/14	960 973	Qtz vein in schist	?
YR12	Hunker Creek road	115 0/15	004 943	Chloritic schist	Disc
YR13	Hunker Creek road	115 0/15	046 882	Chloritic schist	-
YR14	Hunker Creek road	115 0/15	046 882	Qtz lens	Ffm
<i>Hunker Dome</i>					
YR15	Hunker Dome trenches	115 0/15	025 843	Qtz-carb vein	Disc
YR16	Hunker Dome trenches	115 0/15	025 843	Serpentinite	-
YR17	Hunker Dome trenches	115 0/15	030 825	Glassy qtz vein	?
YR18	Hunker Dome trenches	115 0/15	030 825	Milky qtz vein	Disc
YR19	Hunker Dome trenches	115 0/15	030 825	Qtz-mica schist	-
<i>Dominion Creek road</i>					
YR20	Dominion Ck road	115 0/15	144 795	Qtz vein	Disc
YR21	Dominion Ck road	115 0/15	157 785	Gnt-mica schist	-
YR22	Dominion Ck road	115 0/10	212 671	Qtz lens	Ffm
YR23	Dominion Ck road	115 0/10	212 671	Hbde-bi schist	-
YR24	Dominion Ck road	115 0/10	200 664	Qtz lens	Ffm
YR25	Dominion Ck road	115 0/10	200 664	Large qtz vein	Disc
<i>Sulphur Creek road</i>					
YR26	Sulphur Ck road	115 0/10	135 631	Qtz vein in o.gneiss	?
YR27	Sulphur Ck road	115 0/10	135 631	Qtz-fspar vein	Ffm
YR28	Sulphur Ck road	115 0/10	095 662	Qtz-py-gal vein	Disc
YR29	Sulphur Ck road	115 0/10	090 665	Qtz lens	Ffm
YR30	Sulphur Ck road	115 0/10	090 665	Qtz-sulf vein	Disc
<i>Lloyd Occurrence</i>					
YR31	Lloyd occurrence	115 0/15	058 793	Qtz vein, mineralized	Disc
YR32	Lloyd occurrence	115 0/15	058 793	Qtz lens	Ffm
YR33	Lloyd occurrence	115 0/15	058 793	Qtz lens	Ffm
YR34	West of Yukon river	N/A	N/A	Vein in greenstone	Disc
YR35	West of Yukon river	N/A	N/A	Qtz lens	Ffm
YR36	Oro Fino adit	115 0/14	814 925	Qtz vein	Disc
YR37	Trail Hill	116 B/3	800 995	Qtz vein	Disc
YR38	Trail Hill	116 B/3	800 995	Qtz lens	Ffm
YR39	East of airport	N/A	N/A	Qtz-carb vein	?
YR60	Virgin lode	116 B/3	862 982	Qtz-carb vein	Disc
YR61	Dominion Ck	115 0/15	155 785	Qtz lens	Ffm

Appendix 5 continued

Sample no.	Approximate location	1: 50,000 map sheet	UTM* grid ref.	Sample description	Vein Type
YR62	Gold Run Ck	115 0/10	153 683	Qtz lens	Ffm
YR63	Sulphur Ck	115 0/10	N/A	Qtz vein	Disc
<i>Aime idde</i>					
YR64	Aime dump	115 0/10	153 683	Vuggy qtz vein	Disc
YR65	Aime dump	115 0/10	153 683	Qtz lens	Ffm
YR66	Aime dump	115 0/10	153 683	Qtz vein	Disc
<i>Plink claims</i>					
YR67	Plink claims	115 0/14	N/A	Qtz vein	Disc
YR68	Plink claims	115 0/14	N/A	Qtz lens	Ffm
YR69	Plink claims	115 0/14	N/A	Qtz-gal-asp vein	Disc
YR70	Adams Ck	115 0/14	820 904	Qtz vein	Disc
YR71	Adams Ck	115 0/14	820 904	Qtz lens	Ffm
YR72	Clinton Ck road	N/A	N/A	Qtz vein	Ffm?

* Universal Transverse Mercator grid reference: see 1: 50,000 sheet for explanation.

¹ Abbreviations: Ffm= foliaform, Disc= discordant, qtz= quartz, carb= carbonate, musc= muscovite, gal= galena, asp= arsenopyrite, sph= sphalerite, fspar= feldspar, bi= biotite, hem= hematite, bar= barite, serp= serpentinite, chal= chalcedony, QFP= quartz-feldspar-porphry, lim= limonite, chl= chlorite, gnt= garnet, hbde= hornblende, sulf= sulfide

Appendix 6

The geology of selected discordant vein locations

Brief descriptions of the principal discordant vein locations which were examined in the course of the present study are given below. Au-grades are taken from a number of sources including Maclean (1914), the Northern Cordilleran Mineral Inventory (NCMI) data base compiled by Archer Cathro Associates, Debicki (1984, 1985), and unpublished company reports compiled for the Hughes-Lang group of companies. Locations are described from approximately southeast to northwest across the field area.

Aime

The Aime claims cover two discordant quartz veins, trending between east-west to northwest-southeast and dipping to the north at about 45° (Debicki, 1985). The veins are hosted by chloritic schists, and are in the hanging wall of a major thrust fault (see Figures 1b and 2) (Mortensen, 1990). Gold grades were reportedly as high as 308 g/t, with minor silver, but when resampled in 1984, pyritic quartz yielded assays of 0.4 to 12.3 g/t Au (Debicki, 1985).

Lower Dominion

A large milky quartz vein outcrops at the Lower Dominion occurrence, hosted by chloritic schists, within a few hundred meters of the major thrust fault which defines the southeastern margin of assemblage I (Figures 1b and 2). The vein is only partially exposed, but is believed to be discordant, and strikes 070° dipping steeply to the west. No sulfide or gold mineralization was seen.

Gold Run

The Gold Run occurrence consists of a series of adits which were developed on a northwest-southeast trending discordant milky quartz vein. Samples of quartz collected from the adit dumps contained trace galena and gold. The vein(s) is hosted by felsic schist in the immediate footwall to the assemblage I thrust sheet (Figures 1b and 2) (Mortensen, 1990). Clasts of the hostrock can be seen completely enclosed by vein quartz in some float samples. Maclean (1914) reports grades of between 5 and 50 g/t Au in two samples of quartz from the adits.

Lloyd

Several quartz veins, trending approximately 120°, dip steeply to the northeast or southwest and cut through the hanging wall and footwall of the same thrust fault which

runs close to the Gold Run and Aime claim groups (Figure 2). The veins are hosted by felsic and chloritic schists. Clasts of wallrock can be seen locally within the vein quartz. The veins can be traced for approximately 250 m and may be semi-continuous with other claims in the area, perhaps with as much as 2.5 km of strike length. Grades of up to 20 g/t Au have been reported (NCMI).

Hunker Dome

The hardrock claims in this area are some of the most extensively explored in the Klondike, with an exploration history stretching back to 1900 (NCMI). A number of shafts and adits were developed in the area (Figures 5a and 6). Recent trenching has exposed a swarm of minor, discontinuous, gold-bearing milky quartz veins in the footwall and hanging wall of a major thrust fault (Figure 6). The veins are hosted predominantly by chloritic schists. Trench mapping in the area has revealed a possible splay from the major thrust fault, with a body of serpentinite exposed along the thrust surface. Both the veins and the thrust fault trend approximately north-south (Figure 6). It is uncertain whether the micaceous quartzite shown in Figure 6 represents a unit within assemblage II, or a quartzitic unit within the chloritic schists of assemblage I.

Some veins display evidence of brecciation and infilling of vugs by late stage amethyst, and in trench MAC-88-18, a possible cross-cutting relationship was observed between two discordant veins, suggesting that more than one generation of veining may be present. Debicki (1985) reports a grade of 150 g/t Au from galena-bearing quartz.

Sheba and Mitchell

Mineralization on the Sheba claim group consists of a prominent, discordant quartz vein approximately 1.0 to 1.5 m thick which has been cut by a minor fault, and a number of smaller, coeval(?) veins hosted within chloritic schist. K-Ar ages for mica from discordant veins exposed on the Sheba property are reported in Chapter IV. The Sheba vein contains "floating", angular clasts of wallrock, and is notable for its abundant sulfide mineralization (Friedrich and Hoymann, 1989); it is the most sulfide-rich of all of the discordant veins examined in this study (see above). A bulk sample of handpicked sulfides assayed 1.4 g/t Au, and 4680 g/t Ag from 3.7 tonnes (Debicki, 1985).

The Mitchell veins, which occur slightly to the north of the Sheba lodes, are possibly an extension of the Sheba vein system and form an en echelon system trending approximately north-south with steep dips (Mortensen et al., in press). Numerous smaller veins outcrop within the area, hosted by chloritic schists. The chloritic schists are stained brown due to carbonate flooding. Sulfidation of magnetite porphyroblasts within the

wallrocks has been reported by Mortensen et al. (in press). A small shaft was developed on this property at the turn of the century, and visible gold has recently been reported from the tailings pile adjacent to the shaft (J. McFaul, pers. comm.; J. Mortensen, pers. comm.)

Violet

The Violet vein was discovered in 1901, and three shafts were subsequently developed on the property (Van Angeren, 1989). Debicki (1985) reports that several westerly-trending veins are present in the area of the main shaft. These can be traced into a lineament that may extend along strike for up to 500 m. Exposure is poor, and all sampling was carried out from material on mine dumps. The main vein is approximately 1.8 m wide, and occurs at the sheared contact between orthogneiss and a mafic dyke (LeBarge and Bremner, in press). The veins contain a high proportion of gangue-phase barite and also appear to be brecciated locally (Debicki, 1985; this study). Grades of approximately 2.5 g/t Au have been reported.

27 Pup

A number of small (ca. 3 to 4 cm thick) discordant quartz veins are hosted by quartz-augen schist, and cut by a number of minor faults. With one exception, the veins trend roughly north-south. A single east-west trending vein was exposed in shallow trenching, with a thick selvage of limonitic material against its margin. The limonite contained extremely high gold grades, and reportedly yielded approximately 5 oz. of gold from 2 5-gallon pales of material (D. Johnston, pers. comm.) (Plate 7).

Lone Star

The only hardrock property in the Klondike to achieve a significant level of production, nearly 8500 tons of ore were produced from the Lone Star mine, and approximately 35 kg of gold were recovered (Debicki, 1985; NCMI, 1972; MacLean, 1914). Hand-picked sulfide mineralization returned gold values as high as 9 kg/t Au (NCMI, 1972). In common with much of the Klondike region, the geology of the Lone Star area is uncertain due to poor outcrop and a lack of detailed mapping. Gold-bearing veins are hosted by pyritized quartz-muscovite schists. A minor 2-3 cm thick discordant vein exposed in the Boulder Lode trench yielded numerous samples of visible gold over a 2 m length of vein.

Hilchey

Recent trenching and drilling identified a number of minor, gold-bearing discordant veins hosted by felsic schists (Figure 2). The quartz veins are milky white and unbanded with local visible gold (S. Tomlinson, pers. comm.; this study). One vein is approximately 50 cm thick, but pinches and swells significantly. The veins trend roughly east-west and dip towards the north. Gold grades vary from trace to over 200 g/t (Hughes-Lang Group, unpublished company report).

Virgin

Minor discordant veins, locally quite vuggy, occur within quartz-augen schists. The veins are generally sulfide poor and contain barite as a gangue phase. MacLean (1914) reported a grade of approximately 25 g/t Au for one sample of quartz. No structural data is available for this showing, and all material was collected from the tailings dump.

Appendix 7

Graphical construction methods for inclusion fluid pressure estimation.

A) 2-phase curve/isochore intersection.

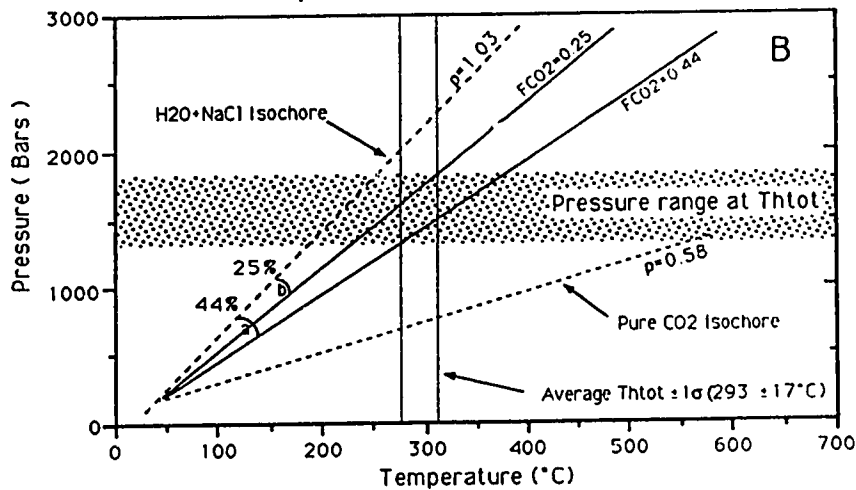
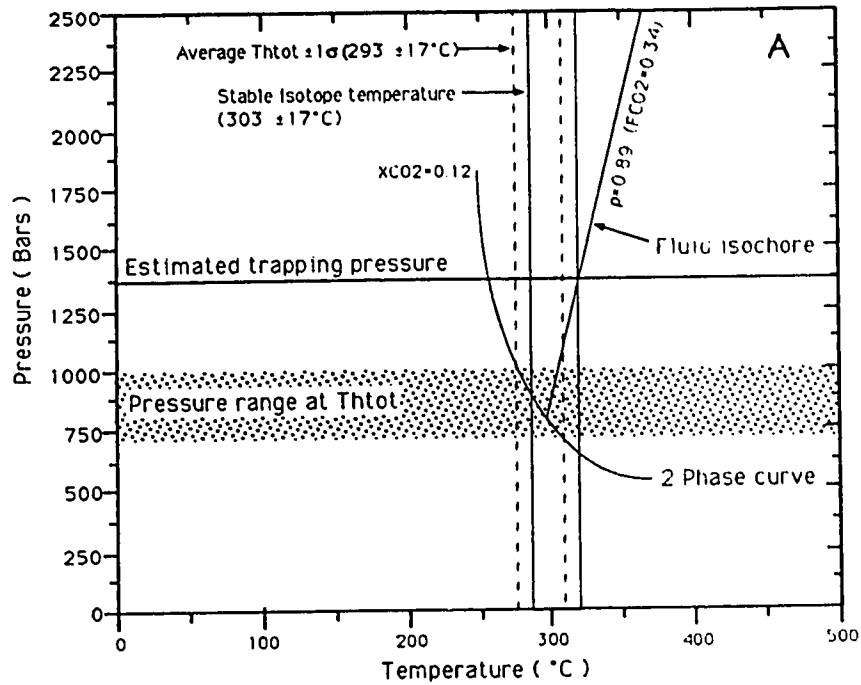
2-phase curves and fluid isochores are constructed using the data of Takenouchi and Kennedy (1965), Bowers and Helgeson (1983), and the corrected fluid compositions in Table 1. The pressure at T_{hot} is defined by the intersection of the fluid isochore with the 2-phase curve (Figure A). Trapping pressures are defined by the intersection of the fluid isochore with the appropriate, independent trapping temperature estimate, in this case, the quartz-muscovite stable isotope mineral pair (Chapter VI). This method is essentially the same as the graphical method of Schwartz (1989).

B) Brown and Lamb's (1989) construction.

Brown and Lamb (1989) assume that mixing in the H_2O -NaCl- CO_2 system, between an H_2O -NaCl solution and a pure CO_2 phase, is ideal (linear). This allows a simple graphical construction method to be used to fix the position of the H_2O - CO_2 -NaCl bulk fluid isochore if i) the relative salinity (NaCl/ H_2O +NaCl), ii) the bulk CO_2 -density, and iii) the volume percent estimate of the CO_2 phase are known.

Isochores are first constructed for the H_2O -NaCl, and CO_2 phases from standard data tables, for example Angus et al. (1976), Potter and Brown (1977), Haas (1976) and Bowers and Helgeson (1983). In Figure B isochores (shown as dashed lines) have been plotted for data from the Gold Run lode; an H_2O -NaCl solution (density= 1.03 g/cc) of approximately 4 eq.wt.% NaCl, and a "pure" CO_2 fluid (density= 0.58 g/cc).

To construct isochores for the ternary mixture, the angle made by the intersection between the end-member isochores (angle A on Figure B) is subdivided into volume percent estimates, and the ternary fluid isochore is then plotted at the appropriate angle away from the end-member isochore. For example, the fluid isochore for a volume percent CO_2 phase estimate of 0.25, is plotted as a straight line at 25 % of angle A away from the H_2O -NaCl isochore, towards the pure CO_2 isochore. The intersection of the ternary isochore with the homogenization and trapping temperature estimates then defines the homogenization and trapping pressures.



Appendix 7, Figure A. Example of pressure estimation from isochore origin, and from intersection of independent geothermometer with an isochore. Figure B. Brown and Lamb's construction method (see text). 2-phase curves constructed from the data of Takenouchi and Kennedy (1965). Isochore coordinates calculated from the data of Bowers and Helgeson (1983), Potter and Brown (1977) and Angus et al. (1976).